Luminal accessory protein regulation of wild type and mutant human cardiac ryanodine receptors (hRyR2)

By

Chloe Elizabeth Maxwell

A thesis submitted for the degree of Doctor of Philosophy

September 2014

Institute of Molecular & Experimental Medicine

School of Medicine

Cardiff University

DECLARATION
This work has not been submitted in substance for any other degree or award at this or any other university or place of learning, nor is being submitted concurrently in candidature for any degree or other award.

Signed .....

Date .....

STATEMENT 1
This thesis is being submitted in partial fulfillment of the requirements for the degree of PhD

Signed .....

Date .....

STATEMENT 2
This thesis is the result of my own independent work/investigation, except where otherwise stated. Other sources are acknowledged by explicit references. The views expressed are my own.

Signed .....

Date .....

STATEMENT 3
I hereby give consent for my thesis, if accepted, to be available for photocopying and for inter-library loan, and for the title and summary to be made available to outside organisations.

Signed .....

Date .....

Acknowledgments:

I would first like to thank my supervisor Professor Alan Williams for giving me the opportunity to work at the Wales Heart Research Institute, for his continual support throughout the course of my PhD and giving me the chance to present my work at an international conference. I also give special thanks to my co-supervisor and friend, Dr Lowri Thomas, to whom I'm extremely grateful for her scientific expertise, patience and guidance that helped me to accomplish this work. To my other colleagues and friends at the WHRI, thank you for making life in the laboratory enjoyable and providing me with useful advice when needed.

I especially want to acknowledge my family and friends for their continual love and support throughout my life and career - you're the best. I'm very grateful to my fiancé Damon for his constant encouragement, guidance and love; and to our cats Hugo and Flossie who welcome me home from work everyday with such enthusiasm. Finally, I would like to thank my parents John and Julie Maxwell for making me into the person that I am today, supporting and believing in me, and encouraging me to always try my best.

Summary:

Human cardiac ryanodine receptors (hRyR2) are major Ca^{2+} release channels in the heart, which form quaternary complexes with luminal proteins, calsequestrin (CSQ2), junctin (JUN) and triadin (TRD1). These proteins facilitate Ca^{2+} release during excitation-contraction coupling, modulating the response of hRyR2 to luminal Ca^{2+} changes. Catecholaminergic Polymorphic Ventricular Tachycardia is an arrhythmogenic disorder, caused by mutations in *RyR2* and *CSQ2* genes. Defective sensing of cytosolic/luminal Ca^{2+} by hRyR2 is a candidate mechanism underlying disease pathogenesis, likely caused by defective luminal protein regulation. Using a recombinant approach, this study aimed to evaluate if mutant (N4104K and A4556T) hRyR2 respond to or interact differently with, these accessory proteins.

Expression constructs corresponding to CSQ2 and JUN were generated and expressed stably and transiently with wild-type (WT) or mutant hRyR2 in HEK293 cells. Immunofluorescent co-localisation confirmed successful co-expression and association of these luminal proteins with hRyR2 *in situ*. Ca^{2+} activation of wild-type/mutant hRyR2 in the absence/presence of CSQ2 and/or JUN was assessed by [^{3}H]-ryanodine binding, while luminal Ca^{2+} effects were monitored using single-cell Ca^{2+} imaging - examining spontaneous Ca^{2+} release events. A4556T-hRyR2 displayed similar cytosolic and luminal Ca^{2+} dependence to wild-type channels, whilst N4104K-hRyR2 displayed a remarkably different Ca^{2+} activation profile, demonstrating functional heterogeneity between hRyR2 mutants.

Ca^{2+} imaging revealed an inhibitory effect of CSQ2 on WT and N4104K-hRyR2 activity, both in the presence and absence of JUN. In line with this, CSQ2 was found to bind directly to hRyR2 by co-immunoprecipitation, an observation that has not been previously demonstrated in the literature. Immunofluorescence studies suggested reduced CSQ2 and JUN association with A4556T-hRyR2, but this could not be confirmed with co-immunoprecipitation. Ca^{2+} imaging investigations with this mutant however, suggested that CSQ2 wasn't able to regulate these channels in the same way as WT, implying a change in functional effect.

Abstract related to this work:

Maxwell, C., Williams, A.J, Mukherjee, S., & Thomas, N.L. (2013). Regulation of Wild Type and CPVT-linked mutant Cardiac Ryanodine Receptors by Junctin and Calsequestrin. *Biophysical Journal*, 104 (2), p441a.

Other peer reviewed publications:

Thomas, N. L., Maxwell, C., Mukherjee, S., & Williams, A. J. (2010). Ryanodine receptor mutations in arrhythmia: The continuing mystery of channel dysfunction. *FEBS Letters*, *584*(10), pp. 2153–2160.

Zissimopoulos, S., Seifan, S., Maxwell, C., Williams, A.J. and Lai, F.A. 2012. Disparities in the association of the ryanodine receptor and the FK506-binding proteins in mammalian heart. *Journal of cell science* 125(Pt 7), pp. 1759–1769.

Table of Contents:

Chapter 1: General Introduction

Chapter 2: Materials and Methods

List of Figures and Tables:

Chapter 1: General Introduction

Figures

Tables

Chapter 2: Materials and Methods

Figures

Tables

Chapter 3: Generation of recombinant luminal accessory protein constructs and co-expression with wild type and mutant hRYR2

Figures

Tables

Chapter 4: Influence of cardiac CSQ2 and JUN on the intracellular Ca^{2+} regulation of WT and mutant hRyR2

Figures

Abbreviations List

AM	Acetoxymethyl
ANOVA	Analysis of variance
AP	Action Potential
ARVD	Arrhythmogenic Right Ventricular Dysplasia
ASPH	Aspartate beta-hydroxylase
AT or AThRyR2	A4556T mutant hRyR2
β-AR	Beta-adrenergic
BLAST	Basic Local Alignment Search Tool
BSA	Bovine serum albumen
CaM	Calmodulin
CaMKII	Calcium/Calmodulin-dependent Kinase II
cDMEM	Complete / supplemented DMEM
CICR	Calcium-induced calcium release
Co-IP	Co-immunoprecipitation
CPVT	Catecholaminergic polymorphic ventricular tachycardia
Cryo-EM	Cryo-electron microscopy
CSQ	Calsequestrin
CSQ1	Calsequestrin, skeletal isoform 1
CSQ2	Calsequestrin, cardiac isoform 2
DAD	Delayed after-depolarisation
DMEM	Dulbecco's modified eagles medium
DMSO	Dimethyl sulfoxide
Dpm	Decays (or disintegrations) per minute
EAD	Early after depolarisation
ECC	Excitation-contraction Coupling
ECG	Electrocardiogram
ECL	Enhanced chemiluminescence
eGFP	Enhanced green fluorescent protein
EGTA	Ethylene glycol tetraacetic acid
ER	Endoplasmic reticulum
F	Fluo-3 peak signal intensity
F_0	Fluo-3 basal signal intensity
FBS	Foetal bovine serum
FKBP	FK506 binding protein
F.U.	Fluorescence Units
GFP	Green Fluorescent Protein

HEDTA	Hydroxyethyl Ethylenediamine Triacetic Acid
HEK293	Human embryonic kidney 293 cells
HF	Heart failure
HRC	Histidine-rich Ca^{2+} binding protein
HRP	Horseradish peroxidase
iPSCs	Induced Pluripotent Stem Cells
jSR	Junctional Sarcoplasmic Reticulum
JP2	Junctophillin
JUN	Junctin
LB	Luria-Bertani medium
LTCC	L-type Ca^{2+} channel (or Dihydropyridine receptor)
mDMEM	Minimal / unsupplemented DMEM
NCX	Sodium-calcium exchanger
NK or NKhRyR2	N4104K mutant hRyR2
NTA	Nitrilotriacetic Acid
PBS	Phosphate Buffered Saline
PCR	Polymerase Chain Reaction
PKA	Protein kinase A
PLB	Phospholamban
pmol	Picomole
P_o	Open probability
PVDF	Polyvinylidene difluoride
ROI	Region of Interest
RT	Room temperature
RyR	Ryanodine receptor
RyR1	Ryanodine receptor, Skeletal Muscle Isoform, Type I
RyR2	Ryanodine receptor, Cardiac Muscle Isoform, Type 2
RyR3	Ryanodine receptor, Type 3 Isoform
SCR	Spontaneous Ca^{2+} release
SDS	Sodium Dodecyl Sulphate
SDS-PAGE	SDS Polyacrylamide Gel Electrophoresis
S.E.M.	Standard error of the mean
SERCA2a	Sarco/endoplasmic reticulum Ca^{2+} ATPase
SOC	Super optimal broth supplemented with glucose
SOICR	Store Overload-Induced Calcium Release
SR	Sarcoplasmic Reticulum
TAE	Tris-acetate-EDTA
TBS	Tris-buffered saline

TBS-T	Tris-buffered saline with added 0.1% (v/v) Tween-20
TEMED	Tetramethylethylenediamine
TRD	Triadin
TRD1	Triadin, cardiac isoform 1
T-tubule	Transverse tubule
VT	Ventricular Tachycardia
v:w	Volume to weight/volume by weight
v:v or v/v	Volume to volume/volume by volume
WT	Wild Type
w/v	Weight by volume

Chapter 1

General Introduction

1.1. Calcium Signalling in the heart:

In cardiac muscle, ionised calcium (Ca^{2+}) acts as a ubiquitous intracellular signalling messenger directly regulating a multitude of processes such as the electrical activity of the heart, ion channel gating and contractile processes. All of which are central to the synchronous systolic-diastolic cycles (ventricular contraction and relaxation, respectively) that produce the heartbeat. During the physiological process of Excitation-Contraction Coupling (ECC), intracellular Ca^{2+} homeostasis must be carefully regulated, such that cardiac myocytes can distinguish between a series of spatially and temporally discrete localised Ca^{2+} signalling pathways (occurring simultaneously within the cell) which combine to produce an overall global Ca^{2+} transient to generate muscle contraction (Bers, 2002). Since Ca^{2+} cannot be metabolised, Ca^{2+} homeostasis is maintained by a subset of critical signalling molecules and protein complexes that function against a background of tightly regulated changes in the intracellular free Ca^{2+} concentration (Scoote and Williams, 2004, Bers et al., 2008).

1.2. Excitation-Contraction Coupling:

ECC refers to the co-ordinated process that pairs electrical stimulation of the cardiomyocytes with the movement of intracellular Ca^{2+} around the cell to induce muscle contraction (Bers, 2008). Ca^{2+} exerts its major signalling function when elevated in the cytosolic compartment of cardiac cells, which is achieved by a specialised intracellular architecture that acts in a coordinated manner to regulate Ca^{2+} handling during each heartbeat. Figure 1.1 (A) illustrates major proteins involved in ECC within cardiac muscle.

1.2.1. The systolic phase of the cardiac cycle (muscle contraction):

When the heart is at rest (diastole), intracellular Ca^{2+} is sequestered into the sarcoplasmic reticulum (SR), which is the major internal Ca^{2+} store of cardiomyocytes. Responsible for elevating intracellular Ca^{2+} within the cytosol, the transverse tubules (or T-tubules) are a coalescence of the myocyte cell surface (the sarcolemma), which exist as deep invaginations and provide a close apposition between the sarcolemma and the intracellular space (the junctional SR membrane (jSR)) of cardiomyocytes (Berridge, 2003, Fearnley, 2011). During systole, specific ion fluxes between the extracellular space and cytosol initiates electrical excitation of the myocyte sarcolemma, a process known as depolarisation. Described further in section 1.2.4, the resultant change in membrane potential initiated by depolarisation is known as the action potential (AP), a phenomenon

that forms distinct phases which correspond to a specific membrane ion flux, as illustrated in Figure 1.1 (B).

When the myocyte becomes depolarised, a small influx of extracellular Ca^{2+} enters the cytosolic compartment of the cell through voltage-gated L-type Ca^{2+} channels (LTCC) present on the sarcolemmal membrane. This inward Ca^{2+} current initiates Ca^{2+}-induced-Ca^{2+} release (CICR), where a much larger Ca^{2+} efflux from the SR significantly amplifies the cytosolic Ca^{2+} concentration. The amplitude of the resultant Ca^{2+} transient determines the contractile force of the cardiac myocyte (Bers and Guo 2005). A major Ca^{2+} release channel found embedded in the SR membrane facilitates this process, and plays a crucial role in CICR. Ryanodine receptors (cardiac isoform known as RyR2) traverse the SR membrane and function as regulated Ca^{2+}release channels, allowing Ca^{2+} to pass from the intracellular store into the surrounding cytoplasm, elevating cytosolic [Ca^{2+}] from approximately 100 nM during diastole to ~1 μM during the systolic phase of the cardiac cycle (Fearnley et al., 2011). The tenfold increase in intracellular Ca^{2+} induces a conformational change in the cardiac muscle myofilaments responsible for cardiomyocyte contraction (Bers and Guo, 2005).

1.2.2. Calcium sparks and transients:

Clusters of RyR2 channels are localised in discrete areas along the jSR membrane (known as calcium release units) and are positioned adjacent to L-type Ca^{2+} channels (Franzini-Armstrong, 2005). The global Ca^{2+} transient that generates contractile function is a summation of many localised intracellular Ca^{2+} release events known as Ca^{2+} sparks, which were first described as spontaneous elementary Ca^{2+} signals arising from the SR (Cheng et al., 1993, Cheng and Lederer 2008). We now know that Ca^{2+} sparks reflect the concerted opening of a cluster of RyR2 Ca^{2+} release channels, which were first visualised in the cell by fluorescent indicators (Cheng et al., 1993). It has been estimated that up to 20 RyR2 channels may open during each Ca^{2+} spark, and that the Ca^{2+} dependence of spark frequency is in line with that of the Ca^{2+} dependence of RyR2 open probability (P_o) (Zahradníková et al., 2012).

1.2.3 The diastolic phase of the cardiac cycle (relaxation):

Allowing cardiac muscle relaxation (reduced activation of contractile proteins), RyR2 channel activity declines and the cytosolic Ca^{2+} concentration is returned to resting levels. This is achieved via two primary mechanisms: the Na^{+}/Ca^{2+} exchangers (NCX), located in the sarcolemma, and the sarco/endoplasmic reticulum Ca^{2+} ATPase pump (SERCA2a), located in the SR membrane (Figure 1.1 (A)). In human ventricles, approximately 70% of intracellular Ca^{2+} is removed by SERCA2a (the predominant isoform in the heart), 28% by NCX, and the remaining 2% by a mitochondrial Ca^{2+} uniporter, a pattern also observed in other species such as dog, guinea pig and rabbit (Fearnley, 2011, Bassani et al., 1994, Bers, 2001). SERCA2a sequesters Ca^{2+} back into the SR store, which is subsequently buffered by the luminal Ca^{2+} binding protein, CSQ2 (section 1.6). SERCA2a activity is regulated by an integral membrane protein, phospholamban (PLB). NCX catalyses the electrogenic exchange of Na^{+} and Ca^{2+}, extruding Ca^{2+} from the cell and thus restoring the intracellular Ca^{2+} concentration to diastolic levels (Bridge et al., 1990). Given the fact that for each Ca^{2+} ion that is extruded, three Na^{+} ions enter the cell, it has also been suggested that RyR2 Ca^{2+} sparks stimulate NCX activity and contributes to the generation of a net inward Na^{+} current that is required for action potential initiation (Berridge et al*.,* 2003).

1.2.4. The cardiac action potential:

Generation of an action potential (AP) at the sarcolemma causes the electrical excitation required to initiate ECC. The cardiac AP consists of 5 phases as shown in Figure 1.1 (B) and is the product of changes in the membrane potential, generated by the activation and deactivation of specific ion channels in a time-dependent manner (Scoote & Williams, 2004). Under diastolic conditions, the resting membrane potential (E_m) of a ventricular cardiomyocyte is approximately -80 mV (Bers, 2008) and is represented as Phase 4 of the AP cycle. Initiating excitation, Phase 0 of the AP represents activation of voltage-dependent fast inward Na^{+} currents, responsible for generating rapid depolarisation of the sarcolemma to approximately +40 mV. This phase is represented in Figure 1.1 (B) as a sharp upstroke. Once depolarisation is complete, this inward Na^{+} current becomes inactivated and a movement of K^{+} and Cl^{-} ions from the cell cytosol triggers early repolarisation of the membrane potential, represented as a downward deflection in the AP cycle (Phase 1). Phase 2 corresponds to a plateau phase, generated by the manifestation of an inward Ca^{2+} current, primarily through L-type Ca^{2+} channels, and a K^{+} efflux through slow delayed rectifier channels. In order to return to resting state, rapid (late) repolarisation (Phase 3) occurs within the myocyte, whereby the RyR2 channels prevent any further Ca^{2+} influx into the cytosolic compartment by initiating Ca^{2+} efflux from the SR

store, inactivating the L-type Ca^{2+} channels by the raised [Ca^{2+}] and at the same time, rapid and slow delayed rectifying K^+ channels remain open and allow the efflux of the remaining K^+ ions out of the cell. This reduction in positive charge causes the cell to repolarise, and the K^+ channels close once the membrane potential is restored to -80 mV. At the same time, the additional Na^+ and Ca^{2+} that entered the cell during the course of the action potential are extruded by NCX, whilst SERCA2a sequesters Ca^{2+} back into the SR store. The Na^+/K^+ ATPase pump also facilitates the removal of excess Na^+ from the cell. Following AP repolarisation, cytoplasmic Ca^{2+} falls and the myocardium relaxes (Bers, 2008). The action potential lasts approximately 300 milliseconds during which time the cell remains refractory to any further activation.

(A)

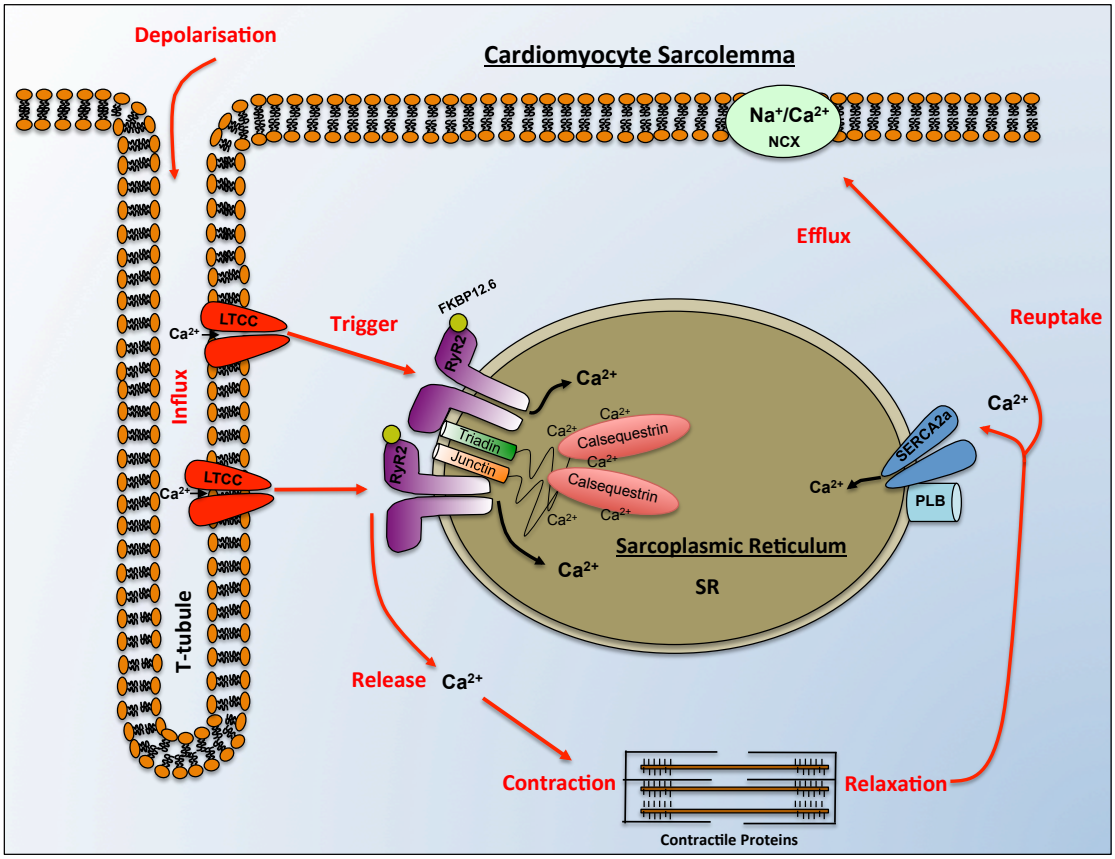

(B)

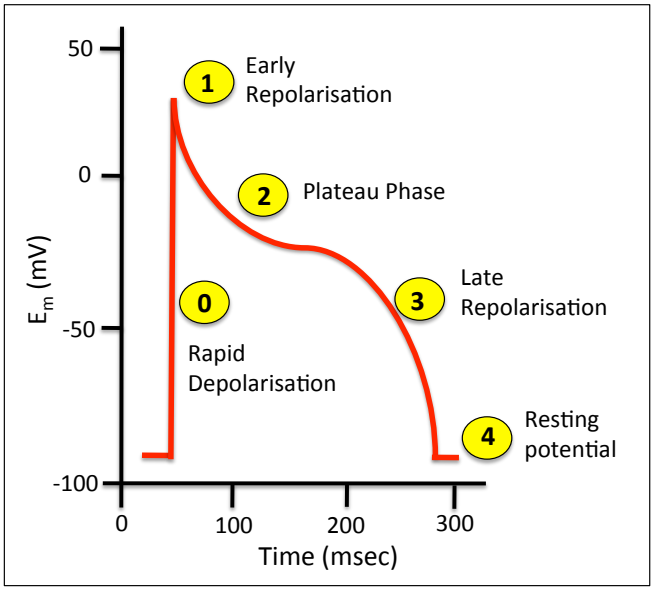

Figure 1.1: Cardiac Muscle Excitation Contraction Coupling: Illustrated are the major protein components involved in ECC described in sections 1.2-1.2.3 **(A)** Depolarisation of the cardiomyocyte sarcolemma initiates an influx of Ca^{2+} through LTCC that subsequently triggers greater Ca^{2+} release from the SR store through RyR2 Ca^{2+} release channels. Following contraction, Ca^{2+} dissociates from the contractile proteins and is removed from the cytoplasm primarily by the SERCA2a pump that sequesters Ca^{2+} back into the SR (modulated by PLB) and via NCX, which extrudes Ca^{2+} from the cell. Distinct phases of the cardiac action potential are highlighted in **(B)** and described further in section 1.2.4.

1.2.5. ß-adrenergic stimulation modulates cardiac EC coupling activity:

During times of emotional stress and exercise, a rapid change in the rate (chronotropy), force of contraction (inotropy) and relaxation (lusitropy) of the heart is achieved by stimulation of the sympathetic nervous system and subsequent activation of a well-characterised ß-adrenergic signalling cascade within the myocardium (Bers, 2002). This process is often known as the "fight-or-flight" response and vitally enhances cardiac myocyte activity in situations where there is a higher metabolic demand (Shan et al., 2010). As summarised in Figure 1.2, neuronally released adrenaline/noradrenaline or circulating catecholamines bind to ß-adrenergic receptors present on the cardiomyocyte sarcolemma, which initiates a downstream signalling cascade that first activates adenylate cyclase and the production of cyclic AMP, which in turn activates phosphorylation enzymes such as protein kinase A (PKA). Alterations in the phosphorylation status of several proteins central to the regulation of contractility, leads to elevations in the Ca^{2+} mediated responses seen during normal EC coupling (Lakatta, 2004, Bers, 2004, Reiken et al., 2003).

The proposed functional consequences of PKA phosphorylation include: (1) *positive inotropic effects*, such as increased activity of LTCC and RyR2 receptors, causing a greater influx of extracellular Ca^{2+} and larger efflux of luminal Ca^{2+} from the SR, respectively (Bers, 2002, Scoote and Williams, 2004); and (2) *positive lusitropic effects*, including phosphorylation of PLB, which relieves SERCA2a inhibition and speeds up Ca^{2+} re-uptake into the SR, increasing the 'Ca^{2+} load'. In addition, a reduction in myofilament Ca^{2+} sensitivity occurs via phosphorylation of troponin I, a protein that mediates myofilament contraction. This lowered activity is however compensated for by the dramatic rise in Ca^{2+} transient amplitude seen after ß-adrenergic stimulation (Li et al., 2000). Taken together, ß-adrenergic activation elicits a cascade of phosphorylation reactions that increase Ca^{2+} levels within the SR and produce larger and faster Ca^{2+} transients. These enhanced processes combine to increase cardiac output and improve overall cardiac performance. It is however important to note that whilst catecholamines can improve contractile function and increase SR Ca^{2+} content, Ca^{2+} load can increase to a level which induces spontaneous Ca^{2+} release from the SR through RyR2 channels, as seen in cardiovascular disease (section 1.7-1.7.1).

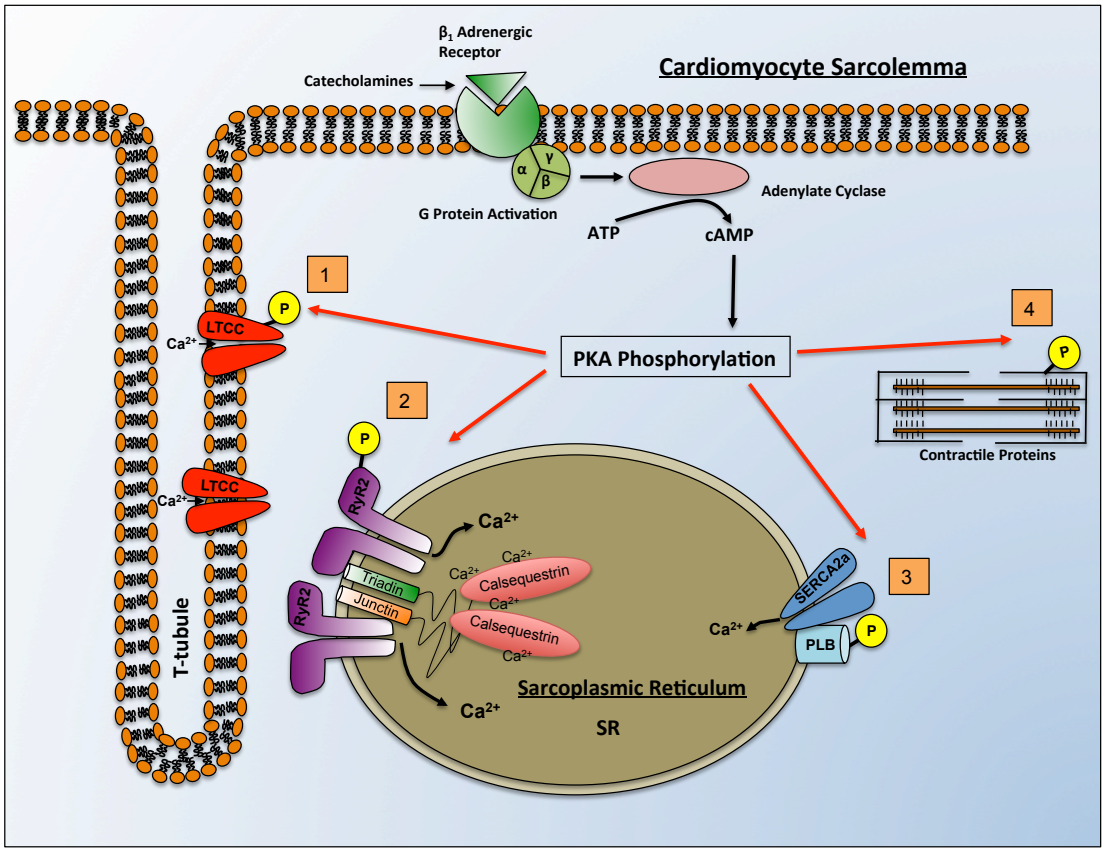

Figure 1.2: Activation of the ß-adrenergic receptor and phosphorylation of protein targets: Activation of ß-adrenergic receptors by circulating catecholamines (or adrenaline/noradrenaline) triggers downstream signalling cascades that culminate in phosphorylation of protein targets. Illustrated here is the G protein (guanosine nucleotide-binding protein) cascade and activation of PKA. Activation of the G protein complex stimulates adenylate cyclase to produce a secondary messenger cAMP (from ATP). This in turn stimulates PKA. The effects of phosphorylation of protein targets highlighted here with numbers: (1) LTCC, (2) RyR2, (3) PLB and (4) contractile proteins (specifically troponin I) is discussed further in section 1.2.5.

1.3. Cardiac ryanodine receptors (RyR2):

Ryanodine receptors are the largest known Ca^{2+} channels in the human body and are named after the muscle-paralysing plant alkaloid, ryanodine. Ryanodine exists naturally in the roots and stems of the *Ryania speciosa* and was found in the late 1980s to bind to the Ca^{2+} release channels with very high affinity and specificity (Lai and Meissner, 1989). The advantages of using this property to assess RyR2 function will be discussed in Chapter 4. RyR channels exist as three mammalian isoforms, each encoded by a distinct gene (*RyR1*, *RyR2* and *RyR3*) and residing on separate chromosomes (Capes et al., 2011). Although the regulation and expression of the three known isoforms is tissue specific, all three share similar characteristics, functioning as cation-selective ion channels that are modulated by Ca^{2+}, Mg^{2+} and ATP (Lanner et al., 2010).

RyR2 is the predominant isoform found in cardiac muscle (Lai et al., 1988), encoded by the *RyR2* gene and located on chromosome 1 (1q42-q43), (Otsu et al., 1993, Tunwell et al., 1996). Aside from the myocardium, RyR2 is also expressed at lower levels in the somata of neurons, the stomach, brain, adrenal glands and ovaries (Lanner et al., 2010, Kuwajima et al., 1992, Giannini et al., 1995, Nakai et al., 1990). Biochemical analysis and three-dimensional reconstruction studies have revealed that RyR2 Ca^{2+} release channels exists as large homotetramers that traverse the SR membrane, and consist of four identical 565 kDa subunits, surrounding a centrally located pore (Lai et al., 1989, Sharma et al., 1998). The four protein monomers combine to form a 2.2 MDa complex, with 4967 amino acids per monomer (Otsu et al., 1993, Tunwell et al., 1996). Channels are characterised by their large N-terminal domain which protrudes into the cytosol and is recognised in electron micrographs as a “foot-like” structure observed at the junction between terminal cisternae of SR and the T-tubule network. A number of associated regulatory proteins make the structure a huge macromolecular complex (Franzini-Armstrong et al., 1999, Yano et al., 2009). Hydropathy plot analysis has revealed that the first 4000 amino acids of the RyR2 channel are hydrophilic and correspond to the N-terminal region of the protein, the smaller C-terminal region is predicted to contain large hydrophobic stretches plus highly charged sequence repeats which are thought to be important for accessory protein association (Zorzato et al., 1990). The C-terminal section of the protein comprises a pore-forming region and approximately 6 transmembrane (TM) helices, with one potential TM stretch forming a pore loop from the luminal side of the channel, as proposed by Du et al., 2002.

Figure 1.3 illustrates predicted structures of the RyR channel complex. In recent years, studies using single-particle cryo-electron microscopy (cryo-EM) have provided us with

invaluable structural information regarding the architecture of RyR Ca^{2+} release channels, as well as the identification of binding regions for a multitude of intracellular molecules responsible for modulating RyR activity (Hamilton and Serysheva, 2009, Huang et al., 2012, Efremov et al., 2015, Yan et al., 2015). Numerous allosteric interactions are predicted to contribute to the conformational changes necessary within the channel domain to allow channel opening, which are largely achieved through extensive van der Waals contacts (Samsó et al., 2005, Yan et al., 2015). Furthermore, cryo-EM studies have facilitated the mapping of CPVT-associated mutation hotspots within the Ca^{2+} release complex. Closed channel structures of rabbit RyR1 (Yan et al., 2015) have recently been achieved at the near-atomic resolution of 3.8 Å (Figure 1.3 (A)), while the open state structure has been captured at 8.5 Å (Efremov et al., 2015). Figure 1.3 (A) and (B) (i) demonstrate the characteristic mushroom-shaped architecture of the RyR1 channel (that is highly conserved between RyR isoforms), which has 4-fold rotational symmetry (Hamilton and Serysheva, 2009) and its macromolecular assembly, generated from cryo-EM imaging and the formation of electron microscopy density maps by Yan et al (2015). The distinct domains established by Yan et al (2015) are highlighted in Figure 1.3 (B) (i)-(iii) and are colour coded for identification (see labelled domains in (B) (ii)). Characterisation of RyR2 channels by cryo-EM has been hindered by the difficulty to isolate large enough quantities of purified, structurally intact channels from cardiac muscle (Liu et al., 2001).

As shown in (B) (i), the large N-terminal cytoplasmic domain of RyR constitutes the bulk of the protein (~80% (Huang et al., 2012)), which is adjoined to the C-terminal luminal domain via a transmembrane region (TM) that together resembles a stalk-like structure (Hamilton and Serysheva, 2009). A structural scaffold for the large N-terminal region is formed by a α-solenoid domain, which consists of ~30 α-helices packed into parallel layers (Yan et al., 2015). Within the cytoplasmic domain, direct interactions between the central and channel domain (marked in Figure 1.3 (B) (ii)) are thought to primarily regulate the conformational changes necessary to control RyR opening and closing (Yan et al., 2015). Described by Yan et al (2015) the handle and two helical structures (indicated as HD1 and HD2 in (B) (ii)) of the cytoplasmic central region (Figure 1.3 (B) (ii)) appear to form a discontinuous corona (a protein adsorption layer which surrounds the protein surface, del Pino et al., 2014), which is predicted to contain the interaction sites for the ligand binding of channel modulators such as FKBPs and CaM. As highlighted in Figure 1.3 (B) (iii), FKBP12 appears to bind within a cleft situated between the N-terminal domain and the handle region (residues 1651-2145), and close to the SPRY domains (Yan et al., 2015). Earlier studies however, have reported that the binding site for FKBP12 lies between amino acids 2458-2468 of rabbit RyR1 (Hamilton and Serysheva, 2009 and Lanner et al.,

2010), which in the model proposed by Yan et al (2015) locates FKBP12 binding to the helical HD1 region (residues 2146-2712). In further studies using cryo-EM analyses, Huang at al (2012) established the binding region for the Ca^{2+} binding protein calmodulin (CaM) between RyR1 residues 3614 and 3643. Interestingly, two distinct but overlapping areas for CaM binding have been identified, where binding at each site is governed by the absence or presence of Ca^{2+} (Samsó et al., 2005, Huang et al., 2013). When CaM switches between Ca^{2+} free- and bound states, cryo-EM studies revealed that the regulatory protein appears to shift approximately 30 Å along the surface of the RyR1 channel (Huang et al., 2013). As highlighted in (B) (ii) and (iii), three SPRY domains are localised within the periphery of the cytoplasmic region, named according to their discovery within dual-specificity sp1A kinase and RyR channels (Ponting et al., 1997, Efremov et al., 2015). The precise function of these domains remains unclear, yet their positioning close to the N-terminal and helical domains (Figure 1.3 (B) (iii) suggests that the domains provide a scaffold and maintain structural integrity throughout this channel region (Yan et al., 2015, Efremov et al., 2015). As shown in Figure 1.3 (B) (iii), the SPRY domains (1-3) are composed primarily of ß-sheets (forming “ß-sandwiches”) and lie close to a phosphorylation hotspot labelled P1 (Yan et al., 2015). Another phosphorylation hotspot (P2) is highlighted in Figure (B) (ii), which has been predicted to reside within the helical domain of RyR1 between residues 2734 and 2940 (Yan et al., 2015). Within this region of channel phosphorylation, Zhu et al (2013) reported the presence of eleven disease-causing mutations.

The secondary structure of the RyR1 pore formulated by Yan et al (2015) is shown in Figure 1.3 (C) (i)-(iii), where six α-helical transmembrane regions (labelled S1-S6) per monomer are predicted, which together exhibit a voltage-gated ion channel fold (although RyR does not exhibit voltage-dependence) (C) (ii), (Samsó et al., 2005, Yan et al., 2015). As highlighted in (B) (ii) and (C) (ii), VSC refers to a cytoplasmic subdomain (named according to its location within the voltage-sensor fold region), formed by the intervening sequences in between transmembrane regions S2 and S3 (Yan et al., 2015). This previously unknown VSC domain appears to link a previously unidentified C-terminal subdomain (labelled CTD) close to the S1-S4 regions (shown in (C) (i)) and together with the central domain forms the “column-like” structure reported in earlier investigations (Samsó et al., 2005, Yan et al., 2015). Finally, as shown in (C) (i)-(iii), the luminal loop is a hairpin loop situated between S5 and the pore helix, which projects into the SR lumen and sits above the selectivity filter; this structure together with the S6 transmembrane region forms the entire ion-conducting pore (as demonstrated in (C) (iii)).

The cytoplasmic region of the S6 segment (labelled in (C) and forming part of the transmembrane domain) is enriched in aspartic and glutamic acid residues and together with the selectivity filter (length ~10 Å, labelled SF in (B) (ii)), forms a long (~90 Å) pathway for ion-conduction, allowing rapid Ca^{2+} transport across the SR membrane (Yan et al., 2015). As proposed by Yan et al (2015) opening of the activation gate may simply result from twisting within this S6 bundle, this however requires further investigation. Interactions between the CTD and the S6 region appear to be stabilised via a zinc-finger motif, whereby structural transitions of these domains are predicted to determine allosteric regulation of the channel's activation gate (Yan et al., 2015).

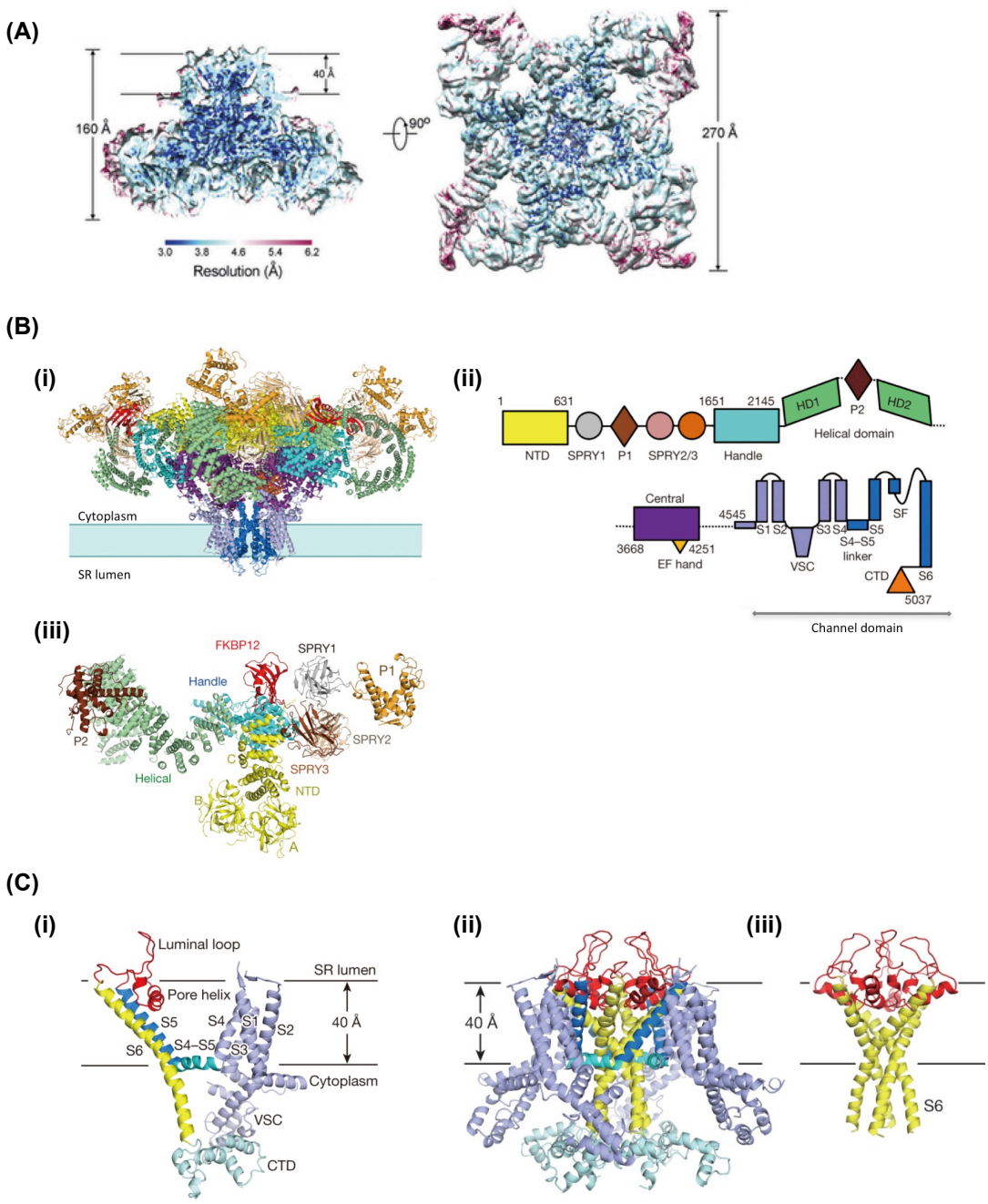

Figure 1.3: Illustration of the ultrastructure of RyR channels: *Established by cryo-EM analysis* ***(A)*** *illustrates an EM density map of the RyR1 channel (in complex with FKBP12) which is colour coded to highlight the ranges of resolutions achieved by Yan et al (2015), with the highest being at the central region of the structure.* ***(B)*** *(i-iii) depicts the overall RyR1 structure and the predicted domain organization and their orientation within the* Ca^{2+} *release channel. These domains are discussed in detail in section 1.3 and are colour coded according to the labelling shown in (B) (ii).* ***(C)*** *Illustrates the predicted structure of the channel domain, which constitutes the pore-forming region of the channel. Colour coding of structures in (ii) and (iii) correlates with those labelled in (C) (i). The labelled transmembrane regions (S1-6), luminal loops, pore helix, etc. in one RyR1 protomer are shown in (i) and per tetramer (ii); and are discussed in section 1.3. As mapped by cryo-EM, the pore helix and luminal loops (which make up the selectivity filter) of the channel are hotspots for CPVT-associated mutations (Yan et al., 2015). As shown in (iii) the ion-conducting pathway of the channel is predicted to consist of the selectivity filter and the S6 transmembrane segments. Image modified from Yan et al., 2015.*

1.4. Modulation of RyR2 channel gating by physiological ligands:

1.4.1. RyR2 regulation by Ca^{2+}:

A variety of physiological ligands, cellular processes, accessory proteins and pharmacological agents can modulate RyR2 activity, but Ca^{2+} is by far the most important effector of channel function. There is still however no consensus as to how exactly cytoplasmic and luminal Ca^{2+} regulates channel activity, but at least four Ca^{2+}-sensing sites on each RyR2 subunit have been proposed. As shown in Figure 1.4, using all known information derived from single channel recordings, Laver et al (2007) developed a model of RyR2 Ca^{2+} sensing sites and their relative contribution to channel activation is discussed below.

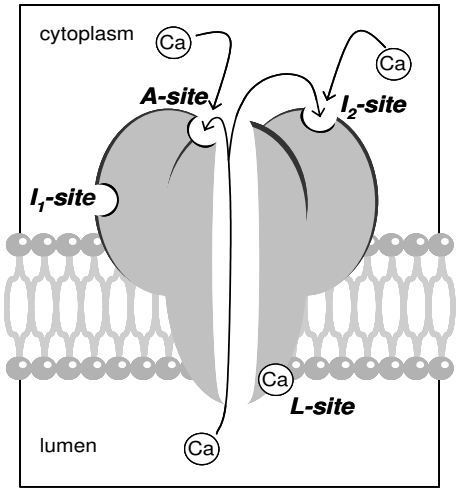

Site	Regulatory Effect	Ligand	Dissociation constant
A-site	Cytoplasmic Activation	Ca^{2+}	1-10μM
L-site	Luminal Activation	Ca^{2+}	60μM
I_1-site	Cytoplasmic Inhibition	Ca^{2+} and Mg^{2+}	~10mM
I_2-site	Cytoplasmic Inactivation	Ca^{2+}	1μM

Figure 1.4: Schematic illustrating the location of predicted RyR2 Ca^{2+} binding sites: *The exact locations of these Ca^{2+} sensing sites remain to be identified. Image taken from Laver, 2007.*

- ***Cytosolic Ca^{2+}:***

Laver (2007) suggests that RyR2 channels are activated by low micromolar concentrations (1-10 μM), but inactivated at millimolar concentrations (1-10 mM) of cytoplasmic Ca^{2+}. As shown in Figure 1.4, two cytoplasmic facing Ca^{2+} binding sites have been attributed to this response, termed the A-site (activation, 1 μM affinity) and the I_1-site (inhibition, 10 mM affinity), which is also known as the Ca^{2+}/Mg^{2+} inhibition site due to its lack of discrimination between these divalent cations (Laver, 2007, Balog et al., 2001). Another high affinity inhibitory site is also predicted, termed the I_2-site. This site has the same affinity as the A-site (1 μM) and causes brief (1 ms) channel closures upon binding Ca^{2+} (Laver, 2007). The bimodal dependence reported by Laver (2007) however has been contested, since other research groups including our laboratory have demonstrated that the effects of cytoplasmic Ca^{2+} on channel open probability (P_o) exhibits a sigmoidal relationship (Li and Chen et al., 2001, Mukherjee et al., 2012). Mukherjee et al (2012) demonstrated that the greatest increase in purified recombinant human RyR2 P_o was evident between 100nM-1 μM cytoplasmic Ca^{2+}, whilst an increase in cytosolic Ca^{2+} concentration >10 μM caused channel P_o to reach saturation levels. The sensitivity of RyR2 to inactivating Ca^{2+} has also been reported as heterogeneous, where the levels of Ca^{2+} imparting an inhibitory effect has been shown to vary in single recombinant mouse (Li and Chen, 2001) and rabbit RyR2 channels (Copello et al., 1997).

- ***Luminal Ca^{2+}:***

Recognised as early as 1975 (Fabiato and Fabiato, 1975), luminal Ca^{2+} also modulates RyR2 Ca^{2+} release (Sitsapesan and Williams, 1994, Györke and Györke, 1998). More than one model has been proposed for this, though it is likely that there is interplay between each of them:

(1) Luminal Ca^{2+}feed through:

Luminal Ca^{2+} passes though the channel pore and modulates activity by binding to regulatory sites (A-, I_1- and I_2-site – Figure 1.4) on the cytoplasmic domain of RyR2 (Xu et al., 2004, Laver, 2007). Single channel recordings identified that activation of RyR2 by luminal Ca^{2+} was governed by the Ca^{2+} flux in the luminal-to-cytoplasmic direction (Tripathy and Meissner, 1996, Xu and Meissner, 1998). Ruling out the possibility of Ca^{2+}-sensing sites present on the luminal domain, Xu and Meissner (1998) reported that in the

absence of cytoplasmic Ca^{2+} (<0.1 μM) i.e. when the channel is closed, elevating the luminal Ca^{2+} up to as high as 10 mM did not activate channel activity.

(2) Direct luminal Ca^{2+} activation:

Termed the "true luminal" model by Laver in 2007, evidence also suggests that the effects of luminal Ca^{2+} could involve distinct Ca^{2+} binding site(s) present on the luminal face of the RyR2 channel (Györke and Györke, 1998). In the Laver model, this site is denoted the L-site (Figure 1.4). Györke and Györke demonstrated that under conditions which favoured a net Ca^{2+} flux in the cytoplasmic-to-luminal direction, raising the luminal Ca^{2+} concentration from 20 μM to 10 mM produced a 10-fold increase in the channel P_o, and was attributed to unique luminal Ca^{2+} sensing sites present on the RyR2 channel itself or via an associated protein, such as calsequestrin (Györke and Györke, 1998). Ching and co-workers reported similar findings, and revealed that tryptic digestion of the luminal side of the RyR channel altered channel activity such that an increase in luminal Ca^{2+} (from 10 μM to 1 mM) no longer enhanced RyR2 P_o, but instead reduced channel activity. This observation led to suggestions that activation sites present on the luminal side of RyR2 channels was destroyed with protease digestion, but inactivating sites may also exist on the luminal side that remained intact after digestion (not shown on the Laver model), (Ching et al., 2000).

(3) Luminal-triggered Ca^2 feed-through mechanism:

RyR2 gating is influenced by Ca^{2+} sensing mechanisms on both the luminal and cytoplasmic sides of the channel, which has led to the development of a unified theory of activation termed the "luminal-triggered Ca^{2+} feed-through" hypothesis. This model integrates all of the predicted activation (A- and L-sites) and inactivation sites (I_1- and I_2-sites) that can be functionally linked by Ca^{2+} feed-through (Laver, 2007). During diastole, when Ca^{2+} is loaded back into the SR, channel activation may occur via the luminal, L-site, producing brief RyR2 openings that allow luminal Ca^{2+} to pass through the channel pore and initiate further activation at the cytosolic A-site (Laver et al., 2007). Compounds that enhance RyR2 activity at the A-site (such as ATP, see section 1.4.3) may therefore enhance luminal Ca^{2+}-dependent activation and render the channels more sensitive to Ca^{2+} loading within the SR (Györke and Györke, 1998, Tencerová et al., 2012). This observation is important, since under pathological conditions enhanced activation of mutant RyR2 by luminal Ca^{2+} has been proposed as a contributing factor of channel dysfunction (Jiang et al., 2005). During systole, the L-site does not appear to influence channel activity, since under conditions of high cytosolic Ca^{2+}, raising the luminal Ca^{2+} concentration did not appear to impart any further increase in the duration of channel

openings (Laver and Honen, 2008). Aside from the interplay between cytoplasmic and luminal Ca^{2+} microdomains, which are clearly critical determinants of RyR2 activity, other intracellular ligands such as Mg^{2+} and ATP are also thought to play important regulatory roles (Zahradníková et al., 2003).

1.4.2. RyR2 regulation by Mg^{2+}:

Mg^{2+} is a physiological inhibitor of RyR2 and plays a role in shaping the cytoplasmic and luminal Ca^{2+} dependencies of channel activity within the cell (Laver and Honen, 2008). Mg^{2+} levels within the millimolar range can inflict an inhibitory effect on channel behaviour (reducing channel P_o), which has been suggested to occur at the I_1- cytoplasmic site (Figure 1.4), (Györke and Györke, 1998, Zahradníková et al., 2003). In cardiac muscle at rest, the free Mg^{2+} concentration has been predicted to lie within the 0.5-1.2 mM range, and is thought to remain relatively constant throughout the cardiac cycle (Zahradníková et al., 2003). It is therefore likely that the free Ca^{2+} concentration within the cell acts as the critical determinant of the degree of channel inhibition seen with Mg^{2+}. It has also been proposed that when cytosolic [Ca^{2+}] is at resting levels (during diastole) and the SR store is depleted of Ca^{2+}, Mg^{2+} may also occupy the A- and L- activation sites and render RyR2 inactive (Laver et al., 2010). Once the SERCA2a Ca^{2+}-ATPase pump sequesters Ca^{2+} back into the SR store and luminal [Ca^{2+}] is increased, Laver et al (2010) proposed that Ca^{2+} displaces Mg^{2+} at the L-site, relieving inhibition and allowing further RyR2 channel activation at the cytoplasmic A-site (Laver et al., 2010).

1.4.3. RyR2 regulation by Adenine Nucleotides (ATP):

Single channel recordings have revealed that the presence of millimolar concentrations of ATP enhances the Ca^{2+} induced activation of RyR2 (Györke and Györke, 1998, Kermode et al., 1998). Since this channel effector is unable to activate RyR2 alone, but enhances both channel openings and open duration in the presence of both cytosolic and luminal Ca^{2+} (Tencerová et al., 2012), it has been suggested that the primary role of ATP is to stabilise the open state of RyR2. Other adenosine nucleotides such as adenosine diphosphate (ADP) and adenosine monophosphate (AMP), which are by-products of ATP hydrolysis, can also potentiate RyR2 Ca^{2+} release, but appear less effective (Sitsapesan and Williams, 1998). The cytoplasm of resting cardiac muscle contains approximately 3-5 mM total ATP, which like Mg^{2+} is thought to remain consistent throughout EC coupling (Zahradníková et al., 2003). Since most ATP in cells exists as a complex with Mg^{2+}, under normal physiological conditions, it is likely that a complex of MgATP (rather that free ATP alone) is responsible for regulating RyR2 Ca^{2+} release (Lanner et al., 2010).

1.5. RyR2 macromolecular signalling complex:

Existing as a huge macromolecular complex, a multitude of regulatory proteins interact directly or indirectly with RyR2 channels to modulate their activity (Wehrens, 2005). Whilst most regulatory proteins interact with the cytoplasmic side of the Ca^{2+} release channel, others traverse the SR membrane or function as luminal accessory proteins. In this chapter, the best characterised of the RyR2 accessory proteins will be discussed.

1.5.1. Regulation of RyR2 by FKBP-binding proteins:

Classed as immunophillins, FKBPs are a family of binding proteins for the immunosuppressant drugs FK506 and rapamycin, and display peptidylpropyl-cis-trans-isomerase (PPIase) activity thought to be important for their roles in protein folding and trafficking (Marks, 1996, Kang et al., 2008). This enzymatic activity however, is not thought to contribute to their role in modulating RyR2 function (Marks, 1996).

Two isoforms of FKBP are known to interact with RyR2: FKBP12.6 and FKBP12 (Chelu et al., 2004, Zissimopoulous et al., 2012). However, since RyR2 exhibits a higher binding affinity for FKBP12.6, this is considered the cardiac-specific isoform, associating with a stoichiometry of one FKBP12.6 molecule per RyR2 subunit (Timerman et al.,1993). FKBP12.6 and FKBP12 share ~85% homology, both consist of 108 amino acids and as determined by X-ray crystallography, their structures are nearly identical both alone and as a drug complex with rapamycin (Deivanayagam et al., 2000). It is thus unsurprising that both are predicted to physically interact with RyR2 channels to regulate their activity (Galfré et al., 2012, Zissimopoulous et al., 2012).

It has been hypothesised that the binding of FKBP isoforms to RyR2 channels inhibit Ca^{2+} release activity and act to stabilise the channels closed state (Marx et al., 1998, 2001, Ondrias et al., 1998). During ß-adrenergic stimulation it has been suggested that FKBP12.6 is partially dissociated from RyR2 channels upon PKA phosphorylation, which subsequently enhances intracellular Ca^{2+} release and improves contractility (Wehrens et al., 2003). However, in disease states (discussed in section 1.8.1), defective interaction between the two proteins following phosphorylation is consequently proposed as a mechanism underlying RyR2 dysfunction. This hypothesis however has been extensively challenged, since not all groups have observed the same effects of the RyR2/FKBP12.6 binding interaction as a channel 'stabiliser' (Xiao et al., 2007). Marx et al (2000) demonstrated at the single channel level that FKBP12.6-deficient RyR2 channels exhibited pronounced subconductance states and enhanced activity recognised by high

channel P_o. Consistent with this study, mice with gene-targeted knockout of FKBP12.6 displayed an enhanced predisposition to heart failure (HF) and sudden cardiac death (SCD), tested using a pre-designed exercise program (Wehrens et al., 2003). However, Xiao et al (2007) reported following single channel, Ca^{2+} imaging and [^{3}H] ryanodine binding investigations that the addition or removal of FKBP12.6 had no observable effects on RyR2 channel activity.

Providing a possible explanation for these discrepancies, Galfré et al demonstrated in a more recent single channel investigation that FKBP12, which is largely overlooked in cardiac cells in terms of function, activated RyR2 channels at very low concentrations, whilst FKBP12.6 did not. The FKBP12.6 isoform did however antagonise the effects imparted by FKBP12 (lowering channel P_o), which led to the idea that dual regulation between both isoforms may be important for channel function; and that an alteration in the ratio of FKBP12/FKBP12.6 ultimately contributes to the defective Ca^{2+} handling seen in HF (Galfré et al., 2012).

1.5.2. Kinase and Phosphatase regulation of RyR2:

Recent studies have revealed that kinases and phosphatases are targeted directly to the cytoplasmic domain of RyR isoforms and modulate channel function in response to extracellular signals (Marx et al., 2001, Reiken et al., 2003). RyR2 channels have highly conserved leucine/isoleucine zipper motifs that associate with adaptor proteins (such as, spinophillin and muscle-specific anchoring protein (mAKAP)) that in turn bind serine/threonine kinases such as: protein kinase A (PKA) and Ca^{2+} Calmodulin Kinase II (CaMKII), and phosphatases: protein phosphatase 1 (PP1) and 2A (PP2A), that control phosphorylation/dephosphorylation in a spatially and temporally regulated manner (Marx et al., 2000, Hulme et al., 2004, Blayney et al., 2009).

PKA is a heterodimeric protein kinase activated during the “fight and flight” response to enable rapid increases in the heart rate and cardiac contractility in times of stress (Wehrens et al., 2006). A secondary messenger, cAMP, the concentrations of which are elevated by adrenergic stimulation of the cardiac ß-adrenoreceptors, activates PKA (section 1.2.5). An increase in heart rate raises intracellular Ca^{2+} levels, which in turn activates CaMKII. The importance of these interactions in regulating RyR2 activity however is still debated. Phosphorylation of RyR2 is predicted to occur at three distinct sites: serine-2808 (PKA and CaMKII), serine-2815 (CaMKII) and serine-2030 (PKA) (Xiao et al., 2006, Huke et al., 2008). PKA phosphorylation at Ser-2030 has been suggested as

the major site that responds to ß-adrenergic stimulation (Xiao et al., 2006). However, other groups have reported more recently that phosphorylation of RyR2 at Ser-2030 has no functional effect on channel activity (Marx and Marks et al., 2013). Other phosphorylation sites have also been detected with mass spectrometry, the significance of which has yet to be investigated (Yuchi et al., 2012).

Since kinases directly influence other major Ca^{2+} handling proteins aside from RyR2 and indirectly modify accessory proteins (section 1.2.5), understanding how Ca^{2+} release is regulated by phosphorylation within the cell is difficult to determine (Mackrill, 1999). It has therefore proved useful to study the effects of RyR2 phosphorylation using *in vitro* investigations. At the single channel level, phosphorylation with exogenous PKA and CaMKII has been reported to increase channel P_o, enhance sensitivity to luminal (Xiao et al., 2007) and cytosolic Ca^{2+} (Marx et al., 2000) and reduce cytoplasmic Mg^{2+} inhibition (Uehara et al., 2002). However, an inhibitory component of phosphorylation has also been suggested, since some research groups have demonstrated a reduction in RyR2 channel activity with kinase association (Hain et al., 1994) and enhanced channel P_o following RyR2 dephosphorylation (Carter et al., 2011). These differences however could be owed to different functional effects of different PKA-phosphorylation sites (Xiao et al., 2006). Carter et al proposed that at rest, RyR2 is phosphorylated up to 75% of full stoichiometry at S2808 and suggested the stimulatory effects of PKA only occur when channels are phosphorylated above this level (Carter et al., 2006). Consistent with this proposal, under basal conditions Li et al (2013) reported that S2808 and S2814 (in rats) displayed phosphorylation levels of 69% and 15%, respectively. However, these levels increased substantially to 83% (S2808) and 60% (S2814) following ß-adrenergic stimulation (Li et al., 2013). Phosphorylation of S2030 however was not included in this investigation since phosphorylation at this site could not be detected (Li et al., 2013).

With regards to the role of phosphatases, PP1 and PP2A are thought to be responsible for both RyR2 (Terentyev et al., 2003a) and PLB dephosphorylation (MacDougall et al., 1991). Terentyev et al reported that PP1 enhances RyR2 activity, whilst others report that channel activity is decreased upon phosphatase association (Terentyev et al., 2003a, Li et al., 2013). Although such discrepancies need to be investigated further, it is clear that the phosphorylation status of RyR2 has notable effects on Ca^{2+} release activity.

1.5.3. Regulation of RyR2 by Calmodulin and Sorcin:

Sharing common structural and functional features, calmodulin (CaM) and sorcin are EF-hand-containing Ca^{2+} binding proteins, proposed to inhibit Ca^{2+} release activity (Balshaw et al., 2001, Farrell et al., 2003).

CaM is a 17 kDa, ubiquitously expressed cytosolic protein that associates directly with RyR2 channels, as well as other several other proteins and ion channels (Meissner, 2004, Lanner et al., 2010). In terms of structure, CaM consists of four EF-hand Ca^{2+} binding domains (two in the carboxy-terminal and two in the amino-terminal of the protein) and binds to one site (1:1 ratio) on each RyR2 monomer (Fruen et al., 2000). Interestingly, modulation of RyR2 activity by CaM, over a wide range of Ca^{2+} concentrations, differs from that of other RyR isoforms, suggesting the protein plays a unique role in EC coupling regulation (Tripathy et al., 1995, Hamilton et al., 2000). At the single channel level, application of CaM can either activate (at low luminal Ca^{2+} concentrations) or inhibit (at high luminal Ca^{2+}) RyR1 and RyR3 channels, thus having a biphasic response, whilst the protein appears to only inhibit RyR2 channel function (Tripathy et al., 1995, Hamilton et al., 2000). Highlighted by Xu and Meissner, evidence suggests that CaM plays an important role in the termination of SR Ca^{2+} release (Xu and Meissner, 2004). CaM application significantly reduced the frequency of RyR2 channel openings, lowering P_o, and increasing the mean closed times (Xu and Meissner, 2004). CaM is predicted to regulate RyR2 gating both in its Ca^{2+} free (apoCaM) and Ca^{2+}-loaded state, and has been suggested to fine-tune the channels sensitivity to intracellular [Ca^{2+}] (Tripathy et al*.,* 1995, Van Petegem, 2012).

First discovered in multidrug-resistant cells, sorcin is a 22 kDa Ca^{2+} binding protein identified in cardiomyocytes as directly interacting with RyR2 channels (Meyers et al., 1998, Bers, 2004). The protein binds Ca^{2+} with high affinity, with half-maximal binding reported to occur at ~1 μM (Zamparelli et al., 2000) Although its precise role remains to be established, sorcin is thought to act in a similar way to CaM, causing RyR2 inhibition, as demonstrated with [^{3}H]-ryanodine binding and single channel investigations (Lokuta et al., 1997, Farrell et al., 2003). Farrell et al (2003) demonstrated that sorcin reduces the P_o of single RyR2 channels, and that inhibition was relieved by PKA-mediated phosphorylation - suggesting an indirect role for this protein kinase. Other EF-hand containing proteins have also been predicted to regulate RyR2 activity but have not been well studied. S100A1 for example has been reported to enhance the opening of RyR2 channels (Prosser et al., 2011).

1.5.4. Regulation of RyR2 by Junctate, Junctophillin and the histidine-rich Ca^{2+} binding protein:

Junctate is a functionally distinct, 33 kDa splice variant of the aspartyl ß-hydroxylase (ASPH) gene (Hong et al., 2007, Scriven et al., 2013, Treves et al., 2000). Another splice variant of *ASPH*, junctin, will be discussed in section 1.6.3. Thought to regulate intracellular Ca^{2+} concentration, junctate is an SR located Ca^{2+} binding protein, composed of a single membrane-spanning transmembrane domain, a short N-terminal (cytoplasmic) region and a long, highly acidic C-terminal segment that protrudes into the lumen of the SR (Hong et al., 2007). Hong et al (2008) used a transgenic mouse model of junctate overexpression to assess its effect in cardiac cells, where impairment in SR function was reported. This was likely due to a notable downregulation in two major Ca^{2+} handling proteins, SERCA2a and CSQ2 (section 1.6.1), (Hong et al., 2008). Prolonged junctate overexpression led to a compensatory enhancement in sarcolemmal protein expression, cardiac hypertrophy and consequently a greater susceptibility to cardiac arrhythmias (Hong et al., 2008). Although this evidence implies that junctate plays a regulatory role in maintaining Ca^{2+} homeostasis, whether it directly modifies RyR2 activity remains to be elucidated.

Junctophillin-2 (JP2), a component of plasma membrane/SR complexes, has a molecular weight of approximately 100 kDa and recognised as the primary isoform expressed in the heart (Takeshima et al., 2000). Spanning the SR membrane, the cytoplasmic region of the protein is reported to interact with the cell membrane/T-tubule network and anchors it close to the SR, forming T-tubule-SR junctions (Nishi et al., 2000, Takeshima et al., 2000). Since in heart failure, JP2 is significantly downregulated, the protein is hypothesised to be critical to the normal operation of CICR between L-type Ca^{2+} channels and RyR2 (Wu et al., 2012). Aside from its role as a structural protein, recent studies have revealed a direct interaction between JP2 and RyR2 (using immunoprecipitation, Beavers et al., 2013) and its ability to regulate intracellular Ca^{2+} release (Wang et al., 2014).

Wang et al (2014) suggested that JP2, under normal circumstances, negatively regulates RyR2 gating, since cardiac-specific knockdown of the modulatory protein triggered severe RyR2-mediated SR Ca^{2+} leak. In JP2 knockdown mice, two notable molecular mechanisms were proposed to explain the arrhythmogenic Ca^{2+} leak through RyR2 channels (Wang et al., 2014). Firstly, at the single channel level, the group demonstrated that severely low JP2 expression significantly enhanced the P_o and mean open time of RyR2; whilst the mean closed time was reduced. An earlier single channel study carried out by Beavers et al (2013) was consistent with this finding, where a decrease in RyR2 P_o

was evident when a small synthetic peptide derived from the JP2 primary sequence was added back to the reconstituted channel. Furthermore, Ca^{2+} sparks in JP2-knockdown cardiac myocytes showed increased width, duration and frequency, thought to result from the enhanced opening of RyR2 clusters (Cheng et al., 1993, Wang et al., 2014). JP2-deficient cardiomyocytes displayed a ~50% reduction in NCX activity, with no observable differences in protein expression, which may also have altered the Ca^{2+} spark profile (Wang et al., 2014).

Proposed to play a prominent role in maintaining Ca^{2+} homeostasis, the histidine-rich Ca^{2+} binding protein (HRC) is 170 kDa and resides within the SR lumen of cardiac cells (Arvanitis et al., 2011). Although it is not thought to interact directly with RyR2 channels, HRC associates with both the SERCA2a pump (section 1.2.3) and the transmembrane protein triadin (discussed in section 1.6.3), and has thus been implicated both in Ca^{2+} uptake (Gregory et al., 2006) and release (Lee et al., 2001). In mouse hearts with HRC overexpression, the rate of Ca^{2+} re-uptake into the SR was drastically reduced, without any notable effects on the SR Ca^{2+} load. This therefore led to the hypothesis that HRC directly suppresses SERCA2a function (Gregory et al., 2006). Binding of HRC to triadin is Ca^{2+}-dependent and the interaction between the two proteins has been implicated in sensing changes in SR Ca^{2+} concentration (Arvanitis et al., 2011). This however requires further investigation. A recent study by Singh et al (2013) described a genetic variant of the HRC protein (Ser96Ala), which generated defective Ca^{2+} cycling and cardiac arrhythmias. The underlying mechanism of this dysfunction was attributed to a reduction in the stability of RyR2 channels, imparted by disrupted protein-protein associations of HRC with triadin (Singh et al., 2013).

1.6. Calsequestrin, Junctin and Triadin:

Existing as a quaternary complex with RyR2 channels at the jSR membrane, calsequestrin (CSQ2), junctin (JUN) and triadin (TRD1) are thought to directly regulate the sensitivity of RyR2 channels to luminal Ca^{2+}, with CSQ2 in particular hypothesised to act as RyR2s luminal Ca^{2+} sensor (Györke et al., 2004). A key question regarding the role of these luminal proteins is whether they can function as direct modifiers of RyR2 channels independently, or if to regulate channel function they must assemble as a complex. The specific properties of CSQ2, JUN and TRD1, and their importance in regulating RyR2 channel activity, will be discussed next in sections 1.6.1-1.6.4 (Tables 1.1-1.3).

1.6.1. Properties of cardiac calsequestrin:

First identified in the early 1970s, CSQ2 is the most abundant Ca^{2+} binding protein present within the SR lumen of cardiac myocytes, binding Ca^{2+} with high capacity (60-80 moles of Ca^{2+} per CSQ molecule) and relatively low affinity (K_d = 1 mM) (MacLennan and Wong, 1971, Mitchell et al., 1988). Isoform 2 (CSQ2) is the major variant expressed in cardiac muscle and is also found in lower quantities in skeletal slow-twitch muscle fibres (Bers et al., 2004). Despite dog cardiac CSQ2 being the most extensively studied, sequence alignment has estimated approximately 86% homology between dog and human CSQ2 (Beard et al., 2004).

Contributing to its ability to bind large amounts of Ca^{2+}, CSQ2 is a highly acidic protein (Lee et al, 2012). Human CSQ2 is composed of 391 amino acids with an additional 19-residue signal peptide at the N-terminus (Lahat et al., 2001, Lee et al., 2012), the C-terminal region of CSQ2 is thought to contain ~60% acidic (in particular aspartate) residues (Shin et al., 2000) and provides the sites of interaction for other accessory proteins (Shin et al., 2000, Kobayashi et al., 2000). CSQ2 is not embedded in the SR membrane, but instead is localised to the junctional face within close proximity to RyR2 channels by integral SR membrane proteins JUN and TRD1. The two proposed 'anchoring proteins' facilitate communication between CSQ2 and RyR2, positioning Ca^{2+} ions accumulated by CSQ2 close to the Ca^{2+} release sites (Györke et al., 2004, Shin et al., 2000, Rossi and Sorrentino, 2002, Franzini-Armstrong et al., 1987, Bers, 2000). Preventing premature Ca^{2+} release, CSQ2 stores large amounts of releasable Ca^{2+} within the SR lumen, whilst at the same time, maintaining a low level of free Ca^{2+} that triggers Ca^{2+} re-uptake following muscle contraction (Beard et al., 2004, Novák and Soukup, 2011). The association of CSQ2 with JUN and/or TRD1 has been suggested to strongly affect its disposition (Franzini-Armstrong et al., 2005). In electron micrographs, the protein has been reported to exist alone as linear polymers folded randomly within the SR lumen, yet when positioned closer to the jSR membrane, the protein appears condensed (described as "dense spots"), owing to its association with the two accessory proteins (Franzini-Armstrong et al., 2005).

CSQ2 is thought to exist as a mixture of monomers, dimers and polymers, where polymerisation and depolymerisation occurs in a [Ca^{2+}]-dependent manner (Beard et al., 2009, Kim et al., 2007, Lee et al., 2012). Studied using rabbit skeletal CSQ, in the absence of Ca^{2+}, the protein is predicted to exist as a random coil monomer with lowered alpha-helical content (~11%), which is increased to >20% upon Ca^{2+} binding and folding of CSQ2 monomers into thioredoxin-like domains (Cozens and Reithmeier, 1984, Beard et

al., 2009). Investigating the Ca^{2+}-dependent conformational changes of the protein, the thioredoxin-like folds are required for protein compaction and subsequent Ca^{2+} binding at intracellular [Ca^{2+}] >10 μM (He et al., 1993, Wang et al., 1998, Beard et al., 2009). Further increases in luminal Ca^{2+} induce conformational changes in CSQ2 monomers, causing them to self-associate and assemble into dynamic linear polymers that allow high capacity Ca^{2+} binding (Beard et al., 2004, Kim et al., 2007). CSQ2 polymers are thought to consist of two types of dimer termed “back-to-back” (C-terminal) and “front-to-front” (N-terminal) interactions, both of which are predicted to form Ca^{2+} binding pockets essential for storage (Park et al, 2003). The conformational state of CSQ2 at luminal [Ca^{2+}] >1mM however has been debated in the literature, with both CSQ2 polymers (Wang et al., 1998, Kim et al., 2007) and monomers (Wei et al., 2009b, Murphy et al., 2011) predicted as responsible for the proteins regulatory function.

1.6.2. Physiological role of CSQ2 and functional interaction with RyR2:

For a number of years, the sole purpose of CSQ2 was believed to be the maintenance of Ca^{2+} homeostasis within the SR by acting as a major Ca^{2+} storage protein. However, in recent years, substantial evidence has suggested that CSQ2 also plays a direct role in regulating RyR2 activity, coordinating time-dependent Ca^{2+} release with recovery (Györke et al., 2004, Beard et al., 2004, Terentyev et al., 2005). Since the role of CSQ2 in regulating RyR2 activity (and the relative contribution of JUN and TRD1 to this regulation) will be discussed further in other chapters, some of the experimental systems used to study CSQ2 function and their reported findings, will be summarised in Table 1.1.

CSQ2 Investigations			
Study Type/species:	**Ca^{2+} handling observations:**	**Phenotypic Alterations:**	**Further Details:**
CSQ overexpression (10-fold) in transgenic mice (**Jones *et al.*, 1998**).	Whole-cell clamped isolated cardiomyocytes displayed a reduced frequency in both spontaneous and Ca^{2+}-triggered Ca^{2+} sparks. Reflecting increased CSQ2-stored Ca^{2+}, caffeine-induced Ca^{2+} release amplitude was enhanced (10-fold).	Severe cardiac hypertrophy, ~1.9 fold increase in heart mass and cell size, exercise intolerance.	RyR2, JUN and TRD downregulated (~50%). SERCA and PLB expression unchanged.
Cardiac –specific overexpression of CSQ2 (20-fold) in transgenic mice (**Sato *et al.*, 1998**).	Reduced Ca^{2+}-induced SR Ca^{2+} release amplitude	Depressed contractility, cardiac hypertrophy	No alterations in RyR2, JUN or TRD expression. Increased protein levels of SERCA and PLB.
Adenoviral-mediated increase or decrease in CSQ2 levels in rat ventricular myocytes (**Terentyev *et al.*, 2003b**).	In permeabilised myocytes, CSQ2 overexpression slowed termination of Ca^{2+} release from the SR and slowed Ca^{2+} spark recovery time.	Premature activation evident in myocytes with lower CSQ2 expression. Upon electrical stimulation, arrhythmogenic Ca^{2+} transients observed (in myocytes with low levels of CSQ2).	Suggests CSQ2 controls Ca^{2+} release by prolonging the Ca^{2+} flux duration. CSQ2 may be involved in the termination of RyR2 Ca^{2+} release.
Gene-targeted ablation of CSQ2 in mice (**Knollmann *et al.*, 2006**).	Under basal conditions normal SR Ca^{2+} release. However, CSQ2-null myocytes displayed increased diastolic Ca^{2+} leak upon catecholamine stimulation. Spontaneous Ca^{2+} oscillations evident and an increased propensity for arrhythmia.	Increased SR volume (size). Functional SR Ca^{2+} storage unaltered.	JUN and TRD1 levels undetectable. No alterations in other Ca^{2+} handling proteins.
Single channel investigation utilising purified canine CSQ2 (**Györke *et al.*, 2004**)	In the presence of JUN and TRD1, CSQ2 added back to purified RyR2 channels inhibited activity (reduced channel openings).	N/A	First proposal that CSQ2 (together with anchoring proteins JUN and/or TRD1) may act as a luminal Ca^{2+} sensor for RyR2 channel activity.

Table 1.1: Functional assays investigating the role of CSQ2 in cardiac muscle

1.6.3. Properties of cardiac junctin and triadin:

Human cardiac muscle JUN is a 26 kDa, 210-amino acid protein that spans the SR membrane and exists as a functionally distinct, non-catalytic splice variant of the aspartate-β-hydroxylase gene (together with junctate, section 1.5.4), (Lim et al., 2000, Wei et al., 2009a). Expressed as a single isoform in cardiac and skeletal muscle (Dulhunty et al., 2009), the protein contains a cytoplasmic N-terminal domain (residues 1-22), a single transmembrane segment (residues 23-44), and a longer, SR intraluminal C-terminal region (residues 45-210) that contains several charged sequence repeats (>13 amino acids) of lysine or glutamic acid residues (predicted from the dog cardiac JUN isoform, Jones et al., 1995). Known as "KEKE" motifs, these repeats are thought to be important for the binding interaction of JUN with the other luminal accessory proteins and RyR2 (Jones et al., 1995, Shin et al., 2000, Fan et al., 2008). The current accepted model of RyR2 regulation by SR luminal proteins suggests JUN has the ability to bind directly to the luminal and/or transmembrane regions of RyR2 and acts as an anchoring protein (together with TRD1) to position CSQ2 near the channel (Zhang et al., 1997, Györke et al., 2004). Although the exact physiological role of JUN in regulating the response of RyR2 channels to luminal Ca^{2+} is a topic of current research, its function in maintaining normal Ca^{2+} release from the SR lumen has been highlighted in studies of HF, where the protein is almost undetectable (Gergs et al., 2007).

JUN may serve as a direct regulator of channel activity or transduce signals from CSQ2 to RyR2 in a Ca^{2+}-dependent manner, or both (Beard et al., 2009). In terms of interaction, Kobayashi and co-workers demonstrated that JUN does not have a single discrete binding domain for CSQ2, since deletions in several "KEKE" motifs along the C-terminal tail all reduced CSQ2 binding (Kobayashi et al., 2000). However, binding of JUN to RyR2 channels has been predicted to occur at two distinct domains (Altschafl et al., 2011). Using blot overlay assays, recombinant JUN and RyR2 polypeptides designed to different proposed intraluminal binding regions, Altschafl et al (2011) demonstrated that the N-proximal intraluminal domain of JUN interacted with intraluminal loop I of RyR2, whilst the KEKE-motif of JUN interacted with RyR2 at intraluminal loop II; with the latter being comparable to the single binding site for TRD1 at intraluminal loop II of the RyR1 protein (Goonasekera et al., 2007, Altschafl et al., 2011). The binding of JUN to different sites on the RyR2 channel could reflect the ability of the protein to regulate Ca^{2+} release activity by more than one mechanism (Altschafl et al., 2011).

Several isoforms of triadin exist in striated muscle, all of which are splice variants of a single *TRDN* gene (Guo et al., 1996). Whilst sharing a common amino terminus (264

residues), each isoform is predicted to differ in their C-terminal regions, which in smaller proteins is truncated (Kobayashi and Jones, 1999, Dulhunty et al., 2012). Three cardiac-specific isoforms have been identified (which are 32, 40 and 75 kDa), with TRD1 (~32 kDa) being the most abundant, comprising of more than 95% of total TRD found in cardiac muscle (Kobayashi and Jones, 1999, Györke and Terentyev, 2007). Like JUN, TRD1 is an integral SR membrane protein and is composed of a short cytoplasmic N-terminal tail, a hydrophobic segment that spans the SR membrane and a longer, highly charged C-terminal region located within the SR lumen which comprises the bulk of the protein (Györke and Terentyev, 2007, Beard et al., 2009). Interaction sites within TRD1 for its molecular partners, i.e. RyR2, CSQ2 and JUN are predicted to reside within the proteins C-terminus (Kobayashi et al., 2000). This region of the TRD1 sequence is characterised by the frequent occurrence of long stretches of alternating positively and negatively charged residues known as KEKE motifs, as previously identified in JUN. Interestingly, the CSQ2-binding domain of TRD1 has been localised to a single KEKE motif (amino acids 210-224) of approximately 15 residues (Kobayashi et al., 2000). The binding regions on RyR2 for cardiac TRD1 remain undetermined (Dulhunty et al., 2012). TRD1 and JUN binding to CSQ2 was found to be Ca^{2+}-dependent such that the proteins dissociate at high Ca^{2+} (10 mM), whilst TRD binding to RyR2 is thought to occur regardless of changes in Ca^{2+} concentration (Zhang et al., 1997, Kobayashi et al., 2000, Qin et al., 2008).

1.6.4. Physiological roles of JUN and TRD1 and their functional interaction with RyR2:

Although the functional role of JUN is still largely undetermined, its experimental manipulation, primarily in animal models, has yielded some interesting observations. Table 1.2 summarises some of the functional studies undertaken to establish the physiological importance of JUN in maintaining normal cardiac function. Further investigations where the ability of JUN to modulate RyR2 channel activity has been explored will be discussed in other chapters of this project.

Given the close structural homology of TRD1 and JUN and the fact that they both communicate with RyR2 and CSQ2, it was first anticipated that the two related proteins share a similar function of simply anchoring CSQ2 within close proximity to RyR2. In this scaffolding capacity, TRD1 is thought to facilitate SR Ca^{2+} release indirectly, permitting CSQ2 to buffer luminal Ca^{2+} in the vicinity of the Ca^{2+} release sites (Zhang et al., 1997, Kobayashi et al., 2000). Aside from its role as an anchoring protein, unique roles of cardiac TRD1 have been reported in recent years, suggesting that TRD1 and JUN may serve different functions to regulate EC coupling. Table 1.3 summarises some of the functional assays carried out to specifically investigate the role of TRD1 in cardiac muscle.

JUN Investigations			
Study Type/species:	**Ca^{2+} handling observations:**	**Phenotypic Alterations:**	**Further Details:**
24-29-fold overexpression of canine JUN in transgenic mice (**Hong *et al.*, 2002**).	N/A	Atrial fibrillation, fibrosis and bradycardia	RyR2 and TRD1 downregulated. L-type Ca^{2+} channel upregulated.
Adenoviral-mediated overexpression of JUN in rat cardiomyocytes (**Gergs *et al.*, 2007**).	Decreased SR Ca^{2+} transient amplitude	Cell shortening (observed by the cell-edge detection system), reduced contractility.	Impaired Ca^{2+} homeostasis suggested.
Adenoviral-mediated, 40% downregulation in JUN expression (by antisense mRNA) in adult rat cardiomyocytes (**Fan *et al.*, 2007**)	Improved Ca^{2+} kinetics – increased Ca^{2+} transient amplitude, increased rate of Ca^{2+} decay in isolated cardiomyocytes	Increased contractility (increased rate of contraction/relaxation).	No changes in the levels of other Ca^{2+} handling proteins.
Gene-targeted JUN ablation in mice (**Yuan *et al.*, 2007**).	Enhanced NCX current, no difference in the L-type Ca^{2+} current. Increased Ca^{2+} transient amplitude, SR Ca^{2+} content and Ca^{2+} spark frequency (isolated JUN-null cardiomyocytes).	Increased cardiac function reported (assessed by echocardiography). However, stimulation-evoked ventricular tachycardia triggered by DADs.	25% of mice died prematurely (~3 months of age) with no structural abnormalities. No significant alterations in CSQ2, TRD1, SERCA2a, PLB,HRC, FKBP12.6, L-type Ca^{2+} channel, protein expression. However 70% reduction in the expression of NCX.
Investigation of intracellular Ca^{2+} homeostasis in JUN-deficient cardiomyocytes (**Altschalf *et al.*, 2011**).	Increased Ca^{2+} transient amplitude and increased SR Ca^{2+} content in JUN-null cardiomyocytes. Despite SR Ca^{2+} overload, no diastolic Ca^{2+} leak evident. Suggests an altered ability of RyR2 channels to “sense” changes in intra-SR Ca^{2+} load.	ß-adrenergic stimulation diminished RyR2 inhibition and induced spontaneous Ca^{2+} oscillations	JUN affects SR Ca^{2+} release directly, no altered expression of other jSR Ca^{2+}-handling proteins. Dual response of JUN suggested at the single channel level, where at low luminal $[Ca^{2+}]$ (<1mmol) JUN activates RyR2 activity, but inhibits it at high luminal $[Ca^{2+}]$.

Table 1.2: Functional assays investigating the role of JUN in cardiac muscle

TRD1 Investigations			
Study Type/species:	**Ca^{2+} handling observations:**	**Phenotypic Alterations:**	**Further Details:**
Single Channel Analysis, canine cardiac TRD1 (together with JUN) added back to purified RyR2 channels (**Györke *et al.*, 2004**)	Increased channel openings indicating TRD1 and/or JUN may have a stimulatory role on RyR2 activity.	N/A	Effects were reversed by CSQ2 addition (reduced channel openings)
Adenoviral-mediated TRD1 overexpression (3-fold) in rat cardiomyocytes (**Terentyev *et al.*, 2005**).	Ca^{2+} spark frequency increased, amplitude reduced, lowered SR Ca^{2+} content.	Arrhythmogenic Ca^{2+} oscillations upon stimulation.	No change in SERCA2a, PLB, NCX, JUN or RyR2.
Adenoviral-mediated infection of rat ventricular myocytes with a TRD1 peptide corresponding to the CSQ2 binding domain (residues 206-230, rat), (**Terentyev *et al.*, 2007**).	Disruption of the protein-protein interactions between TRD1 and CSQ2 - enhanced responsiveness of depolarised myocytes to L-type Ca^{2+} currents - thus increased SR Ca^{2+} release. Permeabilised myocytes displayed increased frequency of Ca^{2+} sparks and waves.	Rhythmically paced peptide-expressing cardiomyocytes exhibited arrhythmogenic, spontaneous Ca^{2+} oscillations.	The peptide did not directly affect purified single RyR2 channels.
Transgenic mice, gene-targeted ablation of TRD (**Chopra *et al.*, 2009**).	Slower Ca^{2+}-dependent inactivation of L-type Ca^{2+} currents.	Electron microscopy revealed altered Ca^{2+} release unit architecture, ~50% reduction in jSR and T-tubule contacts. Catecholamine challenge induced spontaneous Ca^{2+} release in TRD-null myocytes.	Downregulation of RyR2, CSQ2, JUN, Junctophillin 1 and 2. Expression of L-type Ca^{2+} channel and SERCA2a unchanged. TRD suggested as essential to the structural organisation of the SR.

Table 1.3: Functional assays investigating the role of TRD1 in cardiac muscle

1.7. RyR2 and CSQ2 mutations cause ventricular tachycardia and sudden cardiac death:

Linkage studies and direct sequencing has revealed that inherited mutations mapped to chromosome 1q42-q43 (Swan et al., 1999), of the human cardiac ryanodine receptor gene (*hRyR2*), are predominantly associated with two conditions: Catecholaminergic Polymorphic Ventricular Tachycardia (CPVT) and Arrhythmogenic Right Ventricular Cardiomyopathy/Dysplasia type 2 (ARVC/D2), both of which share the clinical feature of exercise- or stress-induced ventricular tachycardia and SCD (Tiso et al., 2001, George et al., 2003b, Priori et al., 2001, Lahat et al., 2001, Laitinen et al., 2003, Thomas et al., 2006).

CPVT is an arrhythmogenic disorder with a high mortality rate in children and young adults (Leenhart et al., 1995, Priori et al., 2002). The disease was recently estimated at a prevalence of 1:10,000 (Jabbari et al., 2013). Two genetic variants of CPVT have been described: an autosomal-dominant form caused by mutations in RyR2 and a recessive form associated with mutations in CSQ2. Mutations in the *RyR2* gene are much more prevalent than those of *CSQ2*, their autosomal dominant fashion means that the inheritance of a single disease-linked allele is sufficient to result in a CPVT phenotype (Fisher et al., 1999). The majority of CPVT patients display a family history of symptoms associated with the disorder such as VT or SCD, suggesting that it is hereditary (Priori et al., 2001, Postma et al., 2005). Conversely, some patients have been found to be the only symptomatic family member, with neither parent carrying the mutant allele. This suggests that CPVT-linked mutations can also arise in a *de novo* manner (Postma et al., 2005). The phenotypic manifestation of the disorder is also very heterogeneous, even affected members of the same family can display symptom variations (Thomas et al., 2007).

Since the majority of arrhythmias in patients affected by CPVT occur during physical exercise or emotional distress, ß-adrenergic stimulation (section 1.2.5) is thought to be a major trigger of the condition (Priori et al., 2002). Moreover, clinical electrophysiological investigations have revealed that exercise testing or catecholamine infusion can induce arrhythmias in patients with CPVT (Priori et al., 2002). Affected individuals may display adrenergically mediated syncopal events, seizures and arrythmogenic episodes, yet have structurally normal hearts and normal resting ECGs (Scheinman and Lam, 2006, Leenhardt et al., 1995). Arrhythmias take the form of bi-directional and/or polymorphic VT, both of which are capable of degenerating into ventricular fibrillation and SCD, which sadly often constitutes the first manifestation of the disorder (Priori et al., 2002, Sumitomo et al., 2003).

Another syndrome associated with missense mutations in *RyR2* is ARVC/D2, a condition characterised by progressive degeneration of the right ventricular myocardium (Györke et al., 2007). Confusion however still surrounds the link between RyR2 and the disease, since few RyR2 mutations are known to cause right ventricular dysplasia (Györke et al., 2009). However, phenotypic heterogeneity in symptomatic families has suggested an overlap between the two conditions (Thomas et al., 2007). For example, d'Amati et al (2005) reported a male CPVT patient as showing right-ventricle abnormalities characteristic of ARVD2, whilst two female members of the same family exhibited stress-induced polymorphic VT in the absence of any structural alterations of the heart, a characteristic phenotype of CPVT (d'Amati et al., 2005, Thomas et al., 2007).

The current preferred treatment of arrhythmia is administration of ß-adrenergic receptor antagonists (ß-blockers), which target the effects of adrenergic drive activated during stress or exercise. Although often effective in preventing the recurrence of arrhythmia, approximately 30% of patients still experience at least one episode of life-threatening adrenergically mediated arrhythmia, leading to syncope or cardiac arrest (Priori et al., 2002, Liu et al., 2011). In patients who display persistent reoccurrence of tachyarrhythmia, implantation of an automated cardioverter-defibrillator (ICD) has proved successful. However, this treatment is not fully effective, since shocks can cause catecholamine release and subsequently generate further arrhythmia (Thomas and Williams, 2012). Identifying new therapeutic agents for the treatment of RyR2-linked diseases is therefore of primary importance. In patients with RyR2 mutation and using long-term ß-blocker therapy, intravenous administration of verapamil (an L-type Ca^{2+} channel blocker) reduced the frequency of isolated and successive premature ventricular complexes during exercise stress testing by 76% (Swan et al., 2005). However, the drug has limited success since although attenuating VT, its use does not appear to prevent the occurrence of arrhythmias (Sumitomo et al., 2003). Although additional studies into the use of Ca^{2+} channel antagonists combined with other therapeutic agents may prove useful in the treatment of CPVT.

1.7.1. Genetic Basis of CPVT:

There are >150 CPVT-linked RyR2 mutations discovered to date which localise in several discrete regions of the polypeptide (Figure 1.5), within which three clusters of mutational frequency are evident at the N-terminus, central domain and C-terminus of the Ca^{2+} release channel (Postma et al., 2005, Capes et al., 2011). Highlighting the importance of these regions, which appear highly conserved between species and isoform, similar clustering patterns of mutation are seen in human RyR1 channels and are implicated in the pathogenesis of two neuromuscular disorders, malignant hyperthermia (MH) and central core disease (CCD).

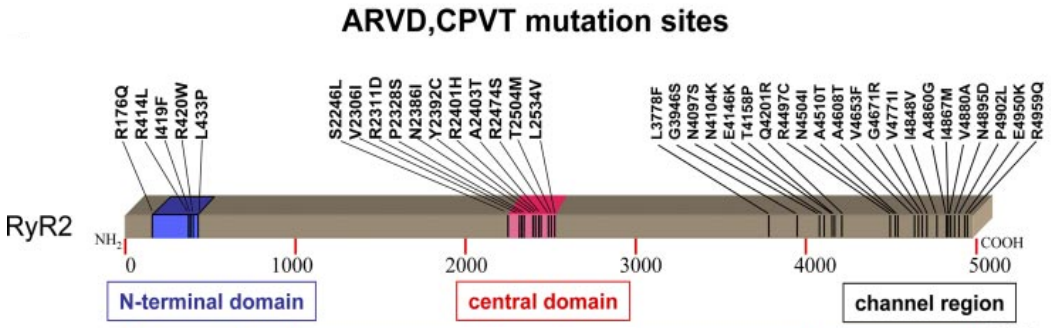

Figure 1.5: Schematic demonstrating RyR2 mutation "hot-spots": *RyR2 mutations tend to cluster within three distinct regions of the protein, the N-terminal domain, central domain and C-terminal region (referred to as the channel region here). The amino acid residues comprising these regions are indicated. The figure highlights only a few of the >150 RyR2 mutations discovered to date. Image modified from Yano et al., 2006.*

Although the molecular mechanisms underlying the pathogenesis of CPVT remain unresolved, it is accepted that most mutant RyR2 channels typically display gain-of-function defects, following ß-adrenergic stimulation (Wehrens et al., 2003, Leenhardt et al., 1995). Specifically, it is thought that enhanced SR Ca^{2+} "leak" through RyR2 channels during diastole increases the propensity for triggered arrhythmias (Wehrens et al., 2007, Novák and Soukup 2011). Triggered activity is thought be initiated by sub-threshold membrane depolarisations, termed afterdepolarisations, which proceed from the previous AP. If such membrane depolarisations occur during the repolarisation phase of the previous AP, they are known as early afterdepolarisations (EADs), whereas delayed afterdepolarisations (DADs) occur after repolarisation and are believed to be the major underlying cause of cardiac VT seen in CPVT (Scoote and Williams, 2002). However, using induced pluripotent stem cells (iPSCs) derived from a patient carrying a P2328S

mutation in RyR2, Kujala et al (2012) recently implicated the contribution of both EADs and DADs in disease pathogenesis. In support of the proposal that DADs occur as a consequence of intracellular Ca^{2+} leak, cell-based assays have demonstrated that overexpression of mutant RyR2 channels generate a diastolic Ca^{2+} leak and spontaneous Ca^{2+} oscillations following catecholamine infusion or caffeine stimulation (which sensitises RyR2 to Ca^{2+}), (George et al., 2003a, Jiang et al., 2004).

1.8. Mechanisms of mutant RyR2 dysfunction:

Given the dispersion of mutations across the RyR2 sequence and their phenotypic variability, it is unlikely that a single universal mechanism is responsible for channel dysfunction. Candidate mechanisms hypothesised to underlie CPVT that dominate in the field are discussed in sections 1.8.1-1.8.3.

1.8.1 Disruption of the RyR2-FKBP12.6 interaction may be involved in the pathogenesis of CPVT:

As aforementioned in section 1.5.1, under normal conditions, ß-adrenergic stimulation and subsequent phosphorylation of RyR2 channels by PKA, has been suggested to partially dissociate FKBP12.6 from the Ca^{2+} release channel (Wehrens et al., 2003).

However in failing hearts, Marx et al demonstrated that the stoichiometry of FKBP12.6 to RyR2 was reduced significantly and implicated a mechanism of PKA “hyperphosphorylation” (enhanced PKA phosphorylation) as a contributing factor of triggered arrhythmias in HF (Marx et al., 2000). In recent years, this proposal has also emerged as a candidate mechanism of CPVT pathogenesis, where mutant RyR2 channels are thought to display a reduced binding affinity for FKBP12.6 under basal conditions, which is further diminished by PKA phosphorylation of RyR2 (Yano et al., 2006, Wehrens et al., 2003, 2007). Since this protein is thought to stabilise the closed conformational state of RyR2, it has been proposed that “hyperphosphorylation” by PKA and subsequent dissociation of FKBP12.6 from the channel complex, contributes to the diastolic SR Ca^{2+} release evident in RyR2 mutants (Wehrens et al., 2007).

The proposed model of FKBP12.6 dissociation outlined by Marx however is not universally accepted. The hypothesis has been challenged by other research groups such as George et al, who found comparable FKBP12.6 association in WT and mutant RyR2 expressed in a murine cardiac cell line (HL-1) both under resting conditions and upon catecholamine

stimulation (George et al., 2003a). Furthermore, FKBP12.6 null-mice were not found to exhibit enhanced susceptibility to triggered arrhythmias in a study by Xiao et al., 2007. Recently, CaMKII-mediated phosphorylation has been implicated in the pathogenesis of CPVT whereby Liu et al demonstrated that CaMKII inhibition attenuated the enhancement Ca^{2+} sparks and diastolic Ca^{2+} leak induced by ß-adrenergic stimulation in the R4496C$^{+/-}$ mouse model of CPVT (Liu et al., 2011). In addition, CaMKII inhibition appears to exert its antiarrhythmic effect by targeting other regulatory proteins of Ca^{2+} homeostasis, since a reduction in SERCA2a function (lowered Ca^{2+} re-uptake into the SR) was also reported (Liu et al., 2011). Finally, CaMKII inhibition reduced the frequency of DADs in an induced pluripotent stem cell (iPSC) derived cardiomyocyte model of CPVT (Di Pasquale et al., 2013) further suggesting the involvement of CaMKII phosphorylation in regulating mutant RyR2 Ca^{2+} leak.

1.8.2. Defective RyR2 intermolecular domain interactions in CPVT:

Inter-domain interactions between discrete regions of the RyR2 cytoplasmic assembly (and notably in mutation “hot-spots”) are thought to participate in the proper folding of the protein complex, acting to stabilise the closed state of RyR2 channels (Liu et al., 2010). Disruption of such interactions is implicated as a potential mechanism of RyR2 dysfunction (Yamamoto & Ikemoto, 2002, George et al, 2004). Ikemoto et al termed this disruption of interactions as “domain unzipping” and it is thought to be caused by RyR2 mutation, thereby weakening the tight ‘zipping’ of the domains that serve to stabilise the channel closed state, enabling the channel to remain open under resting conditions (Yamamoto and Ikemoto, 2002). Using a FRET-based approach to assess the distance between the domains, Liu et al demonstrated that the N-terminal and central domains are involved in inter-subunit interactions (on separate RyR2 subunits) rather than intra-subunit interaction (Liu et al., 2010).

In support of Ikemotos’ model, peptide studies have revealed that interacting regions of RyR2 can be disrupted by mutation to promote channel instability and SR Ca^{2+} leak (Yamamoto and Ikemoto, 2002, Oda et al., 2005, Yang et al., 2006). In two separate studies, a short synthetic peptide homologous to the central domain of RyR2 (DPc10, Gly2460-Pro2495) was used to mimic the effect of a cardiac disease mutation found in CPVT patients (Yang et al., 2006, Oda et al., 2005, Liu et al., 2010). Oda et al reported that the peptide destabilised the interaction between the central and N-terminal domains and acted competitively to reversibly enhance channel activity and Ca^{2+} leak (Oda et al., 2005). Furthermore, rat cardiomyocytes perfused with the DPc10 peptide displayed an enhanced sensitivity to activating Ca^{2+}, increased Ca^{2+} spark frequency and a sustained

increase in resting Ca^{2+} levels, all indicative of an increased propensity towards diastolic Ca^{2+} leak (Yang et al., 2006). The effects of the peptide were found to be abolished following insertion of the CPVT-linked mutation R2474S into the central domain peptide, suggesting that the residue mutated is important for maintaining the interaction between the two domains (Yamamoto & Ikemoto, 2002, Yang et al., 2006). Other peptides located in the N-terminal (DP163-195) and C-terminal (DP4090-4123) regions of RyR2 that mimic CPVT mutations R176Q and N4104K, respectively, have also been found to alter inter-domain interactions and enhance spontaneous Ca^{2+} release from the SR (Tateishi et al., 2008, Liu et al., 2010). George et al reported that this C-terminal region, known as the I-domain, plays an important role in RyR2 autoregulation (George et al., 2006). Mutations in the I-domain (including N4104K) of RyR2 were reported to enhance spontaneous Ca^{2+} release following channel activation, which is likely a consequence of channel destabilisation between the central domain and C-terminus of the protein (George et al., 2006).

1.8.3. CPVT mutations alter the cytoplasmic and/or luminal Ca^{2+} sensitivity of RyR2:

Discussed in greater detail in Chapter 4, section 4.1.3, it has been demonstrated that several CPVT-linked RyR2 mutations alter the channels sensitivity to cytoplasmic and/or luminal Ca^{2+} activation, generating aberrant SR Ca^{2+} release (Jiang et al., 2002, 2004). Since almost all CPVT mutations occur in the cytoplasmic domain of the channel, however, it still remains to be established precisely how these mutations confer hypersensitivity to Ca^{2+} within the SR lumen.

Yang et al demonstrated that mimicking the effects of a central domain mutation by peptide-induced disruption of RyR2, specifically lowered the threshold for cytoplasmic Ca^{2+} activation and generated sustained SR Ca^{2+} leak (Yang et al., 2006). Furthermore, a recent investigation reported that the RyR2 mutation G230C increases sensitivity to both luminal and cytosolic Ca^{2+} activation, as demonstrated at the single channel level (Liu et al., 2013). An alternative hypothesis is that RyR2 mutations principally enhance the channels sensitivity to luminal Ca^{2+} (Jiang et al., 2004). Following observations that many CPVT-linked mutations exhibit a similar cytoplasmic Ca^{2+} dependency to WT RyR2 channels, Chen and colleagues proposed that the major functional consequence of RyR2 mutation is an enhanced sensitivity to luminal Ca^{2+} and subsequently, a lowered threshold for Ca^{2+} release from the SR (Jiang et al., 2004, 2005). This mechanism is termed “Store Overload-Induced Ca^{2+} Release” (SOICR) (Jiang et al., 2004, 2005). Examined in heterologous systems, the functional consequences of a number of RyR2-linked mutations were investigated and found to display increased spontaneous Ca^{2+} release, coupled with

a decrease in the levels of the ER Ca^{2+} load (Jiang et al., 2005, Jones et al., 2008). Highlighting the functional heterogeneity of RyR2 mutations, a decrease or complete ablation of luminal Ca^{2+} sensitivity has also been observed with some channel mutants (Jiang et al., 2007). This model of RyR2 dysfunction is generally favoured since is shows some parallels with the mechanism of aberrant Ca^{2+} release thought to occur in the autosomal recessive form of the disease (section 1.8.4).

1.8.4. Autosomal recessive form of CPVT (CPVT2) evoked by mutations in CSQ2:

Among suspected CPVT2 patients, alterations in CSQ2 generally arise from either missense mutations, that alter the functional properties of the protein, or nonsense mutations that completely abolish protein expression (Lahat et al., 2001, Eldar et al., 2003, Postma et al., 2005, Viatchenko-Karpinski et al., 2004). It is reported that CSQ2 mutations account for approximately 3% of CPVT patients (Katz et al., 2009). Different animal and cell models of CSQ2-linked CPVT have demonstrated alterations in SR Ca^{2+} handling via different mechanisms, yet all culminate in ventricular arrhythmia and DADs following sympathetic stimulation (Györke et al., 2009).

First identified in 7 consanguineous Bedouin families in northern Israel, the CSQ2 missense mutation D307H converts a negatively charged aspartic acid residue into a histidine, in a highly conserved region of the protein identified as a putative Ca^{2+} binding site (Lahat et al., 2001, Elder et al., 2003, Houle et al., 2004). Houle et al reported that the D307H mutation blunts the proteins ability to interact with Ca^{2+}, TRD1 and JUN, and thus its associations with RyR2 (Houle et al., 2004). Complementing this study, it was later proposed that this mutation caused a conformational change in the protein that prevents polymerisation and consequently alters the Ca^{2+} binding capacity of CSQ2 (Kim et al., 2007). Overexpression studies revealed that this mutation suppressed EC coupling and Ca^{2+} spark frequency, which was consistent with an apparent reduction in Ca^{2+} storage capacity of the SR despite the presence of endogenous WT CSQ2 (Viatchenko-Karpinski et al., 2004, Dirksen et al., 2007). Interestingly, a reduction in the expression level of CSQ2 was also reported in a D307H knock-in mouse model (Song et al., 2007).

Another CSQ2-linked mutant (R33Q) completely abolishes the ability of CSQ2 to inhibit RyR2 channels at low luminal Ca^{2+} (Terentyev et al., 2006, Qin et al., 2008). Terentyev et al also demonstrated that in rat cardiac myocytes overexpressing R33Q, EC coupling and Ca^{2+} spark frequency were enhanced and consequently promoted spontaneous diastolic Ca^{2+} release. Unlike the D307H mutation, Terentyev et al found no alteration in the Ca^{2+} storage capacity with *CSQ2*-R33Q overexpression (Terentyev et al., 2006). In contrast,

Rizzi et al reported that in CSQ2-R33Q knock-in mice, the SR Ca^{2+} content was significantly reduced (Rizzi et al., 2008). In addition, the group reported that the mutant caused a 50% reduction in the expression level of CSQ2, TRD1 and JUN, despite the presence of normal levels of mRNA (Rizzi et al., 2008). A functional knock-out phenotype is generated by the CSQ2 mutation L167H, identified in the first patient known to carry heterozygous CSQ2 mutations (di Barletta et al., 2006). Characterisation of the *CSQ2*-L167H mutant *in vitro* has revealed that the mutant does not respond to Ca^{2+} and prevents CSQ2 polymerisation that may be required for Ca^{2+} binding (Kim et al., 2007, Valle et al., 2014). Consistent with these findings, Qin et al demonstrated that at the single channel level, the L167H mutant was unable to reduce RyR2 channel openings at low luminal Ca^{2+} concentrations (Qin et al., 2008).

In summary, CPVT-linked mutations in CSQ2 can exert their deleterious effects by at least two mechanisms: (1) affecting the protein's conformation and ability store Ca^{2+}, and (2) affecting the ability of CSQ2 to regulate RyR2 function (Györke, 2009). CSQ2 mutations that impair the Ca^{2+} storage capacity of the protein or reduce its expression are suggested to accelerate the restitution of Ca^{2+} release from the RyR2 (Terentyev et al., 2006). Following SERCA2a-mediated Ca^{2+} re-uptake, a lower number of Ca^{2+} storage sites within the SR may result in an overload of free releasable Ca^{2+} that can no longer be buffered, and thus may generate spontaneous Ca^{2+} release and DADs (Györke et al., 2009, Knollmann, 2009). The *CSQ2* mutant variants that abolish protein associations between CSQ2, other luminal proteins and RyR2, compromise Ca^{2+} signalling refractoriness following systole, by preventing the ability of CSQ2 to inhibit RyR2 activity when the SR Ca^{2+} content is low (Terentyev et al., 2006).

1.8.5. Newly identified CPVT-linked mutations in other EC coupling components:

It has been proposed that approximately one-third of symptomatic patients referred for genetic screening of CPVT-linked *RyR2* and *CSQ2* gene mutations remain without an identified molecular defect and thus suggests the existence of mutations in other key EC coupling proteins (Roux-Buisson et al., 2012). This hypothesis has recently been emphasised by Roux-Buisson et al (2012) who screened 97 CPVT-patients without RyR2 and CSQ2 mutations, and identified three patients with mutations in cardiac triadin TRD1. Two of the mutants were found to introduce a premature stop codon, suggesting that TRD is degraded in these patients. Interestingly, the identified mutations were mapped to a region of the *TRD* gene common to all isoforms, suggesting that these mutants could also lead to an absence of TRD in skeletal muscle (Roux-Buisson et al., 2012). Although this discovery of a new gene implicated in CPVT is significant, it is important to note that no gene mutations were identifiable in 94 patients, despite being screened for RyR2, CSQ, ASPH (within which JUN is a splice variant) and TRD mutants (Roux-Buisson et al., 2012). A later investigation by a different research group (Nyegaard et al., 2012) described the identification of two CaM mutations detected in screened clinical samples of 64 individuals with unspecified arrhythmia, a gene which was not screened by Roux-Buisson (2012) and co-workers. A recent investigation published this year by Hwang et al (2014) described the functional investigation of two CaM mutants (N54I and N98S), which were found to activate RyR2 activity and enhanced the frequencies if spontaneous Ca^{2+} waves in isolated mouse ventricular myocytes. Taken together, these studies not only highlight the limitations to a gene candidate approach, but also strongly suggest that other mutations in relation to CPVT have yet to be discovered. In a clinical setting these findings highlight the importance of assessing mutations in other EC coupling protein genes, the discovery of which may lead to advances in the development of patient-specific CPVT therapies.

1.9. Research Project Aims:

Taking into consideration the proposed role of the luminal proteins CSQ2, JUN and TRD1 in regulating the hRyR2 channels response to luminal Ca^{2+}, altered regulation or protein-protein association of mutant RyR2 with the accessory proteins could be a contributing factor in the aberrant Ca^{2+} release seen in CPVT patients. To investigate this hypothesis, this project aims to:

- Co-express recombinant human RyR2 (WT or mutant) with the luminal accessory proteins in a heterologous cell system. Evaluate if the protein-protein interactions between the luminal proteins and hRyR2 can be re-created in our chosen experimental system.

- Assess if CPVT-linked RyR2 mutation can disrupt protein-protein associations between the Ca^{2+} release channels and the luminal accessory proteins.

- Assess the effects of luminal accessory proteins on WT hRyR2 Ca^{2+} release.

- Assess the functional consequences of mutant hRyR2 expression on luminal accessory protein regulation. Two CPVT-linked mutants will be investigated in this work: N4104K and A4556T (Figure 1.6). These two mutants in particular were chosen firstly due to their location, since N4104K hRyR2 resides on the cytosolic side of the channel, whilst A4556T is located within the luminal region. It will be of interest to establish if an altered response to luminal protein regulation or interaction is specific to the location of mutation. Furthermore, the consequences of the A4556T hRyR2 mutation are previously uncharacterised; whilst N4104K hRyR2 has been studied previously by numerous research groups (Jiang et al., 2004, George et al., 2006), allowing the data collected in this work to be compared.

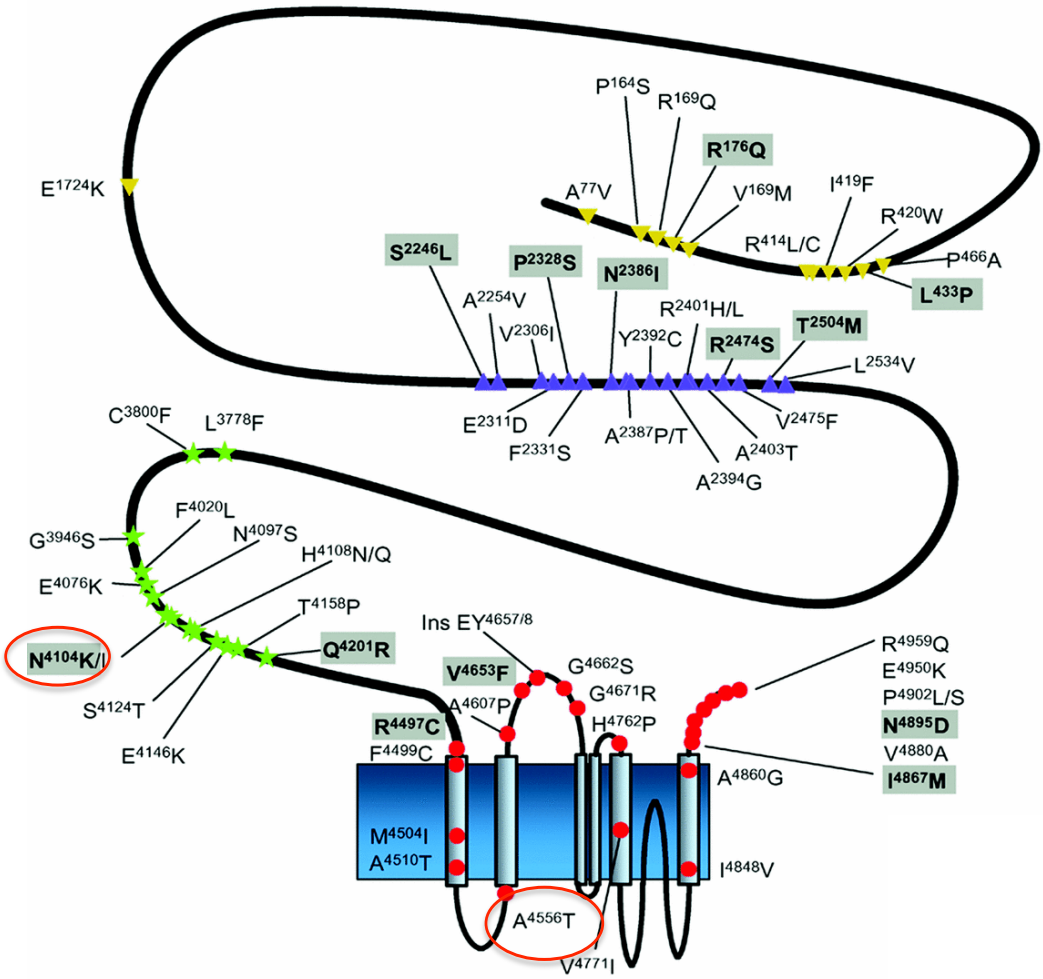

Figure 1.6: Schematic illustrating the hRyR2 mutations investigated in this project: *As circled, the N4104K hRyR2 mutation resides on the cytosolic side of the channel, whilst a previously uncharacterised mutation A4556T is located on the luminal region of hRyR2. Image modified from Thomas et al., 2006.*

Chapter 2

Materials and Methods

2.1 Materials:

2.1.1. General laboratory reagents and chemicals:

All chemicals and reagents were of analytical grade and obtained from Sigma-Aldrich or Fisher Scientific and all cell culture reagents were from Life Technologies, unless otherwise stated. All reagents were dissolved in deionised water (dH_2O) and stored at room temperature unless an alternative is noted. All reagents and equipment used for agarose and polyacrylamide gel electrophoresis were purchased from Bio-Rad, with the exception of the iBlot™ Gel transfer system, purchased from Life Technologies. Centrifugation steps were undertaken using a range of Beckman Coulter centrifuges, solution pH was measured using a Mettler Toledo FE20 pH meter (Camlab) and adjusted using either 1M HCl or 1M KOH, unless otherwise stated. Solutions were filter sterilised where required using a 0.22µM Millex® syringe filter (Millipore).

2.1.2. Molecular Biology Kits and Reagents:

(A) Zero Blunt® PCR Cloning kit (Life Technologies) – stored at -20ºC

i. *pCR™-Blunt II-TOPO® vector:* 10ng/µl plasmid DNA in: 50% glycerol, 50mM Tris-HCl (pH 7.4), 1M EDTA, 2mM DTT, 0.1% Triton X-100, 100µg/ml BSA and 30µM bromophenol blue
ii. *10x Ligation Buffer:* 60mM Tris-HCl (pH 7.5), 60mM $MgCl_2$, 50mM NaCl, 1mg/ml BSA, 70mM β-mercaptoethanol, 1mM ATP, 20mM dithiothreitol and 10mM spermidine
iii. *T4 DNA ligase:* (4U/µl)
iv. *Sterile water:* deionised and autoclaved
v. *M13 reverse primer*: 0.1 µg/µl in Tris-EDTA buffer. Used in DNA sequencing reactions.

(B) Polymerase chain reaction reagents

i. *Phusion™ DNA Polymerase (Finnzymes):* (2 U/µl). Also provided with the enzyme: DMSO (100%) and 5x Phusion™ reaction buffer containing 7.5mM $MgCl_2$.
ii. *dNTP mix, 20mM (Thermo Scientific):* dATP, dCTP, dGTP and dTTP neutralised in water (pH 7.5).
iii. *Human cardiac muscle cDNA library (BD Biosciences).*

(C) ABI Prism® BigDye® terminator v3.1 cycle sequencing kit (Applied Biosystems) and sequencing reagents

i. *BigDye® Terminator Premix:* containing fluorescent BigDye® terminators *(ddNTPs: ddATP, ddTTP, ddGTP and ddCTP).*

ii. *BigDye® Terminator 5x sequencing buffer:* 400mM Tris, 10mM $MgCl_2$ optimised for use with the BigDye® Terminator premix.

iii. *DyeEx ™ kit (Qiagen):* Used to remove unincorporated dye terminators from sequencing reactions.

(D) Agarose gel electrophoresis reagents

i. *TAE, 50x stock (1x diluted stock dissolved with agarose):* 2M Tris, 2M glacial acetic acid, 50mM EDTA.

ii. UltraPure ™ *Ethidium Bromide (10 mg/ml stock):* Used at 0.1µg/ml.

iii. *DNA loading buffer, 1x stock:* 50% 1x TAE buffer, 50% (v/v) glycerol and added orange G to achieve the desired detection colour.

iv. *Molecular weight DNA markers:* 1 kb plus DNA ladder (Life Technologies).

(E) QIAquick Gel Extraction Kit (Qiagen)

i. *Buffer QG:* agarose gel solubilisation and binding buffer containing sodium perchlorate and a pH indicator.

ii. *Buffer PE:* An ethanol-containing wash buffer.

(F) Rapid DNA ligation kit (Roche)

i. DNA dilution buffer (5x), T4 DNA ligation buffer (2x) and T4 DNA ligase (5U/µl). Antarctic phosphatase was used in conjunction with the kit.

(G) Plasmid purification: QIAprep® miniprep spin kit and HiSpeed® maxiprep kit (Qiagen)

i. *Resuspension solution (P1):* 50mM Tris-HCl (pH 8), 10mM EDTA, 100 µg/ml RNase A, pH adjusted to 7.5 with HCl and filter sterilised.

ii. *Lysis solution (P2):* 200mM NaOH, 1% (w/v) sodium dodecyl sulphate (SDS), filter sterilised.

iii. *Maxi-prep neutralisation solution (P3):* 4.09M Guanidine-HCl, 0.759M potassium acetate, pH adjusted to 5.5 with glacial CH_3COOH and filter sterilised.

iv. *Mini-prep neutralisation solution (N3):* 4.2M Guanidine-HCl, 0.9M potassium acetate, and pH 4.8.

v. *Maxi-prep column equilibration buffer (QBT):* 750mM NaCl, 50mM MOPS, pH 7.0, 15% (v/v) isopropanol, 0.15% Triton® X-100.

vi. *Maxi-prep column wash solution, medium salt (QC):* 1M NaCl, 50mM MOPS, 15% (v/v) isopropanol, pH 7.

vii. *Maxi-prep column elution buffer (QF):* 1.25M NaCl, 50mM Tris-HCl, 15% (v/v) isopropanol, pH 8.5.

viii. *Mini-prep spin column wash buffer (PB):* 5 M Guanidine-HCl, 30% isopropanol.

(H) Restriction digest

i. All restriction enzymes and optimised reaction buffers (10x) were purchased from New England Biolabs and stored at -20°C.

2.1.3. Bacterial Cell Culture:

All glassware and sterile plastics were purchased from Fisher Scientific or Greiner. All glassware was washed with dH_2O and autoclaved before use. Bacterial growth media was also autoclaved in the same manner, before cooling to approximately 50°C prior to the addition of antibiotics.

(A) *Luria-Bertani (LB) media:* 10g/L tryptone, 5g/L yeast extract, 5g/L sodium chloride, prepared to 1L with dH_2O.

(B) *LB agar plates:* Prepared with LB media components and 15g/L agar. Autoclaved and antibiotics added before setting within $10cm^2$ sterile petri dishes.

(C) *Ampicillin 100 mg/ml stock*: used at a working concentration of 100µg/ml.
Stored at -20°C.

(D) *Kanamycin 30 mg/ml stock*: used at a working concentration of 30µg/ml.
Stored at -20°C.

(E) DNA Transformation – chemically competent bacterial cells and reagents

i. One Shot® TOP10 chemically competent cells (Life Technologies).

ii. XL10-Gold Ultracompetent cells with provided β-mercaptoethanol (Agilent Technologies).

iii. *SOC medium*: 2% Tryptone, 0.5% Yeast extract, 10mM NaCl, 2.5mM KCl, 10mM $MgCl_2$, 10mM $MgSO_4$ and 20mM glucose.

2.1.4. Oligonucleotides:

Oligonucleotide primers (shown in Chapter 3, Figure 3.1) were designed and ordered from Sigma Genosys or MWG-Biotech AG and were obtained lyophilised. Following the manufacturers guidelines, 100µM and 20µM working stocks were prepared and stored at -20°C.

2.1.5. Plasmid Vectors:

- ***pCR™-Blunt II TOPO® vector (Life Technologies)***

To sequence and confirm that luminal accessory protein constructs were successfully amplified, PCR products were inserted into a pCR™-Blunt II TOPO® vector (Figure 2.1, (A)) using the Topoisomerase I system. The vector was supplied linearised with *Vaccinia* virus, DNA topoisomerase I, bound covalently to the 3' end of each DNA strand. To enable accurate recombinant selection, the vector is designed to encode a lethal *E.coli* gene, *ccdB* fused to the C-terminus of the *LacZ*α fragment. Upon ligation of the blunt ended PCR product, *LacZ*α*-ccdB* gene fusion expression is disrupted, allowing growth of only positive recombinants. Since cleavage sites for restriction enzyme *EcoRI* are positioned either side of the multiple cloning site in the TOPO® vector, restriction digest with this enzyme was used to identify vector clones containing the desired insert. Positive clones were sequenced from the M13 reverse priming site. The DNA sequencing procedure is outlined in section 2.4.1.8.

- ***Mammalian expression vectors – pcDNA™3 and pcDNA™3.1 Hygro $^{(+)}$ (Life Technologies)***

Full length WT and CPVT-linked mutant human eGFP-RyR2 constructs were obtained from Dr Christopher George (WT and N4104K; George et al., 2003b) and Dr Lowri Thomas (A4556T, unpublished), Cardiff University. The hRyR2 constructs were cloned into the mammalian expression vector pcDNA™3 (Figure 2.1, B) and tagged at the N-terminus with an enhanced green fluorescent protein (eGFP), enabling identification of protein expression in a mammalian cell line. The coding sequence for human cardiac muscle CSQ2 was also obtained from Dr Lowri Thomas and isolated as described in Chapter 3, section 3.2.1. Luminal accessory protein constructs were cloned into pcDNA™3.1 Hygro$^{(+)}$ (Figure 2.1, C). The decision to use this vector is outlined in Chapter 3, section 3.3.4. Both pcDNA3™ and pcDNA3.1™ Hygro$^{(+)}$ vectors contain multiple cloning sites in the forward (+) and reverse (-) orientations. To enable plasmid selection in bacteria, the vectors encode for β-lactamase allowing selection by ampicillin resistance. In mammalian cells, transcription is initiated in both expression vectors by the cytomegalovirus (CMV) promoter and terminated by a stop codon inherently encoded by the hRyR2 (TAA), CSQ2 (TAG) and JUN (TAA) sequences. Both vectors replicate autonomously in mammalian and *E.coli* cells from the SV40 and ColE1 origin, respectively.

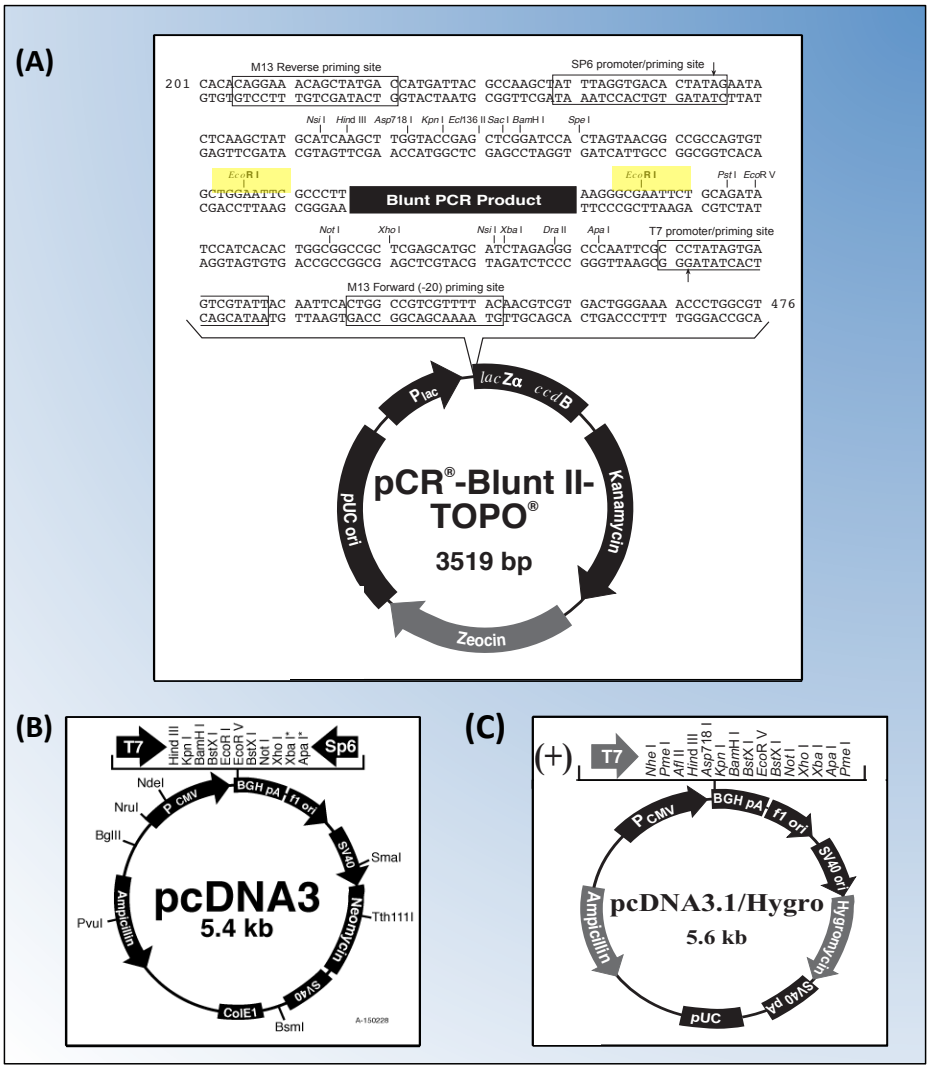

Figure 2.1: Illustration of plasmid vectors used in this study: ***(A)*** *pCR-Blunt II TOPO® vector: PCR amplified products were inserted into the vector for sequencing. As highlighted, EcoRI sites flanking the ligated PCR product enabled easy excision of the insert from the vector by restriction digest. To enhance positive selection of cloned DNA, the vector contains a ccdB gene, plus a kanamycin resistance gene for selection in E.Coli. Sequencing was carried out using the M13 reverse primer site.* ***(B)*** *Mammalian expression vector pcDNA3: full-length WT and mutant eGFP-hRyR2 were constructed in this vector (by Dr Christopher George), which contains an ampicillin resistance gene for positive selection in E.Coli and a gene encoding neomycin (a variant of geneticin/G418) resistance. Expression was driven at the CMV promoter.* ***(C)*** *Mammalian expression vector pcDNA3.1hygro(+): sequence verified luminal protein cDNA constructs were ligated into this vector. The vector enabled positive selection of transformants in mammalian cells via a hygromycin resistance gene. Like pcDNA3, the vector also has an ampicillin resistance gene for positive selection in E.Coli. All images shown were taken from the Life Technologies website (www.lifetechnologies.com) and modified.*

2.1.6. Antibodies:

(A) ab-GFP (B-2): Mouse monoclonal IgG (provided at 200µg/ml). Raised against the entire green fluorescent protein of *Aequoria Victoria*, and cross-reacts with enhanced GFP (eGFP). Purchased from Santa Cruz Biotechnology, stored at 4°C. Used at a 1:10,000 dilution for Western blot analysis.

(B) Anti-Calsequestrin (ab3516, α-CSQ2): Rabbit polyclonal (provided at 0.2mg/ml, stored in PBS, preserved with 0.05% sodium azide). Purchased from Abcam®, stored at -20°C. Used at a dilution 1:5,000 dilution for Western blot analysis. Used at 1:100 for immunofluorescence analysis.

(C) Anti-Aspartate beta hydroxylase (ab72846, α-ASPH): Used for junctin detection (a splice variant of ASPH). Mouse polyclonal (provided at 1 mg/ml, stored in 1x PBS, pH 7.2). Purchased from Abcam®, stored at -20°C. Used at a 1:5,000 dilution for Western blot analysis. Used at 1:100 for immunofluorescence analysis.

2.1.7. Mammalian Cell Culture Reagents:

(A) *Dulbecco's Modified Eagle Medium (DMEM):* containing D-glucose, L-glutamine and pyruvate, and supplemented with 10% (v/v) heat inactivated foetal calf serum, 2mM glutamine and 100µg/ml penicillin/streptomycin (referred to as complete, cDMEM), and stored at 4°C.
(B) *Trypsin-EDTA 0.05%:* 1x, with phenol red. Stored at -20°C.
(C) *Sodium chloride solution (saline):* 0.9% (w/v) supplied by Fresenius Kabi.
(D) *Sodium butyrate (NaB (1M stock prepared)): used at 2mM.*
(E) *Calcium chloride ($CaCl_2$), 1M stock:* purchased from Sigma-Aldrich, stored at -20°C (50ml aliquots).
(F) *Hepes Buffered Saline (HBS):* 280mM NaCl, 10mM KCl, 1.5mM Na_2HPO_4, 10mM glucose, 50mM HEPES, pH 7.05, filter sterilised before storing at -20°C.
(G) *Effectene® Transfection reagent kit (Qiagen):* 1mg/ml Effectene® transfection reagent, 1 mg/ml enhancer and DNA-condensation buffer (EC). All stored at 4°C.
(H) *Cell freezing medium:* 10% (v/v) dimethyl sulphoxide (DMSO) in foetal calf serum, filter sterilised and stored at 4°C.
(I) *Hygromycin B antibiotic:* 50mg/ml stock in PBS (Life Technologies).

2.1.8. Immunofluorescence and calcium imaging reagents:

(A) *Alexa Fluor® conjugated secondary antibodies (Molecular Probes):* Used at a 1/250 dilution.
(B) *Fluo-3 AM:* purchased from Life Technologies, prepared in a solution of 20% Pluronic® acid in DMSO. Added to minimal (unsupplemented) DMEM (mDMEM) to generate a working concentration of 10μM.
(C) *Phosphate buffered saline (PBS):* 137mM NaCl, 2.7mM KCl, 4.3mM Na_2HPO_4, 1.4mM KH_2PO_4, pH adjusted to 7.4 with HCl, filter sterilised.
(D) *Poly-L-lysine:* 0.1% solution, stored at 4°C. Used to coat coverslips/culture dishes.
(E) *Fixing solution:* 4% (w/v) paraformaldehyde in PBS.
(F) *Cell permeabilisation solution:* 0.1% (v/v) Triton X-100 in PBS.
(G) *Krebs*-Ringer-Hepes (KRH) buffer: 120mM NaCl, 5.5mM Glucose, 25mM Hepes, 4.8mM KCl, 1.2mM KH_2PO_4, 1.2mM $MgSO_4$, 1.3mM $CaCl_2$, pH 7.4. Filter sterilised.
(H) *Caffeine:* 100mM stock prepared in KRH buffer, diluted 1/10 to prepare a 10mM stock.

2.1.9. Protein biochemistry reagents:

(A) Western blot analysis

i. *SDS-PAGE running buffer*: 25mM Tris, 250mM Glycine, 0.1% SDS.
ii. *Acrylamide*: 40% acrylamide/Bis mix solution, in 37:5:1 ratio (Bio-Rad).
iii. *Ammonium persulphate 10% (w/v)*: Prepared on the day of use.
iv. *SDS-PAGE loading buffer 2x:* 4% (w/v) SDS, 100mM Tris buffer (pH 6.8), 20% (v/v) glycerol, 0.2% (w/v) bromophenol blue (with added β-mercaptoethanol 10% (v/v)). Stored at -20°C.
v. *Tris-buffered saline (TBS) 1x:* 20mM Tris, 137mM NaCl, pH adjusted to 7.6 before adding 1 ml/L Tween-20 (v/v) (1x TBS-T).
vi. *Blocking solution:* 5% (w/v) non-fat powdered milk in 1x TBS-T.
vii. *Wash buffer/1% blocking solution:* 1% (w/v) non-fat powdered milk in 1x TBS-T.
viii. *Molecular weight markers:* pre-stained Kaleidoscope marker purchased from Bio-Rad.
ix. *Tris 1.5M (separating buffer):* prepared a 1.5M Tris stock, pH adjusted to 8.8.
x. *Tris 0.5M (stacking buffer):* prepared a 0.5M Tris stock, pH adjusted to 6.8.
xi. *Transfer buffer (semi-dry*): 48mM Tris, 39mM Glycine, 0.01% (w/v) SDS, 20% (v/v) methanol.
xii. *Amersham™ ECL™ Western blotting analysis system:* membrane detection reagents used with ECL hyperfilm™ (GE Healthcare).

(B) Mixed membrane preparation

i. *Hypo-osmotic HEK cell lysis buffer:* 20mM Tris, 5mM EDTA, pH adjusted to 7.4 with HCl. 1 protease inhibitor cocktail tablet (Roche), dissolved per 50 ml of buffer.

ii. *Cryopreservant solution ('Solution C'):* 0.4M sucrose, 20mM Hepes and 1x protease inhibitor tablet dissolved per 25ml. Used to re-suspend and freeze membrane preparations at -80°C.

(C) Protein Assay

i. Micro BCA™ protein assay kit (Pierce). Bovine Serum Albumin (BSA) ampules (2mg/ml) were also provided in the kit.

(D) [^{3}H] Ryanodine binding

i. *Ryanodine binding buffer:* 1M KCl, 25mM PIPES, 100μM $CaCl_2$, pH adjusted to 7.4 using KOH.

ii. *'Cold' Ryanodine stock (1mg):* Stored at -20°C under desiccating conditions, purchased from Abcam®, 1 mM working stock prepared in dH_2O.

iii. *'Hot' [^{3}H]-Ryanodine stock (9.25 MBq, 250 μCi):* purchased from Perkin Elmer. Stored at -20°C in secure conditions.

iv. *Ultima™ Gold Scintillation Fluid:* purchased from Perkin Elmer.

(E) Immunoprecipitation studies

i. *Solubilisation buffer:* 20mM Tris, 150mM NaCl, 0.4% CHAPS (w/v), pH 7.4, 25x protease inhibitor solution added (Roche), used at 1x.

ii. *20mM Tris:* solution prepared and used as a final stage wash buffer, pH 7.5.

(F) μ-MACS™ GFP Tagged Protein Isolation Kit (Miltenyi Biotec)

i. *Anti-GFP tagged microbeads:* supplied as a solution containing 0.05% sodium azide. Stored at 4°C.

ii. *SDS-PAGE elution buffer:* 50mM Tris HCl (pH 6.8), 50mM DTT, 1% SDS, 1mM EDTA, 0.005% bromophenol blue and 10% glycerol.

iii. *Protein A microbeads:* solution supplied in 0.05% sodium azide.

2.2. Health and Safety:

All experiments were carried out in accordance with COSHH regulations and full general health and safety training was received from the WHRI safety manager prior to commencing any laboratory work. Use of genetically manipulated organisms was registered and all procedures were carried out in accordance with GMAG guidelines. Microbiology and cell culture safety training was undertaken with the Wales Heart Research Institute (WHRI) biological safety officer. Radioisotope procedures were registered and local rules were followed for use and disposal using the IsoStock® radioisotope accounting software.

2.3. Computer analysis and software:

Microsoft Excel was used to store and plot most numerical data (expressed as mean ± standard error), unless otherwise stated. Statistical analyses and fitting of sigmoidal curves were carried out using GraphPad Prism® (GraphPad Software Inc). Co-incident pixels were counted using Adobe Photoshop and imaging investigations carried out using Leica Microsystems LAS-AF or Zeiss Axiovision software. Quantity-one (Bio-Rad) software was used for image processing and densitometric analysis of Western blots. DNA sequences were verified using the Basic Local Alignment Search Tool (BLAST, http://blast.ncbi.nlm.nih.gov/).

2.4. Methods:

General molecular biology techniques were performed according to protocols outlined in the Molecular Cloning laboratory manual (Sambrook et al., 1989) and procedures optimised by the Williams laboratory or other staff members of the WHRI. When applicable the manufacturers guidelines were followed.

2.4.1. Molecular Biology Methods:

2.4.1.1. Polymerase Chain Reaction (PCR):

A series of PCR reactions were carried out using a GeneAmp® PCR system 9700 thermal cycler (Applied Biosystems). To generate high-fidelity amplification products, Phusion™ DNA polymerase (a *pyrococus furiosus (pfu)* enzyme (Finnzymes)) was used, which possess 5'→ 3' DNA polymerase activity and 3'→ 5' exonuclease (proofreading) activity, allowing recognition and excision of any misincorporated bases during polymerisation. Furthermore, Phusion™ DNA polymerase generated blunt-ended PCR products, which could be ligated directly into a Zero Blunt® TOPO® vector for sequencing.

The complete PCR reactions carried out and the thermal cycling conditions used are highlighted in Table 2.1 and 2.2, respectively. To enrich the PCR products generated from a first round of amplification (PCR reaction 1), a second round of reactions were undertaken using PCR1 products as a template (PCR reaction 2).

PCR Reaction 1	PCR Reaction 2
5µl cDNA library template (20ng) 1µl forward primer (20µM stock) 1µl reverse primer (20µM stock) 10µl reaction buffer (5x) 0.5µl dNTPs (20mM stock) 1µl DMSO 0.5µl DNA polymerase (1 unit Phusion™) 31µl dH_2O TOTAL 50µl	5µl PCR1 as template (20ng) 1µl forward primer (20µM stock) 1µl reverse primer (20µM stock) 10µl reaction buffer (5x) 0.5µl dNTPs (20mM stock) 1µl DMSO 0.5µl DNA polymerase (1 unit Phusion™) 31µl dH_2O TOTAL 50µl

Table 2.1: PCR reaction components: *PCR reaction 1 refers to the first series of PCR reactions undertaken, using a cardiac cDNA library as a template and primers outlined in Chapter 3, Figure 3.1. PCR reaction 2 refers to a second series of PCR reactions carried out to enrich the amplified products. Forward and reverse primers were used at a final concentration of 0.4 µM.*

Step	Temperature (ºC)	Time	Number of cycles
Initial Denaturation	98	30 seconds	1
Denaturation Annealing Elongation	98 62 72	10 seconds 20 seconds 1 minute 30 sec	30
Final Elongation	72	10 minutes	1
Incubation	4	Indefinite	1

Table 2.2: PCR amplification thermal cycling conditions: *The annealing temperature was chosen according to the primer melting temperature (set 10ºC below this value). Elongation time was set according to the length of the expected product.*

2.4.1.2. Agarose Gel Electrophoresis:

Agarose gel electrophoresis was used to verify the size of DNA fragments (such as those generated by PCR amplification). A 1% w/v agarose gel was formed by dissolving the requisite amount of agarose in 1x TAE buffer before heating in a microwave oven, cooling to ~50°C and adding 0.1 µg/ml of ethidium bromide (EtBr). The mixture was set in a gel cast with a comb, forming wells for loading, and assembled according to the manufacturers guidelines (Bio-Rad). Each prepared gel was placed into a Bio-rad mini-sub® gel tank and covered with 1x TAE buffer (section 2.1.2 (D) i) before the samples were loaded. Loading buffer (section 2.1.2 (D) iii) was added to each sample at 1x (from a 3x buffer stock) before gel loading, and a 1 kb DNA molecular weight (MW) marker was run alongside the samples as a reference of fragment molecular mass. Electrophoresis was carried out under constant voltage (typically 90 V) until sufficient DNA fragment separation was evident. The Bio-Rad XRS Chemidoc Imaging System® was used to view the resolved EtBr stained DNA fragments by UV transillumination.

2.4.1.3. Gel Extraction:

The QIAquick Gel extraction kit (Qiagen), (section 2.1.2 (E)) was used to purify DNA fragments separated on agarose gels. The DNA fragments separated by electrophoresis were viewed using a U.V transilluminator light box (Syngene), using an appropriate UV protective face shield. Fragments were excised from the gel using a scalpel, and weighed such that an appropriate volume (3x mass) of a chaotropic salt buffer (QG) could be added, leading to solubilisation of agarose polymers and dissociation of proteins associated with the DNA complex. Incubating the mix at 50ºC in a water bath, for 10 minutes, with vortexing every two minutes, encouraged this solubilisation. Once solubilised, 1x volume of isopropanol was added to the sample. The QG buffer contains a pH indicator, allowing monitoring of pH throughout the reaction, as a pH of <7.5 is essential for efficient DNA adsorption to the silica-gel particles lining a QIAquick membrane spin column. The sample was applied to a QIAquick spin column, placed into a 2ml collection tube and centrifuged at >10,000x*g* for 1 minute. The flow-through was discarded, whilst the QIAquick membrane (with captured DNA) was washed with both 500 µl QG buffer and 750 µl PE buffer to remove any remaining impurities such as agarose and salt. DNA was eluted into a 1.5 ml microcentrifuge tube in 50µl dH_2O following further centrifugation for 1 minute. The purified DNA was verified by agarose gel electrophoresis and stored at -20ºC until required.

2.4.1.4. TOPO® cloning of luminal accessory protein cDNA clones:

Zero Blunt® TOPO® (Life Technologies) allowed fast and efficient cloning of PCR amplicons such that they could be propagated to sufficient quantities of cDNA for automatic sequencing. In contrast to traditional cloning, no restriction digest was necessary and only a minimal amount of insert was required for ligation (10:1 molar ratio of insert:vector recommended in the manufacturers guidelines for optimal efficiency). All reagents used in the ligation reaction were supplied in the Zero Blunt® PCR cloning kit (section 2.1.2, (A)). The reaction contained: 1µl pCR-Blunt TOPO® vector (25ng), 5µl blunt PCR product (250ng), 1µl 10x ligation reaction buffer ((A) ii), 1µl T4 DNA ligase (4U/µl) and 2µl dH_2O (Total volume 10µl). The reaction was incubated for 1 hour at 16 ºC before transformation.

2.4.1.5. Bacterial Cell Transformation:

Transformation of smaller plasmids (i.e., luminal accessory protein constructs) was carried out using chemically competent OneShot®TOP10 *E.coli* cells. For transformation of TOPO® ligations (for example), 2µl (~1ng) of the mix was gently mixed into a chilled 50µl aliquot of TOP10® cells, incubated on ice for 30 minutes before a 30 second heat shock step at 42°C in a water bath. Following heat shock, vials were immediately transferred onto ice for a further 1 minute period, before aseptically adding 1ml SOC medium (section 2.1.3, (E) iii) and placing the vials into a 37°C incubator with shaking at 225 rpm, for 1 hour. Cultures were plated at two different densities onto pre-warmed LB agar containing 100µg/ml of an appropriate antibiotic (kanamycin in the case of TOPO® selection). A cell spreader was used to ensure the cells were dispersed throughout the whole plate, encouraging growth of colonies in isolation and arising from a single transformed cell. The plates were incubated overnight at 37°C (Heraeus Incubator, Thermo Scientific) before colony selection. Individual colonies were selected and seeded under aseptic conditions into 6ml of pre-warmed LB growth medium (section 2.1.3 (A)) containing an appropriate selective antibiotic (100µg/ml), and incubated for 16-18 hours at 37°C with shaking at 225 rpm.

Due to the fragile nature of the eGFP-hRyR2 plasmid construct (primarily owed to its larger size), the amplification technique was executed differently, using a method optimised in close collaboration with my colleagues in Professor Williams' group. Alteration of certain conditions aimed to avoid plasmid degradation and ensured sufficient quantities of purified hRyR2 DNA was generated. Using the transformation protocol aforementioned, the following differences were applied: full-length eGFP-hRyR2 was

transformed into 25µl XL-Gold Ultracompetent *Epicurian coli* cells (in the presence of 1µl ß-mercaptoethanol), which are suitable for propagation of larger plasmids. The cells were placed on ice for 10 minutes and subjected to gentle agitation every 2 minutes, before heat shock and further incubation at 37°C as described previously. After transformation, all culture steps were carried out at 30°C.

2.4.1.6. Small-scale DNA propagation (mini-prep):

To identify positive clones, overnight culture (3ml) inoculated with a single colony was centrifuged at 13,000x*g* for 2 minutes and the resultant pellet subjected to alkaline lysis using the QIAprep® mini-prep spin kit (section 2.1.2 (G) i-viii). Cells were resuspended in P1 buffer (250µl- containing RNAse A) and lysed in an equal volume of P2 containing sodium dodecyl sulphate (SDS) which solubilises the phospholipid components of the cells and sodium hydroxide which creates an alkaline environment that denatures chromosomal DNA and proteins. The lysate was neutralised in a high salt buffer, N3 (350µl) containing potassium acetate, resulting in precipitation of most of the chromosomal DNA, bacterial cell debris and SDS which form insoluble potassium dodecyl sulphate complexes. The precipitated matter was removed by centrifugation at 13,000x*g* for 10 minutes before adding the cleared lysate to a spin column containing a DNA binding silica membrane, which was subjected to further centrifugation at the same speed for 1 minute. The plasmid DNA bound to the membrane was washed with two ethanol-containing buffers (PB and PE) before elution by centrifugation (13,000x*g*, 1 minute) in 50µl dH_2O. Constructs were verified by restriction digest and direct DNA sequencing.

2.4.1.7. Verification of positive transformants by restriction digest:

Restriction endonucleases are widely used in manipulating and analysing DNA, by recognising and cleaving specific short sequence elements. Appropriate enzymes were chosen after constructing a visual digest via http://tools.neb.com/NEBcutter2/. Restriction mapping (prediction of fragment MW) was used to verify all miniprep clones. Restriction digest was typically carried out using 1µg of DNA and 5-10 units of endonuclease (prepared to a total volume of 20µl with 2µl reaction buffer and dH_2O). The plasmid DNA was digested for 2 hours in a 37°C water bath and the resultant products separated by agarose gel electrophoresis. The digest pattern was visualised using UV transillumination. Plasmid preparations that yielded restriction fragments of the expected MW were selected for further propagation (large-scale, maxi-prep culturing, section 2.4.1.10). For cloning, the desired DNA fragments were excised from the gel and purified using the QIAquick Gel Extraction Kit (Section 2.1.2, (E)).

2.4.1.8. DNA sequencing:

Luminal accessory protein constructs were sequenced using a BigDye™ Terminator v3.1 Cycle Sequencing Kit (Applied Biosystems), (section 2.1.2 (C)) following the manufacturers guidelines. The sequencing PCR reaction was prepared to a total volume of 10µl and typically consisted of ~250ng of plasmid DNA, BigDye™di-deoxyterminators, BigDye™ reaction buffer (x1) and a suitable sequencing primer (such as the M13 reverse primer provided in the TOPO® PCR cloning kit (3.5 pmol used)). The thermal cycling conditions are outlined in Table 2.3. Reaction products were purified using a DyeEx™ kit (Qiagen), where unincorporated dye terminators were removed by centrifugation of the samples in spin columns containing a prehydrated gel-filtration resin. Once collected from the columns, the samples were sent for analysis using an ABI 377 automated sequencer (Applied Biosystems, carried out by Central Biotechnology Services, Cardiff University). During analysis, the fluorescence intensities generated from the labelled di-deoxyterminators were translated into electropherograms.

Step	Temperature (ºC)	Time	Number of cycles
Initial Denaturation	96	2 minutes	1
Denaturation Annealing Elongation	96 50 60	30 seconds 30 seconds 4 minutes	30
Incubation	4	Indefinite	1

Table 2.3: PCR sequencing thermal cycling conditions: *The temperatures were chosen according to the BigDye™ Terminator v3.1 Cycle Sequencing Kit guidelines.*

2.4.1.9. Cloning of the luminal accessory protein constructs into a mammalian expression vector:

Verified constructs in pCR™-Blunt II-TOPO® were excised from the vector using a double restriction digest and subsequent gel extraction (sections 2.4.1.3 and 2.4.1.7), and cloned into the mammalian expression vector pcDNA3.1™hygro$^{(+)}$. Prior to preparing the ligation reaction, the DNA was treated with Antarctic phosphatase (5 units, 15 minutes at 37°C with heat inactivation at 65°C for 5 minutes) to prevent any re-ligation of the plasmid vector. Ligations were carried out using the Rapid DNA Ligation Kit (Roche), (section 2.1.2 (F)) and prepared in a 3:1 (insert:vector) molar ratio, as recommended in the manufacturers guidelines (Table 2.4). Reactions were incubated overnight at 4°C before being transformed into competent bacteria (OneShot®TOP10, section 2.4.1.5) and screened for success, as outlined in section 2.4.1.6-2.4.1.8.

Calsequestrin	Junctin
0.5µl pcDNA3.1hygro $^{(+)}$ vector (50ng)	0.5µl pcDNA3.1hygro $^{(+)}$ vector (50ng)
5µl CSQ2 construct (30ng)	2.5µl JUN construct (30ng)
2µl DNA dilution buffer (x5)	2µl DNA dilution buffer (x5)
1.5µl dH_2O (5x)	4µl dH_2O (5x)
----------	----------
10µl T4 DNA ligation buffer (2x)	10µl T4 DNA ligation buffer (2x)
1µl T4 Ligase	1µl T4 Ligase
TOTAL 20µl	TOTAL 20µl

Table 2.4: Luminal accessory protein and pcDNA3.1hygro$^{(+)}$ ligation reaction: *The relative MW of the constructs were used to calculate the molar ratio for ligation reactions (pcDNA3.1hygro$^{(+)}$ = 5600bp, CSQ2 = 1216bp and JUN = 678bp). Estimates of the luminal protein concentration (per µl) were made from the gel recovery (for gel extraction, see section 2.4.1.3), following excision of the constructs from pcDNA pCR™-Blunt II-TOPO®.*

2.4.1.10. Large-scale DNA propagation and maxi-prep purification:

For large-scale plasmid isolation, typically: 2x400ml (luminal protein constructs) or 4x400ml (full-length eGFP-hRyR2) flasks of LB medium (with ampicillin (100 µg/ml) were required to generate one bacterial pellet for DNA purification. Each flask was inoculated at a 1/400 dilution with small-scale culture (from the mini-prep process, described in section 2.4.1.6) and incubated overnight (16-18 hours) at 37°C (luminal protein constructs) or 30°C (full-length eGFP-hRyR2), with shaking at 225rpm (Innova™ 4300 incubator (New Brunswick Scientific)). The bacterial cells were harvested by centrifugation (Avanti J-25, Beckman with JLA16.250 fixed-angle rotor) at 7000 x*g* for 15 minutes at 4°C. Plasmid DNA was isolated from the pelleted cells using a HiSpeed® Plasmid Maxiprep Kit (Qiagen, section 2.1.2 (G)), which employs an ion-exchange resin method for purification. Bacterial cells were treated with the same alkaline lysis reagents used in the mini-prep protocol, before decanting the lysed, neutralised cells into the barrel of a QIAfilter cartridge and incubating at room temperature for 10 minutes. The precipitated cell debris (containing contaminant proteins, detergent and genomic DNA) was removed by filtration and the cleared lysate applied to an equilibrated (with QBT) HiSpeed® maxi tip (containing anion-exchange resin). DNA bound to the resin was washed twice (with buffer QC) before elution in 15ml high salt buffer (QF). Plasmid DNA was desalted and concentrated by isopropanol precipitation; isopropanol (0.7 volumes) was added to the eluate and incubated at room temperature for 30 minutes, before trapping the DNA precipitate in a QIA precipitator® filter using a syringe. Ethanol (70% w/v) was passed through the column to wash the bound DNA, before elution with 1ml dH_2O. Plasmids were quantified and verified by restriction digest, before storing at -20°C.

2.4.1.11. DNA Quantification:

DNA concentration (µg/ml) was established by UV spectrophotometric quantification (LAMBDA Bio$^{(+)}$ spectrophotometer (Perkin Elmer)) of a 1:50 dilution of sample in a quartz cuvette. Absorbance readings were taken at 260 nm (the wavelength at which DNA exhibits peak light absorption) and calculated according to an A260 value/optimal density of 1 corresponds to 50µg/ml of double stranded DNA. Plasmid purity was also quantified by measuring the ratio of A260/A280 (indicative of protein concentration), with values ≥1.8 indicating sufficiently pure preparations.

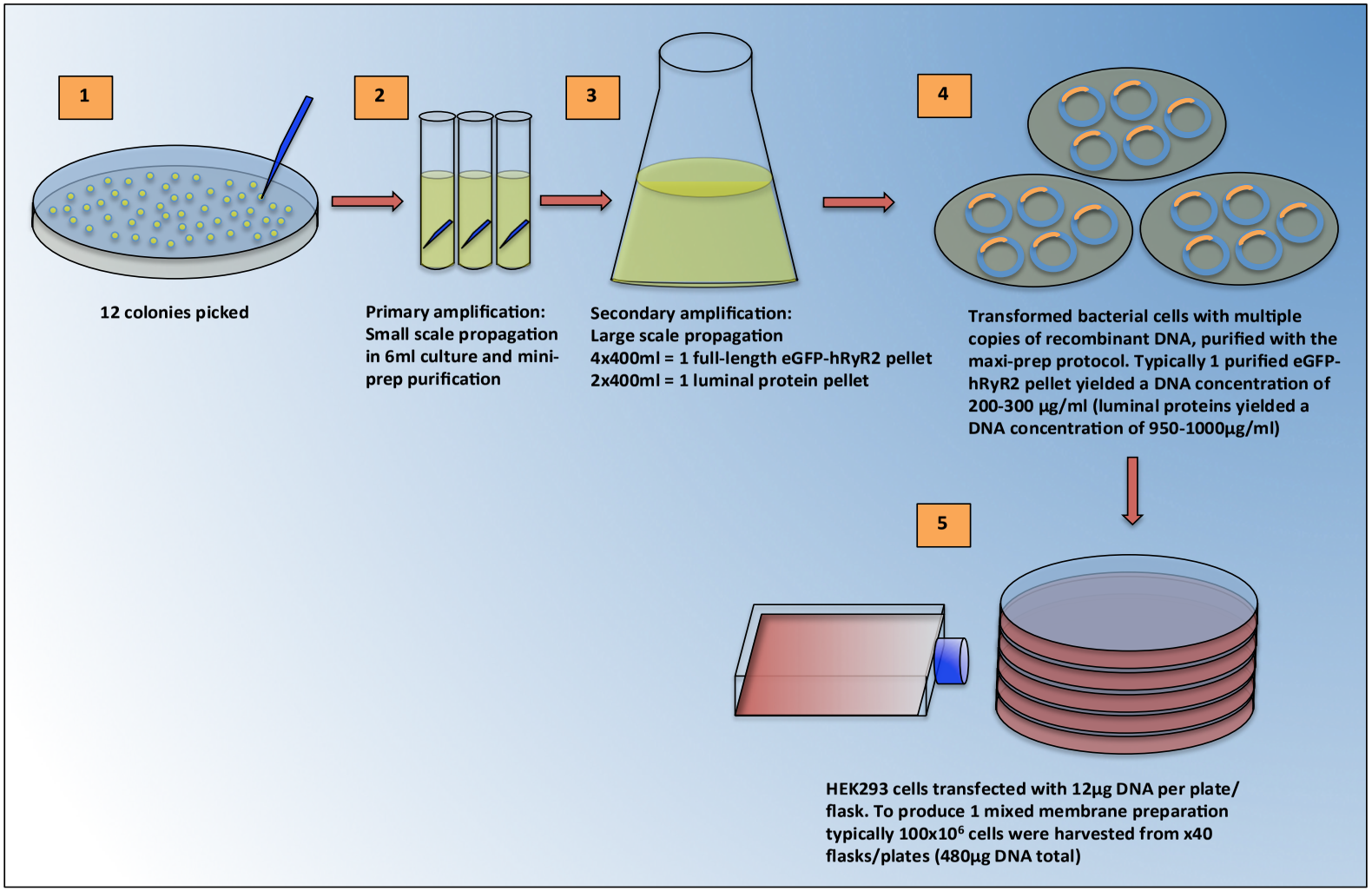

Figure 2.2: Schematic of bacterial cell DNA propagation of full-length eGFP-hRyR2 and luminal accessory protein constructs

2.4.2. Mammalian Cell Culture Methods:

Human embryonic kidney (HEK) 293 cells were developed as an immortal cell line, following transformation with sheared adenoviral DNA (Graham et al., 1977) and are used extensively as an expression tool for recombinant proteins. Although epithelial in origin, the cells' biochemical machinery is able to reproducibly express large-scale, functional, recombinant proteins with high efficiency whilst maintaining any essential post-translational modifications. Importantly, HEK293 cells have no endogenous RyR2 expression (Du et al., 1998), ensuring that the isolated proteins were derived from the transfected plasmid.

2.4.2.1. Maintenance and sub-culture of HEK293 cells:

All cell culture work was undertaken in a designated laboratory in HEPA filtered class II laminar flow containment hoods. Cells were incubated at 37°C, gassed with 5% CO_2, 98% humidity and typically grown in T75 cm^2 culture flasks in the presence of 10ml supplemented (section 2.1.7, (A)) Dulbecco's Modified Eagles Medium (DMEM). To maintain a healthy adherent cell population, routine sub-culturing (passage) of the cell monolayer (at ~80% confluency) was essential to prevent over confluence and cell death. Cells were detached from the culture flasks by trypsinisation (incubated with the cells for no longer than 5 minutes), after washing with 10ml 0.9% w/v saline solution. Dissociated cells were collected as a cell suspension in cDMEM (10ml) and typically 1-1.5ml was subsequently centrifuged at 1000 x*g* for 5 minutes before the resultant pellet was resuspended in 10ml cDMEM and placed into a fresh sterile T75 cm^2 culture flask for further growth.

2.4.2.2. Calcium phosphate transfection of HEK293 cells:

The eGFP-hRyR2 and luminal accessory protein transfection protocol is described in further detail in Chapter 3, section 3.2.3. To generate calcium phosphate-DNA precipitates, plasmid DNA (12µg DNA per $8x10^5$ cells) was mixed with 124mM $CaCl_2$ solution (pH 7) and dH_2O to a total volume of 500µl; and subsequently added dropwise to 500µl of warmed 2x HBS (pH 7.05), (section 2.1.7 (F)) with continuous vortexing. To allow precipitate formation, the DNA/$CaCl_2$/HBS mix was incubated for 20 minutes at room temperature, before adding dropwise (1000µl/plate) to the cell monolayer. It was essential that this process formed a fine precipitate (i.e., not clumpy), such that the DNA could be actively introduced into the cells by endocytosis. Cells were incubated at 37°C, 5% CO_2 for 24 hours before upregulation of expression with 2mM NaB, and determination of

transfection efficiency (see Chapter 3, section 3.3.5), following a further 24 hour incubation. Harvested by trypsinisation, the total cell numbers were established using a haemocytometer, before being pelleted by centrifugation (1000 xg, 5 minutes) and stored at -80°C.

2.4.2.3. Effectene® transfection of stable cell lines:

Described in Chapter 3, section 3.3.4, stable cell lines were transfected using Effectene® reagent (Qiagen). To prepare for Ca^{2+} imaging (section 2.4.3.9), the stable cells were seeded at a density of $1x10^5$ cells into 35mm glass bottom dishes (MatTek™ Corporation), which were coated with poly-lysine before seeding. The cells were maintained in 200 µl menisci of cDMEM for 4-5 hours (to encourage adhesion) before adding 2ml fresh cDMEM to each well and incubating overnight at 37°C, 5% CO_2 before transfection. Briefly, following the manufacturers guidelines, 0.2 µg of recombinant DNA (per micro well) was mixed with an enhancer and a DNA-condensing buffer, and incubated for 5 minutes (room temperature) before addition of the Effectene® reagent. Following incubation for 10 minutes at room temperature, the resultant condensed Effectene®-DNA complexes were mixed with cDMEM and added directly to the cells. Addition of the Effectene® reagent to the DNA generates micelle structures that are actively taken up by the cells.

2.4.3. Protein Biochemistry Methods:

2.4.3.1. Preparation of mixed membranes from transfected HEK293 cells:

Transfected cell pellets (produced as described in section 2.4.2.2, typically ~$100x10^6$ cells per pellet) were resuspended in ice-cold hypo-osmotic buffer (1ml for every $1x10^6$ cells) before two stages of cell lysis (on ice), (for composition of hypo-osmotic buffer, see section 2.1.9 (B) i). Cells were first lysed in a glass homogeniser (x20 strokes) to manually disrupt the cells, followed by passing the homogenate 20x through a sterile 23G needle (BD Microlance™) aided by the use of an automated cell homogeniser (the "montygeniser", designed and constructed by Richard Montgomery, illustrated in Figure 2.3, A). The resultant homogenate was centrifuged at 2700 rpm (1200 x*g*) for 15 minutes, at 4°C (using an Allegra™ 6R centrifuge (Beckman Coulter)) and the supernatant collected (whilst the pellet consisting of cell debris and nuclear fraction was discarded). Microsomal membranes were collected by high-speed centrifugation for 90 minutes at 28,000 rpm (100,000 x*g*), 4°C, using an Optima L-90K ultracentrifuge (50.2 Ti fixed angle rotor (Beckman Coulter). Membranes were resuspended in 'solution C' (section 2.1.9 (B)

ii) and homogenised further using a glass homogeniser, before storing as 30µl aliquots at -80°C, following flash freezing in liquid nitrogen.

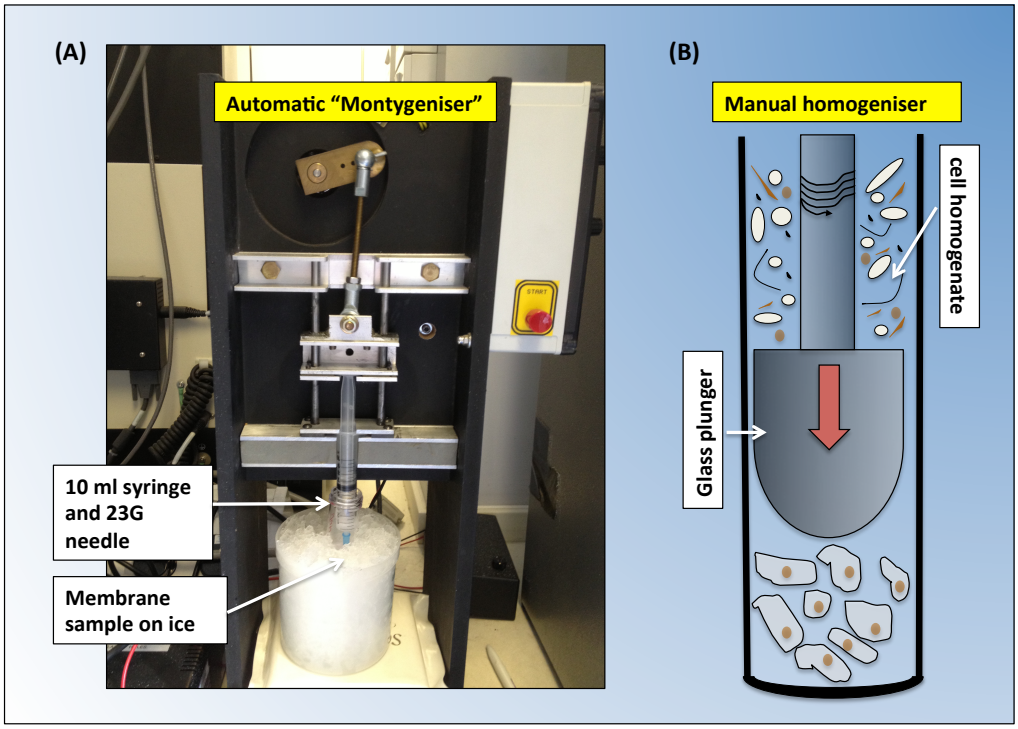

Figure 2.3: Apparatus used to homogenise transfected HEK293 cell pellets: *(A) Illustrates the automatic cell homogeniser and (B) is a schematic of a manual glass homogeniser.*

2.4.3.2. Protein assay and analysis of protein expression:

Total protein in all samples was quantified using the BCA™ system (Thermo Scientific). This kit uses bicinchoninic acid (BCA) as the detection reagent for Cu^{+1} (univalent copper), formed when protein reduces Cu^{2+} in an alkaline environment. The chelation of two BCA molecules with one cuprous ion (Cu^{+1}) generates a purple coloured reaction product. The absorbance of which at 595 nm can be read using a spectrophotometer. Dilutions (1/50, 1/100 and 1/200) of membrane samples along with protein standards (0-500µg/ml BSA) were mixed with the kit reagents according to the manufacturers guidelines, before incubating at 30°C for 20 minutes for chromogenic development. Absorbance readings at 595nm were taken using a Labsystems Multiscan™ spectrophotometer and Genesis software. A standard curve was plotted of absorbance (595nm) vs. protein concentration (µg/ml). Sample protein concentration was derived from the values given by the standards, using the linear equation y=mx+c. Protein expression levels were ascertained by Western blot analysis following separation by SDS-polyacrylamide gel electrophoresis (SDS-

PAGE). Densitometric analysis of Western signals was used to standardise protein samples for expression level before use in further investigations.

2.4.3.3. SDS-PAGE gel electrophoresis:

eGFP-hRyR2 protein samples were separated using a 4% acrylamide gel (supplemented with 1% agarose to strengthen), whilst luminal proteins were resolved on a 10% gel. Gels were cast and run using the Bio-Rad mini-gel apparatus. Separating gels were prepared as in Table 2.5 and set (~1 hour) between glass plates, assembled into a gel casting system. A stacking gel mixture (4% used for all proteins detected) was layered on top of the separating gel (with an inserted comb to form loading wells) and left to set for ~45 minutes. To prepare the samples for electrophoresis, the proteins were denatured in the presence of SDS-containing loading buffer, for 20 minutes at 42°C. The buffer also contained 10% ß-merceptoethanol, a reducing agent that prevented the formation of protein aggregates. A Kaleidoscope protein MW marker (Bio-Rad) was loaded alongside the protein samples. Gel electrophoresis was carried out at a constant current (typically 20 mA) and run until the appropriate coloured MW markers were resolved.

Separating acrylamide gel composition			
Reagents	Typical Volumes (µl)		Final concentration
	4%*	**10%****	
Acrylamide/Bis (37:5:1) 40%	1000	2500	Dependent on % acrylamide used
Tris-HCl 1.5M, pH 8.8	2500	2500	25% (v/v)
SDS 10%	100	100	1% (v/v)
Ammonium Persulphate 10%	50	50	0.5% (v/v)
TEMED	5	5	0.05% (v/v)
dH_2O (supplemented with 1% agarose in 4% gels)	6345	4845	Up to a final volume
Gel **%** determined according to the size of the proteins to be separated and is indicative of the amount of acrylamide required.			
* Used for running WT and mutant hRyR2 protein. ** Used for running luminal accessory proteins.			

Table 2.5: Components used to prepare SDS-PAGE gels: *The composition of SDS-PAGE 4% and 10% separating gels are shown. Stacking gels were all 4% and prepared as described above (4% separating gel) but the Tris-HCl 1.5M, pH 8.8 was replaced with Tris-HCl 0.5M, pH 6.8.*

2.4.3.3.1. Protein transfer onto a polyvinylidene difluoride (PVDF) membrane:

The separated proteins were transferred onto a PVDF membrane (Immobilon-P, Millipore) using either a semi-dry system (Bio-Rad), for CSQ2/JUN transfer or an iBlot™ dry blotting system (Life Technologies) to transfer eGFP-hRyR2. The iBlot™ system was chosen for hRyR2 analysis because of the reduced transfer time (14 minutes) required compared to using the semi-dry blotting technique (4 hours), but with equivalent transfer efficiency. For semi-dry transfer, the PVDF membrane was soaked in methanol for 1 minute, then for a further 45 minutes in transfer buffer, along with the SDS-PAGE gel (soaked for 5 minutes) and filter paper. The transfer apparatus was assembled as follows: the SDS-PAGE gel was placed on top of the PVDF membrane and both were sandwiched between six pieces of soaked filter paper. A roller was used to remove air bubbles. 'Semi-dry' transfer of CSQ2 and JUN was carried out at 400mA (limited to 25V) for 50 minutes at 4°C. Protein transfer using the iBlot™system was carried out using specialised iBlot™ gel transfer stacks (Life Technologies), eliminating the need for any pre-soaked membranes/filter paper and transfer buffer. Based on a dry blotting concept, the iBlot™ transfer stacks consisted of: (1) an anode stack (on top of which the pre-activated PVDF (0.2μM) membrane was placed), (2) a cathode stack (with the SDS-PAGE gel placed underneath, on top of the membrane) and (3) a disposable sponge with metal contact to associate the electrodes of the iBlot™ device with the assembled gel stacks. The design of the iBlot™ system created a shorter distance between electrodes and thus enabled the generation of high field strength and currents, and enhanced transfer speed. The program selected for hRyR2 transfer consisted of a 13 minute run at 20V.

2.4.3.4. Immunodetection of Western Blotted proteins:

Immediately after transfer, membranes were incubated for 1 hour at room temperature in blocking solution (5% non-fat milk in TBS-T, see section 2.1.9 (A) vi) on a rocker. To enable immunodetection, the primary antibodies were prepared in 1% blocking buffer (section 2.1.9 (A) vii) and applied to the membrane as a 1/5,000 or 1/10,000 dilution, as recommended in the manufacturers guidelines (see section 2.1.6 for antibody details), and incubated for 2 hours at room temperature or overnight at 4°C. The membrane was subsequently washed 3 times (5 minute durations) with wash buffer (section 2.1.9 (A) vii) before further incubating the membrane with a horseradish peroxidase (HRP)-linked secondary antibody, chosen according the species within which the primary antibody was generated. Used as a 1/10,000 dilution in 1% blocking buffer, the secondary antibody was incubated with the membrane at room temperature for approximately 90 minutes. Before the final stage of detection, the membrane was washed five times (5 minute incubations)

with TBS-T buffer (section 2.1.9 (A) v), to remove any remaining traces of unbound antibody or milk solution.

To visualise the immunoreactive protein bands, enhanced chemiluminescence detection reagents were used (ECL™ Western blotting analysis system, Amersham™, GE Healthcare) according to the manufacturers guidelines. The membrane was then exposed to X-ray film (Amersham Hyperfilm™, GE Healthcare) for a suitable length of time, determined according to the intensity of the chemiluminescence signal detected using a Compact x4 x-ray film developer. The obtained immunoblots were subsequently used for densitometric analysis, undertaken using a GS-700 imaging densitometer and Quantity One® software (Bio-Rad).

2.4.3.5. [^{3}H] Ryanodine Binding Protocol:

The details of the [^{3}H] ryanodine binding assays undertaken in this project are discussed further in Chapter 4, sections 4.2.1-4.2.1.1. Each reaction contained 100µg of membrane proteins, 10nM [^{3}H] ryanodine and was prepared to a final volume of 500µl using ryanodine binding buffer (adjusted to a given free Ca^{2+} concentration). To control reactions, the final volume of binding buffer was adjusted to accommodate the addition of 10µM 'cold' (non-radiolabelled) ryanodine. All reactions were prepared in duplicate, materials outlined in section 2.1.9 (D) i-iv.

Following thorough mixing, the reactions were incubated in a water bath at 37°C for 90 minutes, at which equilibrium binding is achieved (Holmberg and Williams, 1990). To terminate the reaction, x10 excess (5 ml) ryanodine binding buffer was added. All reactions were then filtered through pre-soaked Whatman™ glass fibre filters (0.25 µM) under vacuum by attaching the filter apparatus to a Heto™ masterjet lab suction pump. The full apparatus is shown in Figure 2.4. At this stage, unbound [^{3}H]-ryanodine passed through the filter with washing, whilst eGFP-hRyR2 (and any bound [^{3}H]-ryanodine) was retained on the filter. Each filter was placed into a 10 ml scintillation vial (Fisher Scientific) and fully submerged in 5 ml Ultima™ Gold Scintillation Fluid (Packard Bioscience). All samples were mixed and incubated at room temperature for 24 hours before reading in a Packard (2100TR) liquid scintillation counter. Decontamination of used plasticware was carried out according to local rules.

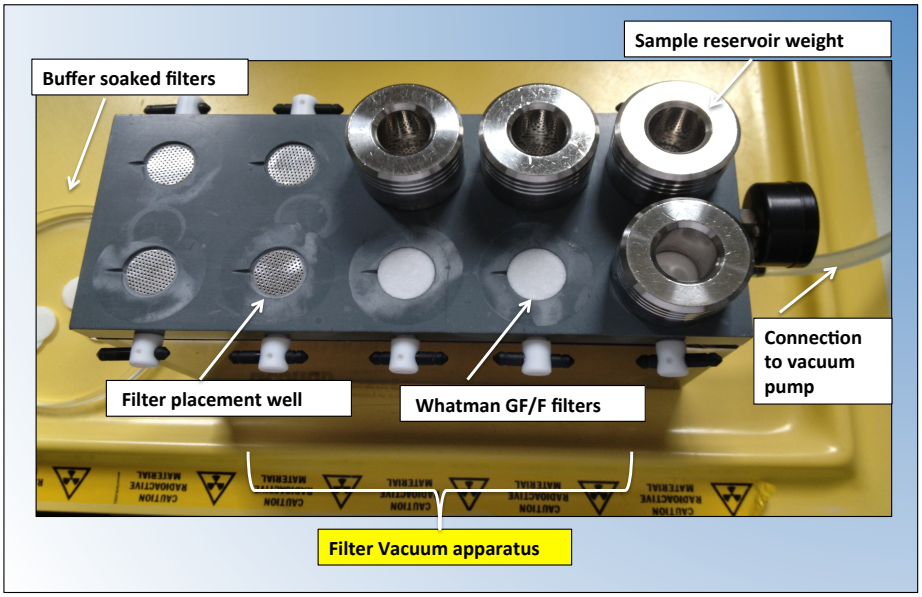

Figure 2.4: [^{3}H] Ryanodine binding filter apparatus.

2.4.3.6. Co-immunoprecipitation (Co-IP) of hRyR2 with luminal proteins:

Co-IP studies are described in Chapter 5 and were carried out using a μMACS™ GFP protein isolation kit (Miltenyi Biotec), (section 2.1.9 (F) i-iii), whereby WT and mutant eGFP-hRyR2 proteins and their interacting partners were isolated from solubilised membrane preparations using super-paramagnetic μMACS™ microbeads, conjugated to an anti-GFP monoclonal antibody. Using the same protocol described below, luminal protein associations were investigated using μMACS™ Protein A microbeads (Miltenyi Biotec).

All samples used for co-IP studies were first analysed by Western blot and densitometry to ensure that equal amounts of both WT and mutant eGFP-hRyR2 used. Using a solubilisation buffer, 1-1.5 mg of ER membranes were solubilised overnight at 4°C, before removal of any unsolubilised, unbound material using centrifugation (10 minutes, 11500 rpm (16,000 x*g*) in an Allegra 6R Beckman Coulter, at 4°C). All samples were made up to a total volume of 1 ml with solubilisation buffer and the appropriate volume of protease inhibitor. Anti-GFP paramagnetic microbeads (50μl, 50 nm in diameter) were mixed and incubated with the solubilised WT/mutant eGFP-tagged hRyR2 protein for at least 30 minutes, on ice.

To isolate the proteins bound to the anti-GFP-microbeads, the samples were applied to μMACS™ columns, which were equilibrated (with solubilisation buffer, section 2.1.9 (E) i) and placed into a μMACS™ separator (a magnetic stand, Miltenyi Biotec). μMACS™ columns are packed with steel spheres that enhance the magnetic field necessary to capture the μMACS™ microbeads and bound target protein/s. Assembly of the set-up is shown in Figure 2.5. The immunoprecipitates were applied to the μMACS™ columns where the magnetically labelled proteins were retained. The columns were washed four times with 200 μl solubilisation buffer, before a final wash step with 20 mM Tris, pH 7.4 (100 μl), ensuring removal of any non-interacting material (such as detergent and salt) that would interfere with analysis. The samples of interest were eluted in 50μl of an SDS-containing elution buffer (composition detailed in section 2.1.9), which was heated to 95°C in a hot block before use. Eluted proteins were analysed by SDS-PAGE and Western blotting.

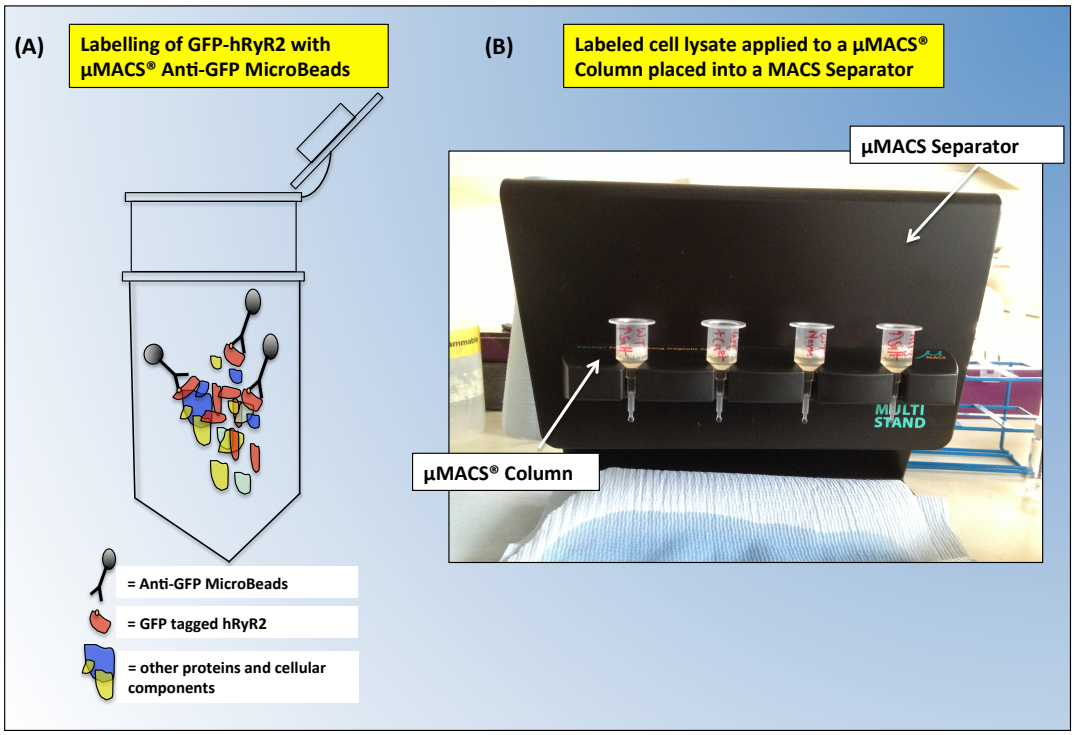

Figure 2.5: Co-immunoprecipitation investigations: *(A) Schematic of the labelling of eGFP-hRyR2 with µMACS™ anti-GFP microbeads, prepared within a microcentrifuge tube and incubated for at least 30 minutes (B) image of the µMACS™ column and separator apparatus used for immunoprecipitate isolation.*

2.4.3.7. Immunofluorescent co-localisation investigations:

Transfected HEK293 cells were collected and plated as a 200µl meniscus onto poly-lysine coated glass coverslips (22 x 22 mm) at a density of $8x10^4$ cells/coverslip, and left to adhere overnight at 37°C with 5% CO_2. The cells were washed three times in 1x phosphate buffered saline solution (PBS, section 2.1.8 (C)) before fixing with a 4% paraformaldehyde/PBS solution (pH 7.4) for 10 minutes in the dark. The fixed cells were washed and re-hydrated with PBS solution for 60-90 minutes before permeabilisation at room temperature in 0.1% v/v Triton X-100 in PBS for 30 minutes. The cells were further washed in PBS before blocking in 10% FCS (in PBS) for 30 minutes at room temperature. Primary antibody (used at 1/100) was then added as a 150µl meniscus in PBS, for 90 minutes at room temperature. Coverslips were then washed and incubated with a fluorescent secondary antibody (used at 1/250), again at room temperature for 90 minutes. Following three final wash steps in PBS and dH_2O, the coverslips were dried and mounted onto ethanol washed glass slides using Fluorsave™ (Millipore). The slides were left to dry for 30 minutes before storing at 4°C until required. The slides were visualised using a confocal Leica SP5 microscope (Leica, Heidelberg, Germany), with an oil immersion, 63x objective lens. Co-incident eGFP- and Alexa® Fluor- labelled cells were identified using the Leica LAS-AF software.

2.4.3.8. Loading of transfected HEK293 cells for Ca^{2+} imaging studies:

Cells for Ca^{2+} imaging investigations were prepared as described in section 2.4.2.3. Fluo-3 AM (50µg) was dissolved in 15µl DMSO containing 20% w/v Pluronic® F-127, making a 3mM stock. This was added to mDMEM at a concentration of 10µM and incubated with the cells at 30°C with 5% CO_2 for 45 minutes. Cells were then de-esterified in mDMEM for 10 minutes prior to Ca^{2+} imaging.

2.4.3.9. Ca^{2+} imaging protocol:

Fluo-3 loaded cells were imaged using a laser scanning confocal microscope (Leica SP5, Leica, Heidelberg, Germany), with an oil immersion, x63 objective lens and Argon laser, controlled with Leica software. To visualise Ca^{2+} dependent Fluo-3 fluorescence, excitation was initiated at a wavelength of 488 nm and fluorescence detected by a photomultiplier tube (PMT) at 520±28. To view, the cells were immersed in a 200µl meniscus of Krebs-Ringer-Hepes (KRH) buffer containing 1.3 mM $CaCl_2$ (section 2.1.8 (G)) and spontaneous Ca^{2+} release events were imaged (5 frames/second) for 2 minutes at 512 x 512 pixel resolution. To estimate cell ER load, the transient amplitude following 10 mM caffeine addition was assessed. A caffeine response also verified the presence of functional RyR2 channels.

Chapter 3

Generation of recombinant luminal accessory protein constructs and co-expression with wild type and mutant hRyR2

3.1 Introduction:

It is now well accepted that in addition to the diverse range of interacting proteins reported to regulate hRyR2 activity from the cytosolic side of the channel, luminal accessory proteins also play a prominent role in Ca^{2+} release regulation. In particular, a quaternary complex located at the junctional SR membrane, comprising: RyR2, the Ca^{2+} buffering protein CSQ2 and two SR transmembrane proteins JUN and TRD1, are thought modulate the ability of RyR2 channels to sense changes in SR luminal [Ca^{2+}] (Zhang et al., 1997, Dulhunty et al., 2012). While defective Ca^{2+} sensing by RyR2 is a candidate mechanism in CPVT, it is unknown if mutant channels respond to or interact differently with luminal accessory proteins; a concept investigated in this project.

3.1.1 Regulation of ryanodine receptor Ca^{2+} release by luminal accessory proteins at the junctional domain of the sarcoplasmic reticulum membrane:

A detailed understanding of precisely how CSQ2, JUN and TRD1 modulate normal SR Ca^{2+} cycling (and specifically RyR2 function) as a complex or individually, is an active area of research (Beard et al., 2009, Lee et al., 2012, Rossi et al., 2014). Investigations using overexpression/knockout CSQ2/JUN/TRD1 animal models or *in vitro* techniques have provided us with an insight into how the luminal proteins may control normal SR Ca^{2+} cycling, however some functional differences have been reported (as highlighted in Chapter 1 (Tables 1.1-1.3)) which likely reflect species variability or inconsistencies between experimental conditions.

To exemplify this, single channel investigations carried out by Györke et al (2004) with dog isoforms of the luminal accessory proteins demonstrated that CSQ2, when added back to the RyR2/JUN/TRD complex inhibited channel activity (decreased RyR2 P_o); whilst Wei et al (2009b) with cardiac isoforms isolated from sheep, reported that CSQ2 activated RyR2 channels (increased P_o) when associated with RyR2/JUN/TRD1 in a lipid bilayer system (Wei et al., 2009b). Discrepancies in studies of protein-protein interaction have also been attributed to differences between species (Qin et al., 2009), whereby at physiological concentrations of luminal Ca^{2+}, Zhang et al (1997) demonstrated an interaction between dog JUN and CSQ2, whilst using similar conditions no binding between rabbit JUN and CSQ2 was evident (Qin et al., 2009). Across species, CSQ2 shares ~75% homology (Prins and Michalak, 2011, Beard et al., 2004), whilst both JUN and TRD1 display their greatest divergence in C-terminal regions (Lim et al., 2000, Marty et al., 2009). Human, rabbit and dog JUN sequences for example, demonstrate ~97% homology in N-terminal

and putative transmembrane domains among species, but <72% similarity in C-terminal sequence (Wetzel et al., 2000), which could explain disparities in functionality. Thus, in order to reliably investigate the physiological roles of CSQ2, JUN and TRD1 in the human heart, human isoforms of the luminal accessory proteins should be used. *In vitro* techniques however have proved more useful for closely investigating the molecular mechanisms and protein-protein interactions that mediate RyR2 luminal Ca^{2+} sensitivity (Zhang et al., 1997, Lee et al., 2012). In transgenic animal models with gene-targeted over-expression, down regulation or complete ablation of CSQ2, JUN or TRD1 (Jones et al., 1998, Fan et al., 2008, Chopra et al., 2009, Altschafl et al., 2011), compensatory mechanisms are often reported, such as down regulation of other critical EC coupling proteins or structural remodelling (as in Chopra et al., 2009). As a consequence, the observed alterations in cellular Ca^{2+} homeostasis cannot be confidently attributed to one particular luminal component or their role as a complex confidently established (Dulhunty et al., 2012).

Taking the aforementioned into consideration, a recombinant approach has been employed in this project, firstly to explore how the sensitivity of RyR2 channels to cytosolic and/or luminal Ca^{2+} may be modulated by luminal accessory protein co-expression and to assess the protein-protein interactions between them. To provide a simplified model by which luminal accessory protein regulation of RyR2 channels could be investigated (without the presence of other specialised SR proteins complicating findings), the recombinant proteins were expressed a mammalian HEK293 cell system, which does not endogenously express RyR2 or any associated proteins. Allowing the proteins to assemble *in situ*, without the need for purification, the combination of luminal accessory protein(s) co-expressed with RyR2 channels (for example, CSQ2 alone with hRyR2 or in the presence of JUN) could be manipulated. Furthermore, expression of recombinant RyR2 in HEK293 cells enabled the functional effects of CPVT-linked RyR2 mutations found in cardiac disease to be examined (Thomas et al., 2010). Although defective cytosolic/luminal Ca^{2+} sensing has been reported as a common mechanism in CPVT pathogenesis (Terentyev et al., 2006, Jiang et al., 2005), it is unknown if mutated RyR2 channels respond differently to luminal accessory protein regulation or if their association is altered. Thus, the response and interaction of mutant hRyR2 channels (N4104K and A4556T) with the luminal proteins has also been explored in this investigation, and directly compared with data obtained using WT hRyR2.

3.1.2 Chapter Objectives:

HEK293 cells are currently the most widely used RyR2-deficient cell line (Du et al., 1998) for studies of recombinant RyR2; and have been used extensively by Professor Wayne Chen (University of Calgary, Canada) to study the molecular mechanisms underlying Ca^{2+} release through RyR2 channels and spontaneous Ca^{2+} release events seen with channel mutation (Jiang et al., 2002, 2004, 2005; Li and Chen, 2001). This expression system has also been used previously by the Williams laboratory to investigate the Ca^{2+} handling dynamics of both WT and mutant RyR2 channels (Euden et al., 2013, Thomas et al., 2005, 2004) and as a vehicle for RyR2 expression prior to purification and use in single-channel investigations (Mukherjee et al., 2012, Mason et al., 2012). The benefits of using a mammalian cell system for human recombinant protein expression are significant, since any post-translational modifications such as glycosylation, which is important for junctional SR trafficking (Kiarash et al., 2004) are likely to be native or near-native (Hopkins et al., 2012); and the expressed proteins are able to associate within a mammalian cell environment (section 3.3.5). This chapter will focus exclusively on generating the luminal accessory protein constructs and optimising recombinant protein co-expression in a heterologous HEK293 cell system. Specifically, the following strategies will be discussed:

(1) Amplification of cDNA encoding CSQ2, JUN and TRD1 from a human cardiac muscle library with a view to clone and express each protein alone and in combination with WT and mutant eGFP-hRyR2.

(2) Selection of an appropriate vector system for luminal accessory protein stable cell line generation in HEK293 cells for Ca^{2+} imaging studies (Chapter 4) and optimisation of expression conditions such that sufficient hRyR2/CSQ2/JUN expression levels are obtained for [^{3}H] ryanodine binding (Chapter 4) and immunoprecipitation studies (Chapter 5).

3.2 Methods:

3.2.1. Strategies used for cloning and expression of luminal accessory protein constructs:

- ***Junctin and Triadin (isoform 1, TRD1)***

PCR amplification (section 2.4.1.1, Tables 2.1 and 2.2) was used to isolate the open reading frames (ORFs) of human cardiac muscle JUN and TRD1 *in vitro*, from a human cardiac muscle complementary DNA (cDNA) library (BD biosciences). PCR primers designed to the desired luminal accessory protein cDNAs (NCBI accession numbers: AF184241 (cardiac JUN), U18985 (TRD1 skeletal), U31540 (TRD1 rabbit) and AF165915 (TRD1 dog) are shown in Figure 3.1 (also see results, section 3.3.1). The components of each PCR reaction are outlined in Table 2.1. Several different primers were used in attempts to amplify human cardiac muscle TRD1 (Figure 3.1, B), however this was unsuccessful (see section 3.3.1.).

- ***Calsequestrin (isoform 2, CSQ2)***

The coding sequence for human cardiac muscle CSQ2 (accession number: NG_008802) was obtained by direct cloning from an existing expression construct (obtained from Dr N.L Thomas, cloned into the pECFP-N1 vector and inserted at the *XhoI*/*SacII* sites). The full open reading frame including kozak sequence and a TAG stop codon was digested from pECFP-N1-CSQ2 using restriction enzymes *XhoI*/*ApaI* and ligated directly into pcDNA3.1™hygro$^{(+)}$ (ligation reaction outlined in section 2.4.1.9, Table 2.4).

All constructs were verified at each cloning stage by restriction mapping (using NEB cutter) and digest, followed by automated sequencing (sections 2.4.1.7-2.4.1.8). To sequence JUN and TRD1 amplicons, cDNAs were cloned into the Zero Blunt® II TOPO® vector (Life Technologies), transformed into bacterial cells and propagated to sufficient quantities, as outlined in Chapter 2, sections 2.4.1.4-2.4.1.6 and 2.4.1.10-2.4.1.11. Clones containing the desired insert were sequenced using the protocol described in section 2.4.1.8. Those successfully verified were subsequently cloned into the mammalian expression vector pcDNA3.1™hygro$^{(+)}$ (section 2.4.1.9), following PCR amplification using primers containing restriction sites for *BamHI* and *NotI* endonucleases (Figure 3.1, shown in bold). The resultant amplified fragment was cut with *BamHI* and *NotI* to enable ligation into the multiple cloning site of the similarly digested pcDNA3.1™hygro$^{(+)}$ vector. Restriction digest

and further automated sequencing was used to confirm ligation of the luminal proteins (CSQ2 and JUN) into pcDNA3.1™hygro$^{(+)}$.

(A)

pcDNA3.1hygro$^{(+)}$-JUN Forward: 5'CCGCAG**GGATCC**ACCATGGCTGAAGATAAAGAG3'
clamp ***BamHI*** hJUN sequence

pcDNA3.1hygro$^{(+)}$-JUN Reverse: 3'CCATC**GCGGCCGC**TTAGCCGTTTCTTTTCTGGGT5'
clamp ***Not I*** hJUN sequence

(B)

pcDNA3.1hygro$^{(+)}$-TRD Forward: 5'CCGCAG**GGATCC**ACCATGACTGAGATCACTGCTG3'
clamp ***BamHI*** cTRD sequence

(i) pcDNA3.1hygro$^{(+)}$-TRD Reverse: 3'CCATC**GCGGCCGC**TTACTGTCCTTGTTGCTTCTG5'
clamp ***Not I*** cTRD sequence

(ii) Matchmaker AD pACT2 Reverse: 3'GTGAACTTGCGGGGTTTTTCAGTATCTACGA5'

(iii) Non-specific-TRD Reverse: 3'CCAYTGNATYTGYTTYTTNCCNAGNGT5'

Figure 3.1:

(A) Luminal accessory protein forward (5') and reverse (3') primers used in PCR isolation of junctin from a human cardiac muscle cDNA library. *The primers were designed to contain restriction sites for BamHI (forward primer) and Not I (reverse primer), found in the multiple cloning site of the mammalian expression vector pcDNA3.1hygro$^{(+)}$. Human cardiac muscle JUN exists as a splice variant of the ASPH gene, encoding aspartyl ß-hydroxylase (AspH) (Jones et al., 1995).*

(B) Primer combinations used in the attempt to isolate cDNAs encoding human cardiac muscle triadin. *Initial PCR reactions were carried out using primers designed to contain BamHI and NotI restriction sites. The sequence for human cardiac muscle TRD, isoform 1 (TRD1) was unknown at the time of this work and thus the human sequence for the skeletal isoform and rabbit and dog cardiac sequences were consulted for primer design. The forward primer (5') was designed to a conserved region found in all known TRD isoforms, established using BLAST. However, since the C-terminal regions of each isoform differed in sequence (and each protein differed in size between species), the reverse (3') primer was designed to the C-terminal end of human skeletal TRD (i). Due to unsuccessful PCR amplification of TRD1, alternative reserve primers were used in additional reactions as shown in (ii) and (iii), with the intention that the resultant product could subsequently be used as a template for further amplification using the reserve primer containing the Not I site. This will be discussed further in section 3.3.1.*

3.2.2. Comparison of G418 and hygromycin mediated selection of luminal accessory protein expressing stable cell lines:

Hygromycin and G418 (Geneticin Sulphate) are often used as positive selection markers for stable protein expression, where only cells expressing the gene of interest display antibiotic resistance (Massignan et al., 2010). As a consequence, transfected cells lacking permanent integration of the recombinant DNA are subsequently eliminated upon antibiotic treatment. Prior to producing the stable cell lines, comparisons were made between the effectiveness of the two antibiotics on HEK293 cells, and an optimal selection concentration established.

To determine a working concentration of G418 or hygromycin treatment that would enable long-term selection of HEK293 cells stably expressing the luminal proteins, a series of kill curves were constructed (n=3 curves formulated for each antibiotic dose range). Untransfected HEK293 cells were plated into 6 well culture dishes, seeded at a density of 1 x 10^6 cells/well and once at ~80% confluency (~24 hours later), exposed to increasing concentrations of G418 or hygromycin (100µg/ml-1000µg/ml). The cells were incubated in the presence of the given antibiotic for 48 hours before analysis.

To generate each stable cell line, HEK293 cells transfected with CSQ2, JUN or CSQ2+JUN were cultured in the presence of the chosen antibiotic (400µg/ml hygromycin). To achieve a clonal population, the cells were subjected to a limiting serial dilution, achieved by diluting a harvested stable cell population in excess cDMEM containing hygromycin and plating out the generated cell suspension in a series of 1/10 dilutions across a 96 well plate, until only ~1 cell/well was evident. Isolated cells were grown to confluency in 96 well plates before seeding the cell populations into T75 cm^2 culture flasks for further growth, and positive selection with hygromycin treatment (approximately 28 days to obtain a confluent (70-80%) flask).

3.2.3 Optimisation of eGFP-hRyR2 expression in HEK293 cells using calcium phosphate mediated transfection:

To establish an effective, reproducible method of achieving high levels of recombinant gene expression, it was imperative that the transfection protocol was first optimised. eGFP tagged full-length WT and mutant (N4104K and A4556T) hRyR2 mammalian expression constructs (obtained from Dr Chris George and Dr N. Lowri Thomas (Cardiff University), respectively) allowed the transfection efficiency, established from using two different

calcium phosphate ($CaPO_4$) protocols, to be effectively estimated (section 3.3.5). To optimise WT hRyR2 expression, the following protocols were compared:

(1) Protocol A was designed by Dr N.L Thomas (modified from Sambrook et al, 1989) and used previously to express eGFP-hRyR2 for Ca^{2+} imaging investigations (as used in Thomas et al, 2005).

(2) Protocol B was designed by Professor.W.Chen (modified from Chen and Okayama, 1987) and used to express high levels of mouse RyR2 for single channel analysis (Li and Chen, 2001, Jiang et al., 2002).

To establish optimum conditions that would consistently generate high protein expression, the transfection variables most likely to affect transfection efficiency were considered:

(i) ***Cell density:*** HEK293 cells were transfected at either ~75% (Thomas et al., 2005) or ~30% (Jiang et al., 2002) confluency, achieved by plating the cells at higher ($8.5x10^4$ cells/cm^2, plated into a 6 well culture dish with a growth area of $9.6cm^2$ ($8x10^5$/well)) or lower ($1.5x10^4$ cells/cm^2, plated into a $10cm^2$ petri-dish with a growth area of $55cm^2$ ($8x10^5$/dish)) starting cell densities respectively. Sparse distribution of cell populations will increase the surface area over which the condensed DNA/Ca^{2+} precipitates can be endocytosed likely leading to higher transfection efficiencies. However, a high DNA/cell ratio can result in a cytotoxic effect suggesting the cells need to be at a sufficient confluency before transfection, without being too confluent to result in too low a transfection efficiency or detachment of fully confluent sheets of cells.

(ii) ***DNA concentration:*** Expressed as the quantity of DNA/cell (estimated according to the starting cell number), comparisons were made between the use of 5 pg DNA/cell (4µg DNA per $8x10^5$ cells), (Thomas et al., 2005) and 15 pg DNA/cell (12µg DNA per $8x10^5$ cells), (Jiang et al., 2002). Higher DNA concentrations can reduce cell growth and may become cytotoxic, especially if the cell density is too low. In addition overexpression could promote protein malfunction. However, use of lower DNA concentrations may limit $CaPO_4$ precipitate formation and uptake and as a consequence, produce lower transfection efficiencies.

All transfection reactions were formed by adding the DNA and $CaCl_2$ to 2x HBS with vigorous vortexing, followed by incubation of the transfection mix at room temperature (20 minutes), to allow precipitates to form before adding to the cell monolayer. The cells were incubated for 24 hours, before the addition of 2mM sodium butyrate (NaB) to culture

medium, which upregulates transcription (Gorman et al., 1983, George *et al*., 1998). The cells were incubated for a further 24 hours (in the presence of NaB), before the transfection efficiency was established. Chapter 2, sections 2.4.2-2.4.2.1 and 2.4.3.1 further describes culturing and harvesting of transfected HEK293 cell populations. Transfection efficiencies were calculated as outlined in section 3.3.5.

3.2.4. Co-expression of luminal accessory protein constructs with wild type and mutant eGFP-hRyR2 in HEK293 cells:

Using an optimised $CaPO_4$ precipitation protocol (sections 3.2.3 and 3.3.5), the luminal accessory protein constructs were co-transfected in an equimolar ratio with WT or mutant eGFP-hRyR2. Typical DNA concentrations used per reaction (12 µg total) are summarised below (Table 3.1). Each cell population was harvested 48 hours post-transfection and microsomal membrane vesicles subsequently isolated from these cells, as described in section 2.4.3.1.

Transcript Length:	**hRyR2+CSQ2+JUN**	**hRyR2+CSQ2**	**hRyR2+JUN**
hRyR2 15,219 bp	10.7 µg (89%)	11 µg (92%)	11.5 µg (95.6%)
CSQ2 1216 bp	0.80 µg (6.7%)	1 µg (8%)	-
JUN 678 bp	0.5 µg (4.3%)	-	0.5 µg (4.4%)
Total DNA	12 µg	12 µg	12 µg

Table 3.1: Co-expression of hRyR2 and luminal accessory proteins was achieved by transfection of cDNA constructs in an equimolar ratio: *WT/mutant hRyR2 were transfected in equimolar quantities with each of the luminal proteins, individually (CSQ2/JUN) or in combination (CSQ2+JUN). The DNA transfection ratio was calculated according to the relative length of the transcripts.*

3.3 Results:

3.3.1 PCR amplification of cDNA sequences encoding the luminal accessory proteins JUN and TRD1 from a human cardiac muscle cDNA library:

- ***Isolation of JUN cDNA***

Using the primers detailed in Figure 3.1 (A), initial PCR amplification from the human cardiac muscle cDNA library yielded a band of the expected molecular weight for human cardiac muscle junctin (~700bp, Table 3.2). However, the target DNA amplified in the initial PCR reaction (PCR1) was not of sufficient quantity for gel extraction and needed further enrichment (as described in section 2.4.1.1). As demonstrated in Figure 3.2 (A) sufficient quantities of the target JUN cDNA were generated by a second PCR reaction (PCR2), achieved using the PCR1 recovered cDNA as a template (Table 2.1, section 2.4.1.1). The desired fragment was subsequently gel extracted to eliminate non-specific amplification products and purified using a QIAEX® II kit (Qiagen), the recovery of which is shown in Figure 3.2 (D).

- ***Isolation of TRD1 cDNA***

Using primers designed to try and target the cardiac protein (Figure 3.1, B), PCR isolation of human TRD1 generated four distinct cDNA fragments (Figure 3.2, B (i)), but did not yield any products with the predicted molecular weights of ~950-1000bp, expected of TRD1 (Table 3.2). The bands closest to this predicted molecular weight were evident at ~600bp or ~1600bp (indicated with an asterisks in Figure 3.2, B (i)), which were subsequently sequenced. In further attempts to isolate TRD1, the variant known to be the predominant isoform expressed in the myocardium (Kobayashi and Jones 1999, Roux-Buisson et al., 2012) and thus the target in this project, the amplification strategy was consequently re-designed. Since TRD isoforms seem to be well conserved in their N-terminal sequences, showing great variability in their C-terminal tail (due to differential splicing, Feng et al., 2009), the original 5' primer was used with less specific 3' ones. A series of additional PCR reactions were carried out using the primers outlined in Figure 3.1 B, (ii) and (iii), with the idea that the generated amplicons could be subsequently used as templates for additional amplification using the pcDNA3.1hygro$^{(+)}$-TRD specific primers.

In an attempt to amplify TRD1, repeat PCR reactions were carried out using the forward 5' pcDNA3.1hygro $^{(+)}$-TRD primer and the following alternative 3' reverse primers:

(1) Matchmaker (pACT-2 specific) 3' AD, targeting the human cardiac muscle cDNA library cloned into the pACT2 vector (Clontech).

(2) A "non-specific" 3' TRD primer designed to the 3' end of the known TRD sequences and targeted towards conserved regions within the sequence (established using BLAST).

The two PCR reactions yielded some prospective clones, with fragments at ~1000bp Figure 3.2, B, (ii) and ~1500bp, Figure 3.2, B, (iii) being of particular interest, since they appeared at the expected molecular weight of TRD1.

3.3.1.1 Isolation of cDNA encoding CSQ2 from a pECFP-N1 expression vector:

A double digest with restriction enzymes *XhoI* and *ApaI* was used to excise the coding sequence for human cardiac muscle CSQ2 from a pECFP-N1 expression vector (section 3.2.1). As highlighted in Figure 3.2 (C), the digest yielded two fragments at ~4486, corresponding to cut pECFP-N1 vector, and ~1200bp, which was at the correct molecular weight of the desired CSQ2 target (Table 3.2). Gel extraction and purification of this band generated a sufficient cDNA recovery as shown in Figure 3.2 (D).

Accessory protein:	Base Pairs:	Protein size in kDa
CSQ2	**~1200 bp**	**~45 kDa** (Scott *et al*., 1988)
JUN	**~700 bp**	**~26 kDa** (Jones *et al*., 1995)
TRD1	**~950-1000 bp**	**~35 kDa-40kDa** (Kobayashi and Jones, 1999), or **~37 kDa** (Roux-Buisson *et al*., 2012)

Table 3.2: Predicted molecular weights of CSQ2, JUN and TRD1. *Highlighted are the molecular sizes of each luminal accessory protein cDNA in base pairs (bp), and estimates of their protein size in kilodaltons (kDa). TRD1 is thought to exist in two forms, glycosylated and deglycosylated, reported by Kobayashi and Jones to be appear as 40 and 35 kDa, respectively with Western anaylsis. However, Roux-Buisson et al., 2012, reported that TRD1 appears as a double band at 37kDa (with no 5 kDa difference evident). Although CSQ2 has been predicted to exist in numerous glycosylated and phosphorylated states (12 structural forms in native heart tissue), all are predicted to run as a single band in SDS-PAGE analysis (Scott et al., 1988, O'Brian et al., 2002).*

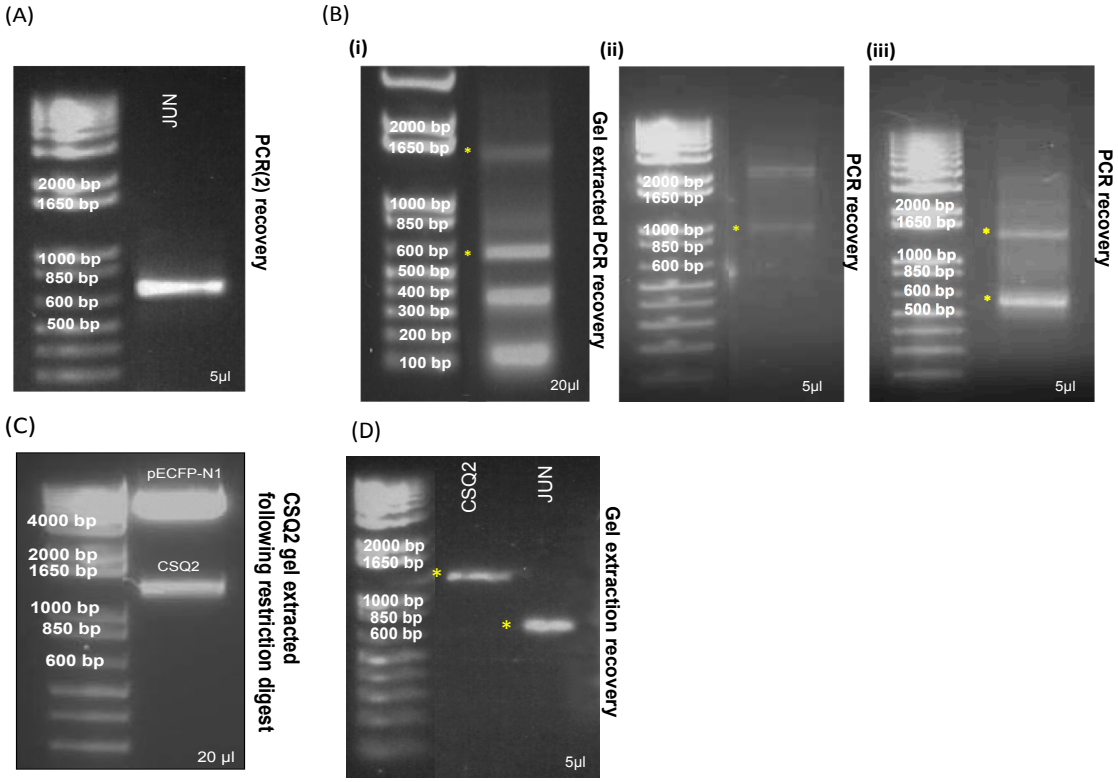

(E)

	Expected product size:	Generated product size:
CSQ2	~1200 bp	~1200 bp
JUN	~700 bp	~ 700 bp
TRD1	~950-1000 bp	**(i)** **Band 1:**1600 bp, **Band 2:** 600 bp, **Band 3:** 400 bp **Band 4:** 150 bp **(ii)** **Band 1:** 2100 bp, **Band 2:** 1000 bp, **(iii)** **Band 1:**1500 bp **Band 2:** 550 bp

Figure 3.2: Agarose (1%) gel electrophoresis to visualise PCR and gel extraction products: *A fragment corresponding to amplified JUN cDNA appeared at the expected molecular weight (MW) of ~700 bp* ***(A)****. Initial attempts at PCR amplification of cardiac TRD1 generated four distinct fragments, which were not at the MW expected for the cardiac isoform* ***(B),(i)****. The amplification strategy was designed as discussed in section 3.3.1. Using a 3' reverse primer designed to target the pACT2 vector (into which the human cardiac muscle cDNA library was cloned), a fragment at ~1000bp evident in the PCR reaction was of particular interest as it appeared at the expected MW of TRD1* ***(B),(ii)****. An additional PCR reaction carried out using a "non-specific" 3' reverse primer, designed to target conserved regions within the C-terminus of the known TRD sequences, generated distinct fragments at ~1500bp and ~550bp* ***(B),(iii)****. CSQ2 cDNA was excised from an existing pECFP-N1-CSQ2 expression construct (section 3.2.1) by a double digest with XhoI/ApaI, the desired fragment at ~1200bp was subsequently gel extracted and purified* ***(C)****. Isolation of CSQ2 and JUN cDNA appeared successful, where fragments indicative of the two luminal proteins (~1200bp and ~700bp, respectively) was evident in the gel extraction recovery* ***(D)****. The expected product sizes corresponding to luminal accessory protein cDNA, compared with those obtained, are summarised in* ***(E).*** *All bands highlighted by asterisks were isolated and sequenced as outlined in section 3.3.2. A 1 kb DNA ladder was used in all gels shown. Where cropped for presentation purposes, the original photos will be shown in the Appendix, Figure 1.*

3.3.2 Sequence verification of luminal accessory protein constructs:

Sequences were identified and verified using the Basic Local Alignment Search Tool (BLAST, http://blast.ncbi.nlm.nih.gov), where an alignment report was generated against known, related sequences currently present within the NCBI database. The generated cDNA construct corresponding to JUN (in TOPO® vector) displayed exact sequence homology (100% identification, including start, kozak and TAG stop sequences) to the known human cardiac muscle JUN sequence (current accession number: AF224468 (Lim et al., 2000)). As discussed in section 3.2.1, the CSQ2 construct was sequenced once inserted into the pcDNA3.1 hygro$^{(+)}$ vector and was also found to display 100% sequence identity to the known cardiac CSQ2 sequence (current accession number: NM_001232 (Kawamura et al., 2013)). Conversely, sequence analysis of the prospective TRD1 clones did not display any sequence homologies to the known TRD isoforms following a BLAST search. In addition, the isolated fragments were also manually aligned against the known TRD1 sequences of other species to assess the degree of homology, yet no significant similarities were found. Table 3.3 lists the outcomes of the BLAST search following sequencing of all prospective TRD amplicons. As further considered in the discussion section of this chapter (section 3.4.1), when this section of the project was carried out, the human cardiac muscle TRD1 sequence was unknown, thus designing PCR primers with significant specificity to TRD1 proved problematic, and reliable verification of the obtained PCR products difficult. In light of this, and considerable evidence in the literature suggesting that TRD1 and JUN have functionally distinct roles in regulating RyR2 activity (Altschafl et al., 2011, Chopra et al., 2013), I decided to focus my investigations on the interaction and functional regulation of hRyR2 by luminal proteins CSQ2 and JUN.

PCR isolated Fragment:	BLAST homologous sequence:	Accession Number:
~600 bp (Figure 3.2, B (i)) ~550 bp (Figure 3.2, B (iii))	Homo sapiens chromosome 14, alternate assembly	NC_018925.2
~1000 bp (Figure 3.2, B (ii))	Homo sapiens chromosome 11, alternate assembly	NC_018922.2
~1600 bp (Figure 3.2, B (i)) ~1500 bp (Figure 3.2, B (iii))	Homo sapiens chromosome 1, alternate assembly	AC_000133.1

Table 3.3: Identification of prospective TRD amplicons using BLAST.
The obtained sequences of each isolated fragment were assessed using BLAST, but did not display any sequence homologies to human cardiac muscle triadin 1 (TRD1). The human TRDN gene is located on chromosome 6 (Thevenon et al., 2003).

3.3.3 Cloning CSQ2 and JUN constructs into mammalian expression vector pcDNA3.1hygro $^{(+)}$:

- ***pcDNA3.1hygro (+)-JUN***

Sequence verified JUN cDNA was excised from TOPO® vector using an overnight double digest with *BamHI* and *NotI* restriction enzymes at 37°C and subsequently cloned into the pcDNA3.1 hygro$^{(+)}$ expression vector (Life Technologies) following the ligation protocol described in section 2.4.1.9.

- ***pcDNA3.1hygro (+)-CSQ2***

Following an overnight digest of pcDNA3.1hygro $^{(+)}$ with *XhoI* and *ApaI* (section 3.2.1), a ligation reaction was undertaken (Table 2.4) to directly clone the isolated CSQ2 cDNA into the new expression vector.

To confirm successful generation of full-length luminal protein-pcDNA3.1hygro$^{(+)}$ expression constructs, restriction enzymes *Psi I* (JUN-pcDNA3.1hygro$^{(+)}$) and *Bpu10I* (CSQ2-pcDNA3.1hygro$^{(+)}$) were used for restriction mapping (using NEB cutter, http://tools.neb.com) and subsequent digest, chosen on the basis that recognition sites for the given enzymes were present in both the pcDNA3.1hygro$^{(+)}$ vector and the luminal protein insert. Restriction fragments were resolved according to their molecular weight using 1% agarose gels (section 2.4.1.2) and further automated sequencing confirmed that the luminal protein inserts were successfully cloned into the mammalian expression vector before using the constructs in further investigations.

3.3.4 Hygromycin is a better selection antibiotic than G418 for making stable cell lines in HEK293 cells:

Optimal concentrations of selection antibiotic were determined by plotting dose-response (or kill-) curves for hygromycin and G418 (Figure 3.3) carried out on untransfected HEK293 cells, as outlined in section 3.2.2. In contrast to hygromycin treatment, HEK293 cells displayed a high level of resistance to G418, which resulted in very little cell death (Figure 3.3). In light of this, hygromycin selection was chosen as the most efficient treatment. As shown in Figure 3.3, a concentration of 400 µg/ml was chosen, since treatment of cells with this dose eliminated ~65% of cells and increases in concentration from here did not cause an appreciable increase in cell death. Shown in Figure 3.4 are representative images of HEK293 cell death when treated with increasing doses of hygromycin. Three HEK293 cell lines stably expressing CSQ2, JUN or CSQ2+JUN were generated as described in section 3.2.2, cultured in the presence of 400 µg/ml hygromycin. Western Blotting was used to establish the expression levels of each protein (section 3.3.6).

Illustrated as a bar graph in Figure 3.5 (A), the growth rate of stable cell lines was significantly slower than that of untransfected HEK293 cells, which consequently reduced transient $CaPO_4$-mediated expression of hRyR2 (generating lower transfection efficiencies, examples of which are shown in Figure 3.5, (B)). This hindered original plans to use luminal accessory protein-expressing stable cells for large-scale hRyR2 co-expression. Since it was necessary for sufficient [^{3}H] ryanodine binding and co-immunoprecipitation investigations (discussed in Chapter 4 and 5, respectively) to produce large amounts of hRyR2, recombinant material was generated from transient transfection of hRyR2 (alone or in the presence of luminal accessory proteins) in normal HEK293 cells, achieved using the $CaPO_4$ precipitation method (outlined in section 3.2.4 and Table 3.1).

Since the luminal accessory proteins were not tagged with fluorescent proteins, it was essential to ensure that all cells imaged expressed the luminal accessory proteins of interest. WT or mutant hRyR2 could then be transiently expressed on top, as these cells would be able to be identified by their caffeine response (Thomas et al, 2004). Thus, stable cells were transfected with hRyR2 using the lipid-based Effectene® reagent (Life Technologies), (section 2.4.2.3), which requires less DNA than the $CaPO_4$ method and is therefore less cytotoxic, ensuring cell viability is maintained (which is of the utmost importance for single-cell Ca^{2+} imaging studies, since damaged cells will not show agonist response). In addition, Effectene® does not form a precipitate and its efficacy is not

dependent on cell doubling rate. As illustrated in Figure 3.6 (A), sufficient transfection efficiencies of hRyR2 for Ca^{2+} imaging was achieved in stable cells using this method.

However, [^{3}H] ryanodine binding and immunoprecipitation experiments require large-scale transfection and high hRyR2 expression levels. For these purposes Effectene®-mediated hRyR2 transfection of stables was not deemed adequate because: 1) The growth rate of the stable cell lines was prohibitively slow for large-scale transfection to be achieved, 2) the volume of Effectene® required was prohibitive, and 3) the overall expression level of hRyR2 was lower that that achieved using transient co-transfection of all constructs using $CaPO_4$. As highlighted in Figure 3.6 (B), although Effectene® and $CaPO_4$-mediated transfection of hRyR2 in HEK293 cells displayed similar transfection efficiencies (i.e. the percentage of cells that were green), higher protein levels per cell were achieved using $CaPO_4$ precipitation, as indicated by the appearance of brighter green cells. However, due to higher protein expression, the cells did not appear as healthy as those transfected with Effectene® (which is essential for Ca^{2+} imaging), but this was not a concern for investigations which required the cells to be harvested and lysed.

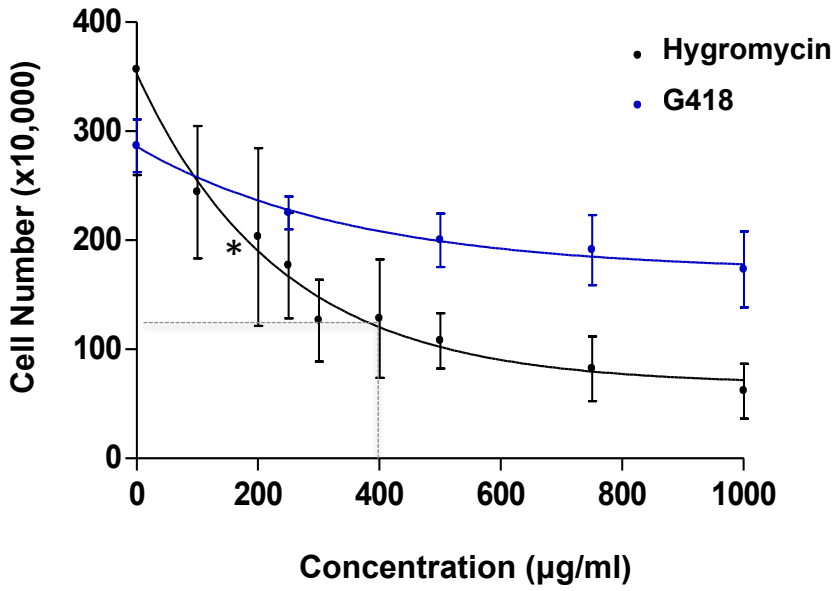

Figure 3.3: Hygromycin and G418 Kill-Curves: *HEK293 cells were seeded at a density of 1 x 10^6 cells/well and exposed to increasing concentrations of hygromycin and G418. Following 2 days culture in the presence of the antibiotic, the surviving cells were counted using haemocytometry. The kill-response curves were constructed using an average of the surviving cell number/dose determined from an n=3 experiments. HEK293 cells displayed high levels of resistance to G418 treatment, resulting in very little cell death. Hygromycin proved more effective, yielding an LD_{50} (the dose of antibiotic which killed 50% of cells) of 164 µg/ml (asterisks). A treatment of 400 µg/ml, that killed 65% of cells (indicated with a dashed line) was chosen as the optimum dose to select for stable expression, since treatment at this concentration appeared to eliminate a significant proportion of cells without causing detrimental cell loss (plateau phase).*

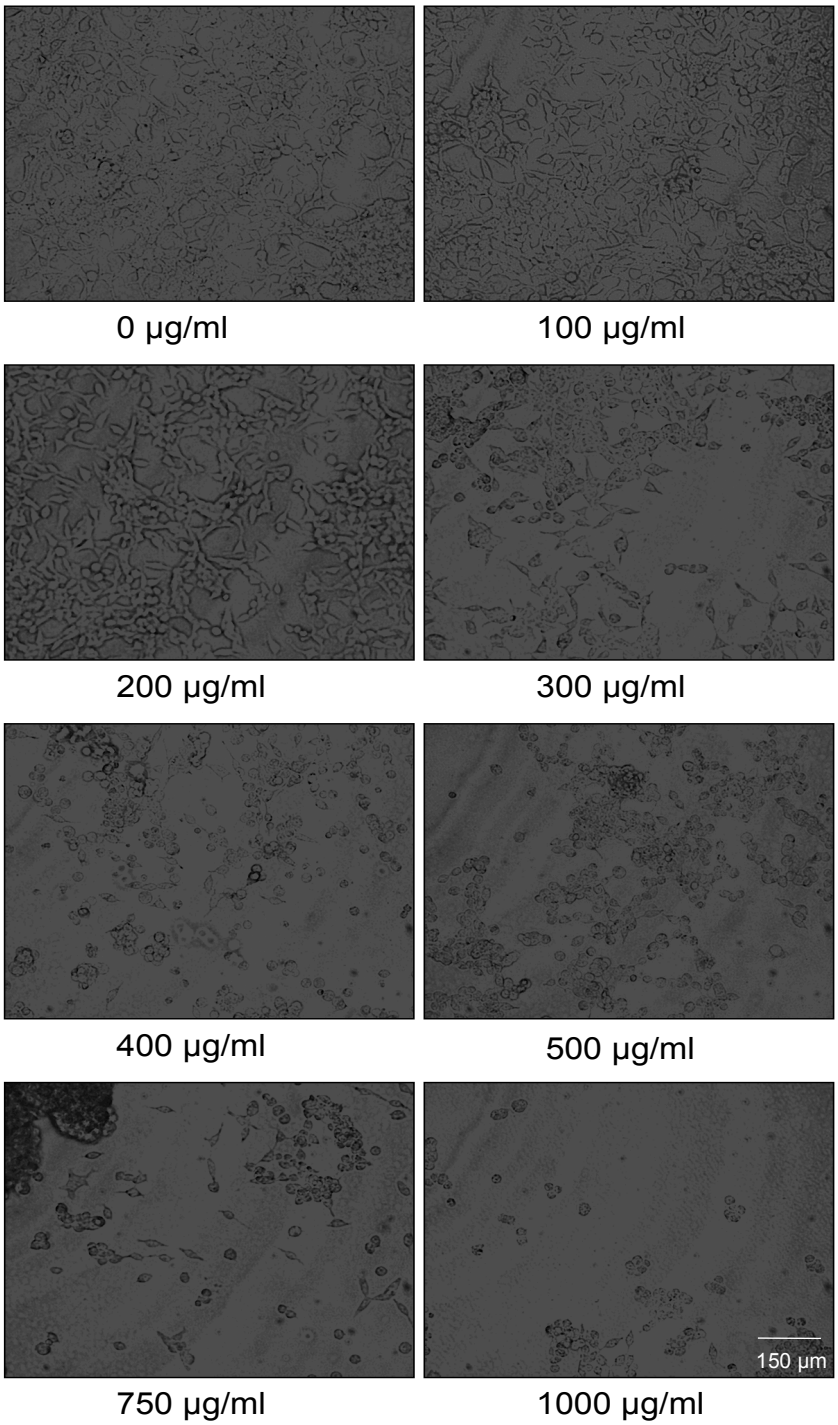

Figure 3.4: Representative images of HEK293 cell populations following treatment with hygromycin. *To find an optimal dose of hygromycin treatment that would allow selection of transfected HEK293 cells stably expressing the luminal proteins, a hygromycin dose-dependence curve was constructed. Shown here are representative images of HEK293 cells treated with increased concentrations (µg/ml) of hygromycin. Once cultured for 48 hours in the presence of the antibiotic, the number of surviving cells was counted. As illustrated, cell death increased in a dose-dependent manner.*

(A)

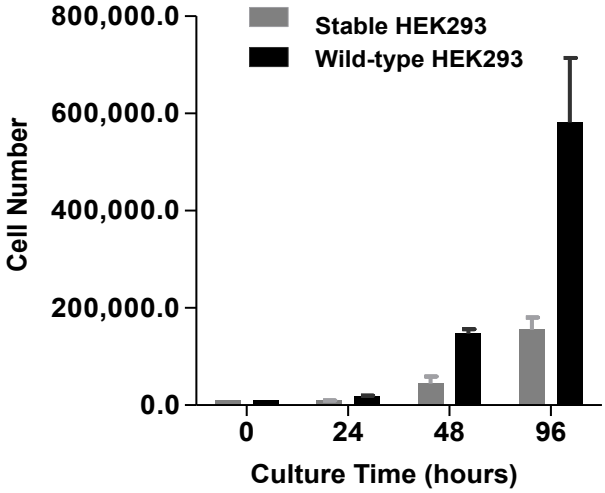

(B)

(i)

WThRyR2 expression in CSQ2-expressing HEK293 stable cells

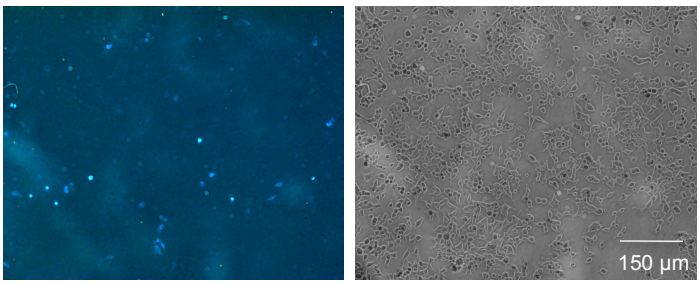

Transfection efficiency = 11 ±5%

(ii)

WThRyR2 expression in JUN-expressing HEK293 stable cells

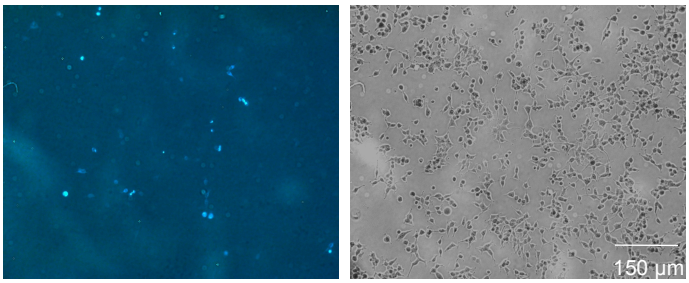

Transfection efficiency = 8 ±3%

Figure 3.5: Assessment of transient hRyR2 expression in stable HEK293 cells: *(A) As illustrated using CSQ2 stables as an example, stable cells displayed a much slower growth rate than untransfected HEK293 cells and likely explains why using the $CaPO_4$ precipitation method, transient transfection of WT hRyR2 into CSQ2 (B) i and JUN (B) ii-expressing stable cell lines, generated low transfection efficiencies (established by counting the percentage of green cells from 4 fields of view). Thus, the stables were not considered suitable for large-scale hRyR2 expression.*

(A)

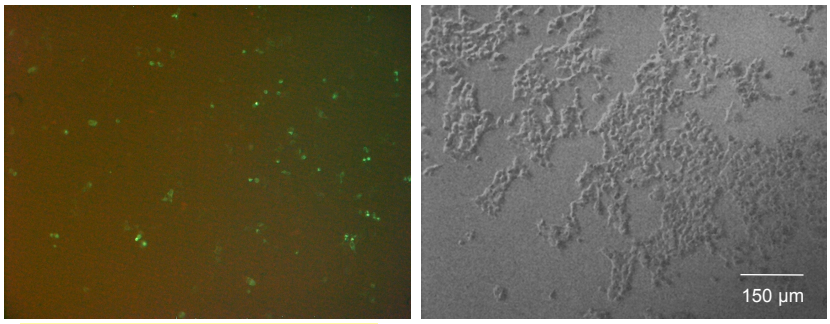

Transfection efficiency = 20±1.25%

(B)

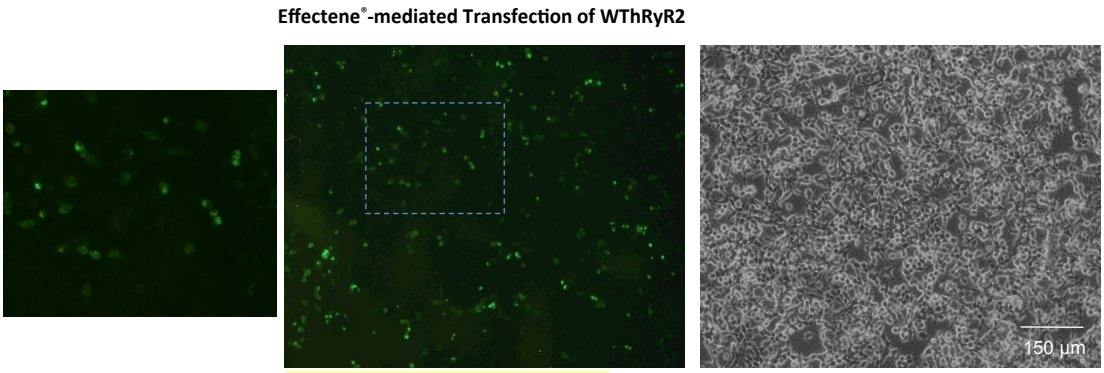

Transfection efficiency = 30±3%

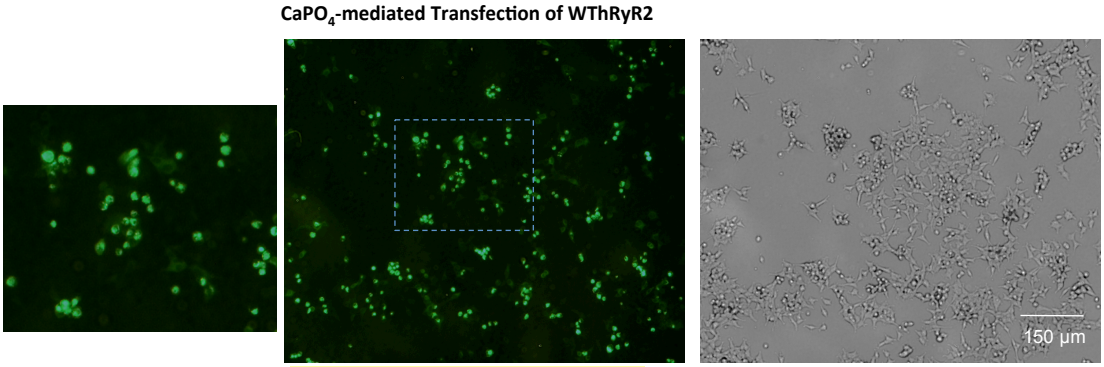

Transfection efficiency = 40±4%

<u>Figure 3.6:</u> Assessment of the Effectene®-mediated transfection protocol: *Transfection of WT hRyR2 into stable CSQ2-expressing cells (used here as an example) with Effectene® reagent, generated sufficient transfection efficiencies for Ca^{2+} imaging studies (A). Use of the reagent to transfect hRyR2 into wild-type HEK293 cells was also compared with the optimised $CaPO_4$ precipitation protocol (for large-scale transfections) outlined in section 3.3.5 (Fig. 3.7 and 3.8). As shown in (B), whilst both methods generated similar transfection efficiencies, hRyR2 expression in cells transfected with $CaPO_4$ appeared brighter (brighter green, bottom panels left and centre), indicative of higher protein expression per cell. Cells transfected using the Effectene® protocol appeared healthier (top left panel vs bottom left panel), likely due to lower protein expression. However, although more cytotoxic, in cells which were ultimately going to be harvested and lysed to produce microsomal mixed membranes necessary for further investigations, the $CaPO_4$ precipitation method produced higher quantities of recombinant hRyR2 protein.*

3.3.5. Assessment of HEK293 cells transiently transfected with eGFP-hRyR2:

Prior to large-scale transfections of WT/mutant hRyR2 alone or in the presence of CSQ2 and/or JUN, it was important to determine the optimal conditions required to generate high-levels of recombinant protein expression. Optimisation focused on the use of different starting cell confluency at the point of transfection and incubation with different concentrations of DNA. Each experiment was replicated 4 times and the results expressed as the mean transfection efficiency±S.E.M. Fluorescence microscopy was used to visualise WT eGFP-hRyR2 expression in cell populations 48 hours post-transfection, and images were taken of 3 fields of view (bright field and the corresponding fluorescence of the same field of view). To assess transfection efficiency, bright field and corresponding fluorescent fields of view were selected at random, cells were counted and the efficiency calculated as the percentage of green cells of the total number of cells in a mutual field of view.

Figure 3.7 (A) illustrates typical fields of view of transiently transfected HEK293 cells, corresponding to each set of variables tested. Transfection of cells with a low DNA: cell ratio of 5 pg/cell (determined according to starting cell numbers) yielded transfection efficiencies of ~41±2% and ~30±1.5%, when at lower or higher cell densities, respectively (Figure 3.7, A (iii), (iv) and B). In comparison, the use of higher concentrations of DNA per cell (~15 pg/cell) appeared to increase the transfection efficiency to ~51±3%, at lower cell densities (Figure 3.7, A (i) and B), and ~39±1% at higher cell densities (Figure 3.7, A (ii) and B), respectively. Taken together, optimal eGFP-hRyR2 expression was achieved using lower starting cell densities and a higher DNA: cell ratio, as illustrated in a bar graph, Figure 3.7 (B).

Expression levels of WT hRyR2 achieved using the different transfection variables, were also assessed by Western Blot analysis (Figure 3.8 A). Consistent with calculations of transfection efficiency, cell populations transfected at a lower starting cell density and higher DNA: cell ratio (Figure 3.8, A), expressed WT hRyR2 to a significantly higher level than in other variable combinations tested, as measured by densitometric analysis (Figure 3.8, B).

Once optimised, all $CaPO_4$ transfections were carried out using lower starting cell densities i.e. 30-40% confluency and transfected using a DNA concentration of 15 pg/cell. Since CSQ2 and JUN constructs were untagged, transfection efficiencies of the luminal proteins co-expressed with WT/mutant hRyR2 could not be assessed (48 hours post-transfection) in the same manner as eGFP-hRyR2. Therefore, in addition to Western Blot

analysis (section 3.3.6), luminal protein expression was visualised by confocal microscopy and immunofluorescent co-localisation (the investigations of protein-protein interactions using this method are outlined in Chapter 5, section 5.3.3). As illustrated in Figure 3.9, the localisation of hRyR2 (A, (ii) and B (ii)), CSQ2 (A, (iii)) and JUN (B, (iii)) to the ER in transfected HEK293 cells could be assessed using this technique. Determination of the transfection efficiencies of CSQ2 and JUN (together with eGFP-hRyR2) detected by immunofluorescent labelling is shown in Figures 5.2 and 5.3 in Chapter 5 (described in results section 5.3.1).

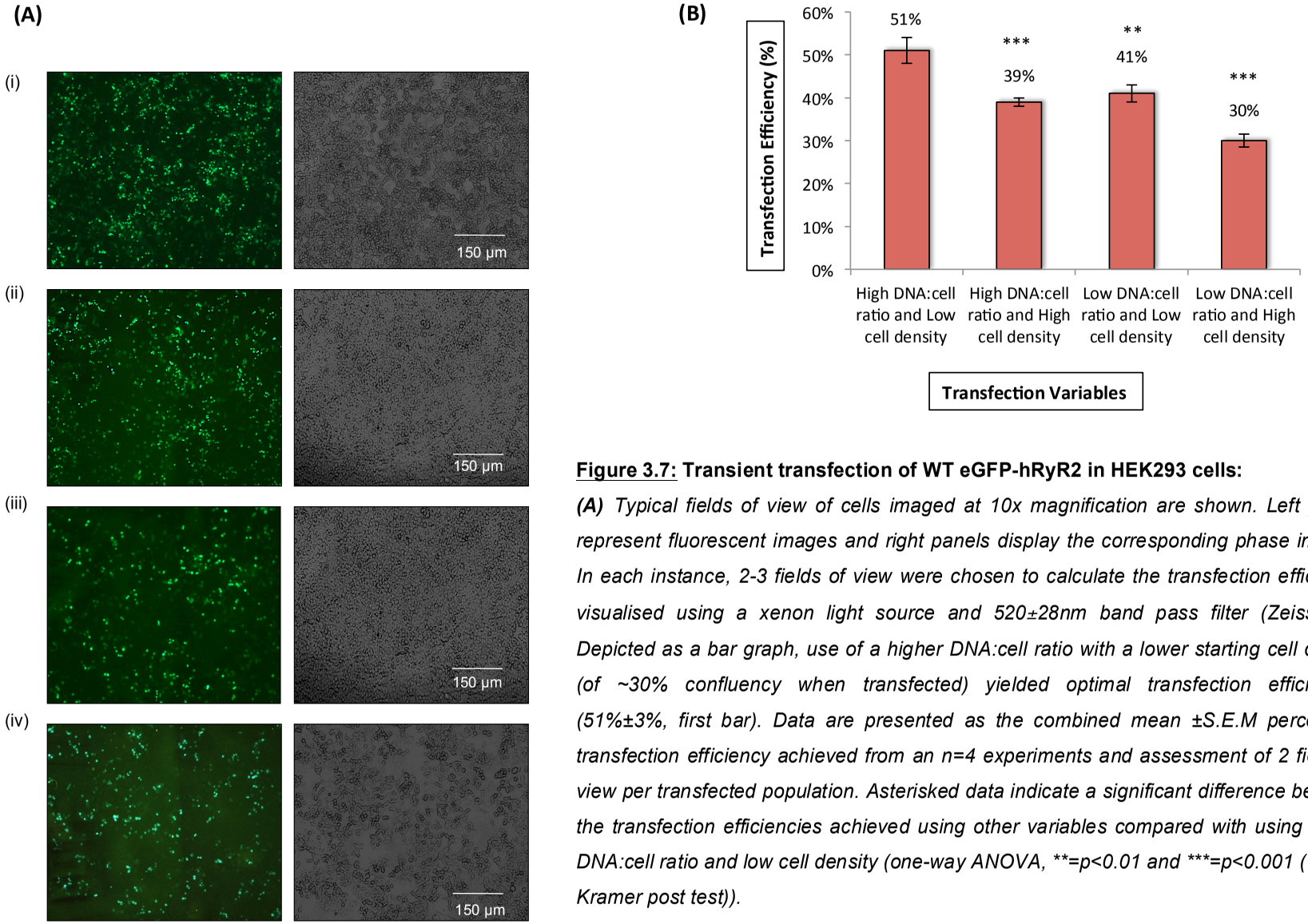

Figure 3.7: Transient transfection of WT eGFP-hRyR2 in HEK293 cells:

(A) *Typical fields of view of cells imaged at 10x magnification are shown. Left panels represent fluorescent images and right panels display the corresponding phase images. In each instance, 2-3 fields of view were chosen to calculate the transfection efficiency, visualised using a xenon light source and 520±28nm band pass filter (Zeiss).* ***(B)*** *Depicted as a bar graph, use of a higher DNA:cell ratio with a lower starting cell density (of ~30% confluency when transfected) yielded optimal transfection efficiencies (51%±3%, first bar). Data are presented as the combined mean ±S.E.M percentage transfection efficiency achieved from an n=4 experiments and assessment of 2 fields of view per transfected population. Asterisked data indicate a significant difference between the transfection efficiencies achieved using other variables compared with using a high DNA:cell ratio and low cell density (one-way ANOVA, **=p<0.01 and ***=p<0.001 (Tukey-Kramer post test)).*

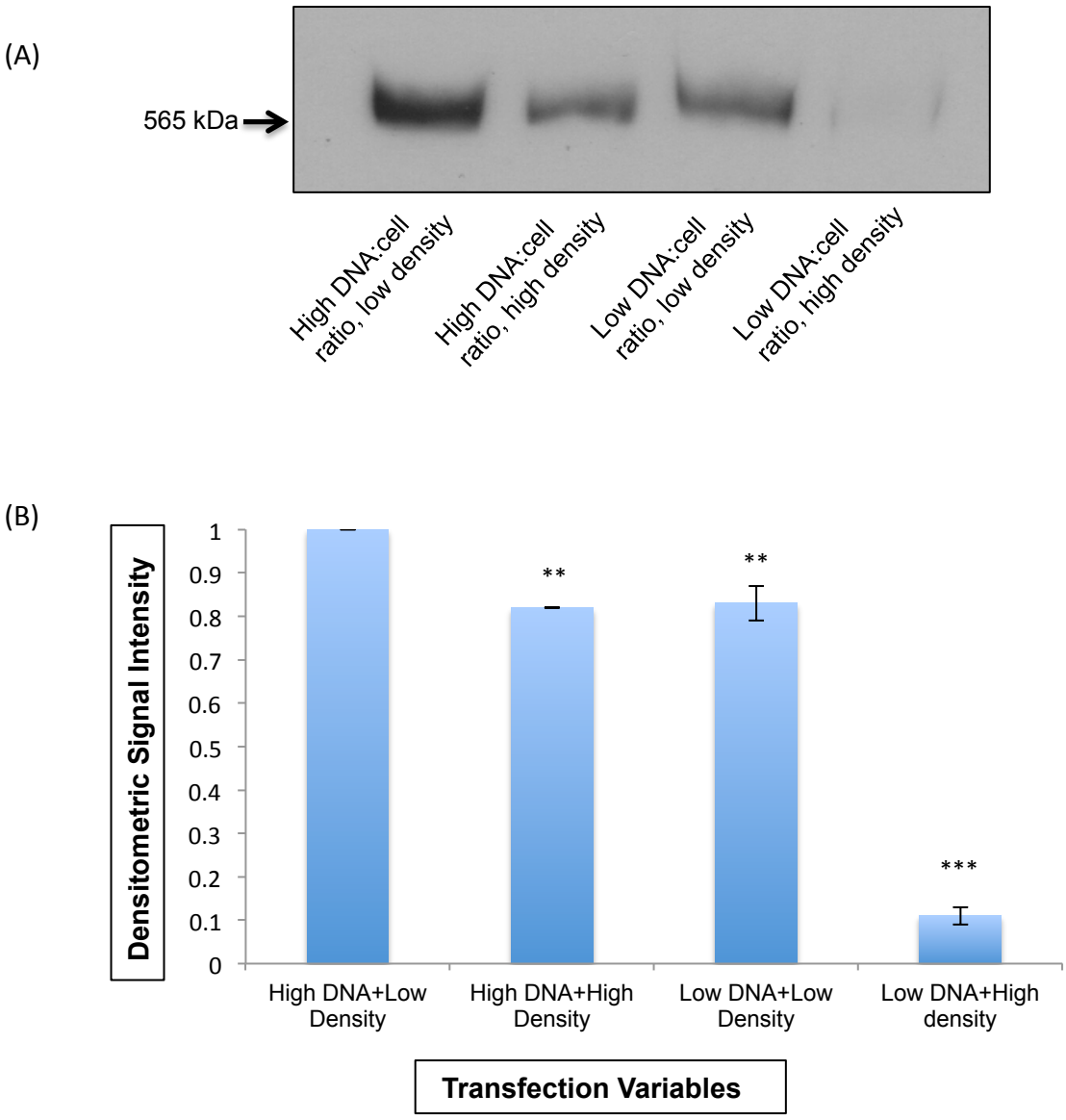

<u>Figure 3.8:</u> Comparison of transfection variables by protein expression, assessed by Western Blot analysis. ***(A)*** *Resolved by SDS-PAGE (50µg of each mixed membrane preparation), transient expression of WT hRyR2 was examined by Western blotting, using an eGFP-specific mouse-monoclonal anybody. As indicated with an arrow, Western signals corresponding to hRyR2 were detected at 565 kDa, which appeared above the highest Kaleidoscope™ prestained marker at 250kDa (as shown in the Appendix, Figure 3 (D)). Protein expression were much higher in cell populations transfected at a lower cell confluency and a high DNA:cell ratio, compared to expression detected in other preparations, and was in accordance with the higher transfection efficiencies calculated in Figure 3.7. Densitometric analyses were carried out on two experiments (following the generation of 1 preparation per variable, 4 in total), the results of which are presented in* ***(B)****. Data are presented as the mean±S.E.M. Asterisked data indicates a significant difference in the relative densities measured in all other transfected cell populations compared with densitometric analysis of Western signals achieved from membrane preparations where higher DNA:cell ratios and low starting cell densities were used for transfection (one-way ANOVA, ** = p<0.01 and ***=p<0.001 (Tukey-Kramer post test)).*

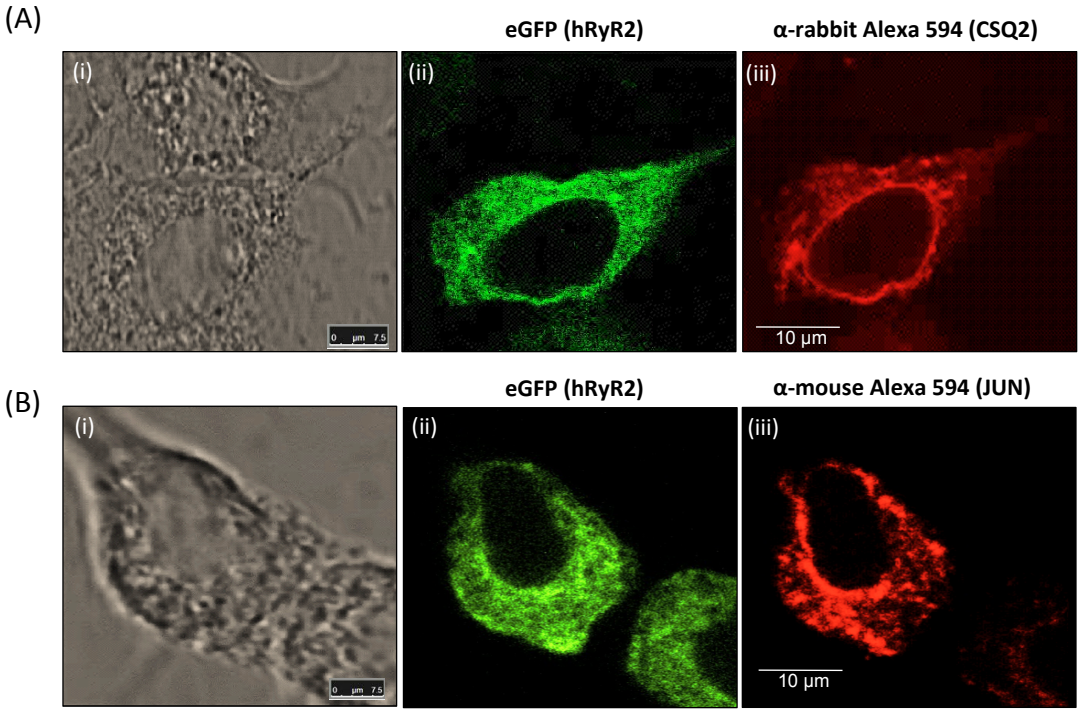

Figure 3.9. Immunofluorescent detection of hRyR2, CSQ2 and JUN expression confirms ER trafficking. *Cells co-expressing eGFP-hRyR2 and CSQ2 or JUN were imaged by confocal microscopy (at x63 magnification). WT hRyR2 was visualised using eGFP fluorescence (A (ii) and B (ii)) whereas accessory proteins were immunolocalised using anti-CSQ2 or anti-JUN antibodies with α-rabbit (CSQ2) or α-mouse (JUN) Alexa-594 conjugated secondary antibodies, A (iii) and B (iii), repectively. Corresponding phase images are shown in A (i) and B (i). Both eGFP and Alexa 594 signals displayed a reticular pattern of fluorescence, indicating trafficking of all membrane proteins to the ER in situ.*

3.3.6 Successful expression of recombinant hRyR2, CSQ2 and JUN in HEK293 cells confirmed by Western Blot analysis:

Prior to investigating the functional regulation and interaction of the luminal proteins with hRyR2, it was essential to determine the relative expression levels of each recombinant protein in the microsomal membranes, and confirm that full-length eGFP-hRyR2, CSQ2 and JUN were being expressed. Western analysis confirmed successful co-expression of CSQ2 and/or JUN with WT/mutant hRyR2 in HEK293 cells. Figure 3.10 (A) illustrates typical bands detected by Western blotting, where sufficient protein expression was evident in all the microsomal membrane preparations generated. High levels of transient protein expression of (A) WT/mutant hRyR2 (~565kDa), (B) CSQ2 (~45kDa) and/or (C) JUN (~26kDa) was evident in all preparations assessed (n=4 blots were generated for each recombinant protein). Comparable levels of luminal accessory protein expression were seen in all microsomal membrane preparations (Figure 3.10, B). Furthermore, transient (co-expressed hRyR2 with CSQ2 and/or JUN) and stable expression of CSQ2 and JUN were compared (50µg mixed membranes loaded into each lane, Figure 3.11 A, (i-iii)). In addition, membrane proteins from untransfected HEK293 cells were loaded alongside samples to verify the lack of any endogenous CSQ2 or JUN in HEK293 cells. All three stable cell lines appeared to sufficiently express the desired luminal proteins: (i) CSQ2 only, (ii) JUN only and (iii) double stables co-expressing CSQ2+JUN. However, levels of expression were lower than those achieved by transient expression (expression in CSQ2 stables was 23±2.5% less than in mixed membranes transiently expressing CSQ2 with WT hRyR2, whilst expression in JUN stables was 24±3% less than in membranes transiently expressing JUN with WT hRyR2). As discussed in section 3.3.4, the relative expression levels of hRyR2 achieved by transient expression in stable HEK293 cells was not sufficient for reliable detection by SDS-PAGE and Western blot analysis, and thus were deemed unsuitable for use in [^{3}H] ryanodine binding experiments. Therefore, transiently transfected cell populations (Figure 3.10) were used for [^{3}H] ryanodine binding experiments (Chapter 4, section 4.3.1), which required prior standardisation of hRyR2 expression in all mixed membrane preparations by densitometric analysis (described in Chapter 4, Figure 4.4).

(A)

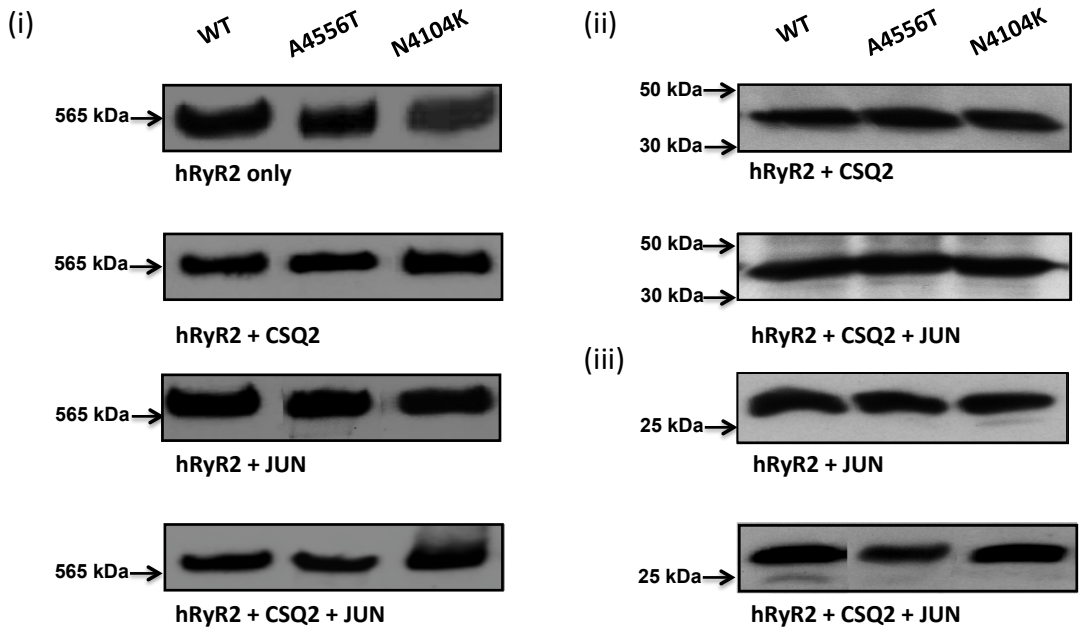

(B)

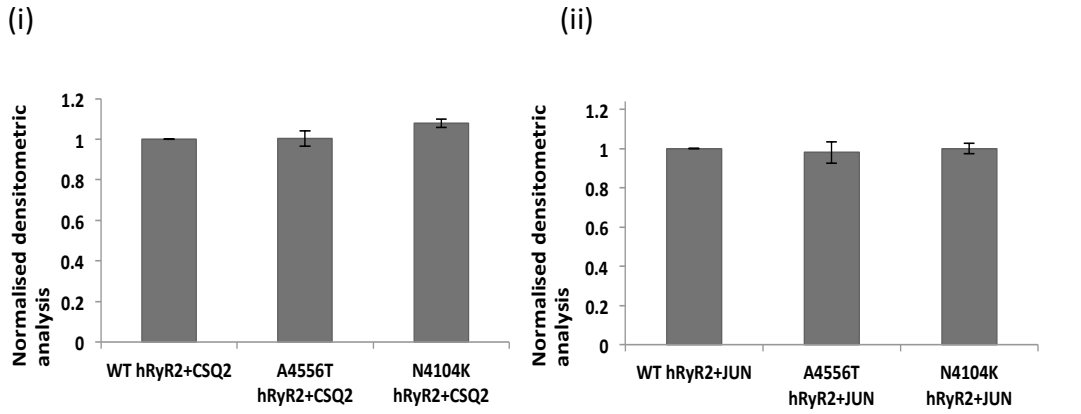

<u>Figure 3.10:</u> Western Blotting confirms transient expression of hRyR2, CSQ2 and JUN in co-transfected HEK293 cells: ***(A)*** *Representative bands achieved from Western blot analysis of (i) hRyR2 (~565kDa), (ii) CSQ2 (~45kDa), and (iii) JUN (~26kDa) expression (n=4), detected in the various microsomal membrane preparations generated (4 per recombinant protein combination). Original and additional Western blots are shown in the Appendix, Figures 3 and 4.* ***(B)*** *Expression levels of CSQ2 and JUN in mutant hRyR2 mixed membrane preparations were comparable to WT. Densitometric analysis shown here was carried out on Western signals of CSQ2 and JUN expression obtained from membranes expressing hRyR2+CSQ2 (i) and hRyR2+JUN (ii), respectively.*

(A)

(i)

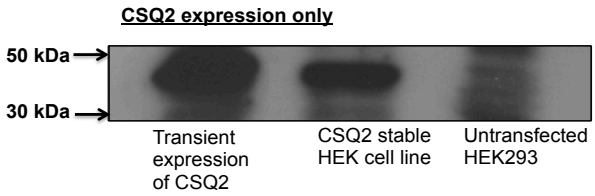

(ii)

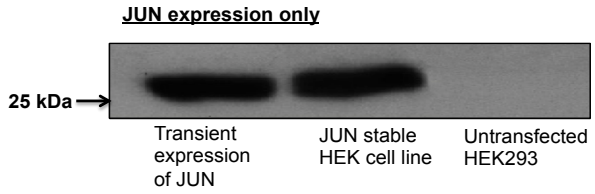

(iii)

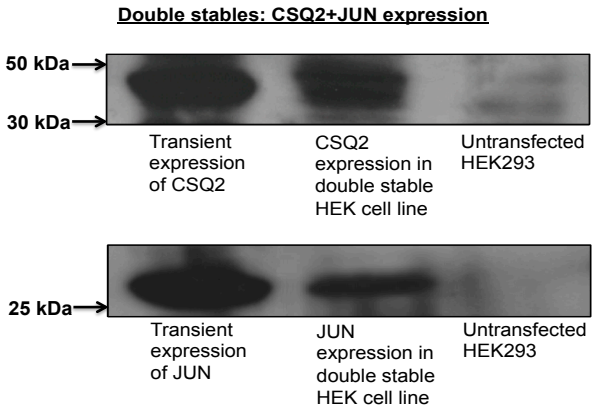

(B)

(i) (ii)

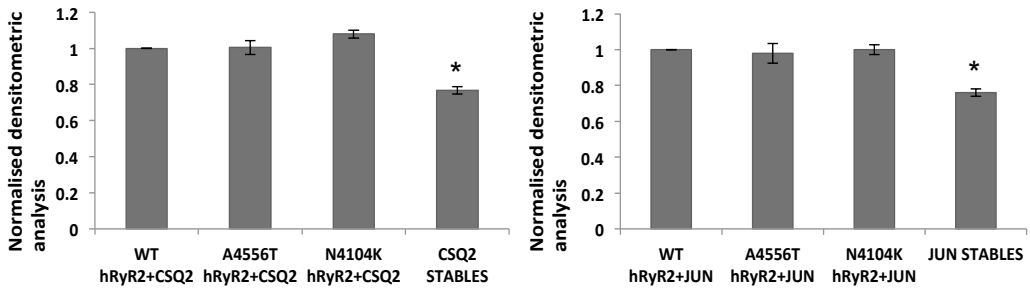

Figure 3.11: Stable expression of luminal proteins in HEK293 cells confirmed by Western Blot analysis: ***(A)*** *Detected using 50µg of isolated microsomal membranes, Western blotting revealed significant protein levels in stable cell lines expressing: (i) CSQ2 only (~45kDa), (ii) JUN only (~26kDa) and (iii) CSQ2 (top bands) and JUN (bottom bands) double stables. Representative bands were selected from an n=3 blots. It is possible that untransfected HEK293 cells may express a small amount of endogenous CSQ2, suggested by the presence of bands at ~45kDa shown in A (i). In comparison to transient expression however, the Western signals detected were very low (as highlighted in A (iii)).* ***(B)*** *Assessed by densitometric analysis, expression levels of CSQ2 only (i) and JUN only (ii) in stable cell lines were less than those achieved with transient expression. Nevertheless, the expression levels obtained in stable cell lines were sufficient for use in further investigations. *=p<0.05 compared with expression in membranes expressing WT hRyR2+CSQ2 or JUN, respectively (one-way ANOVA, Tukey-Kramer post test). It is important to note that these differences could reflect the fact that Western signals for transient expression are slightly over-exposed, leaving room for error with densitometry. However, the blots needed to be left for a longer exposure time in order to detect the Western signals for stable expression, thus suggesting transient expression is higher.*

3.4 Discussion:

- In order to assess the response and interaction of WT and mutant hRyR2 channels to luminal accessory protein co-expression, pcDNA3.1 hygro$^{(+)}$-CSQ2 and pcDNA3.1 hygro$^{(+)}$-JUN expression constructs were generated and sequence verified. The TRD1 sequence could not be isolated from the human cardiac library used.

- High-levels of WT/mutant hRyR2 expression and subsequent luminal protein co-expression in HEK293 cells was achieved by optimising the transfection protocols, using transient and stable HEK293 cell lines.

- Successful expression of all recombinant proteins in HEK293 cells was confirmed by Western blotting, trafficking to the ER was confirmed by immunofluorescence.

3.4.1. Successful generation of human cardiac muscle CSQ2 and JUN mammalian expression constructs

Cloning of full-length cDNA encoding CSQ2 (~1200bp) and JUN (~700bp) into the mammalian expression vector pcDNA3.1hygro$^{(+)}$ was verified by restriction digest and automated sequencing (ABI 3700, Applied Biosystems). Generated constructs displayed 100% sequence homologies with the known cDNA sequences of human cardiac muscle CSQ2 and JUN, respectively (NCBI, Genbank).

Isolation of the open reading frame of human cardiac muscle TRD1 however, proved problematic and was hindered by the absence of the published human cardiac muscle sequence within the NCBI database at the time this work was carried out. Described in section 3.3.1, a series of PCR reactions were carried out using several primer combinations designed to target the luminal protein (Figures 3.1, B). Specifically, different PCR reverse 3' primers were used (section 3.3.1), taking into consideration that: (1) the C-terminus of TRD1 is known to contain numerous positively and negatively charged sequence repeats ("KEKE" motifs) which may limit primer specificity and (2) suggestions in the literature that each TRD isoform displays a unique C-terminal sequence, which also varies between species. As reported by Kobayashi and Jones (1999) the C-terminal regions of rabbit (Guo et al., 1996) and dog TRD1 share only ~77% homology, and it is likely that the human isoform also diverges from these species with its own unique C-terminal sequence. In support of this concept, Kobayashi and colleagues (1999) described

that poor cross-reactivity was evident when probing human cardiac muscle microsomes with an antibody designed to the distinct C-terminal region of dog TRD1, and detection of TRD1 in the human preparation was only achieved following the use of five times more concentrated antiserum and much longer exposure times (Kobayashi and Jones, 1999).

As shown in Figure 3.2 (B), (i)-(iii), several prospective amplicons were generated and subsequently sequenced, but none of which were found to show any homology to cardiac TRD1 using a BLAST search (Table 3.3), and manual alignment against the known TRD sequences (human skeletal, rabbit and dog cardiac) that were currently published. Kobayashi and Jones (1999), also encountered difficulties in isolating full-length cardiac TRD isoforms from dog cDNA libraries, where screening identified numerous partial or corrupt clones with unrelated sequences ligated adjacent to the correct coding sequence of the protein. The group carried out reverse transcription-PCR of dog left ventricle total RNA using dog-specific primers to predict the correct size of TRD1 and TRD3. These data were subsequently used to eliminate false clones and to confirm the generation of full-length isolated cDNA of both TRD isoforms, which were assembled from overlapping partial clones (Kobayashi and Jones, 1999).

Although released towards the end of the tenure of this project (and thus it was too late to obtain the clone), it is important to note here that a sequence corresponding to human TRD1 (also known as Trisk 32) is now accessible via the NCBI database (accession number: NM_006073.3), published by Roux-Buisson et al in 2012. To formulate this sequence, the group identified a sequence in the human *TRDN* gene that displayed significant homologies with the specific cardiac TRD1 sequence in rats. Total RNA was extracted from a human cardiac muscle sample obtained from the “Myobank-AFM” tissue bank (Paris, France) and the full-length coding sequence amplified by RT-PCR, using a 3’ reverse primer designed to the homologous genomic sequence identified in both the rat and human *TRDN* gene, and a 5’ forward primer designed to the first exon of the human *TRDN* gene. Using the same primers, the amplified transcript was bidirectionally sequenced and although differing in the specific C-terminal region (as also reported by Kobayashi and Jones, 1999), displayed significant homologies to rat, rabbit and dog protein sequences (Roux-Buisson et al., 2012). The potential TRD1 sequences obtained in this investigation were subsequently aligned against this new sequence, but no significant homologies were identified.

Due to the difficulties encountered isolating human TRD1 from the cardiac cDNA library, the remainder of this project focussed solely on the functional effects and interactions of WT and mutant hRyR2 with luminal accessory proteins CSQ2 and JUN. The use of

cardiac TRD1 isolated from a different species was not favoured, since some investigations of luminal accessory protein function have reported species variability (Wei et al., 2009b, Qin et al., 2008).

3.4.2 Optimised co-expression of hRyR2 channels with CSQ2 and JUN in transient and stable HEK293 cell lines

By comparison of two calcium phosphate precipitation methods (section 3.2.3), a modified transfection protocol was established, and subsequently used to routinely achieve high transfection efficiencies. Representative images taken 48 hours post-transfection are shown in Figure 3.7 (A), following transfection of WT hRyR2 into HEK293 cells using different starting cell densities and DNA: cell ratio (section 3.3.5). As used in Jiang et al., 2002, the use of lower starting cell densities was found to prevent over-confluence and provided a greater surface area over which DNA precipitates could be endocytosed. Furthermore, although using higher concentrations of DNA can enhance cytotoxicity, transfecting with 15 pg DNA/cell (providing the cells with a greater concentration of DNA for uptake) was found to yield significantly higher transfection efficiencies of 51±3%, achieved in combination with a low starting cell density. In agreement with the higher transfection efficiencies calculated, WT hRyR2 protein expression was found to be significantly higher in these cell populations as assessed by densitometric analysis of Western blot signals (Figure 3.8, A and B).

Using the optimised transfection protocol, different combinations of the luminal accessory proteins CSQ2 and JUN, were transiently co-expressed with WT or mutant hRyR2 in an equimolar ratio (Table 3.1). Using this approach, CSQ2 and JUN constructs were expressed both individually and in combination (CSQ2+JUN) with hRyR2 channels. Transfection efficiency 48 hours post-transfection could only be monitored via eGFP expression (detection of hRyR2), since the luminal accessory proteins were untagged, however the efficiencies achieved were comparable to those obtained when hRyR2 channels were expressed alone, suggesting that co-expression of all recombinant proteins did not cause any cytotoxic effects. In addition, WT and mutant hRyR2 expression yielded similar transfection efficiencies (see Appendix, Figure 2).

HEK293 cells stably expressing CSQ2, JUN and CSQ2+JUN (double stables) were also generated. Attributed to constitutive expression of the target genes and the pressures of antibiotic selection, cell proliferation was found to be much slower in stable cell lines compared to untransfected HEK293 cells (Figure 3.5, A). Consequently, using $CaPO_4$

mediated transfection, hRyR2 expression was found to be much lower in the stable cell lines (Figure 3.5, B) and expression could not be clearly visualised by SDS-PAGE and Western Blotting. These cells were therefore considered unsuitable for applications where high levels of recombinant hRyR2 were required (e.g., for [^{3}H] ryanodine binding, where sufficient counts can only be achieved using large quantities of RyR2 channels, see section 4.2.1). However, the stable cell lines were essential for single-cell Ca^{2+} imaging, where experiments require that all cells express both hRyR2 and the luminal protein of interest. As described in Chapter 5, stable cells expressing the luminal proteins which were also transfected with hRyR2 could be identified by the occurrence of spontaneous Ca^{2+} release events, (Jiang et al., 2004, MacLennan and Chen, 2009), which do not occur in the absence of hRyR2 channels.

Therefore, to eliminate the potentially cytotoxic effects of the $CaPO_4$ precipitation method which could diminish cell viability (Jordan and Wurm, 2004), a commercially available Effectene® (lipid-mediated) transfection reagent was used to introduce WT and mutant hRyR2 into HEK293 cells stably expressing the luminal proteins (section 2.4.2.3). Using this transfection reagent proved more suitable to maximise hRyR2 expression in stable cell lines (as demonstrated in Figure 3.6, A). This method however was not used for large-scale transfections, since the overall protein expression generated was lower than that achieved when hRyR2 was transfected into normal HEK293 cells by the optimised $CaPO_4$ precipitation method (Figure 3.6, B). There are however limitations of using HEK cells with transient expression of the luminal proteins with hRyR2, since the existence of mixed populations of complexes are possible. For example, in cells transiently expressing hRyR2+JUN, there may be cells within the preparation that only express hRyR2 (though these will be few due to the overwhelmingly higher transfection efficiency of the accessory proteins, see section 5.3.1) and a larger population of cells that just express JUN. This will thus need to be considered when assessing the response of WT/mutant hRyR2 to luminal protein co-expression. Shown later in Chapter 5, Figures 5.2 and 5.3, immunofluorescent co-localisation studies suggest that high levels of hRyR2 and luminal protein expression were achieved and the given proteins of interest were predominantly expressed within the same cells of a population.

3.4.3 Western blot analysis of recombinant protein expression in HEK293 cells

Western blot analysis of mixed membrane preparations from transfected HEK293 cell populations (section 2.4.3.3-2.4.3.4), confirmed that full-length recombinant proteins were being expressed (hRyR2 detected at ~565kDa, CSQ2 at ~45kDa and JUN at ~26kDa). As highlighted in Figure 3.10 (A), high levels of transient WT and mutant hRyR2 expression in the absence or presence of CSQ2 and JUN was achieved. Furthermore, mutant hRyR2 expression did not affect the expression levels of the luminal proteins (Figure 3.10, B). The luminal proteins were also expressed in sufficient quantities in stable HEK293 cell populations (CSQ2, JUN and CSQ2+JUN), as demonstrated in Figure 3.11. Described in Chapter 4, densitometric analysis of Western signals was used to standardise hRyR2 expression in all test samples before further investigation.

Chapter 4

Influence of cardiac CSQ2 and JUN on the intracellular Ca^{2+} regulation of WT and mutant hRyR2

4.1 Introduction:

4.1.1. Regulation of RyR2-mediated Ca^{2+} release by luminal accessory proteins at the junctional domain of the SR membrane:

Intracellular Ca^{2+} release from the SR store through RyR2 channels is a crucial event during EC coupling, which must be carefully regulated for normal contraction and subsequent relaxation of the mammalian heart (Bers, 2004; Thomas et al., 2004; Györke and Terentyev 2007). As discussed in previous chapters, it is well known that RyR2 activation is governed not only by cytosolic Ca^{2+}, but also by Ca^{2+} accumulated within the SR lumen, where small increases in luminal Ca^{2+} load generate large elevations in Ca^{2+} release (Györke and Györke, 1998; Ching et al., 2000, Shannon et al., 2005; Radwanski et al., 2013). Situated within the SR membrane, the SERCA2a pump (Figure 1.1, A) is responsible for raising the free intra-SR luminal Ca^{2+} concentration close to 1 mM (Beard et al., 2005, Györke et al., 2008, Stevens et al., 2009) and acts in tandem with the luminal accessory protein CSQ2. This Ca^{2+} storage molecule acts as a major luminal Ca^{2+} buffer, which indirectly regulates RyR2 function by altering the releasable (free) Ca^{2+} concentration within the SR (Györke and Terentyev 2007; Gaburjakova et al., 2013).

Independent of its role in global SR Ca^{2+} buffering, a growing number of investigations have suggested that CSQ2 also has the ability to directly regulate channel activity (Shannon et al., 2005, Györke, 2009, Terentyev et al., 2006). First proposed by Györke et al (2004), it is now believed that a quaternary complex assembles at the jSR membrane between RyR2, CSQ2 and two SR transmembrane proteins JUN and TRD1, and forms a putative luminal Ca^{2+} sensor which responds to changes in SR Ca^{2+} load and modulates RyR2 activity accordingly (Zhang et al., 1997; Györke et al., 2004; Terentyev et al., 2003b; Beard et al., 2005). Györke et al (2004) used recombinant dog cardiac CSQ2 (Kobayashi et al., 2000), JUN (Zhang et al., 1997) and TRD1 (Kobayashi and Jones, 1999) to examine the potential role of the luminal proteins in conferring RyR2 luminal [Ca^{2+}] sensitivity. Purified RyR2 channels reconstituted in a lipid bilayer system were reported by Györke et al (2004) to be unresponsive to changes in luminal Ca^{2+} (ranging from 20 μM-5 mM), and luminal Ca^{2+} sensing was only restored in the presence of the accessory proteins. Upon adding CSQ2 back to the luminal side of the channel, it was reported that RyR2 activity was inhibited, but only at low luminal [Ca^{2+}] <20 μM, and in the presence of JUN and TRD1. This inhibition is important, since in CPVT2, CSQ2 mutation cause RyR2 channels to display a short refractory period before release (Terentyev et al., 2006). Furthermore, JUN and TRD1 added back to the purified channels alone (in the absence of CSQ2) enhanced channel open probability, suggesting an additional activatory role of the

two proteins (Györke et al., 2004). Taking into account that CSQ2-RyR2 regulation appeared luminal Ca^{2+} dependent, the group concluded that the intracellular Ca^{2+} binding protein (via its associations with JUN and TRD1) acts to mediate the ability of RyR2 channels to respond to luminal Ca^{2+}(Györke et al., 2004). However, the individual contributions of JUN or TRD1 to the CSQ2-RyR2 functional interaction (since both were added back to the channel complex together) was not addressed in this work, or the potential of each protein as direct modulators of RyR2 activity established (Altschafl et al., 2011; Dulhunty et al., 2012; Gaburjakova et al., 2013). Interestingly, a later single channel investigation using skeletal CSQ1, demonstrated that the inhibitory action of the accessory protein on RyR1 activity was only seen when expressed in the presence of JUN, leading to suggestions that JUN acts distinctively from TRD1, which was also investigated (Beard et al., 2009, Dulhunty et al., 2009).

Although evidence is limited with regards to the role that JUN plays in mediating the effects of luminal Ca^{2+} on RyR2 function (Radwañski et al., 2013), the physiological importance of the luminal protein to Ca^{2+} release activity has been highlighted in animal models. For example, in adult rat cardiomyocytes with acute downregulation of JUN (~40%), (Fan et al., 2008) and in a mouse model with JUN ablation (Yuan et al., 2007), the frequency and amplitude of Ca^{2+} sparks and contractility within isolated cardiomyocytes were enhanced, which consequently increased the propensity for triggered arrhythmias and SCD. In both models, there were no notable alterations in the expression of other Ca^{2+} handling proteins (e.g., CSQ2 or RyR2), which led to the assumption that the effects seen were exclusively due to downregulation/ablation of cardiac JUN (Fan et al., 2008, Yuan et al., 2007). This may suggest that JUN has an inhibitory effect on RyR2 function or that it enhances the inhibitory effects of CSQ2, as discussed previously (Györke et al., 2004, Miller et al., 2005). This however requires further investigation, and will be explored in this project using single cell Ca^{2+} imaging.

Mutations in RyR2 and CSQ2 are both implicated in the development of CPVT and defective luminal Ca^{2+} sensing is a candidate mechanism of disease pathogenesis (Priori and Chen 2011; Jiang et al., 2005). Since the RyR2 channels response to changes in luminal [Ca^{2+}] appears to be modified by the luminal accessory proteins, a better understanding of how each luminal protein contributes to Ca^{2+} release function could also reveal alterations that might occur as a result of mutation. For example, although no CPVT-linked mutations in JUN have currently been identified, changes in the levels of JUN expression led to an increased incidence of arrhythmia, a symptom that defines CPVT (Altschafl et al., 2011; Yuan et al., 2007). In addition, CSQ2 mutations have been proposed to alter the proteins ability to modulate RyR2 luminal Ca^{2+} sensitivity (for

example, the R33Q mutant studied by Houle et al., 2004, Terentyev et al., 2006) or reduce the luminal Ca^{2+} buffering capacity within the SR (D307H mutant, examined by Viatchenko-Karpinski et al., 2004). It however remains to be elucidated whether RyR2 mutation can alter the way in which the channels respond to luminal accessory proteins or whether association of the complex with RyR2 is disrupted by the mutation.

4.1.2. Spontaneous Ca^{2+} release events in CPVT:

Arrhythmogenic episodes in CPVT occur during times of physical or emotional stress, i.e., when the levels of circulating catecholamines are high and the ß-AR signalling cascade is activated (Priori et al., 2002). Known as the "fight or flight" response, increased cardiac output is required to meet the higher metabolic demands of the heart during periods of stress, and subsequently improves contractile force (Marx and Marks, 2013). Discussed further in Chapter 1 (section 1.2.5) stimulation of the ß-AR pathway causes dissociation of PLB from the SERCA2a pump, which relieves inhibition and speeds up Ca^{2+} re-uptake into the SR. As a consequence, the SR Ca^{2+} load is increased and thus the amount of releasable Ca^{2+} available during subsequent action potentials is enhanced. If however, SR Ca^{2+} content reaches a particular level, spontaneous Ca^{2+} release through RyR2 channels can occur in the form of Ca^{2+} oscillations, a phenomenon now known as "Store-Overload Induced Calcium Release" or SOICR (Jiang et al., 2004, Venetucci et al., 2008). In view of the association between Ca^{2+} overload, DADs and CPVT, disease-causing mutations have been suggested to reduced the threshold for SOICR occurrence, which in turn increases the susceptibility for arrhythmogenesis (Priori and Chen 2011).

4.1.3. CPVT-associated mutations enhance the sensitivity of ryanodine receptors to Ca^{2+} activation:

A co-ordinated change in Ca^{2+} concentration on both the cytosolic and luminal side of the jSR membrane is responsible for regulating Ca^{2+} release through RyR2 channels. As illustrated in Figure 4.1, Jiang et al (2004, 2005) proposed that in disease states such as CPVT, mutation causes an enhanced sensitivity of RyR2 channels to luminal Ca^{2+}, which as a consequence, lowers the threshold SR Ca^{2+} load at which SOICR occurs. The group examined a number of RyR2 (recombinant mouse) mutations spanning the length of the protein, expressed in HEK293 cells, including the mutation studied in this project, N4104K (located in the C-terminal region), (Jiang et al., 2004, 2005). Using single-cell Ca^{2+} imaging, all mutations were found to enhance the frequency of spontaneous Ca^{2+} oscillations, resulting in a decrease in the ER Ca^{2+} store (measured by caffeine-induced Ca^{2+} release). Compared with WT RyR2 at the single channel level, mutant RyR2

channels displayed an increased open probability in response to luminal Ca^{2+}, (Jiang et al., 2004, 2005). Consistent with this observation, Ca^{2+} oscillations were evident at lower extracellular Ca^{2+} concentrations in mutant expressing cells, leading to suggestions that spontaneous Ca^{2+} release manifests at a reduced ER load in CPVT. This may also explain how enhanced SOICR occurs with mutant RyR2 expression, despite an observed reduction in the SR Ca^{2+} content (Jiang et al., 2005). Measured using [^{3}H]-ryanodine binding, mutant and WT RyR2 channels responded equivalently to activating Ca^{2+}, which predominantly reflects the channel's sensitivity to cytosolic Ca^{2+} (Jiang et al., 2005). A recent publication by Chen et al (2014) reported the discovery of a key residue (E4872) which may comprise the inherent luminal Ca^{2+} sensor of RyR2, located within the region of the proposed Ca^{2+} sensing gate (helix bundle crossing region). HEK293 cells expressing a mutation of this residue, E4872Q, displayed no SOICR activity, highlighting its involvement in sensing SR Ca^{2+} content. In addition, knock-in of the E4872Q mutation into a mouse model expressing the CPVT-mutant R4496C protected the animals against stress-induced arrhythmia (Chen et al., 2014). To distinguish this mechanism from that of the CSQ2-based luminal Ca^{2+} sensor, the effects of RyR2 E4872Q were also examined in CSQ2-knockout mice (Zhang et al., 2014), where comparable to the aforementioned findings, the mutant eliminated spontaneous Ca^{2+} release and triggered arrhythmia. Currently, the interplay between the luminal Ca^{2+} sensor formed by the luminal accessory proteins and the RyR2-resident sites remains unexplored (Chen et al., 2014).

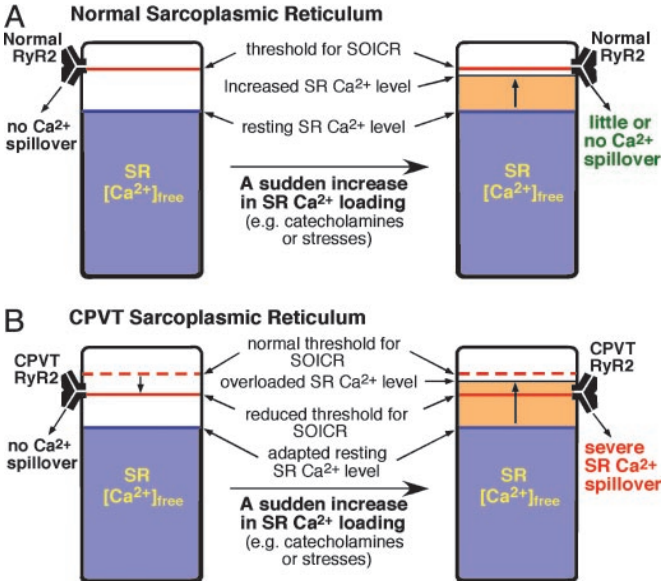

Figure 4.1: Schematic of the store-overload induced Ca^{2+} release (SOICR) mechanism hypothesised for CPVT mutants: *When normal RyR2 are expressed in cardiomyocytes, the levels of free SR luminal Ca^{2+} (blue shading), largely regulated by CSQ2, is below the normal threshold for spontaneous Ca^{2+} release (solid red line, panel A), thus there is no SOICR activity (panel A). Upon ß-AR stimulation under conditions such as stress or exercise, when the levels of free luminal Ca^{2+} are elevated (orange shading) by enhanced SERCA2a actvity, the SR Ca^{2+} level under normal conditions still remains below the SOICR threshold (Panel A, right). It is however hypothesised that as a consequence of RyR2 mutation, the threshold for SOICR occurrence is reduced (panel B, reduced threshold indicated by solid red line, normal SOICR threshold dashed red line). Therefore, under stimulated conditions the raised free luminal Ca^{2+} exceeds the SOICR threshold (orange shading, panel B, right) and spontaneous Ca^{2+} release is generated, greatly increasing the propensity for DADs and triggered arrhythmias. Image modified from Jiang et al., 2004.*

The heterogeneous nature of RyR2 mutant dysfunction, first proposed by Thomas et al., 2004, was highlighted in a more recent investigation by Loaiza et al (2013), where it was demonstrated that a CPVT-linked mutant, V2475F, displayed enhanced sensitivity to both cytosolic and luminal Ca^{2+} regulation. Compared with WT channels, the RyR2 mutant exhibited sensitised activation by increasing concentrations of cytosolic Ca^{2+}, established using a [^{3}H]-ryanodine binding assay. Interestingly, as found by Jiang et al (2005), the V2475F mutation also displayed a pronounced responsiveness to changes in luminal Ca^{2+} (measured by single channel recordings). However, when WT and mutant channels were expressed in HEK293 cells (as in Jiang et al., 2004, 2005) no differences in the SOICR threshold were evident. An earlier investigation by Meli et al (2011) reported that luminal Ca^{2+} sensing is not defective in CPVT and demonstrated that the RyR2 mutation G230C exclusively displays enhanced sensitivity to cytosolic Ca^{2+}. However, characterising the same mutation, Liu et al (2013) provided evidence of an enhanced propensity for SOICR occurrence. This thus highlights the need to assess the functional alterations of RyR2 mutants in more than one experimental system and further demonstrates the complexity in

deciphering the mechanism behind channel dysfunction. Since the studies by Jiang et al (2004) and Loaiza et al (2013) used purified mouse RyR2 channels and expression in HEK293 cells, which are devoid of accessory proteins, the altered sensitivity of RyR2 mutants to luminal/cytosolic Ca^{2+} could not be attributed to changes in channel modulation by the CSQ2-mediated luminal Ca^{2+} sensor. However, given the proposed role of the proteins in regulating RyR2 channel activity and the fact that CSQ2 mutations can also cause the CPVT phenotype (Houle et al., 2004), alterations in the function of these proteins may also contribute to defective RyR2 luminal Ca^{2+} sensing and thus needs to be investigated.

4.1.4. Chapter Aims

Luminal regulation of Ca^{2+} release through RyR2 channels is thought to be influenced both by the sensitivity of RyR2 channels themselves to activating luminal [Ca^{2+}] (Laver et al., 2007) and it's ensuing effect on cytosolic Ca^{2+} sensitivity; and via interaction with the luminal accessory proteins CSQ2, JUN and/or TRD1 (Györke and Györke, 1998). It is possible that two luminal Ca^{2+} sensing mechanisms exist to regulate RyR2 function, one of which forms part of the RyR2 channel itself (Chen et al., 2014) and the other composed of the luminal accessory proteins interacting with the Ca^{2+} release channels (Györke and Györke, 1998, Wei et al., 2009b).

Since it is unknown how RyR2 mutation could affect luminal accessory protein regulation, the behaviour of mutant channels with CSQ2 and/or JUN co-expression has been evaluated, and directly compared with findings using WT hRyR2. Cytosolic and luminal Ca^{2+} regulation of WT and mutant (A4556T and N4104K) channels will be examined in this chapter, since the two are ultimately linked.

In the absence and presence of luminal accessory proteins CSQ2 and JUN, WT and mutant hRyR2 channel regulation by Ca^{2+} has been assessed as follows:

- Quantitative [^{3}H]-ryanodine binding experiments were used to evaluate the cytosolic Ca^{2+} activation profile of WT and CPVT-linked mutant RyR2 channels in the presence/absence of CSQ2 and/or JUN. Used extensively as an effective agent to examine RyR2 function, [^{3}H] ryanodine will only bind RyR channels in their open conformation and thus acts as a surrogate marker of channel activity (Meissner et al., 1988, Li and Chen, 2001, Jiang et al., 2005).

- Since the term SOICR, is somewhat of a misnomer, as it refers to a lowered threshold for spontaneous Ca^{2+} release as opposed to actual store overload, the Ca^{2+} oscillations analysed in this investigation will be referred to as spontaneous Ca^{2+} release (SCR) events. Using single cell Ca^{2+} imaging, the parameters of SCR events (such as amplitude, duration and frequency) were monitored to establish luminal Ca^{2+} effects, where a direct comparison was made between HEK293 cells expressing WT/mutant RyR2 channels alone or in the presence of accessory proteins (achieved using stable cell lines expressing CSQ2, JUN or CSQ2+JUN). This technique was first used to establish if WT and mutant RyR2 are activated differently by luminal Ca^{2+}. The responses of WT and mutant channels to luminal accessory protein co-expression were then compared.

4.2 Methods:

4.2.1. Optimisation of the quantitative [^{3}H]-ryanodine binding assay:

A series of [^{3}H] ryanodine binding reactions (further details described in Chapter 2, section 2.4.3.5, Figure 2.4) were used to test a range of different protein concentrations (50-200µg), where each binding assay included 10nM [^{3}H] ryanodine, prepared to a final volume of 500µl with a binding buffer designed to optimise the open probability of RyR2 channels (containing 1M KCl, 100µM Ca^{2+} and 25mM PIPES (pH 7.4)). To distinguish any non-specific binding, 1000-fold excess 'cold', unlabelled ryanodine (10µM) was added to control samples. Liquid scintillation counting was used to quantify [^{3}H]-ryanodine binding data, where the counts achieved were measured in decays (or disintegrations) per minute (dpm). Subtraction of the non-specific counts achieved in control samples (in the presence of excess unlabelled ryanodine) from the total counts obtained in the test samples (using the same protein concentration) was used to calculate specific [^{3}H] ryanodine binding (for example, if a control sample yielded 2000dpm and a test sample 8000dpm, specific [^{3}H] ryanodine binding was calculated as 6000dpm). In preliminary investigations, the same assay was also carried out using two native sources (rabbit skeletal and rat cardiac heavy SR membranes) where it could be guaranteed that RyR was being expressed to a very high level. The data established using the native material was subsequently used to gauge the expression levels achieved using recombinant protein, by measurement of the specific [^{3}H] ryanodine bound, in pmol/mg of protein.

4.2.1.1. [^{3}H] ryanodine binding as a measurement of hRyR2 Ca^{2+} activation:

A suitable range of Ca^{2+} concentrations for hRyR2 activation (0-500µM (Mukherjee et al., 2012)) was achieved by accurately buffering stock binding solutions with three Ca^{2+} chelators: EGTA, HEDTA and NTA (see abbreviations table, Patton, 2004). To achieve a given free Ca^{2+} concentration, the appropriate amounts of $CaCl_2$ to add to stock binding buffer (in the presence of 1mM of each Ca^{2+} chelator) were calculated using the Maxchelator software (http://www.standford.edu/~cpatton/maxc.html). Prior to using recombinant protein, the Ca^{2+} activation assay was tested using a native sample, as with previous optimisation (section 4.3.1).

To establish enough material for further investigations, 48 microsomal membrane preparations were generated in total (n=4 per protein combination). The following eGFP-hRyR2 and luminal protein combinations were produced: (1) WT hRyR2 alone or in the presence of CSQ2 and/or JUN, (2) A4556T hRyR2 alone or in the presence of CSQ2

and/or JUN and (3) N4104K hRyR2 alone or in the presence of CSQ2 and/or JUN. Harvest of ~100x10^6 transfected HEK293 cells was required to generate each mixed membrane sample, which typically yielded a protein concentration of 4-6 mg/ml (established using a BCA protein assay). To undertake each [^{3}H] ryanodine binding Ca^{2+} activation assay in duplicate, approximately 4.4 mg of protein was necessary (calculated based on the use of 100 µg per reaction).

Densitometric analysis of Western blot signals was used to standardise expression levels of WT/mutant hRyR2 from each mixed membrane preparation, i.e., a representative WThRyR2 sample was used as a densitometric control, ensuring all test samples were standardised for hRyR2 expression prior to use in Ca^{2+} activation experiments. Each [^{3}H] ryanodine binding Ca^{2+} activation curve was fitted using non-linear regression (variable slope) and statistically compared using the extra-sum of squares F-test (GraphPad Prism).

4.2.2. Examination of spontaneous Ca^{2+} release properties using single cell Ca^{2+} imaging:

Generation of stable HEK293 cell lines, Effectene®-mediated transfection and loading of cells with Fluo3-AM are described in Chapter 2 (sections 2.4.2.3 and 2.4.3.8-2.4.3.9). Prior to confocal imaging, mDMEM was removed from the loaded cells and replaced with a 200µl meniscus of Krebs-Ringer-Hepes (KRH) buffer, supplemented with 1.3 mM Ca^{2+}. As demonstrated by Jiang et al., 2004, raising the external Ca^{2+} around HEK293 cells is an effective way to induce SOICR-events. This is an intrinsic property of RyR2 channels (Jiang et al., 2004), since untransfected HEK cells loaded with Fluo3-AM did not display any SOICR-like events (as shown in the Appendix, Figure 5).

The transfected cells were imaged using a laser scanning confocal microscope (Leica SP5, Leica, Heidelberg, Germany), with an oil immersion, 63x magnification objective lens and an argon laser, controlled with Leica software. Ca^{2+} dependent Fluo3-AM fluorescence was visualised by excitation at 488 nm and fluorescence emission detected over a range of 520±28 nm. Using Leica LAS AF confocal software (Leica Microsystems), data were collected over 2 minute recordings (5 frames/second) at 512 x 512 pixel resolution. Acquired as regions of interest (ROIs), all cells displaying SCR-activity (visualised as cell oscillations) representing global Ca^{2+} environments, or caffeine-dependent Ca^{2+} release, were selected. All collated data were exported to Microsoft Excel for further analysis and statistical differences calculated using one-way ANOVA and a Tukey-Kramer post-test (GraphPad prism). Outliers in the collected data were identified using the GraphPad prism Grubbs' test (column scatter plots of all collected data are

shown in the Appendix, Figure 6). Illustrated in Figure 4.2, all properties of the Ca^{2+} SCR events were examined as follows:

1. ***Basal Signal Intensity:*** The basal signal intensity (**F_0**) was measured by taking a mean of the fluorescence values between each SCR event (inter-SCR). F_0 is highlighted by a dashed line in Figure 4.2 (A).

2. ***Amplitude:*** Subtraction of the average inter-SCR basal signal intensity **(F_0)** from peak signal intensity (**F**) of each event was used to determine SCR amplitude (**$F-F_0$**). **F** is indicated with a green arrow in Figure 4.2 (A) and (B). The amplitude was expressed as a proportion of the basal signal intensity (**$F-F_0/F_0$**, denoted as **$\Delta F/F_0$**).

3. ***Duration:*** Measured in seconds (**s**), the duration of each SCR event was established by obtaining the difference between the time at which the SCR-event was initiated and the time when the signal intensity returns to basal levels (**F_0**). The SCR event start (red arrow) and end (brown arrow) are highlighted in Figure 4.2 (A).

4. ***Rate of Ca^{2+} Release:*** The rate of Ca^{2+} release is expressed as a change in the signal intensity over time (**$(\Delta F/F_0)sec^{-1}$**). Firstly, the time taken to reach peak Ca^{2+} levels was established by subtracting the time at which the SCR-event was initiated from the time taken to reach peak signal intensity. To calculate the rate at which spontaneous Ca^{2+} release occurred, the amplitude of the SCR event (**$F-F_0/F_0$**) was divided by the time taken to reach peak Ca^{2+} levels.

5. ***Rate of Ca^{2+} Decay:*** The rate of Ca^{2+} decay is also expressed as a change in the signal intensity over time (**$(\Delta F/F_0)sec^{-1}$**). The time taken for the Ca^{2+} peak to return to F_0 was first established by subtracting the time at peak signal intensity from the time taken for the SCR-event to return to baseline levels (SCR end, indicated with a brown arrow in Figure 4.2 (A)). To calculate the rate at which spontaneous Ca^{2+} release decayed (indicative of it's removal from the cytosol), the amplitude of the SCR event (**$F-F_0/F_0$**) was divided by the time taken for the signal intensity to return back to basal levels.

6. ***Inter-SCR Duration:*** Measured in seconds (**s**), the inter-SCR duration (representing the time period in between each SCR-event) was established by taking the time at which a new SCR-event occurred and subtracting from it the time at which the previous event ended and returned to baseline.

7. ***Frequency of events:*** Measured as SCR-events per minute, the frequency was determined by first adding together the SCR event duration and the inter-SCR duration, which established in seconds is the duration of a full SCR-event, and subsequently calculating the occurrence of these events per minute.

8. ***Estimation of ER Ca^{2+} load:*** Demonstrated in Figure 4.2 (B), ER Ca^{2+} load was estimated by calculating the Ca^{2+} release amplitude induced by caffeine application (10mM, dissolved in KRH). Subtraction of the average basal signal intensity (**F_0**) from peak signal intensity (**F**) was used to determine the SCR event amplitude (**$F-F_0$**). **F** is indicated in (B) with a green arrow. The amplitude was subsequently expressed as a proportion of the basal signal intensity.

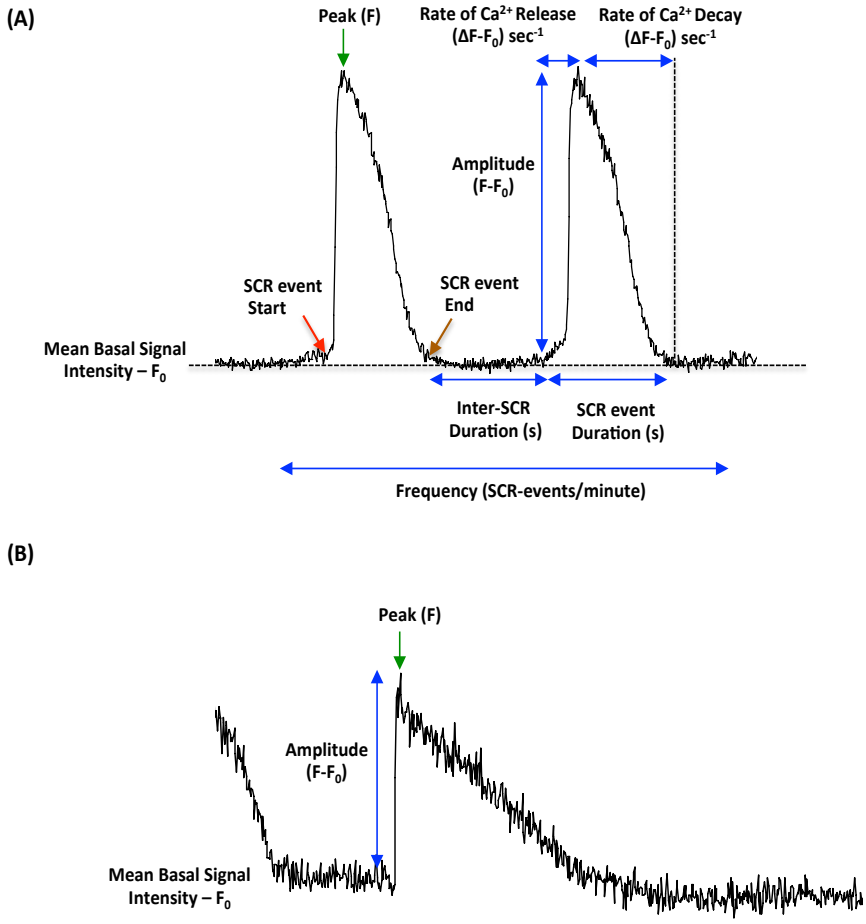

<u>Figure 4.2:</u> Illustration of the SCR kinetic parameters measured in transfected HEK293 cells: *A representative trace of SCR events obtained from Fluo-3 loaded HEK293 cells (in the presence of 1.3mM external Ca^{2+}) are shown in (A), where the parameters assessed are indicated with blue arrows. The start, end and peak of a SCR-event are highlighted with red, brown and green arrows, respectively. F_0 represents the basal Fluo-3 signal intensity. The ER Ca^{2+} store load, was estimated by measuring the amplitude of caffeine-induced Ca^{2} release, as demonstrated in (B).*

4.3 Results:

4.3.1. Optimisation of [^{3}H] ryanodine binding assays using native and recombinant material:

Demonstrated in Figure 4.3 (A), establishing a suitable protein concentration of recombinant hRyR2 for use in future experiments was achieved by plotting an average of the specific [^{3}H] ryanodine binding counts (in dpm) generated when using the recombinant material, against the chosen protein concentration range (0-200µg) used in the assay. 100µg was chosen as the optimal protein quantity for use in subsequent investigations since this concentration appeared to be the minimal protein amount which yielded the least [^{3}H] ryanodine binding variability, and at which sufficient liquid scintillation counts were achieved.

Since the [^{3}H]-ryanodine binding assay requires the use of functional RyR2 channels expressed to a high level, it seemed rational to also carry out the same optimisation experiments using native sources, such that a comparison could be made between the data collected using the recombinant material. Illustrated in Figure 4.3 (B) as a bar graph, despite being lower, the specific [^{3}H] ryanodine bound in 100µg of recombinant protein could be directly compared to native material, a WT hRyR2 mixed membrane preparation bound to 0.3 ± 0.02 pmol/mg [^{3}H] ryanodine, compared with 1.0 ± 0.18 and 16.8 ± 1.30 pmol/mg for native rat cardiac and rabbit skeletal membranes, respectively. Furthermore, native rat cardiac membranes were also used to test the Ca^{2+} activation assay before proceeding with recombinant material. As shown in Figure 4.3 (C), the resultant [^{3}H] ryanodine binding Ca^{2+} activation curve displayed a sigmoidal relationship (EC_{50} = 0.35±0.02µM), indicating that the range of Ca^{2+} concentrations chosen were buffered efficiently (section 4.2.1.1).

As described previously in section 4.2.1.1, before use in [^{3}H] ryanodine binding Ca^{2+} activation assays, all eGFP-hRyR2 mixed membranes (expressed alone/in the presence of CSQ2, JUN or CSQ2+JUN) were standardised for hRyR2 expression by Western blotting and densitometric analysis. Highlighted in Figure 4.4 (A), the same representative WT hRyR2 mixed membrane preparation was loaded alongside all additional mixed membrane preparations during hRyR2 detection and using 100µg of recombinant protein as a benchmark, the concentration of a given mixed membrane sample was adjusted for use in Ca^{2+} activation assays accordingly, ensuring equivalent amounts of hRyR2 protein were used in each experiment (Figure 4.4,B).

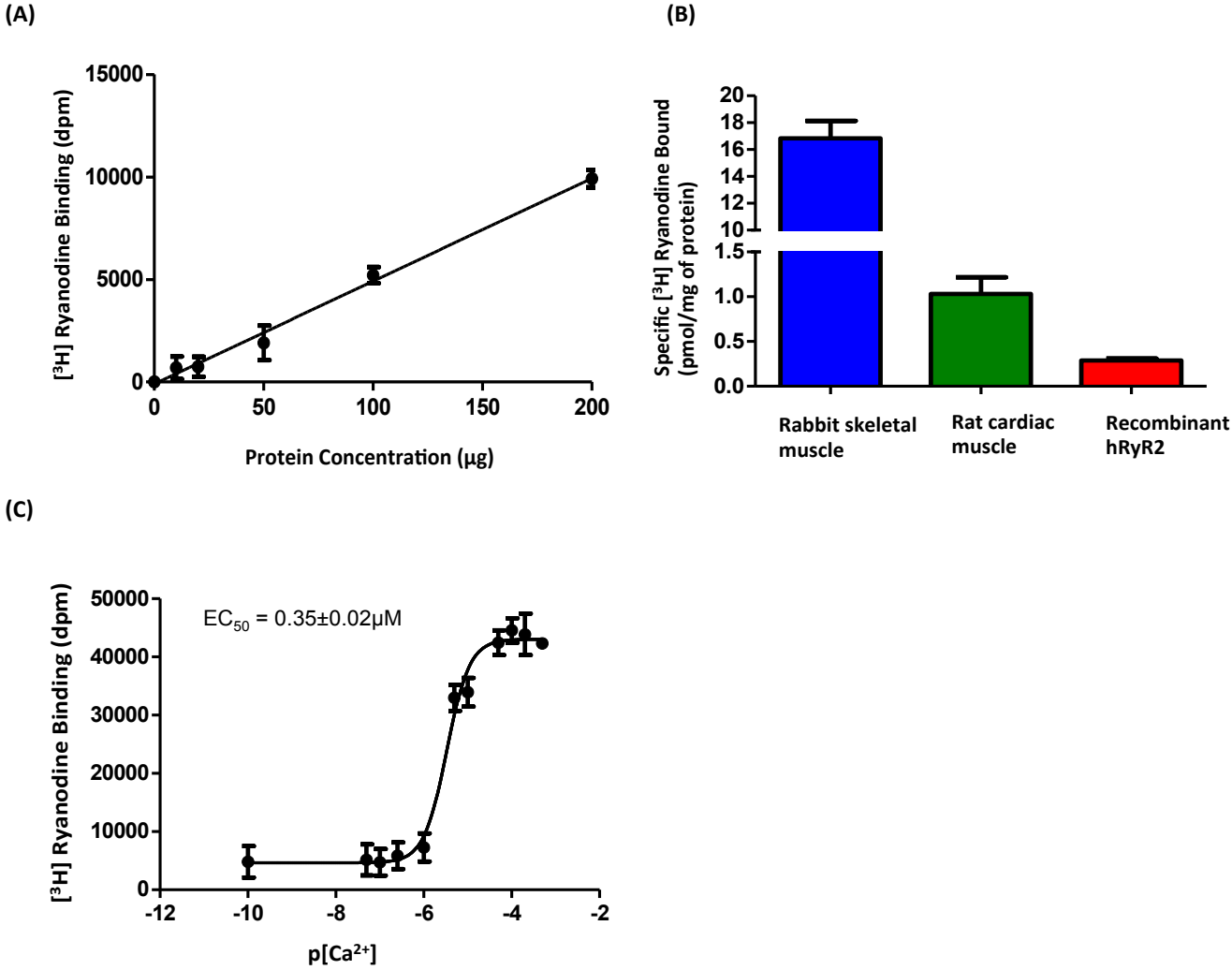

Figure 4.3 Determination of an optimal recombinant protein amount for use in [^{3}H] ryanodine binding assays and a preliminary Ca^{2+} activation assay using native material: *To establish an optimal recombinant protein concentration for use in Ca^{2+} activation assays, the [^{3}H] ryanodine binding counts (in dpm) achieved using increased amounts of recombinant WT RyR2 protein (n=3 experiments) were determined by liquid scintillation counting and the averages plotted as shown in (A). To gauge the success of acquiring sufficient [^{3}H] ryanodine binding counts using the recombinant material generated, two native preparations: rat cardiac and rabbit skeletal membranes were included as controls in optimisation investigations (n=3 experiments for each), (B). The concentration of specific [^{3}H] ryanodine bound to 100µg of recombinant material was calculated as: 0.3 ± 0.02 pmol/mg of protein, compared with 1.0 ± 0.18 and 16.8 ± 1.30 pmol/mg of rat cardiac and rabbit skeletal membranes, respectively. Prior to commencing Ca^{2+} activation experiments, a preliminary experiment (n=4) was carried out using rat cardiac muscle membranes. The [^{3}H] ryanodine binding Ca^{2+} curve obtained is shown in (C), which yielded an EC_{50} of 0.35±0.02µM.*

(A)

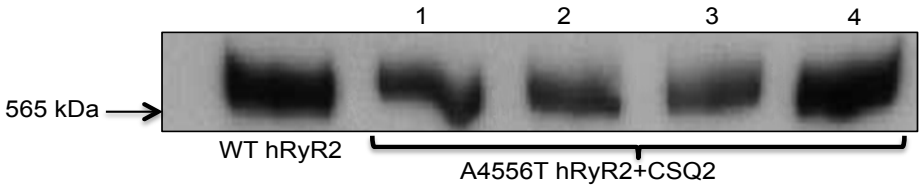

(B)

Mixed membrane Sample	Density (ODu/mm^2)	Normalisation	Protein amount required for [^{3}H] ryanodine binding (µg)
WT hRyR2	21.13749136	1	100
A4556T hRyR2+CSQ2 (Preparation 1)	13.70498893	0.648373577	154.2319711
A4556T hRyR2+CSQ2 (Preparation 2)	12.08151488	0.571567863	174.9573104
A4556T hRyR2+CSQ2 (Preparation 3)	10.61617886	0.502244117	199.1064104
A4556T hRyR2+CSQ2 (Preparation 4)	33.78306817	1.598253624	62.56827763

Figure 4.4: Standardisation of mixed membrane preparations for hRyR2 expression by densitometry before use in [^{3}H] ryanodine binding Ca^{2+} activation assays: *As an example, standardisation of hRyR2 in mixed membrane preparations generated from HEK293 cells expressing mutant A4556ThRyR2+CSQ2 are shown as a Western blot (signal detection: 1.30 minutes) in (A), with a corresponding table of results in (B). The same process was carried out for all other test samples. Following SDS-PAGE and Western blotting, each mixed membrane sample intended for future use was checked for sufficient hRyR2 expression by densitometric analysis of Western signals. Using the levels of hRyR2 expression detected in a WT sample as a standard, 100µg (established as optimal to achieve sufficient [^{3}H] ryanodine binding) of this sample was used as benchmark to adjust the protein concentration of other mixed membrane preparations accordingly, such that equivalent amounts of hRyR2 protein were used in each Ca^{2+} activation experiment.*

4.3.2. Measurement of the Ca^{2+} dependence of [^{3}H]-ryanodine binding for WT, A4556T and N4104K hRyR2 channels in the absence of luminal accessory proteins:

[^{3}H]-ryanodine binding was used to assess the cytosolic Ca^{2+} sensitivity of WT and CPVT-linked mutant human RyR2 when recombinantly expressed alone or co-expressed with CSQ2, JUN or CSQ2 and JUN. Figure 4.5 illustrates the Ca^{2+} activation curve for WT hRyR2 channels expressed alone, which yielded an EC_{50} of 0.58 ± 0.27μM. As demonstrated, the Ca^{2+} activation data can also be plotted as specific [^{3}H] ryanodine bound in pmol/mg of protein, as used in Du et al., 1998 and Li and Chen 2001. Using [^{3}H]-ryanodine binding assays, the sensitivities to Ca^{2+} activation of mouse (EC_{50} of 0.28±0.02μM (Jiang et al., 2005) and 0.31±0.02μM (Jiang et al., 2007)) and rabbit (EC_{50} of 0.79±0.08μM (Du et al., 1998)) recombinant RyR2 are not dissimilar to those obtained in this investigation.

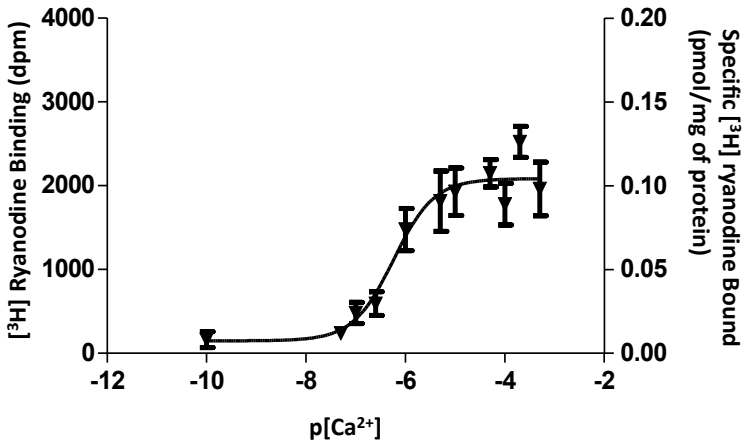

Figure 4.5: [^{3}H] ryanodine binding Ca^{2+} activation curve of WT hRyR2 channels: *The Ca^{2+} activation profile achieved for WThRyR2 was derived from an n=10 assays, where values were obtained from 4-5 separate binding experiments. The curve was constructed using a sigmoidal dose-response (variable slope) fit (GraphPad Prism). As shown, the dose-response data can be presented using the [^{3}H] ryanodine binding counts achieved (in dpm), determined by liquid scintillation counting or the binding counts generated can subsequently be used to calculate the specific [^{3}H] ryanodine bound in pmol/mg of protein.*

Mutant hRyR2 Ca^{2+} activation curves were compared with that obtained for WT hRyR2 channels. Given that all protein samples used in the Ca^{2+} activation assays were first standardised for hRyR2 expression, at first glance, it was not deemed necessary to normalise results to maximal (max) [^{3}H] ryanodine binding, since arguably all max binding should be the same. As shown in Figure 4.6, this is the case for the N4104K hRyR2 mutant (A), which displays similar max binding to WT hRyR2 channels. However, when A4556T hRyR2 channels were assessed (B), [^{3}H] ryanodine binding appeared much higher at

every Ca^{2+} concentration tested and thus max binding differed significantly from the WT. Due to the variable nature of the data, it was therefore decided that in order to rigorously compare the EC_{50} between datasets, the Ca^{2+} activation curves needed to be fitted with constraints (as without it, statistical differences may be difficult to pinpoint), as recommended in the GraphPad Prism Statistics Guide (www.graphpad.com). Often used to exhibit [^{3}H] ryanodine binding data in the literature (Jiang et al., 2005, Li and Chen, 2001), the simplest way to do this was to normalise the data. The [^{3}H] ryanodine binding dose-response curves generated will thus be presented both as non-normalised (raw) and normalised data, as in Figure 4.6.

N4104K hRyR2 channels displayed a significantly sensitised cytoplasmic Ca^{2+} activation profile (seen as a left-shift in the curve) compared to WT hRyR2, which yielded an EC_{50} of 0.22 ± 0.27μM (Figure 4.6 (A), normalised, right-graph). Furthermore, the mutant elevated channel activation at basal Ca^{2+} levels (as evident in the non-normalised Ca^{2+} activation curve (Figure 4.6 (A), left graph)). Normalised WT hRyR2 data yielded an EC_{50} of 1.63μM, which is almost identical to the EC_{50} (1.65± 0.43μM) reported by Mukherjee et al., 2012, at the single channel level.

Displaying the [^{3}H] ryanodine binding results both in the normalised and non-normalised form was important, since interesting aspects of the data might have otherwise been overlooked. In the raw data for example, increased [^{3}H] ryanodine binding was evident at all Ca^{2+} concentrations >1μM with A4556T hRyR2 channels (Figure 4.6 (B), right graph, highlighted with asterisks). However, the Ca^{2+} sensitivity of A4556T hRyR2 channels to activation was comparable to WT hRyR2, and yielded a similar EC_{50} = 0.63 ± 0.08μM (normalised data, right graph, (B)). Discussed further in section 4.4.1.1, the fact that enhanced [^{3}H] ryanodine binding was evident, yet the sensitivity to Ca^{2+} activation was similar to WT channels, may be due to an experimental error or it could reflect a bona fide consequence of channel mutation.

(A)

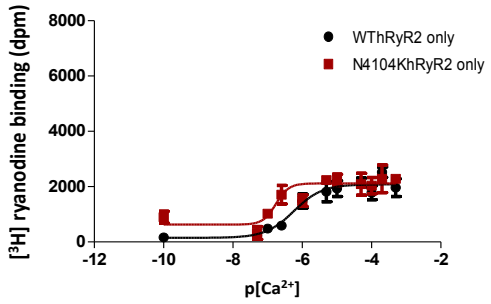

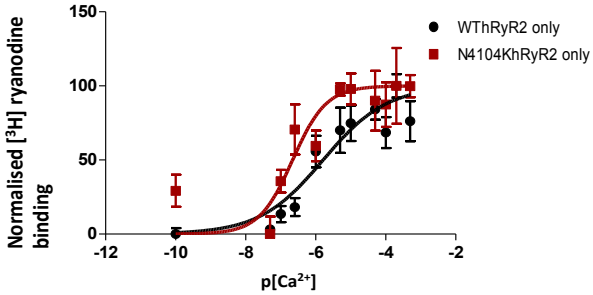

Best-fit values	WT hRyR2	N4104K hRyR2	Significance
EC_{50}	0.58 µM	0.17 µM	nsd

Best-fit values	WT hRyR2	N4104K hRyR2	Significance
EC_{50}	1.63 µM	0.22 µM	p<0.05

(B)

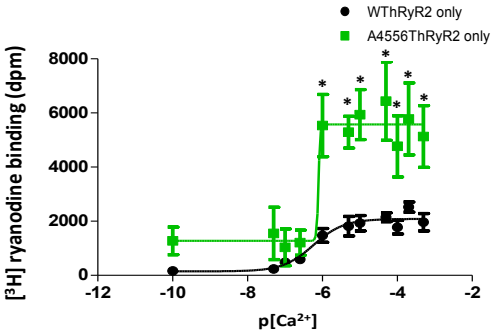

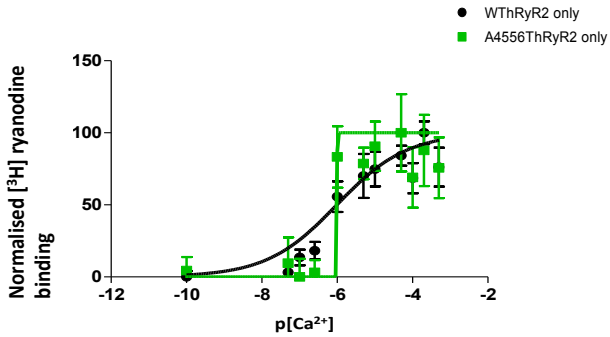

Best-fit values	WT hRyR2	A4556T hRyR2	Significance
EC_{50}	0.58 µM	0.78 µM	nsd

Best-fit values	WT hRyR2	A4556T hRyR2	Significance
EC_{50}	1.63 µM	0.63 µM	nsd

<u>Figure 4.6:</u> A comparison of the [^{3}H] ryanodine binding Ca^{2+} activation curves of WT, A4556T and N4104K hRyR2 channels: *Each dataset was fitted as a non-linear regression, sigmoidal (four parameter logistic) curve using GraphPad Prism. All statistical differences were also detected using this software, evaluated using the sum of squares F test (to reliably assess EC_{50} values), (GraphPad Prism). To normalise (right graphs), the data was constrained to 0 (bottom) and 100 (top) before fitting the curve. The tables indicate best-fit values, where (A) highlights a comparison of N4104K hRyR2 and (B) A4556T hRyR2, where nsd = no significant difference and p<0.05 = a significant difference to WT hRyR2. The Ca^{2+} activation profiles achieved for N4104K and A4556T hRyR2 were derived from an n=6 curves (for each, i.e 12 in total), obtained from 3 separate [^{3}H]-ryanodine binding experiments and using 3-4 different mixed membrane preparations expressing the mutant channel of interest. The A4556T mutant (non-normalised data, left graph (B)) displayed enhanced [^{3}H] ryanodine binding at all [Ca^{2+}] >1µM (* p = <0.05 vs WT hRyR2 response, Student's t-test (GraphPad Prism)).*

4.3.2.1. Ca^{2+} dependence of [^{3}H]-ryanodine binding for WT hRyR2 channels in the presence of CSQ2, JUN or CSQ2 and JUN:

Figure 4.7 shows the Ca^{2+} activation (determined using [^{3}H] ryanodine binding) of WThRyR2 channels in the presence of the luminal accessory proteins. Examination of both non-normalised (left graphs) and normalised Ca^{2+} activation data with constraints (right graphs) revealed that co-expression of CSQ2, JUN or CSQ2+JUN did not significantly affect the cytoplasmic Ca^{2+} activation of WThRyR2 and yielded similar EC_{50} values to WT channels (WThRyR2+JUN = 0.58 ± 0.15μM (A), WThRyR2+CSQ2 = 0.43 ± 0.08μM (B) and WThRyR2+CSQ2+JUN = 0.85 ± 0.21μM (C)). Co-expression of WT channels with JUN alone however, did appear to have a slight activatory effect on channel activity, both at basal and increasing Ca^{2+} levels, though this was not determined as statistically significant. Interestingly, this effect was not evident when WThRyR2 channels were co-expressed in the presence of both accessory proteins, suggesting CSQ2 may dampen any stimulatory effect observed.

(A)

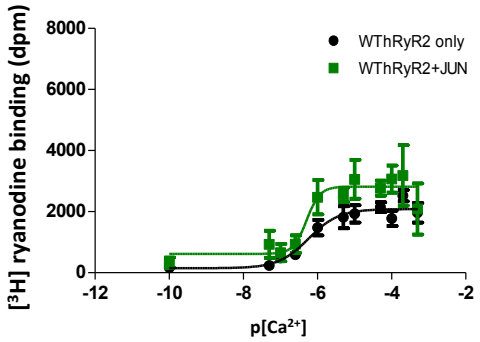

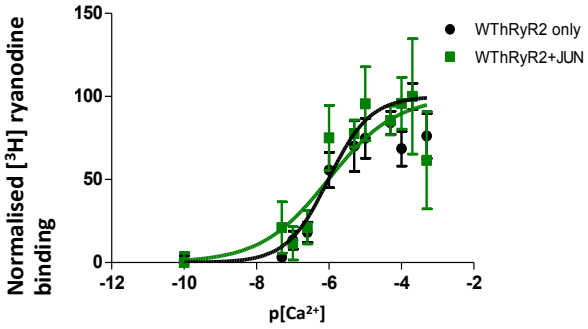

Best-fit values	WT hRyR2	WT hRyR2+JUN	Significance
EC_{50}	0.58 µM	0.50 µM	nsd

Best-fit values	WT hRyR2	WT hRyR2+JUN	Significance
EC_{50}	1.63 µM	0.58 µM	nsd

(B)

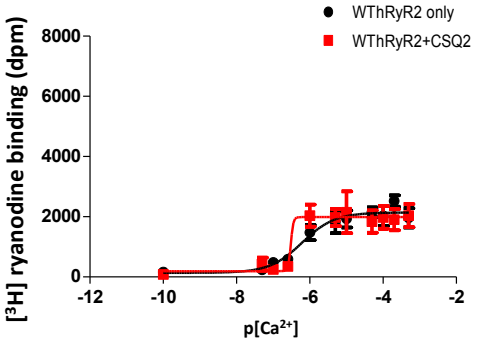

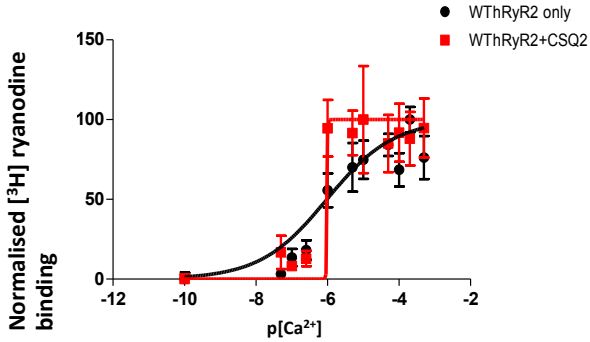

Best-fit values	WT hRyR2	WT hRyR2+CSQ2	Significance
EC_{50}	0.58 µM	0.30 µM	nsd

Best-fit values	WT hRyR2	WT hRyR2+CSQ2	Significance
EC_{50}	1.63 µM	0.43 µM	nsd

(C)

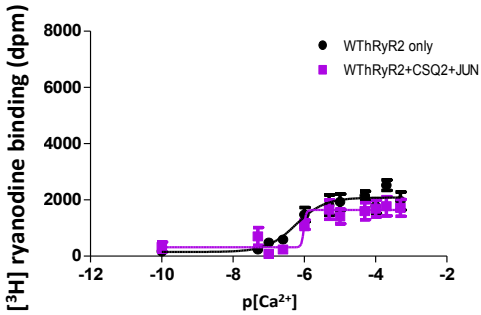

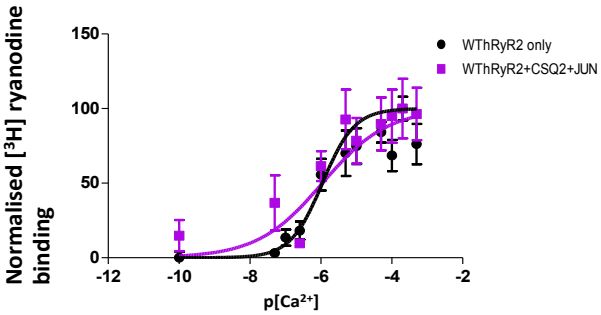

Best-fit values	WT hRyR2	WT hRyR2+ CSQ2+JUN	Significance
EC_{50}	0.58 µM	0.97 µM	nsd

Best-fit values	WT hRyR2	WT hRyR2+ CSQ2+JUN	Significance
EC_{50}	1.63 µM	0.85 µM	nsd

<u>Figure 4.7:</u> [^{3}H] ryanodine binding Ca^{2+} activation curves of WT hRyR2 channels expressed alone and in the presence of luminal accessory proteins CSQ2 and JUN: *Established from 3-4 separate experiments, co-expression of WThRyR2 with (A) JUN (n=6 assays), (B) CSQ2 (n=7 assays) and (C) CSQ2+JUN (n=7 assays) did not have any appreciable effects on the cytosolic Ca^{2+} activation profile achieved for WT channels expressed alone (plotted in (A)-(C)). All curves were fitted and statistically analysed as described in Figure 4.6, nsd = no significant differences in EC_{50} values compared to WThRyR2.*

4.3.2.2. Examination of Ca^{2+} dependence of [^{3}H]-ryanodine binding for CPVT-linked mutant hRyR2 channels in the presence of CSQ2, JUN or CSQ2 and JUN

4.3.2.2.1 A4556T hRyR2 channels:

As observed in the non-normalised data (left graphs), the elevated [^{3}H] ryanodine binding of mutant A4556T hRyR2 channels in response to cytosolic Ca^{2+} was not significantly altered by luminal accessory co-expression, as demonstrated in Figure 4.8 (A)-(C). Each normalised Ca^{2+} activation curve yielded the following comparable EC_{50} values: AT hRyR2+JUN = EC_{50} of 0.50 ± 0.12μM (A), AT hRyR2+CSQ2 = EC_{50} of 1.0 ± 0.4μM (B) and AT hRyR2+CSQ2+JUN = EC_{50} of 1.23 ± 0.37μM (C). Interestingly, although no statistically significant difference was detected, the increased basal [^{3}H] ryanodine binding seen at low [Ca^{2+}] in the non-normalised curves appeared to be restored to WT levels when the mutants were co-expressed in the presence of both CSQ2 and JUN (Figure 4.8, (C), left graph).

4.3.2.2.2 N4104K hRyR2 channels:

[^{3}H]-ryanodine binding Ca^{2+} activation curves obtained using mutant N4104K hRyR2 channels are shown in Figure 4.9. As found previously with WT and A4556T hRyR2 channels, luminal accessory protein co-expression did not significantly affect the cytosolic Ca^{2+} activation profile of this mutant. Each normalised Ca^{2+} activation curve yielded the following EC_{50} values, which were comparable to N4104K channels expressed alone: NK hRyR2+JUN = EC_{50} of 0.49 ± 0.4μM (A), NK hRyR2+CSQ2 = EC_{50} of 0.34 ± 0.1μM (B) and NK hRyR2+CSQ2+JUN = EC_{50} of 0.26 ± 0.02μM (C).

(A)

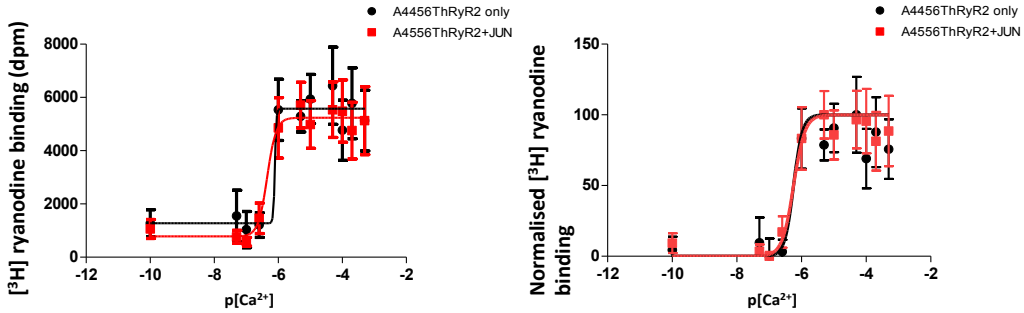

Best-fit values	A4556T hRyR2	A4556T hRyR2+JUN	Significance
EC_{50}	0.78 µM	0.45 µM	nsd

Best-fit values	A4556T hRyR2	A4556T hRyR2+JUN	Significance
EC_{50}	0.64 µM	0.50 µM	nsd

(B)

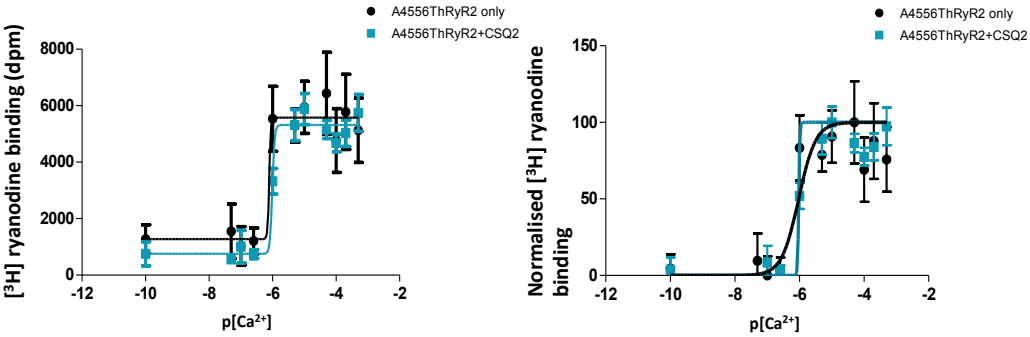

Best-fit values	A4556T hRyR2	A4556T hRyR2+CSQ2	Significance
EC_{50}	0.78 µM	0.98 µM	nsd

Best-fit values	A4556T hRyR2	A4556T hRyR2+CSQ2	Significance
EC_{50}	0.64 µM	1.00 µM	nsd

(C)

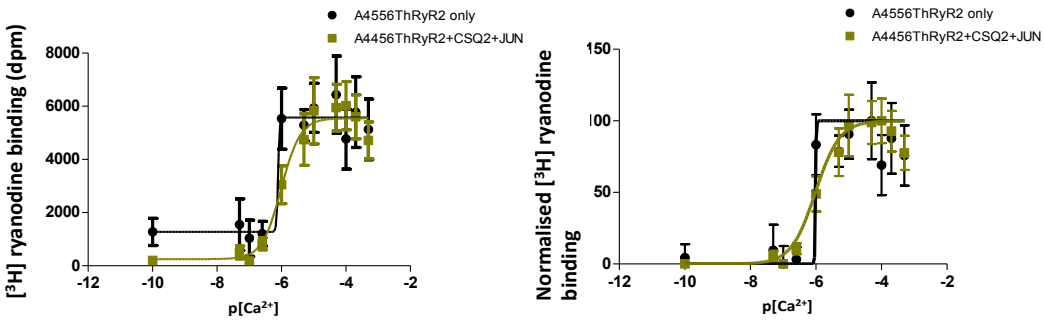

Best-fit values	A4556T hRyR2	A4556T hRyR2+ CSQ2+JUN	Significance
EC_{50}	0.78 µM	0.98 µM	nsd

Best-fit values	A4556T hRyR2	A4556T hRyR2+ CSQ2+JUN	Significance
EC_{50}	0.64 µM	1.23 µM	nsd

Figure 4.8: [^{3}H] ryanodine binding Ca^{2+} activation curves of A4556T hRyR2 channels in the absence and presence of CSQ2 and/or JUN: *Co-expression of AT hRyR2 with (A) JUN (n=6 assays), (B) CSQ2 (n=6 assays) and (C) CSQ2+JUN (n=6 assays) did not significantly alter the response of the mutant channels to increasing cytosolic Ca^{2+} concentrations, as directly compared with the Ca^{2+} activation curve achieved using AT hRyR2 channels expressed alone (A)-(C). Non-normalised (left graphs) and normalised (right graphs) data (collected from 3-4 separate binding experiments) was fitted and statistically analysed as described in Figure 4.6, nsd = no significant differences in EC_{50} values compared to AT hRyR2 expressed alone.*

(A)

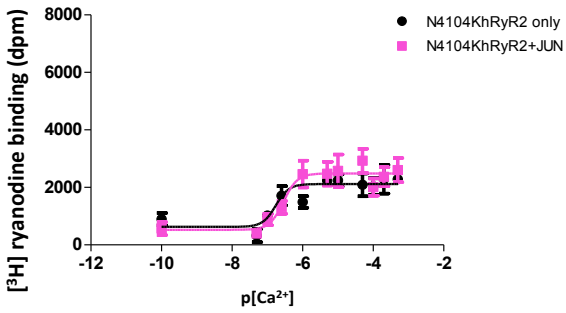

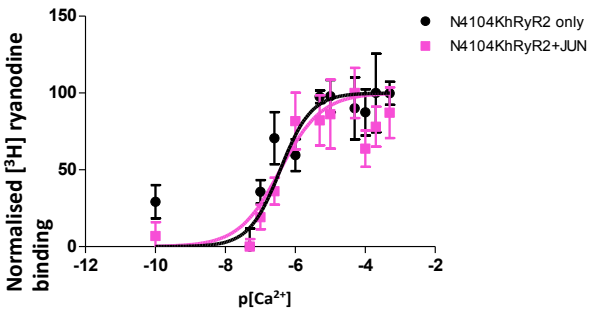

Best-fit values	N4104K hRyR2	N4104K hRyR2+JUN	Significance
EC_{50}	0.174 µM	0.28 µM	nsd

Best-fit values	N4104K hRyR2	N4104K hRyR2+JUN	Significance
EC_{50}	0.21 µM	0.49 µM	nsd

(B)

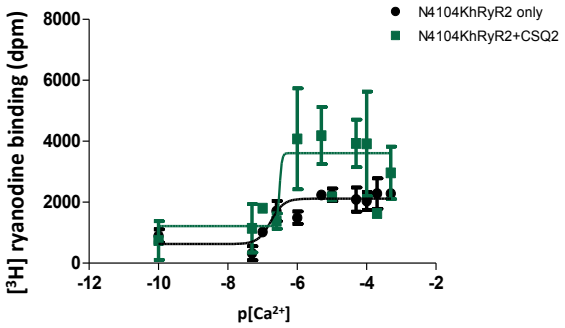

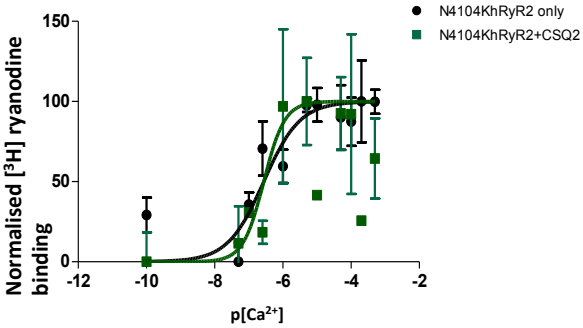

Best-fit values	N4104K hRyR2	N4104K hRyR2+CSQ2	Significance
EC_{50}	0.174 µM	0.30 µM	nsd

Best-fit values	N4104K hRyR2	N4104K hRyR2+CSQ2	Significance
EC_{50}	0.21 µM	0.34 µM	nsd

(C)

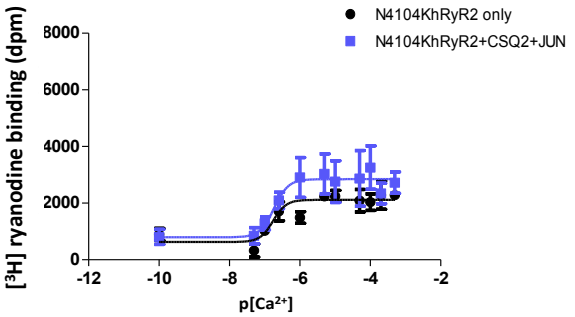

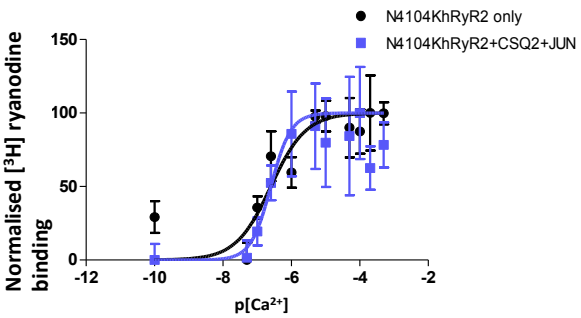

Best-fit values	N4104K hRyR2	N4104K hRyR2+ CSQ2+JUN	Significance
EC_{50}	0.174 µM	0.18 µM	nsd

Best-fit values	N4104K hRyR2	N4104K hRyR2+ CSQ2+JUN	Significance
EC_{50}	0.21 µM	0.26 µM	nsd

Figure 4.9: [^{3}H] ryanodine binding Ca^{2+} activation curves of N4104K hRyR2 channels in the absence and presence of luminal proteins: *The dose-response curve of N4104KhRyR2 expressed alone is shown in (A)-(C). Derived from 3-4 separate binding experiments (using 3-4 different mixed membrane preparations for each combination), co-expression of NK hRyR2 with (A) JUN (n=6 assays), (B) CSQ2 (n=6 assays) and (C) CSQ2+JUN (n=8 assays) did not significantly affect the response of the mutant channels to activating Ca^{2+}. Non-normalised (left graphs) and normalised (right graphs) data was fitted and statistically analysed as described in Figure 4.6, nsd= no significant differences in EC_{50} values compared to NK hRyR2*

4.3.2.3. Are luminal accessory protein interactions disrupted by the optimised [^{3}H] ryanodine binding conditions?

Designed to optimise the open probability of RyR2 and prevent aggregation, [^{3}H] ryanodine binding experiments were carried out using a binding buffer containing 1M KCl (as used in Jiang et al., 2007, Chopra et al., 2009, Euden et al., 2013). As demonstrated in Figure 4.10 (taken from Jiang et al., 2004), when undertaking investigations with recombinant (mouse) RyR2, sufficient [^{3}H] ryanodine binding of WT channels (open circles) was only achieved when higher concentrations of KCl were used. However, since no significant differences in the cytosolic Ca^{2+} activation profile of WT or mutant hRyR2 were detected when co-expressed in the presence of luminal accessory proteins, it seemed logical to establish if the high salt conditions disrupted the binding interactions of CSQ2 and JUN with hRyR2 (Ahmed, 2004). Described in Chapter 5, sections 5.2.2 and 5.3.4, the protein-protein interactions between CSQ2, JUN and hRyR2 were investigated by co-immunoprecipitation (Co-IP), using the µMACS™ system from Miltenyi Biotec (section 2.4.3.6, Figure 2.5). In these experiments, a low salt buffer (containing 150mM NaCl) was used to solubilise all mixed membrane samples. To establish if higher salt disrupts the interaction of the luminal proteins with hRyR2, a series of Co-IP investigations (n=4) were carried out using both the standard solubilisation buffer (section 2.1.9) and the same buffer prepared to contain 1M NaCl. Although not the primary goal of this investigation, it has been reported at the single channel level that high concentrations of luminal Ca^{2+} dissociates CSQ2 from RyR2 channels (Beard et al., 2005, Qin et al., 2008). To test this concept biochemically, 10mM Ca^{2+} was added to the standard solubilisation buffer (150mM NaCl) and also used in Co-IP investigations.

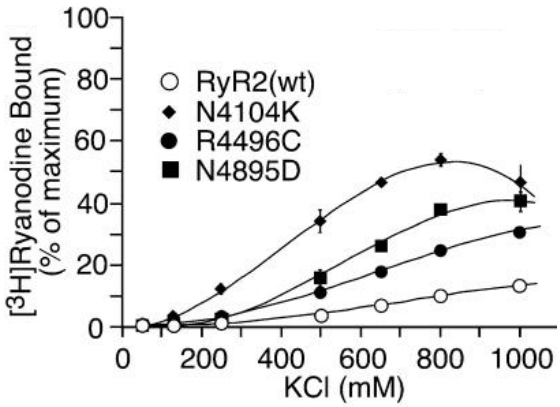

Figure 4.10: [^{3}H] ryanodine binding of WT and mutant RyR2 channels with increasing concentrations of KCl: *The aim of this investigation carried out by Jiang et al., 2004 was to demonstrate that RyR2 mutation enhances [^{3}H] ryanodine binding at basal (~3nM) Ca^{2+} levels. However, the graph also demonstrates that optimal binding in WT recombinant RyR2 (mouse in this case) is achieved at higher concentrations of KCl. (Image modified from Jiang et al., 2004).*

A mixed membrane preparation co-expressing WT hRyR2+CSQ2+JUN was used the Co-IP investigations, following the protocol described in Chapter 2, section 2.4.3.6. The only difference to this protocol was that in addition to using the standard buffer containing 150mM NaCl (no Ca^{2+}) for solubilisation, aliquots of the mixed membranes were also solubilised in the standard buffer (150mM NaCl) but with 10mM Ca^{2+} added and an equivalent buffer containing 1M rather than 150mM NaCl (Figure 4.11).

Figure 4.11 (A) shows an example of the Western blot signals obtained from the detection of CSQ2 or JUN expression captured in immunoprecipitates (eluted from anti-GFP magnetic microbeads (Miltenyi Biotec)). Derived from an n=4 investigations, the results varied somewhat with the use of high salt solubilisation buffer. In some experiments CSQ2 and JUN were unaffected (n=1 of 4 blots assessed), yet in another CSQ2 and/or JUN appeared reduced (n=1 both reduced, n=2 JUN only reduced). In the particular blot shown in Figure 4.11 (A), the association of JUN with hRyR2 channels appears to be diminished when solubilised in high salt buffer (lane 3, at ~26kDa), but the association of CSQ2 was unaffected (lane 3, at ~45kDa). In contrast, a reduction in the interaction of CSQ2 and JUN with hRyR2 channels was consistently observed when membranes were solubilised in the presence of 10mM Ca^{2+}, as demonstrated in Figure 4.11 (A), lane 2 (CSQ2 at ~45kDa and JUN at ~26kDa, respectively). Densitometric analysis was performed on all Co-IP Western signals (Figure 4.11 (B)), where a reduction in the association of CSQ2 and JUN with hRyR2 channels was only found to statistically significant when mixed membranes were solubilised in the presence of 10mM Ca^{2+}.

(A)

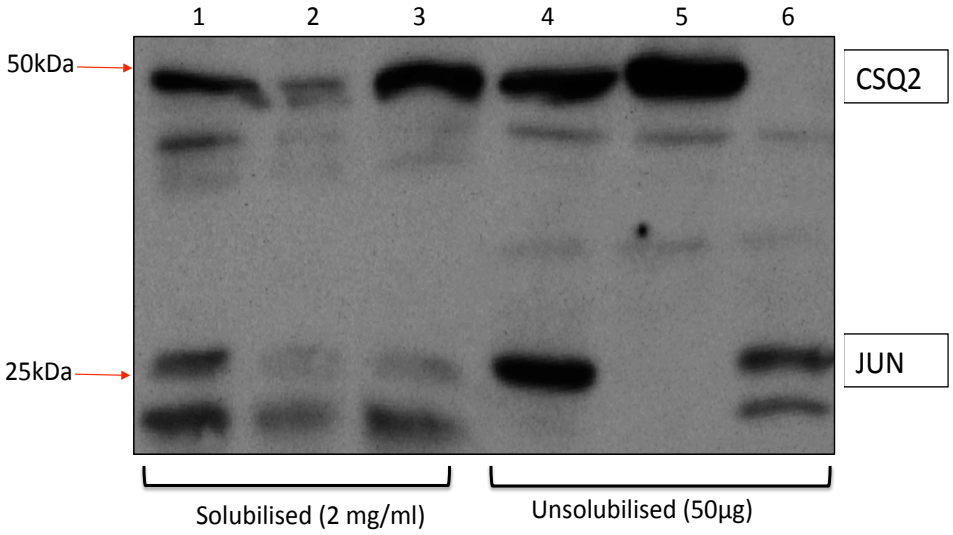

(B)

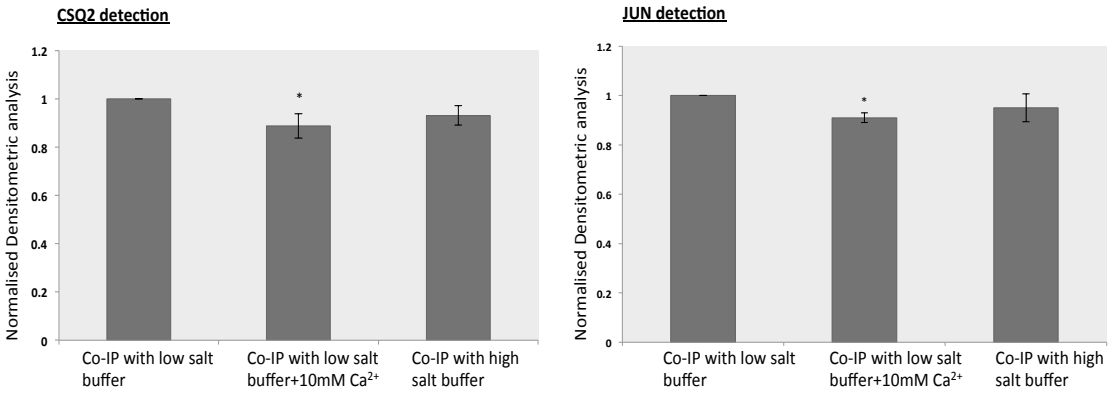

<u>Figure 4.11:</u> Co-immunoprecipitation investigations to establish if the association of CSQ2 and JUN with hRyR2 is altered by high salt and high Ca^{2+} concentrations: *An example of captured immunoprecipitates resolved by SDS-PAGE and detected by Western blotting is shown in (A), where lanes 1-3 = mixed membranes from cells expressing WT hRyR2, CSQ2 and JUN solubilised (at 2mg/ml) in buffer containing: (1) 150mM NaCl in contaminant Ca^{2+}, (2) 150mM NaCl with 10mM Ca^{2+} and (3) 1M NaCl in contaminant Ca^{2+}. Lanes 4,5 and 6 = mixed membranes (50µg, unsolubilised) from cells expressing WThRyR2, CSQ2 and JUN (4) or CSQ2 (5) or JUN (6) only. Each blot was probed with α-CSQ2 and α-JUN antibodies to detect CSQ2 and JUN, respectively. Represented as bar graphs (B), densitometric analysis of Western blot signals (n=4 blots) was used to distinguish any significant alterations in the association of CSQ2 and/or JUN with hRyR2 when solubilised in high salt conditions or in the presence of 10mM Ca^{2+} (normalised to the signals obtained using standard solubilisation buffer). Statistically significant differences (* $p<0.05$) were calculated using an ANOVA and a Tukey-Kramer post-test.*

4.3.3. Imaging of spontaneous Ca^{2+} release events in HEK293 cells expressing WT and mutant hRyR2 channels in the absence of luminal accessory proteins:

As illustrated in Figure 4.12, N4104K hRyR2-expressing HEK293 cells displayed markedly different SCR-events, compared with those observed in cells expressing WT or A4556T hRyR2. Presented as a series of bar graphs in Figure 4.13, the kinetic parameters of these events were examined. The N4104K mutant caused a significant reduction in the amplitude, duration and inter-SCR duration of SCR events, thereby increasing their frequency. In addition, the rate of Ca^{2+} release and decay was also reduced in N4104K hRyR2 expressing cells, which consequently changed the shape of the Ca^{2+} waves (Figure 4.12). Consistent with an enhanced frequency, the ER Ca^{2+} content (measured by the Ca^{2+} transient amplitude induced by caffeine application (10mM)) was significantly reduced (in comparison to cells expressing WT RyR2), which is indicative of Ca^{2+} leak through RyR2 channels (Jiang et al., 2007). In contrast, all SCR parameters in HEK293 cells expressing A4556T hRyR2 appeared similar to WT (Figure 4.13), where no significant differences between the two were detected.

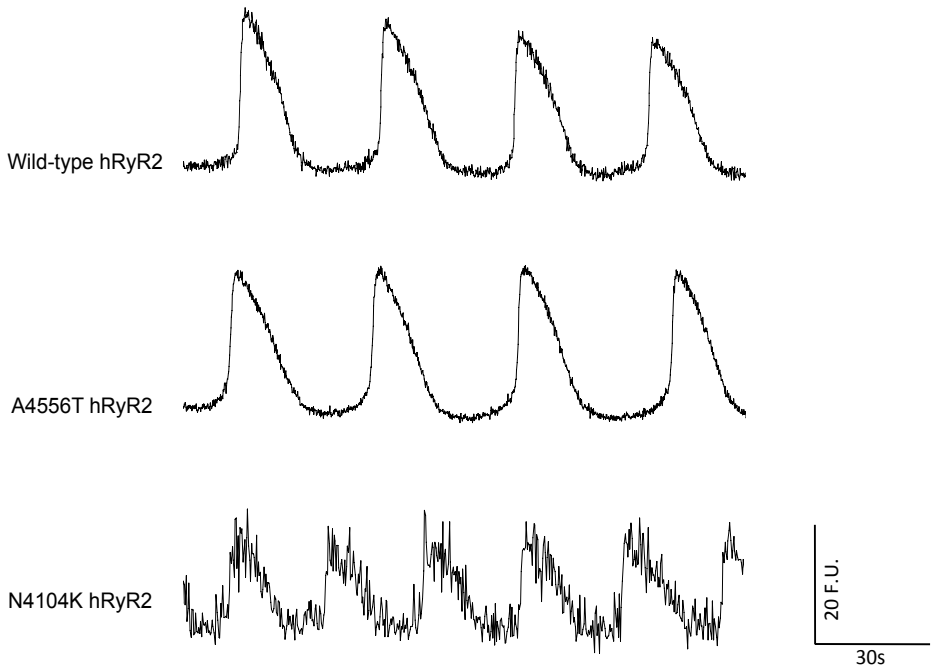

Figure 4.12: Representative traces of spontaneous Ca^{2+} release events from HEK293 cells expressing WT and mutant A4556T and N4104K hRyR2, measured by Fluo-3.

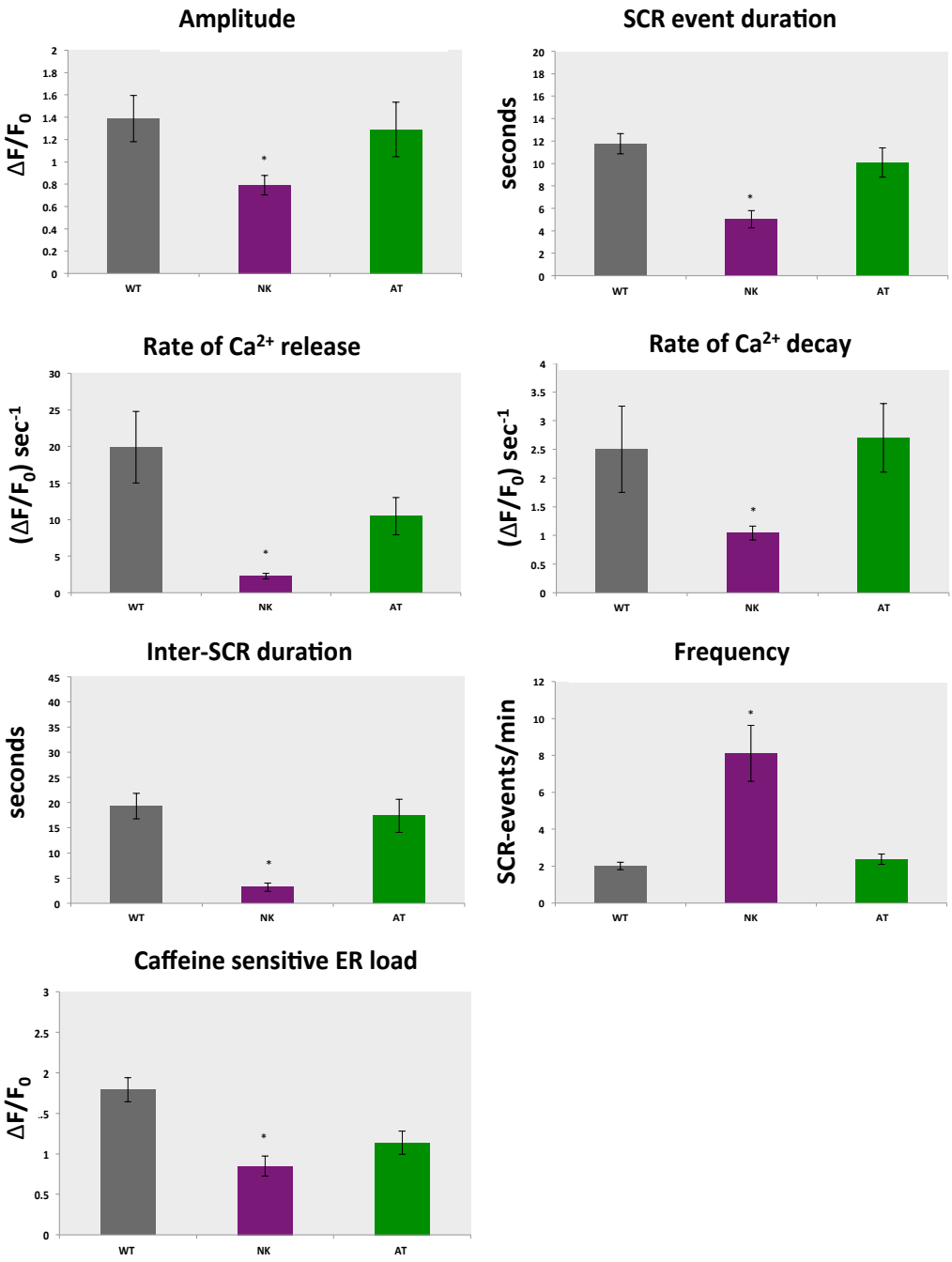

Figure 4.13: Assessment of the spontaneous Ca^{2+} release event properties in HEK293 cells expressing WT and mutant hRyR2 channels alone: *All kinetic parameters of SCR-events were examined as described in section 4.2.2. As shown, all Ca^{2+} oscillation properties were significantly altered by mutant N4104K hRyR2 expression (purple bars), compared with cells expressing WT hRyR2 (grey bars). Unlike expression of the N4104K mutation, HEK293 cells expressing the A4556T hRyR2 mutant (green bars) displayed similar SCR-event properties to the WT. The data are presented for each parameter as the combined mean± S.E.M, collected from between 11-25 transfected cells and 3-4 separate experiments. Statistical significance was calculated using one-way ANOVA, Tukey-Kramer test (GraphPad Prism), where p<0.05 is denoted by * (vs WT hRyR2).*

4.3.4. Expression of CSQ2, JUN and CSQ2+JUN with WT hRyR2 channels alters the properties of spontaneous Ca^{2+} release events:

Representative traces of SCR events from WT hRyR2-expressing HEK293 cells, in the absence and presence of luminal accessory proteins are demonstrated in Figure 4.14. To assess the effects that CSQ2, JUN or CSQ2+JUN co-expression has on the Ca^{2+} handling dynamics of WT channels, the properties of the SCR-events were examined (Figure 4.15). Although luminal protein co-expression did not alter the SCR event amplitude, expression of CSQ2, JUN or CSQ2+JUN with WT hRyR2 channels significantly enhanced their duration, whilst decreasing the rate of Ca^{2+} release and decay. As shown in Figure 4.14, compared with cells expressing WT hRyR2 alone, these effects consequently produced longer Ca^{2+} waves and changed the shape of the SCR-events. In addition to an increase in event duration, co-expression with CSQ2 (both alone and in combination with JUN) notably lengthened the time period in between each SCR event (inter-SCR duration) and subsequently decreased their frequency. This effect was not observed when WT channels were co-expressed with JUN alone. Compared with expression of WT hRyR2 only, the ER Ca^{2+} load was found to be significantly lower in all cells co-expressing the luminal proteins.

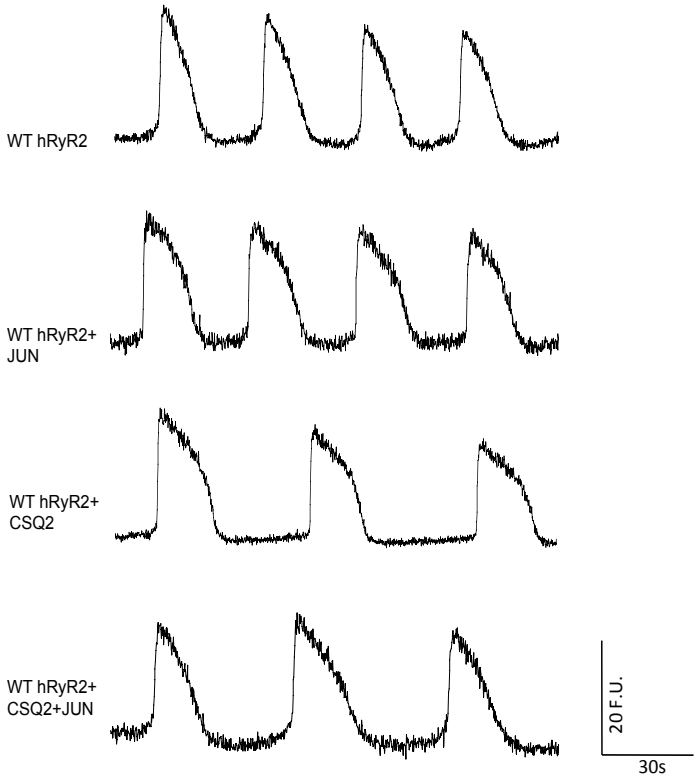

Figure 4.14: Representative traces of spontaneous Ca^{2+} release events in HEK293 cells expressing WT hRyR2, in the absence and presence of luminal accessory proteins CSQ2 and/or JUN, measured by Fluo-3.

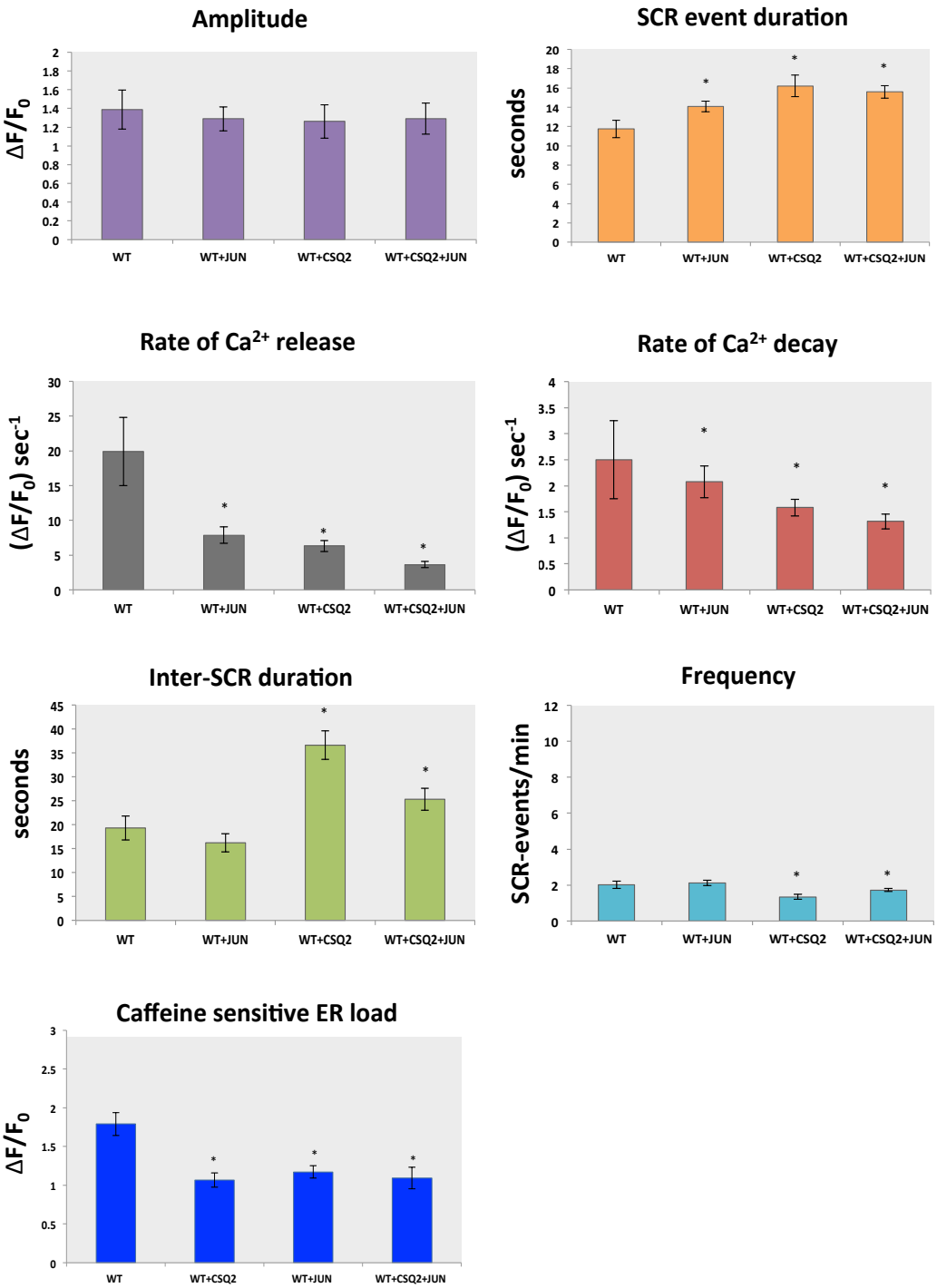

Figure 4.15: Assessment of the effects CSQ2 and/or JUN co-expression has on the spontaneous Ca^{2+} release event properties of WT hRyR2-expressing cells: *The kinetic parameters of SCR-events were examined as described in section 4.2.2. As shown, co-expression of the luminal proteins with WThRyR2 channels significantly altered many of the Ca^{2+} oscillation properties, as discussed in section 4.3.4. Data are presented for each parameter as the combined mean± S.E.M, collected from between 11-25 transfected cells and 3-4 separate experiments. Statistical significance was calculated using one-way ANOVA, Tukey-Kramer test (GraphPad Prism), where $p<0.05$ is denoted by * (vs WT hRyR2 expressed alone).*

4.3.5. Examination of spontaneous Ca^{2+} release parameters in cells co-expressing mutant A4556T hRyR2 channels and the luminal accessory proteins CSQ2 and/or JUN:

Although the SCR-events in cells expressing A4556T hRyR2 channels appeared similar to WT (Figure 4.13), some changes in the effects of luminal protein co-expression were detected. In particular, as presented in Figure 4.17, CSQ2 expressed alone did not appear to have an inhibitory effect on channel activity, suggesting that the way in which the mutant responds to CSQ2 differs from that of WT channels. However, co-expression with both accessory proteins (CSQ2+JUN), appeared to impart similar effects on A4556T as it did to WT SCR parameters - generating an increase in the SCR event duration and inter-SCR duration, whilst reducing their frequency (as illustrated in Figure 4.16). Consistent with WT data, co-expression of both luminal proteins with A4556T channels also reduced the rate of Ca^{2+} release and decay. These data could suggest that the direct effect of CSQ2 on RyR2 has been affected by mutation, but that the interaction via JUN has not, since the effect is the same as that seen on the WT channel. The effects of CSQ2 and JUN co-expression on A4556T hRyR2 Ca^{2+} load however had the opposite effect to that seen with WT hRyR2 co-expression, where ER Ca^{2+} content was significantly augmented in HEK293 expressing A4556T hRyR2+CSQ2+JUN (Figure 4.17).

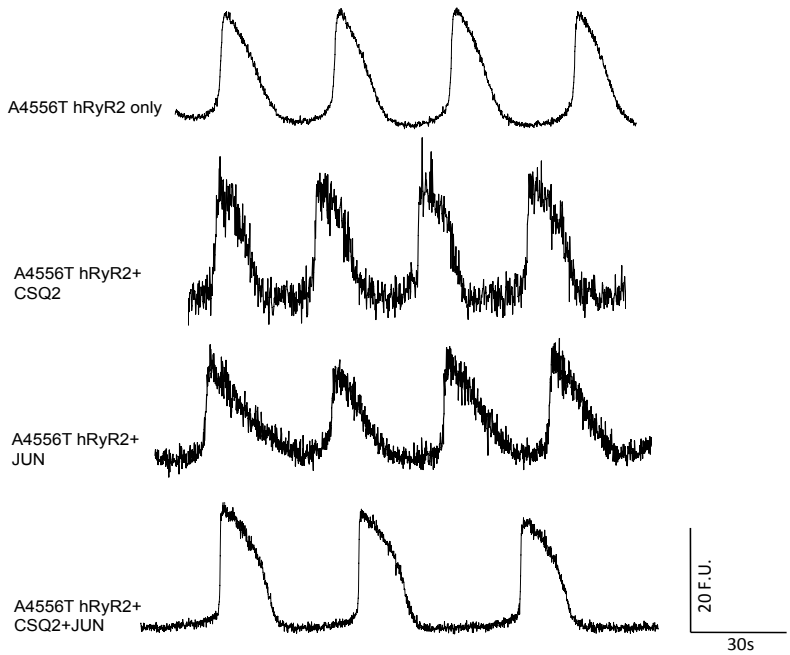

Figure 4.16: Representative traces of spontaneous Ca^{2+} release events in HEK293 cells expressing A4556T hRyR2 alone and in the presence of luminal accessory proteins CSQ2 and JUN, measured by Fluo-3.

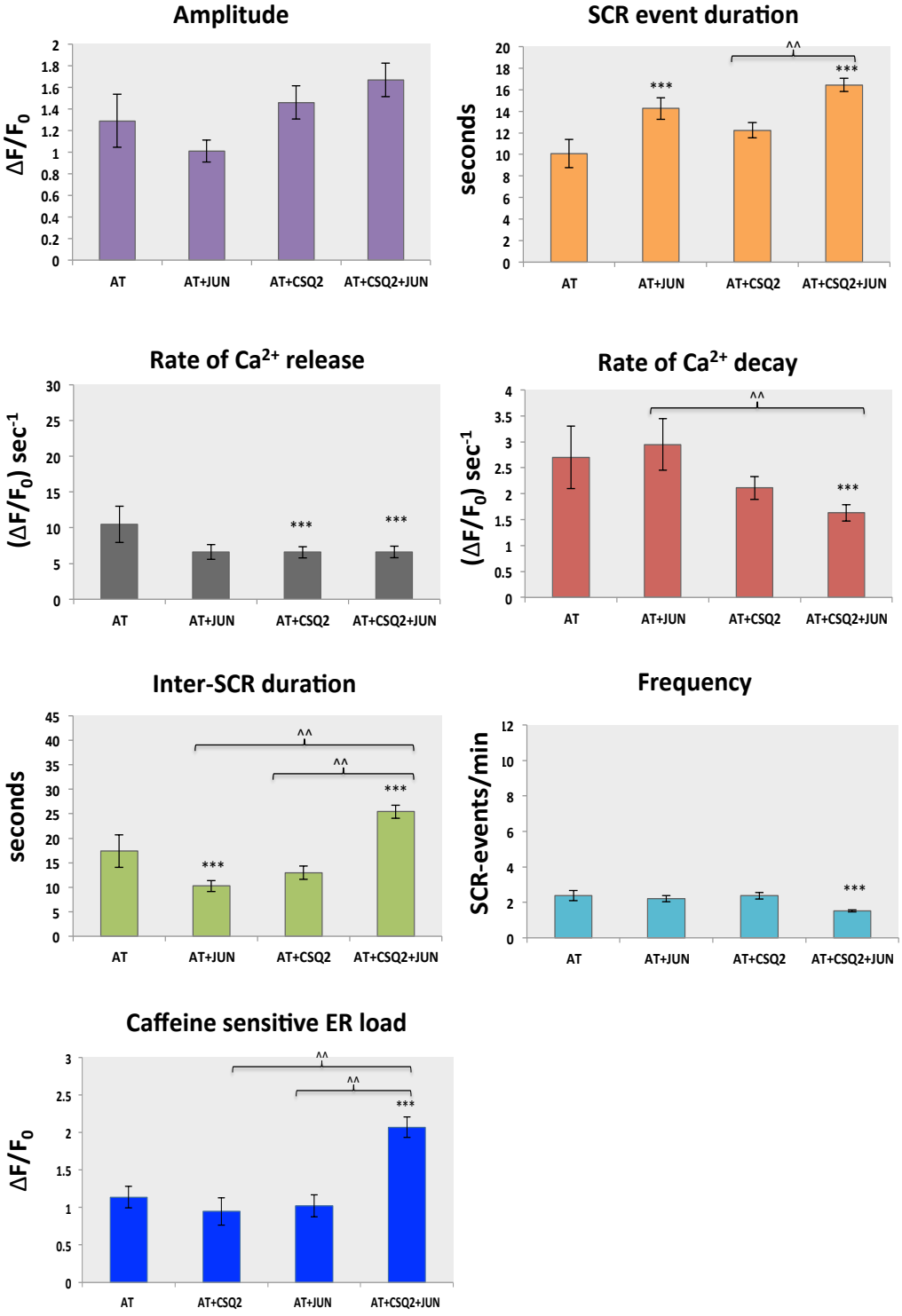

Figure 4.17: Assessment of the effects CSQ2 and/or JUN co-expression has on the spontaneous Ca^{2+} release event properties of A4556T hRyR2-expressing cells: *In particular, co-expression of A4556T hRyR2 channels with both accessory proteins (AT+CSQ2+JUN) appeared to significantly alter the Ca^{2+} oscillation parameters, as discussed in section 4.3.5. Data are presented for each parameter as the combined mean± S.E.M, collected from between 11-25 transfected cells and 3-4 separate experiments. Statistical significance was calculated using a one-way ANOVA, Tukey-Kramer test (GraphPad Prism), where p<0.05 is denoted by *** (vs A4556T hRyR2 expressed alone) and ^^ (vs A4556T+CSQ2+JUN.*

4.3.6. Examination of spontaneous Ca^{2+} release events in cells co-expressing mutant N4104K hRyR2 channels and the luminal accessory proteins CSQ2 and/or JUN:

Although the SCR-events in cells expressing N4104K hRyR2 channels appeared entirely different to WT hRyR2 (Figure 4.13), the effects of luminal accessory protein co-expression were quite similar. Co-expression of CSQ2 and/or JUN with N4104K channels did not alter the SCR amplitude, but generated significant increases in the duration and inter-SCR duration of the events, thus reducing their frequency (as observed in WT hRyR2 channels), (Figure 4.19). Representative traces of SCR events from NK hRyR2-expressing HEK293 cells, in the absence and presence of both luminal accessory proteins, are demonstrated in Figure 4.18. Differing from WT channels however, co-expression of the luminal proteins with N4104K hRyR2 did not have any significant effects on the ER Ca^{2+} levels (Figure 4.19). However, since N4104K hRyR2 channels expressed alone also displayed a significantly reduced Ca^{2+} content, this could be a reflection of the store itself rather than an effect of luminal protein co-expression.

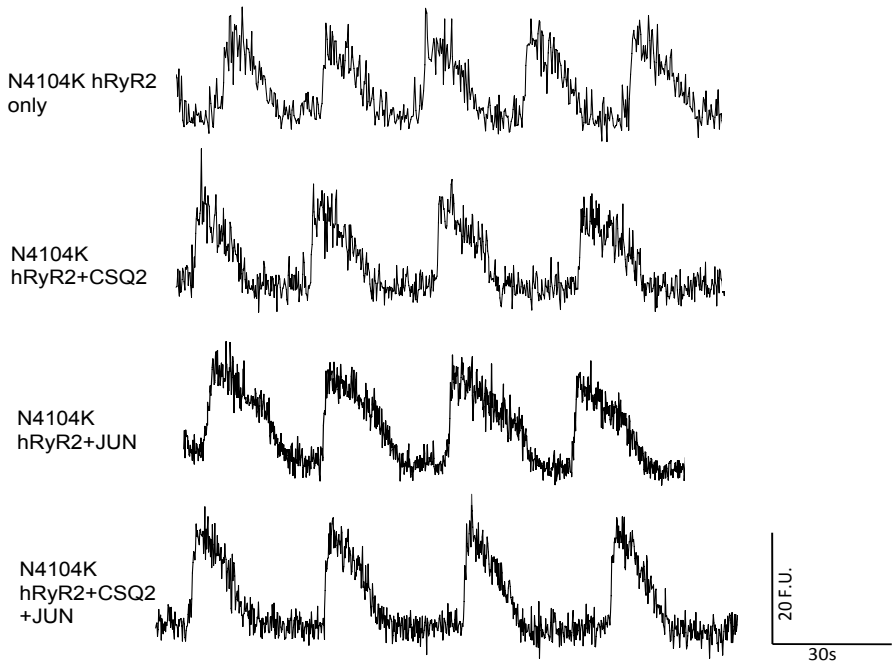

Figure 4.18: Representative traces of spontaneous Ca^{2+} release events in HEK293 cells expressing N4104K hRyR2 alone and in the presence of luminal accessory proteins CSQ2 and JUN, measured by Fluo-3.

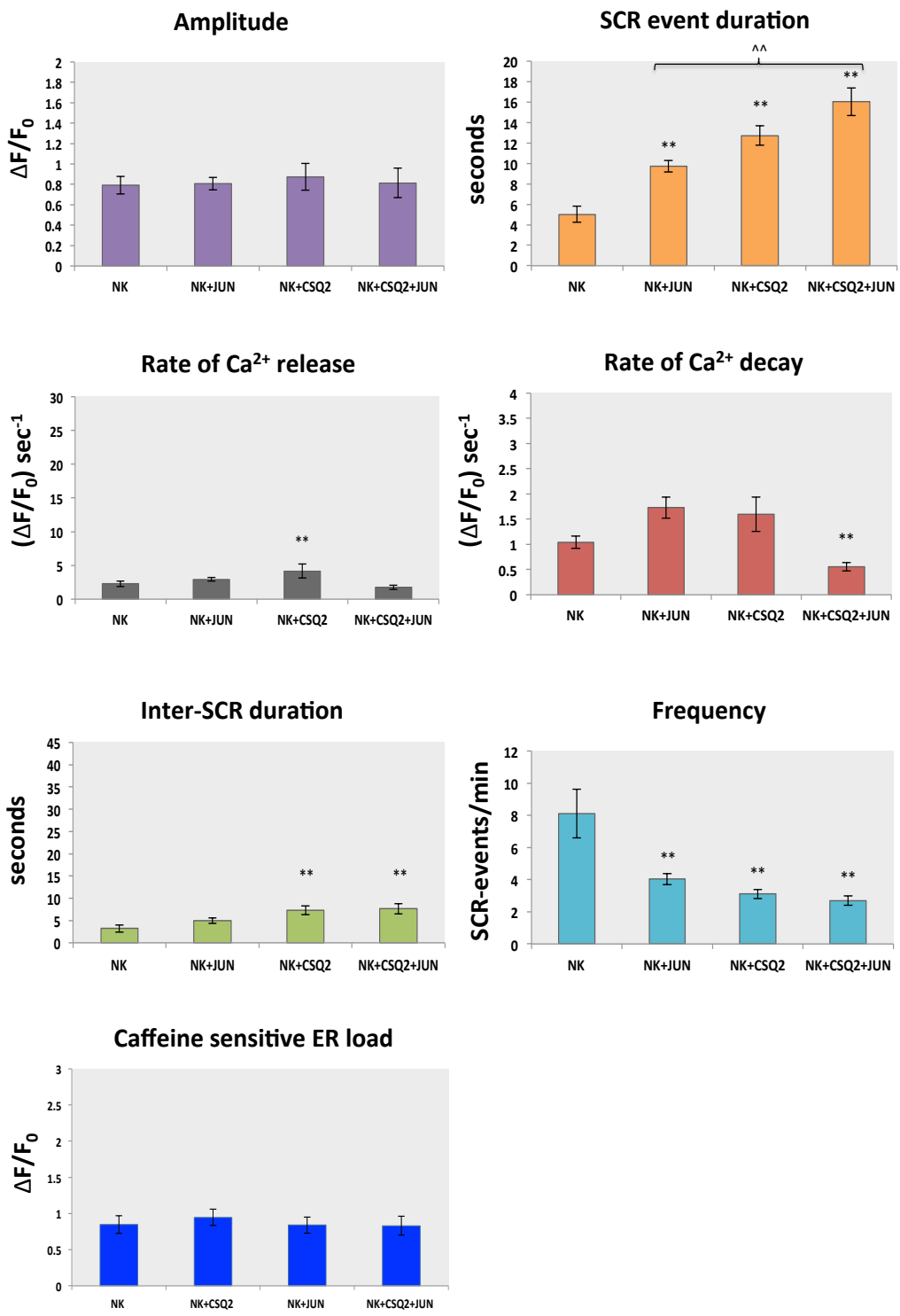

<u>Figure 4.19:</u> Assessment of the effects CSQ2 and/or JUN co-expression has on the spontaneous Ca^{2+} release event properties of N4104K hRyR2-expressing cells: *Examination of the kinetic SCR-event parameters in cells co-expressing the luminal proteins with N4104K hRyR2 channels revealed some significant alterations in the Ca^{2+} oscillation properties, as discussed in section 4.3.6. Data are presented for each parameter as the combined mean± S.E.M, collected from between 11-25 transfected cells and 3-4 separate experiments. Statistical significance was calculated using one-way ANOVA, Tukey-Kramer test (GraphPad Prism), where $p<0.05$ is denoted by ** (vs N4104K hRyR2 expressed alone) and ^^ (vs N4104K+CSQ2+JUN).*

4.4. Discussion:

- Assessment of the cytosolic Ca^{2+} dependence of WT and mutant hRyR2 channel activation showed that CPVT mutants are functionally heterogeneous with A4556T having a comparable half-maximal dose of activation (EC_{50}) comparable to that of the WT, whilst N4104K channels displayed a markedly sensitised response to activating Ca^{2+}.

- Co-expression with the luminal accessory proteins did not significantly alter the Ca^{2+} dependence of [^{3}H] ryanodine binding to WT or mutant hRyR2. Although, as discussed in section 4.3.2.3, altered protein-protein interactions caused by the use of high ionic strength conditions in these experiments may have masked any luminal protein effects.

- Effects on luminal Ca^{2+} regulation were appraised by measuring the properties of spontaneous Ca^{2+} release (SCR) events. HEK293 cells transfected with N4104K displayed significantly enhanced SCR parameters, which were indicative of Ca^{2+} leak through hRyR2. In contrast, A4556T channels displayed similar SCR events to WT hRyR2. Luminal protein co-expression revealed an inhibitory effect of CSQ2 on WT and N4104K hRyR2 activity, both in the presence of JUN and when expressed alone. A4556T hRyR2 differed in their response to CSQ2 co-expression, with no evidence of channel inhibition.

4.4.1. Wild type and mutant hRyR2 channels expressed in the absence of luminal accessory proteins display differences in Ca^{2+} sensitivity:

Quantitative [^{3}H] ryanodine binding was used to directly measure the cytosolic Ca^{2+} dependence of WT and mutant hRyR2 channels expressed alone (Figures 4.5 and 4.6), before assessing the effects of luminal protein co-expression. As discussed in section 4.3.2, the Ca^{2+} activation curves were presented in two ways: as raw (non-normalised) data and normalised data (fitted with constraints). Due to the variable nature of the data (in particular the A4556T hRyR2 mutant), without normalisation statistical differences between the EC_{50} of each dataset could not be accurately measured. As evidenced in this work, a steep dependence of RyR2 open probability or [^{3}H] ryanodine binding on cytosolic Ca^{2+} is not without precedent (see Jiang et al., 2003, 2004 and 2005). Studies on single hRyR2 channels in our own lab have also found this to be the case, with a 10-fold

increase in channel open probability occurring between 100 nM-1μM Ca^{2+} (Mukherjee et al., 2012). Since [^{3}H] ryanodine binding is activated to a greater extent at micromolar concentrations of Ca^{2+} (Pessah et al., 1987), inclusion of additional Ca^{2+} concentrations up to and above this range (between 250nM-1μM and above) could have smoothed out the Ca^{2+} activation curve to resemble a more sigmoidal relationship. When fitting the four-parameter logistic model, the Hill slope was a measure of the curves' steepness (GraphPad.com). This however, was not considered in the results, since we cannot be sure exactly what the Hill slope signifies in the context of this work. The Hill equation is commonly used to quantify the degree of cooperativity in ligand binding, which in this case would be a measure of the cooperativity of [^{3}H] ryanodine binding to hRyR2 with activating Ca^{2+}, in the absence/presence of luminal accessory proteins. It is however more likely to be a measure of the concerted cooperativity of channel activation. As shown in Figures 4.6-4.9, this steep transition was much more apparent in experiments carried out using A4556T hRyR2, and when channels were co-expressed with CSQ2, the significance of which will be considered below (sections 4.4.1.1 and 4.4.2.1). Single cell Ca^{2+} imaging was carried out to assess the properties of spontaneous Ca^{2+} release events in HEK293 cells expressing WT and mutant hRyR2. Using this technique, the sensitivity of WT or mutant channels to luminal Ca^{2+} could be examined, and any changes in the response following luminal accessory protein co-expression ascertained.

4.4.1.1. Investigations of hRyR2 mutation A4556T:

Compared with WT hRyR2, mutant A4556T hRyR2 channels (Figure 4.6 (B) left graph) displayed higher [^{3}H] ryanodine binding at every Ca^{2+} concentration tested, which was statistically significant at all concentrations >1μM (Student's *t*-test vs. WT hRyR2), and may have contributed to the sharp transition (steepness of the slope) seen with increasing [Ca^{2+}]. Since binding of [^{3}H] ryanodine reflects the open state of hRyR2 channels, it is possible the mutant directly affected the sensitivity of channel opening. However, the A4556T Ca^{2+} activation curve yielded a comparable EC_{50} to WT channels (0.63± 0.08μM vs. 1.63± 0.27μM normalised WThRyR2 data), (Figure 4.6 (B) right graph), suggesting that their Ca^{2+} dependence were similar. It is possible the A4556T mutant may have been affecting the association/dissociation rate of [^{3}H] ryanodine itself, since the binding data exhibited great variability (as indicated by the larger error bars seen in the graphs). As demonstrated in Figure 4.4, it is unlikely that standardisation was affected by the mutation, since similar hRyR2 expression levels to WT were evident in mixed membranes expressing A4556T (assessed by densitometric analysis of Western blot signals). The A4556T mutation however is positioned in or near the pore-forming region of the RyR2 channel, within which the residues deemed critical for ryanodine binding are situated, such

as a glutamine residue at position 4863 (Wang et al., 2003). Mutation of this amino acid (Q4863A) was found at the single channel level to considerably reduce the affinity of ryanodine for RyR2 channels (Ranatunga et al., 2005), meaning that no [^{3}H] ryanodine binding was detected (Wang et al., 2003). It is possible that the A4556T mutant may have altered the structure of the ryanodine-binding site, such that the affinity for ryanodine was enhanced. The only way to prove this however would be to investigate A4556T hRyR2 channels at the single channel level, using a reversible ryanoid (as discussed further in Chapter 6).

In single-cell Ca^{2+} imaging investigations, HEK293 cells expressing WT and A4556T hRyR2 channels alone displayed remarkably similar SCR-events (Figure 4.12 and 4.13) and no statistically significant differences were found. Therefore, taking into account both the [^{3}H] ryanodine binding and Ca^{2+} imaging together, no differences in the sensitivity of RyR2 channels to Ca^{2+} were apparent with A4556T mutation. Although listed in the human gene mutation database (HGMD) as a disease-causing variant (Tester et al., 2007), these results suggest that A4556T hRyR2 may not be causative of arrhythmia; especially since altered Ca^{2+} sensitivity in CPVT mutants is a well-documented observation (Jiang et al., 2005, Wehrens et al., 2007, Meli et al., 2011, Loaiza et al., 2013). In agreement with this proposal, Jabbari et al (2013) recently concluded that the A4556T mutation is benign following the use of numerous prediction tools (including SIFT (Sorting Intolerant From Tolerant) and PolyPhen-2 (Polymorphism Phenotyping) to predict its deleterious outcome. Additionally, Papadakis et al (2013) reported of a 17 year old male harbouring the A4556T mutant, who was found in post mortem to have died due to a structural abnormality (marked right ventricular dilatation), unrelated to RyR2 mutation. Thus it is possible that A4556T could be a single nucleotide polymorphism, which can be identified in patients, but not usually causative of disease.

4.4.1.2. Investigations of hRyR2 mutation N4104K:

In contrast, the N4104K mutation was found to be markedly different to A4556T and WT hRyR2 channels in both experimental systems. As shown in Figure 4.6 (A), compared with WT channels, the CPVT-linked mutant displayed enhanced [^{3}H] ryanodine binding at basal (or sub-activating) Ca^{2+} levels (non-normalised data, left graph), an observation also reported by Jiang et al., 2004. Normalisation of the binding data demonstrated that N4104K channels exhibit a sensitised Ca^{2+} activation profile, seen as a left-shift in the dose-response curve (Figure 4.6, (A), right graph); and yielded an EC_{50} that was statistically different from WT channels (0.22 vs. 1.63μM (normalised data)). This result differed from that of Jiang et al (2004) who reported that although enhanced basal levels

of [^{3}H] ryanodine binding was evident, N4104K did not alter the Ca^{2+} dependence of [^{3}H]-ryanodine binding. As illustrated in Figure 4.10 however, the CPVT-linked mutants assessed in their study only exhibited elevated [^{3}H] ryanodine binding at contaminant Ca^{2+} levels, when high (>800mM) concentrations of KCl were used. However, all Ca^{2+} activation experiments were undertaken in low (100mM KCl) salt conditions (Jiang et al., 2004). Thus, it is likely that under such low salt concentrations significant differences in the Ca^{2+} dependence of mutant RyR2 channels compared with WT would not have been distinguished. However, the N4104K hRyR2 Ca^{2+} activation curve in this study appeared left-shifted, as found in this investigation (Jiang et al., 2004).

As illustrated in Figures 4.12 and 4.18, the SCR events in cells expressing N4104K-hRyR2 appeared much smaller and faster than those observed in HEK293 expressing WT (or AT) hRyR2. The kinetics of the SCR events differed significantly to WT, represented by a series of bar graphs in Figure 4.13. Expression of this mutant lowered the amplitude, duration and inter-SCR duration of the Ca^{2+} transients, which consequently increased their frequency (Figure 4.13). Furthermore, the rate of Ca^{2+} release and decay were also decreased. As established by measuring the Ca^{2+} transient amplitude following high-dose caffeine application, (which empties the ER store) the ER Ca^{2+} load in N4104K-hRyR2 expressing cells was also significantly lowered and is indicative of Ca^{2+} leak through mutant RyR2 channels (Jiang et al., 2004, 2005, 2007). These findings are in line with the published data from Jiang et al (2004), where the N4104K mutant enhanced the propensity for SOICR. It was noted that N4104K hRyR2 channels in particular displayed greater signal variability ((noise), as shown in Figures 4.12 and 4.18), which has been suggested by George et al (2006) to represent conformational instability of the Ca^{2+} release channel.

4.4.2. Assessment of the effects that CSQ2 and/or JUN co-expression has on WT hRyR2 channel activity:

When assessing the response of hRyR2 channels to CSQ2 co-expression, the stoichiometry of the luminal protein at the various [Ca^{2+}] used in each experiment should be considered. Discussed previously in section 1.6.1, the oligomeric state of CSQ2 is thought to be [Ca^{2+}]-dependent, with CSQ2 monomers predicted to self-associate to form dimers, tetramers and eventually polymers at higher luminal Ca^{2+} concentrations (>1 mM), where the protein becomes compacted and the Ca^{2+} binding capacity is enhanced (Park et al., 2003, 2004, Kim et al., 2007, Qin et al., 2008, Lee et al., 2012). In a study by Wei et al (2009b) however, even at 1 mM Ca^{2+} under physiological ionic strength, CSQ2 failed to form polymers (as assessed by chemical cross-linking), leading to suggestions by the

author that the cardiac isoform might not polymerise at all. This however does require further investigation.

At low luminal [Ca^{2+}] (<1mM), it is well documented that CSQ2 exists primarily as a monomer (Györke and Carnes, 2008, Murphy et al., 2011) or dimer (Park et al., 2003), which interacts with other luminal accessory proteins such as triadin and junctin to regulate RyR2 activity (Qin et al., 2008, Altschafl et al., 2011). Thus, monomeric CSQ2 (in association with JUN/TRD1) is thought to be responsible for regulating Ca^{2+} release, whilst CSQ2 polymers (if formed) store Ca^{2+} near the site of release (Qin et al., 2008). Although hypothesised in the literature, there is currently no published data demonstrating the ability of CSQ2 to regulate and bind RyR2 channels directly (in the absence of additional accessory proteins). Using a Ca^{2+} concentration range of 0-500μM for [^{3}H] ryanodine binding experiments and in the presence of contaminant (~1-5 μM) Ca^{2+} in Co-IP investigations, CSQ2 was predicted to exist in monomeric/dimeric form, thereby retaining the ability to regulate/bind hRyR2 channels. As discussed further in Chapter 5, section 5.3.4, reduction of CSQ2 binding to RyR2 was only observed at very high (i.e. 10mM) Ca^{2+} concentrations (Figure 4.11). The lack of effect of JUN and CSQ2 on the Ca^{2+} dependence of [^{3}H] ryanodine binding in WT/mutant hRyR2 channels was therefore most likely due to the use of high ionic strength (1M KCl) conditions, rather than the use of an unsuitable [Ca^{2+}] range altering CSQ2 conformation. In single-cell Ca^{2+} imaging investigations, transfected, Fluo-3 loaded cells were maintained in an extracellular Ca^{2+} concentration of 1.3mM. Within the ER, the dynamic changes in free luminal [Ca^{2+}] during SCR could not be reliably measured, however, it was anticipated that CSQ2 remained as a monomer/dimer at a free luminal [Ca^{2+}] <1mM, with the ability to interact and regulate RyR2 activity. Following analysis, this assumption was confirmed with the observation that CSQ2 imparted an inhibitory effect on SCR event parameters compared with hRyR2 channels expressed alone (as discussed below in section 4.4.2.2 and sections 4.3.4-4.3.6).

4.4.2.1. Ca^{2+} activation as measured by [^{3}H] ryanodine binding:

The Ca^{2+} dependence of [^{3}H] ryanodine binding for WT hRyR2 channels did not appear to be altered by luminal accessory protein co-expression. As demonstrated in Figure 4.7, the Ca^{2+} activation curves generated using both the raw (left graphs) and normalised (right graphs) data appeared similar to those constructed for WT hRyR2 channels expressed alone and yielded EC_{50} values that were statistically comparable (A)-(C). The sharper slope evident in [^{3}H] ryanodine binding curves when channels were co-expressed in the presence of CSQ2 could reflect a direct effect of the protein altering the cooperativity of

channel activation (i.e, affecting the population of hRyR2 channels opening). The effect of CSQ2 expression on [^{3}H]-ryanodine binding has been explored previously, with both stimulatory (Kawasaki and Kasai, 1994) and inhibitory effects (Beard et al., 2002) being reported. Since no significant alterations in the Ca^{2+} dependence of hRyR2 channels (in terms of EC_{50}) with CSQ2 co-expression were found in this investigation, it would be beneficial to examine the Ca^{2+}-activation profile of hRyR2+CSQ2 and/or JUN further at the single channel level. JUN co-expressed alone with WT channels did seem to have a slight stimulatory effect on channel activity (Figure 4.7 (A), left graph), seen as a left-shift in the curve. However, the EC_{50} was not significantly different to WT hRyR2. Interestingly, an activatory role of JUN on RyR2 channel activity at lower Ca^{2+} concentrations has been reported in the literature (Altschafl et al., 2011 (Table 1.1)). As tested by co-immunoprecipitation (Figure 4.11), high salt conditions used in [^{3}H] ryanodine binding assays were found to reduce the association of CSQ2 and JUN with hRyR2 channels. Although the difference was not calculated as statistically significant, it is possible that this reduction was enough to alter their functional effects. Imaging at a cellular level however, proved much more effective in detecting the effects of luminal protein co-expression.

4.4.2.2. Single-cell Ca^{2+} imaging investigations:

Co-expression of the luminal proteins with WT channels in HEK293 stable cell lines (section 4.2.2) were found to significantly alter the SCR parameters in Ca^{2+} imaging investigations (Figures 4.14 and 4.15). Although no effects on the SCR amplitude were exhibited, co-expression of all accessory protein combinations (CSQ2, JUN and CSQ2+JUN) with WT hRyR2 enhanced the duration of SCR events, whilst lowering the rate of Ca^{2+} release and decay. CSQ2 co-expression in particular (both alone and with JUN) seemed to have a profound inhibitory effect on WT hRyR2 function, where in addition to an increase in the duration of SCR, the time period in between each Ca^{2+} wave (the inter-SCR duration) was also significantly lengthened and the frequency of events reduced (Figure 4.15). This finding is consistent with the work of Györke et al (2004) where an inhibitory effect of CSQ2 on purified RyR2 channels at the single channel level was reported. However, channel inhibition was said to only occur in the presence of JUN and TRD1 (Györke et al., 2004). Studies of cardiac-specific CSQ2 overexpression in transgenic mice have also implicated an inhibitory role of the accessory protein, where impaired Ca^{2+} release was evident upon sarcolemmal depolarisation (Jones et al., 1998, Sato et al., 1998 (Table 1.1)) and Ca^{2+} spark frequencies were drastically reduced (Jones et al., 1998). It was anticipated that the releasable Ca^{2+} store would be increased by WT hRyR2+CSQ2 co-expression, as observed in CSQ2 overexpression studies (Jones et al., 1998, Sato et al., 1998). However, as shown in Figure 4.15, the ER Ca^{2+} content appeared to be

significantly lower in all cells expressing luminal proteins. However, a greater store capacity is evidenced by the fact that the SCR events in these cells exhibit a reproducibly longer duration. In regards to JUN co-expression, a decrease in the SR Ca^{2+} load has been previously observed in myocytes isolated from JUN-overexpressing mice, together with depressed relaxation kinetics of the Ca^{2+} transient (including a prolonged rate of Ca^{2+} decay as found in this investigation (Figure 4.15)), (Kirchhefer et al., 2006). These effects were attributed to JUN directly modifying RyR2 Ca^{2+} release to regulate the SR Ca^{2+} content (Kirchhefer et al., 2006). Furthermore, in human heart failure it has been suggested that diminished JUN expression may be a compensatory mechanism intended to raise Ca^{2+} levels within the SR (Yuan et al., 2007).

4.4.3. Do mutant hRyR2s respond differently to luminal accessory protein co-expression?

When evaluating the response of mutant hRyR2 channels to luminal protein co-expression and comparing this data to the WT, it was important keep in mind the differences observed between the channels when expressed alone (4.4.1).

4.4.3.1. [^{3}H] ryanodine binding investigations:

Luminal accessory protein co-expression did not modify the enhanced [^{3}H] ryanodine binding exhibited by A4556T hRyR2 channels expressed alone (Figure 4.8, non-normalised data, left graphs) and the EC_{50} of each Ca^{2+} activation curve were comparable (Figure 4.8, right graphs). Similarly, the Ca^{2+} activation profile of mutant N4104K hRyR2 channels, measured by [^{3}H]-ryanodine binding, was unchanged by luminal accessory protein co-expression, as found in all other investigations. As discussed in section 4.4.2.1, the [^{3}H] ryanodine-binding assay was not sensitive enough to pinpoint subtle differences imparted by CSQ2 and/or JUN co-expression (or could reflect altered protein-protein interactions caused by the use of high salt conditions, Figure 4.11).

4.4.3.2. Measurement of SCR parameters by single-cell Ca^{2+} imaging:

At the cellular level, differences in the response of mutant channels to CSQ2 and JUN association (compared to A4556T and WT hRyR2 alone) were detected as presented in Figure 4.17. In particular, the notable inhibitory effects of CSQ2 on the SCR parameters in cells expressing WT hRyR2 were not evident when co-expressed with A4556T channels, suggesting the mutant responded differently to CSQ2 association. Alternatively, this

difference could reflect disrupted association of CSQ2 with A4556T channels, which will be examined in Chapter 5. Interestingly, co-expression of A4556T channels with both accessory proteins (CSQ2+JUN) seemed to alter the SCR properties in a similar manner to WT channels, enhancing the duration of events, inter-SCR duration and causing a subsequent reduction in SCR event frequency, rate of Ca^{2+} release and decay (Figure 4.17). Collectively, this suggests that the effects of CSQ2 on RyR2 were restored in the presence of JUN. Interestingly, in A4556T hRyR2 [^{3}H] ryanodine binding experiments it was also noticed that CSQ2 and JUN co-expression restored the increased basal [^{3}H] ryanodine binding seen at low [Ca^{2+}] to WT levels (Figure 4.8, (C), left graph), although this was not a statistically significant effect. On the contrary, the ER Ca^{2+} load in A4556T+CSQ2+JUN expressing HEK293 cells appeared to be enhanced by luminal protein co-expression, which was the exact opposite to the effects observed in WT channels (Figures 4.15 and 4.17). Although it was first thought that the A4556T hRyR2 mutation could be benign (discussed in section 4.4.1.1), the discrepancies in the response of the mutant (vs. WT) to luminal protein co-expression (observed in Ca^{2+} imaging studies) could reflect an effect on RyR2 activity after all, albeit because it cannot be regulated in the same way by luminal accessory proteins (notably CSQ2), rather than by a direct effect on channel gating. As discussed previously, HEK293 cells expressing N4104K hRyR2 alone displayed an entirely different SCR profile to those expressing WT hRyR2 (Figures 4.12 and 4.13), which therefore needed to be considered when assessing the response to luminal protein co-expression. With this in mind, the observed alterations in the SCR-event properties imparted by CSQ2 and/or JUN co-expression were surprisingly similar to those found in WT investigations. As demonstrated in Figure 4.19, expression of the luminal proteins (all combinations) with N4104K generated a significant increase in the SCR duration and a reduction in SCR-event frequency. The inhibitory effects of CSQ2 (expressed alone and with JUN) exhibited in WT channels were also evident when expressed in combination with N4104K. In addition to the alterations aforementioned, co-expression of CSQ2 with N4104K hRyR2 caused a prolongation of the inter-SCR duration. Unlike WT channels, the ER Ca^{2+} content in cells expressing N4104K was not significantly affected by luminal protein co-expression (Figure 4.19). This difference however could be a refection of the Ca^{2+} store itself, which appeared to be significantly lower in N4104K expressing HEK293 cells without luminal protein co-expression (Figure 4.13).

4.4.4. Concluding Remarks:

Examining the spontaneous Ca^{2+} release kinetic properties in HEK293 cells appeared to be a much more efficient technique than [^{3}H] ryanodine binding to detect small but notable changes in the response of hRyR2 channels to activating Ca^{2+}, generated by luminal accessory protein co-expression. However, unlike [^{3}H] ryanodine binding, direct Ca^{2+} activation could not be measured in these experiments. As highlighted in section 3.4.2, a limitation of using transient expression for [^{3}H] ryanodine binding investigations was the possibility that mixed populations of WT/mutant hRyR2+luminal protein complexes could exist. Immunofluorescent staining however, demonstrated that most cells expressing hRyR2 were likely to also have CSQ2 and/or JUN co-expression, since much higher transfection efficiencies of the luminal proteins in comparison were achieved. Given our limited knowledge of the exact RyR2-JUN-CSQ2 stoichiometry *in vivo* (Terentyev et al., 2006, Lee et al., 2012), it is difficult to establish precisely how such mixed populations could have affected the [^{3}H] ryanodine binding data. In particular, since the technique failed to generate any significant differences when WT hRyR2 channels were co-expressed in the presence of CSQ2 and/or JUN. It is possible that without the physiologically relevant stoichiometry, the degree of hRyR2 channel regulation (whether it be stimulatory or inhibitory) would be reduced or even completely abolished.

It is typically assumed that JUN binds at a stoichiometry of one JUN per RyR2 monomer (or 4 JUN per RyR2 tetramer), and subsequently binds CSQ2, anchoring it close to the site of Ca^{2+} release (Zhang et al., 1997, Terentyev et al., 2006). Further to simply acting as an anchoring protein, JUN has been suggested to also 'sense' changes in luminal [Ca^{2+}] (Altschafl et al., 2011), (Table 1.2). Altschafl et al (2011) proposed that JUN might bind at two distinct sites within RyR2, the binding of which is governed according to the luminal [Ca^{2+}] within the SR. *In vivo*, at low luminal Ca^{2+} (<1 mM), JUN was hypothesised to bind to only one RyR2 site, whilst its other binding site is occupied by CSQ2, preventing its binding to RyR2 (Altschafl et al., 2011). At low luminal Ca^{2+} (and in the absence of CSQ2), a stimulatory role of JUN on RyR2 gating was reported, an effect that is likely masked in the presence of CSQ2 (Altschafl et al., 2011). A small stimulatory effect was evident in [^{3}H] ryanodine binding investigations of hRyR2 channels co-expressed with JUN only, as discussed in section 4.3.2.1, Figure 4.7. CSQ2+JUN and/or TRD1 (added together at the single channel level) were reported by Györke et al (2004) to have an inhibitory effect on hRyR2 channel activity. However, the single-cell Ca^{2+} imaging data carried out in this work (discussed further in section 4.3.4) revealed inhibitory effects of CSQ2 on hRyR2 activity both when expressed alone and in the presence of JUN, suggesting the precise stoichiometry *in vivo* needs to be examined in greater detail. As outlined in section 1.3,

cryo-EM analysis and discovery of CSQ2, JUN and TRD1 binding sites on RyR2 channels, would facilitate this identification.

In Ca^{2+} imaging studies, N4104K hRyR2 channels were considerably different to those observed in both WT and A4556T hRyR2-expressing cells. Thus, further highlighting how functional heterogeneity can exist between CPVT mutants (Thomas et al., 2004). The major differences in the response of WT and mutant hRyR2 channels to luminal protein co-expression were observed when the channels were expressed with each protein individually (CSQ2 or JUN). However, mutant hRyR2 responded similarly to WT channels when co-expressed in the presence of both accessory proteins (hRyR2+CSQ2+JUN). All Ca^{2+} imaging data collected are summarised in the Appendix, Figure 7. Where apparent trends in the Ca^{2+} imaging data were evident, yet no statistically significant differences were detected, it is possible that an insufficient number of experiments were conducted. To test this idea, using Figure 4.17 (cells expressing A4556T hRyR2 in the absence/presence of luminal proteins) and assessment of the inter-SCR duration as an example, a post-hoc power analysis was performed on the data using G*Power 3 software (www.gpower.hhu.de). The power of the study was calculated according to the mean values and standard deviations obtained within each data set (A4556T hRyR2 only vs A4556ThRyR2+JUN and/or CSQ2). In those data where significant differences were identified, the study was considered to be highly powered (A4556T hRyR2 vs A4556T+JUN and vs A4556T+CSQ2+JUN) at >99%; whilst data derived from cells expressing A4556T+CSQ2 (where no significance difference in inter-SCR duration to A4556T only was distinguished) was powered to 80%; which is still an accepted level of power for detecting differences between the specified data (Beck, 2013). It is therefore likely that the number of samples used for analysis were adequate to detect real differences. On the other hand, using the same data as an input for a priori sample size estimation (where the mean and standard deviation of each group are predicted before commencement of the study), it was estimated that a further 10 experiments in total (i.e, 5 more per group (A4556T hRyR2 only and A4556T+CSQ2 compared) would be required to achieve a power of >95%. It is thus possible that undertaking these additional experiments may have revealed a statistical difference. In future experiments, finding the sample size necessary to achieve a high-powered investigation by use of a power calculation, could aid identification of statistically significant differences between datasets.

Chapter 5

Protein-protein interactions of wild type and mutant (A4556T and N4104K) hRyR2 with luminal accessory proteins CSQ2 and JUN

5.1 Introduction:

5.1.1. Interactions of calsequestrin, junctin and the cardiac ryanodine receptor:

Under normal circumstances, intracellular Ca^{2+} handling within the myocardium relies on an intricate interplay between the Ca^{2+} release channel, RyR2, and its associated accessory proteins, which localise to the junctional SR membrane and form a multimeric signalling complex that orchestrates Ca^{2+} release (Guo et al., 1996, Bers, 2004). As discussed further in previous chapters (section 4.1.1), CSQ2 and JUN are thought to form part of a luminal Ca^{2+} sensor, together with the luminal domains of RyR2 and TRD1 (Zhang et al., 2014; TRD1 discussed in section 1.6.3). However, the exact protein-protein interactions underlying assembly of this quaternary complex remain undefined. In particular, although CSQ2 is one of the better characterised RyR2 accessory proteins (Slupsky et al., 1987, Kim et al., 2007, Knollmann et al., 2009), direct evidence of whether CSQ2 interacts directly with hRyR2 channels or indirectly through its anchoring to JUN and/or TRD remains to be properly established (Terentyev et al*.,* 2006, Dulhunty et al., 2012, Chen et al., 2014). This chapter will first describe our current knowledge of the protein-protein interactions that take place between CSQ2, JUN and RyR2 in the jSR lumen, prior to interaction studies with mutant and WT hRyR2 carried out in this investigation.

5.1.2. Evidence of a direct binding interaction between cardiac JUN and CSQ2:

Using an ^{125}I-calsequestrin filter overlay assay, Mitchell et al (1988) first identified JUN as the predominant CSQ2-binding protein present in jSR membranes of dog cardiac muscle, leading to the idea that this transmembrane protein was the major physiological anchor of CSQ2, holding it within close proximity to RyR2 channels (Mitchell et al., 1988, Beard et al*.,* 2004). However, following further investigations, it is now generally accepted that both TRD1 and JUN are likely to mediate the interaction between CSQ2 and RyR2 (Zhang et al., 1997, Györke et al., 2004), as highlighted in Chapter 1, Tables 1.2-1.3. With emphasis on the role of JUN, Zhang et al (1997) used several different techniques to examine the binding interactions of the protein with other jSR components important for Ca^{2+} release, including cardiac CSQ2 and RyR2 (Zhang et al., 1997). Evidence that JUN binds directly to CSQ2 was demonstrated by immunoprecipitation (IP), where endogenous JUN and CSQ2 were immunoprecipitated from detergent-solubilised dog cardiac jSR vesicles by incubation with α-CSQ2 (JUN detection) and α-JUN (CSQ2 detection) antibodies, respectively. Increasing [Ca^{2+}] disrupted the binding interaction between CSQ2 and JUN, with half-maximal inhibition evident between 0.6-0.8 mM $CaCl_2$ (Zhang et al., 1997). The

CSQ2-binding domain of JUN was localised to the luminal region of the molecule, determined by CSQ2-affinity chromatography with Glutathione S-transferase (GST)-fusion proteins corresponding to the cytoplasmic/luminal domains of JUN conjugated to affinity beads (Zhang et al., 1997). In contrast to IP experiments, the binding interaction between the two proteins remained significant at mM Ca^{2+} concentrations. Analysis of the JUN fusion protein, identified the highly charged "KEKE motif" (section 1.6.3) at the intraluminal region (amino acid residues 46-210) of the protein as the site that interacts with the aspartyl-rich region of CSQ2, and proposed that these electrostatic interactions stabilise protein binding (Zhang et al., 1997, Shin et al., 2000, Pritchard and Kranias, 2009). A later investigation by Kobayashi and co-workers however, revealed that JUN does not appear to have a discrete CSQ2 binding domain, since deletions in several KEKE motifs along the C-terminal tail of the protein significantly reduced CSQ2 binding (Kobayashi et al 2000). Furthermore, the aspartyl-rich region of CSQ2 has been suggested as a major Ca^{2+} binding motif, where elevations in [Ca^{2+}] could induce a conformational change in the protein structure and diminish its interaction with JUN and/or TRD1 or the proteins may compete for the Ca^{2+} binding sites (Shin et al., 2000). To further examine the role of JUN in anchoring CSQ2 within close contact to RyR2 channels (Zhang et al., 1997, Guo et al., 1996), the structural effects of JUN overexpression have been investigated (Zhang et al., 2001, Tijskens et al., 2003). Cardiomyocytes isolated from transgenic mice, overexpressing cardiac JUN exhibited changes in cellular morphology, such as a narrowing of the junctional SR cisternae and compaction of its content (Zhang et al., 2001), whilst the opposite was seen in an earlier study of CSQ2 overexpression, where SR cisternae were greatly enlarged and their content displayed a dispersed appearance (Jones et al., 1998). Complementing these findings, Tijskens et al described that although JUN was not necessary for targeting of CSQ2 to the terminal cisternae, enhanced expression of the protein produced a strong-ordering effect and tighter clustering of CSQ2 at jSR sites, condensing the Ca^{2+} binding protein at the jSR membrane within close proximity to RyR2 channels (Tijskens et al*.,* 2003). These findings support the view that JUN, either directly or indirectly (via an effect on jSR structure) has an effect on the functional coupling between CSQ2 and RyR2.

5.1.3. Evidence of cardiac JUN association with RyR2:

Zhang et al (1997) also observed a direct binding interaction between cardiac JUN and RyR2, demonstrated by IP investigations and [^{3}H] ryanodine binding. Dog JUN was first immunoprecipitated from detergent-solubilised jSR vesicles using a JUN monoclonal antibody (mouse 5D8) covalently coupled to protein A agarose beads. Once obtained, the resultant immunoprecipitate was subsequently incubated with a RyR2 specific antibody that detected a substantial amount of RyR2 protein adsorbed to the JUN-bound beads (Zhang et al., 1997). Similar to CSQ2, the RyR2 interacting domain of JUN was located to the luminal region, identified by [^{3}H] ryanodine binding (established by measuring the percentage of purified RyR2 channels precipitated from fusion protein affinity-beads), (Zhang et al., 1997). To confirm direct binding between the two proteins without influence from other jSR components, a GST fusion protein corresponding to the luminal domain of JUN was shown to interact with purified RyR2 channels in a Ca^{2+}-independent manner. Following predictions that a single binding site at intraluminal loop II of the RyR1 protein is responsible for binding the KEKE-motif of TRD (Goonasekera et al., 2007), Altschafl et al in 2011, examined if the KEKE-motif of JUN also binds specifically to the intraluminal loop II of RyR2 (Altschafl et al., 2011). Using recombinant JUN and RyR2 polypeptides designed to different intraluminal binding regions of the two proteins, the group demonstrated biochemically (via a blot overlay assay) that at least two distinct regions of JUN are capable of interacting with RyR2 channels, one of which contained the aforementioned KEKE-motif (Altschafl et al in 2011). It was suggested that the N-proximal intraluminal domain of JUN interacts with intraluminal loop I of RyR2 (residues 4520-4553), whilst the KEKE-motif of JUN interacts with RyR2 at intraluminal loop II (residues 4789-4846), (Altschafl et al., 2011). The existence of multiple protein-protein interactions between the two proteins strengthened the observations reported by the group that JUN plays a dual role in regulating RyR2 activity (as highlighted in Table 1.2.), (Altschafl et al in 2011) and does not merely act as a linker between CSQ2 and the Ca^{2+} release channel.

5.1.4. Does CSQ2 associate directly with RyR2 channels?

CSQ2 is generally considered to interact with the RyR2 Ca^{2+} release channel via its association with JUN and/or TRD1 (Györke et al., 2004, Beard et al., 2009). However, several groups have also proposed that CSQ2 may bind to RyR2 channels themselves (Szegedi et al., 1999, Wei et al., 2009b, Murray and Ohlendieck, 1998), but direct evidence of such an interaction and its significance to myocardial function has not been determined (Murray and Ohlendieck, 1998, Terentyev et al., 2006, Chen et al., 2014). Currently, only investigations of protein-protein interactions between the skeletal isoforms of the two proteins have been reported. For example, Herzog et al (2000) used surface plasmon resonance (SPR) to prove a high affinity molecular interaction between CSQ1 and RyR1. In addition, Murray and Ohlendieck (1998) observed a complex formation between CSQ1 and RyR1 in fast- and slow-twitch muscle rabbit skeletal muscle. Furthermore, lipid bilayer experiments have demonstrated that purified RyR1 (absent of TRD1, JUN and CSQ2 associations) are activated by exogenous CSQ1 added back to the reconstituted channel, providing further evidence that more than one mechanism of CSQ1 association with RyR channels may exist (Beard et al., 2009). Other unresolved questions include whether CSQ2 can bind directly to RyR2 in the presence of JUN and/or TRD, or if the anchoring proteins prevent direct binding of CSQ2 to the Ca^{2+} release channel. It has been hypothesised that the Ca^{2+} binding protein binds directly to RyR2 in both the presence and absence of JUN and/or TRD1, the response of the channel may be altered from activation to inhibition when bound to the anchoring proteins (Györke et al., 2004, Beard et al., 2004, Wei et al., 2009a).

5.1.5. Defective protein-protein interactions contribute to the pathophysiology of CPVT

As discussed previously in Chapter 1 sections 1.7-1.8.4, mutations in RyR2 and CSQ2 are linked to CPVT, where alterations in the two proteins generate significant Ca^{2+} handling defects that can lead to SCD (Laitinen et al., 2003, Jiang et al., 2004; Song et al., 2007; Venetucci et al., 2008). Abnormal expression of JUN is also associated with CPVT (Kirchhof et al., 2007). Taking into consideration the numerous accessory proteins that have been proposed to interact with the hRyR2 Ca^{2+} release channel, it is unsurprising that defective protein-protein interactions are suggested as a contributing mechanism of CPVT (Wehrens et al., 2003, Thomas et al., 2007). For example, a CPVT-linked mutation, R2474S, was found by Xu et al (2010) to disrupt regulation of RyR2 interdomain interactions; and as a consequence reduced the binding affinity of the accessory protein calmodulin (section 1.5.3). Furthermore, a regulatory protein shown by some groups to

stabilise the closed state of RyR2 channels, FKBP12.6 (section 1.5.1), has been suggested to dissociate from the channels during heart failure (Marx et al., 2000, Blayney et al., 2010). Furthermore, the underlying mechanism responsible for the deleterious effects of a CPVT2-linked CSQ2 mutation, R33Q, was ascribed to a disruption in the protein-protein interactions between CSQ2 and the RyR2 Ca^{2+} release complex; rather than a defective Ca^{2+} binding capacity which had been reported for other CSQ2 mutants (Terentyev et al., 2006, Rizzi et al., 2008, Venetucci and Eisner, 2008). Valle et al (2014) recently described how a knock-in mouse model of CSQ2-R33Q displayed not only a significant reduction in CSQ2-R33Q expression in early development, but also down-regulation of JUN and TRD1, and morphological changes of the jSR, all of which may culminate to promote diastolic Ca^{2+} release from the SR (Valle et al., 2014, Knollmann et al., 2006). Given the proposed roles of CSQ2 and JUN in regulating the response of hRyR2 channels to luminal Ca^{2+} (Györke et al., 2004, Fan et al., 2008, Altschafl et al., 2011) and since mutations in CSQ2 appear to alter its structure such that it can no longer associate with the channel (either directly or via its association with JUN and/or TRD1), it is plausible that CPVT-linked RyR2 mutations (in particular those located at the luminal domain of the channel (e.g., A4556T) could affect the interaction of these accessory proteins; a concept that will be investigated in this chapter.

5.1.6. Chapter Aims

This chapter examines the protein-protein interaction between WT/mutant hRyR2 and the jSR luminal accessory proteins, CSQ2 and JUN. The transfection efficiencies of co-expressed CSQ2/JUN, and their intracellular trafficking, will be assessed using immunofluorescent detection. In addition, fluorescent labelling will be used to measure the degree of co-localisation between the luminal accessory proteins and WT/mutant hRyR2, where any differences in mutant protein interaction will be indicated. To specifically establish if defective interaction of the luminal proteins with mutant hRyR2 may be a contributing factor in the pathophysiology of CPVT, co-immunoprecipitation (Co-IP) experiments will also be carried out. Using this technique, the ability of CSQ2 and JUN to directly bind to hRyR2 channels (in the absence of other interacting proteins) will be assessed, before determining whether mutant hRyR2 channels associate differently with CSQ2 and/or JUN *in situ.*

5.2 Methods:

5.2.1. Immunofluorescent detection of hRyR2 and co-localisation with luminal accessory proteins CSQ2 and JUN:

HEK293 cells co-expressing hRyR2 and either CSQ or JUN (or both in combination) were fixed in 4% paraformaldehyde and probed with α-CSQ2 or α-JUN primary and Alexa® Fluor 594 labelled secondary antibodies, as specified in Chapter 2, section 2.4.3.6. WT and mutant hRyR2 expression were detected by their eGFP epitope tag. The transfection efficiencies of CSQ2 and JUN within a transfected HEK293 cell population were calculated by imaging the cells using a Zeiss fluorescence microscope. To visualise the co-localisation of WT/mutant hRyR2 with CSQ2 or JUN, the cells were imaged using an SP5 confocal microscope (Leica) with an oil immersion, x63 objective. Alexa® -594 fluorescence was excited at 590nm with a helium-neon laser and was detected over a 617nm±33 range, whilst eGFP fluorescence was excited with an argon laser (peak excitation = 488nm) and detection of emission at 520nm±28. As described by George et al (2003a), high resolution overlay images of the co-incident eGFP and Alexa® Fluor pixels were captured using Leica Microsystems LAS-AF software, such that the "percentage overlap" of co-incident pixels (corresponding to eGFP-hRyR2 and CSQ2/JUN expression, respectively) could be calculated. Adobe Photoshop was used to quantify the percentage of eGFP (green) pixels that were directly co-incident with Alexa®-594 (red) pixels, which appeared as yellow pixels when directly overlaid (or "merged") with each other (George et al., 2003a).

5.2.2. Co-Immunoprecipitation of CSQ2 and JUN by WT and mutant hRyR2:

Mixed membrane preparations were generated from transfected HEK293 cells (section 2.4.3.1) expressing WT or mutant hRyR2, in combination with either JUN or CSQ2 alone, or co-expression of both accessory proteins (JUN+CSQ2). As demonstrated in Figure 5.1 (A-C), all samples were first standardised for hRyR2 expression by Western blotting (A) and densitometric analysis (B), such that comparable amounts of WT and mutant hRyR2 protein were used in all Co-IP experiments (C). Using the μMACS™ system from Miltenyi Biotec (Figure 2.5), detergent-solubilised ER membranes (2 mg/ml) were incubated with 50μl anti-GFP magnetic microbeads to covalently couple the eGFP-tagged hRyR2 protein and the immunoprecipitated material captured using μMACS™ columns. Details of the Co-IP protocol are described in Chapter 2, section 2.4.3.6, together with those for SDS-PAGE and Western blotting (sections 2.4.3.3-2.4.3.4) which were used to visualise co-immunoprecipitates eluted from the μMACS™ columns. These were subsequently

analysed by densitometry. This protocol was also used to examine the direct association of CSQ2 with JUN, where detergent-solubilised microsomal membranes were captured using µMAC™ Protein A microbeads (Miltenyi Biotec) labelled by incubation with α-CSQ2 antibody and the resultant immunoprecipitate probed via Western blot analysis for JUN detection.

(A)

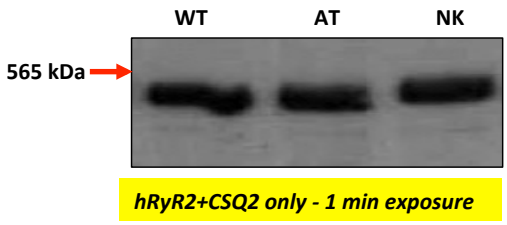

(B)

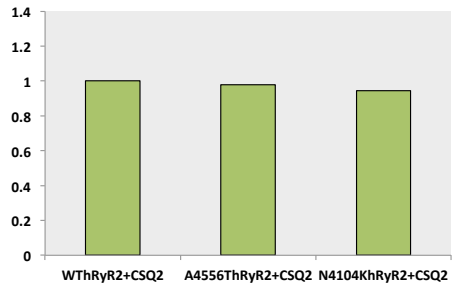

(C)

Protein combination	Density ODu/mm^2	Normalisation	Protein concentration	Volume and concentration of protein required for solubilisation	Final concentration of protein solubilised
WThRyR2 +CSQ2	504.6634	1	4995 µg/ml	200µl (1mg) solubilised in 500µl IP buffer	2 mg/ml
A4556ThRyR2 +CSQ2	355.7151	0.704856	7432 µg/ml	190µl (1420µg) solubilised in 710µl IP buffer	2 mg/ml
N4104KhRyR2 +CSQ2	431.8653	0.855749	8696 µg/ml	130µl (1170µg) solubilised in 585µl IP buffer	2 mg/ml

(D)

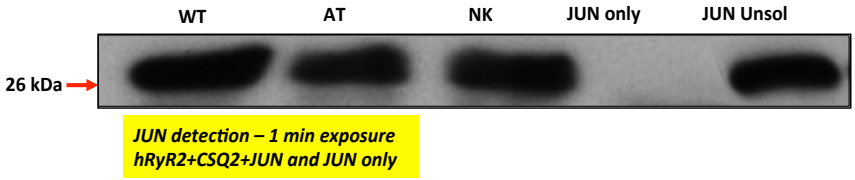

<u>Figure 5.1:</u> All mutant hRyR2 samples were standardised to WT hRyR2 expression before use in Co-IP investigations:

(A) *Illustrates an example of a Western blot of hRyR2 expression in mixed membranes co-expressing WT/mutant hRyR2 and CSQ2 only (NK= N4104KhRyR2, AT=A4556ThRyR2).*

(B) *Represented as a bar graph, to normalise for hRyR2 expression densitometric analysis was carried out on the Western blot signals obtained in (A).*

(C) *Following densitometry and before use, mutant hRyR2 test samples were standardised against WT for hRyR2 expression, such that equivalent amounts of each were used in the Co-IP experiment.*

(D) *Detection of any non-specific CSQ2/JUN binding to the µMACS™ columns was established in preliminary Co-IPs. Shown here is an example of JUN detection by Western blot, where in solubilised (2mg/ml) mixed membranes expressing JUN only, no JUN expression was evident following elution from anti-GFP microbeads. In contrast, JUN was detected in immunopreciptates co-expressing the luminal protein with WT/mutant hRyR2. JUN detection in unsolubilised material expressing JUN only (JUN Unsol) is also demonstrated.*

The preparatory stages described in (A)-(D) were carried out for all test samples before use in Co-IP experiments.

5.3 Results:

5.3.1. Determination of CSQ2 and JUN transfection efficiencies by immunofluorescent labelling:

Alexa® Fluor-594 labelling enabled the transfection efficiencies of untagged CSQ2 and JUN constructs to be calculated. In each field of view analysed, the accessory proteins and eGFP-hRyR2 were expressed to a high level, and predominantly within the same cells of a population (assessed by the % of cells which appeared both green and red, indicative of hRyR2 and CSQ2/JUN expression, respectively). Co-expression of WT or mutant hRyR2 with the accessory proteins yielded similar transfection efficiencies as illustrated in Figure 5.2 (n=4 populations counted for each expressed protein). When the transfection efficiencies of CSQ2 and hRyR2 were assessed, the percentage of cells which appeared both green and red were as follows: WT: 98±1%, A4556T: 97±2% and N4104K: 97±1%. Assessment of JUN and hRyR2 transfection efficiencies yielded similar results (WT: 98±2%, A4556T: 96±1% and N4104K: 98±1%), suggesting a high degree of luminal protein co-expression. An example of JUN and CSQ2 staining in transfected HEK293 populations co-expressing WT hRyR2+CSQ2+JUN is shown in Figure 5.3. To detect any non-specific staining, two controls were used: (1) transfected HEK293 cells treated with the Alexa® Fluor-594 secondary antibodies only and (2) untransfected HEK293 cells treated with both CSQ2/JUN primary and Alexa® Fluor-594 secondary antibodies (Figure 5.3). When imaging the cells by confocal microscopy, the negative controls were used to adjust the photomultiplier tube (PMT) voltage gain (red), such that the cells were imaged at a level where no non-specific staining could be identified.

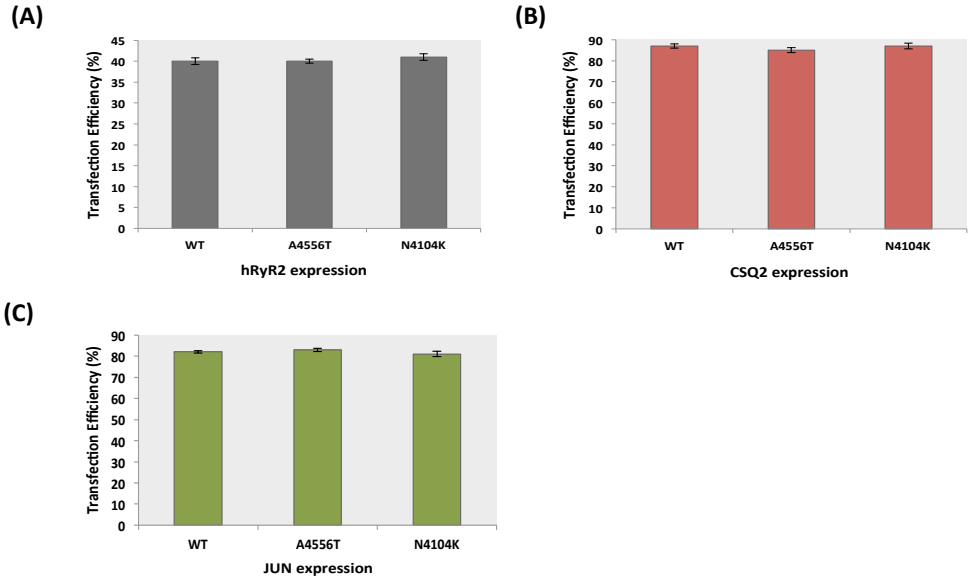

Figure 5.2: Comparable transfection efficiencies of HEK293 cell populations (n=4) expressing WT/mutant hRyR2, CSQ2 and JUN

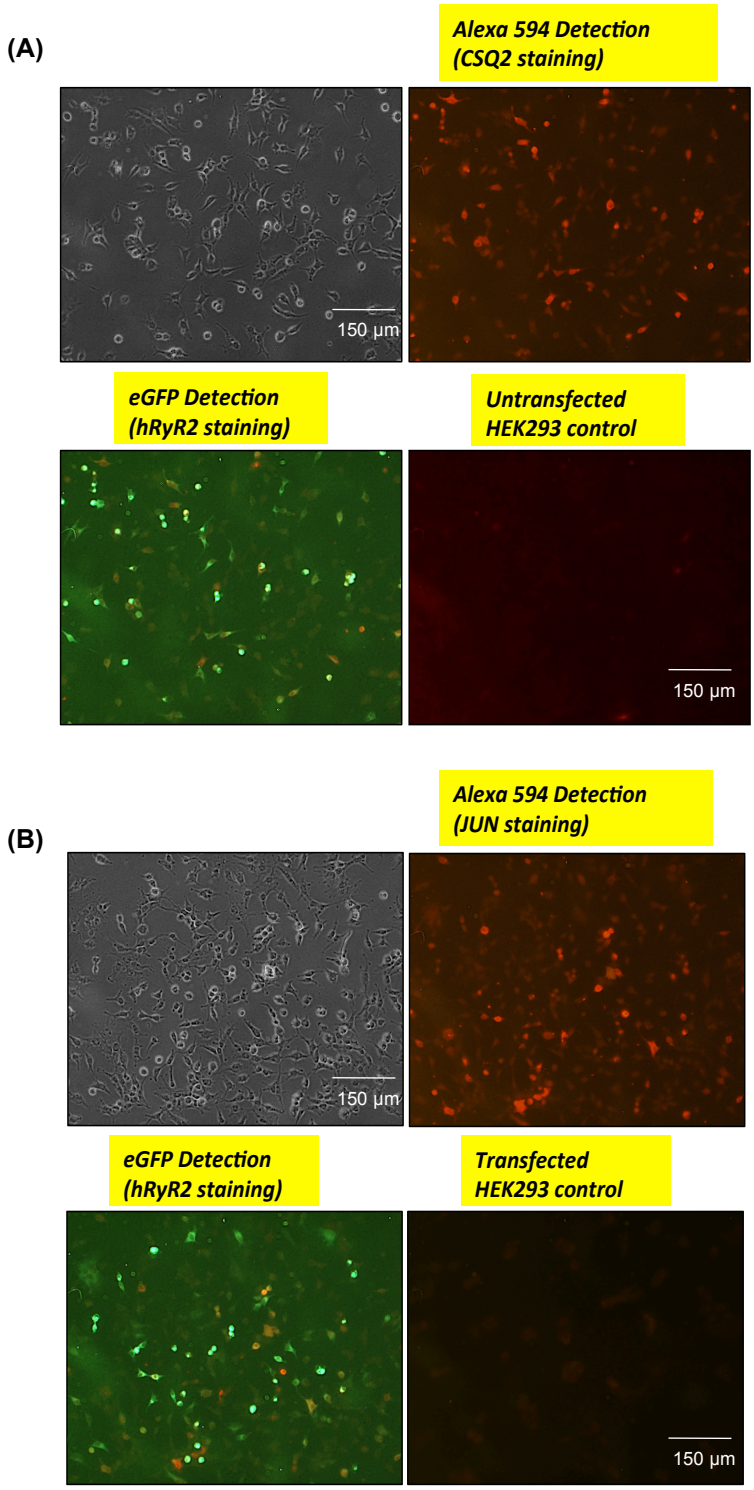

Figure 5.3: Imaging of CSQ2 and JUN co-expression with eGFP-hRyR2 in HEK293 cell populations. *Typical fields of view of cells imaged at 10x magnification are shown, taken using a Zeiss fluorescent microscope. Top left panels represent brightfield images of the transfected cells transiently expressing WT hRyR2, JUN and CSQ2. Top right panels display images of (A) CSQ2 detection and (B) JUN detection, following labelling of the accessory proteins with a red fluorescent secondary antibody. Images of eGFP detection are shown in the bottom left panels. Bottom right panels show immunostaining controls. (A) untransfected HEK293 cells were treated with the same primary and secondary antibodies to ensure no non-specific (background) binding was detected (cells shown were treated with anti-CSQ2 and Alexa®-594 anti-rabbit) and (B) transfected cells were treated with secondary antibodies (cells shown were treated with Alexa®-594 anti-mouse). As illustrated, only very low background fluorescence was evident.*

5.3.2. Evidence of greater CSQ2 condensation with JUN co-expression:

To ensure that any observed functional consequences of luminal protein or mutant RyR2 co-expression was not caused by protein mis-trafficking, immunofluorescence analysis was first used to confirm that all co-expressed recombinant proteins were correctly localised within HEK293 cells (Chapter 3, Figure 3.9), where the ER is thought to be analogous to the junctional SR of cardiac muscle (Milstein et al., 2009; Knollmann et al*.,* 2010). Illustrated in Figure 3.9, hRyR2, JUN and CSQ2 signals could be detected throughout the ER of the transfected HEK293 cells, both surrounding the nucleus and extending towards the central part of the cell. Cardiac CSQ2 has previously been shown to localise primarily to proximal ER compartments in non-muscle cells (Rossi and Sorrentino 2002, Houle et al., 2006), whilst using electrospray ionisation mass spectrometry it has been demonstrated that in HEK293 cells, CSQ2 displays a glycan structure characteristic of an endoplasmic reticulum-localised glycoprotein (O'Brian et al., 2002).

Consistent with these observations, most CSQ2 staining was identified in proximal ER regions (i.e., through the body of the cell but not immediately adjacent to the nucleus), however interestingly, more intense staining in the peri-nuclear membrane (i.e., adjacent to the nucleus) was visualised when CSQ2 was expressed in the presence of JUN. The brighter fluorescence signals corresponding to CSQ2 in this region are demonstrated in Figure 5.4: (A) WThRyR2+CSQ2+JUN, (B) N4104KhRyR2+CSQ2+JUN and (C) A4556ThRyR2+CSQ2+JUN. In HEK293 imaged with hRyR2+CSQ2+JUN co-expression, CSQ2 staining appeared brighter in 68% of cells with WThRyR2 expression, 75% of N4104KhRyR2 and 71% of A4456ThRyR2. In contrast, in cells expressing hRyR2+CSQ2 only, brighter staining in the peri-nuclear membrane was only evident in 20% of cells with WThRyR2 expression, 30% of N4104KhRyR2 and 25% of A4456ThRyR2.

Since CSQ2 does not contain any known ER targeting sequences such as the C-terminal KDEL tetrapeptide found in other resident ER proteins (such as calreticulin (Sönnichsen et al., 1994)), investigations into the molecular mechanism(s) responsible for retaining the Ca^{2+} binding protein in the junctional SR is a popular subject of current research (Knollmann et al., 2010; McFarland et al., 2010; Guo et al., 2012). As highlighted in Figure 5.4, co-expression of JUN with CSQ2 seemed to cause a tighter condensing of the luminal protein within the ER, and thus indicates JUN binding could be an important factor involved in CSQ2 ER/SR retention. Consistent with this suggestion, in cardiomyocytes isolated from transgenic mice with overexpression of both CSQ2 and JUN, CSQ2 was found to be packed within close proximity to the SR membrane, whilst when expressed alone the protein displayed a more diffuse disposition (Tijskens et al., 2003). In this investigation, the

authors concluded that although JUN was not necessary for CSQ2 targeting to the terminal cisternae, JUN plays a significant role in retaining CSQ2 within the jSR lumen of cardiac muscle and that the typical SR "phenotype" is governed by expression of both luminal proteins (Tijskens et al., 2003).

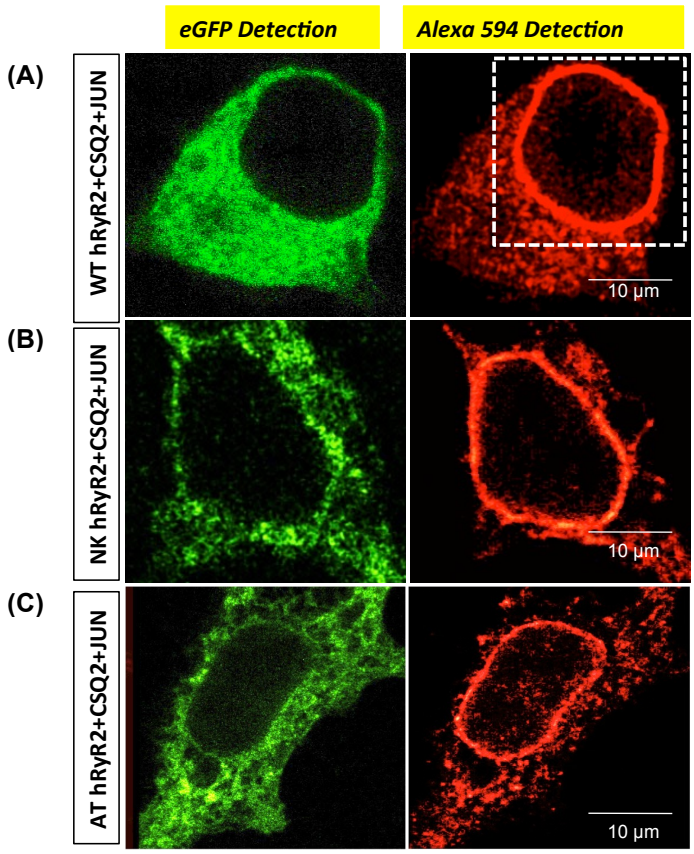

Figure 5.4: Evidence of CSQ2 condensation at the peri-nuclear region in imaged HEK293 cells: *When co-expressed in the presence of JUN, CSQ2 staining appeared brighter within the peri-nuclear region of HEK293 cells (highlighted with a dashed box in (A)). As discussed in section 5.3.2, this brighter staining was evident in a much larger percentage of cells co-expressing CSQ2+JUN, compared with those expressing CSQ2 only; thus suggesting JUN could be condensing CSQ2 within this region. Cells expressing WThRyR2 (A), N4104K hRyR2 (B) and A4556T hRyR2 (C) in the presence of the luminal accessory proteins are shown.*

5.3.3. Immunofluorescence co-localisation studies to examine the interaction of WT and mutant hRyR2 with CSQ2 and JUN:

Fluorescence labelling of hRyR2, JUN and CSQ2 (using an epitope tag or antibody labelling) enabled the degree of co-localisation between the recombinant proteins to be assessed. The extent of Alexa®-594 antibody (CSQ2/JUN) and eGFP (hRyR2) co-localisation was quantified as the percentage of green pixels (eGFP) that were directly co-incident with Alexa®-594 pixels (red) within a chosen image, which when merged (co-incident) were presented as yellow pixels, as demonstrated in Figure 5.5 and 5.6 (right panels, (i) in A and B). Data (mean ± S.E.M) were obtained from the analysis of 8-12 images in each instance and statistical differences detected using a Student's *t*-test (GraphPad Prism). No statistical differences were identified using ANOVA with a Tukey-Kramer post-test. As suggested in the GraphPad Prism handbook (graphpad.com) this may have been due to the conservative nature of this post-test, which can result in subtle, but significant differences in the data being undetected. The findings are represented in Figures 5.5 and 5.6 as a series of bar graphs A and B, (ii).

Figure 5.5 illustrates hRyR2 and CSQ2 detection, where overlay images of individual cells co-expressing WT/mutant hRyR2 with CSQ2 alone (A), (i) or in the presence of JUN (B), (i) are shown. N4104K hRyR2 appeared to co-localise with CSQ2 to a similar extent as WT hRyR2 channels (ii), in cells expressing CSQ2 alone (A): N4104K = 84% co-incident pixels ± 3.0 vs. WT hRyR2 = 93.6% co-incident pixels ± 2.6, and with JUN co-expression (B): N4104K = 85% co-incident pixels ± 6.75 vs. WThRyR2 = 93% co-incident pixels ± 1.46. In cells expressing A4556T hRyR2 however, a significant reduction in the co-localisation of CSQ2 was evident, both when expressed alone with the Ca^{2+} release channel (A), (ii), (81% co-incident pixels ± 2.8) and in combination with JUN (B), (ii), (80% co-incident pixels ± 3.0). Figure 5.6 demonstrates the detection of hRyR2 and JUN. Overlay images of individual cells co-expressing WT/mutant hRyR2 with JUN alone and in the presence of CSQ2 are shown in A, (i) and B, (i), respectively. When JUN was co-expressed alone with hRyR2 channels, no differences in its co-localisation with hRyR2 mutants were identified and a high degree of eGFP and Alexa® 594 co-localisation was evident in all cells imaged: WThRyR2+JUN only = 90%± 2.15, A4456T+JUN =86%± 4.0 and N4104K+JUN = 85%± 6.75 co-incident pixels. In contrast, in the presence of both luminal proteins (CSQ2+JUN), JUN co-localisation appeared to be significantly reduced when co-expressed with A4556T hRyR2 channels B, (ii): A4556T = 79% co-incident pixels ± 6.0 vs. WT hRyR2 = 98% co-incident pixels ± 0.89). As with CSQ2, no difference in the co-localisation of JUN with N4104K hRyR2 channels was evident (90% co-incident pixels ± 5.04, (B), (ii)).

To summarise, using immunofluorescence analysis, the A4556T hRyR2 mutation appeared to significantly reduce binding of CSQ2 in both the presence/absence of cardiac JUN. In addition, a decrease in JUN binding to this mutant was also evident, but was only calculated as significantly different in cells with CSQ2 co-expression (hRyR2+CSQ2+JUN). As discussed in the next section (5.3.4), following these observations, co-immunoprecipitation experiments were carried out to closer examine the association of CSQ2 and JUN with WT/mutant hRyR2.

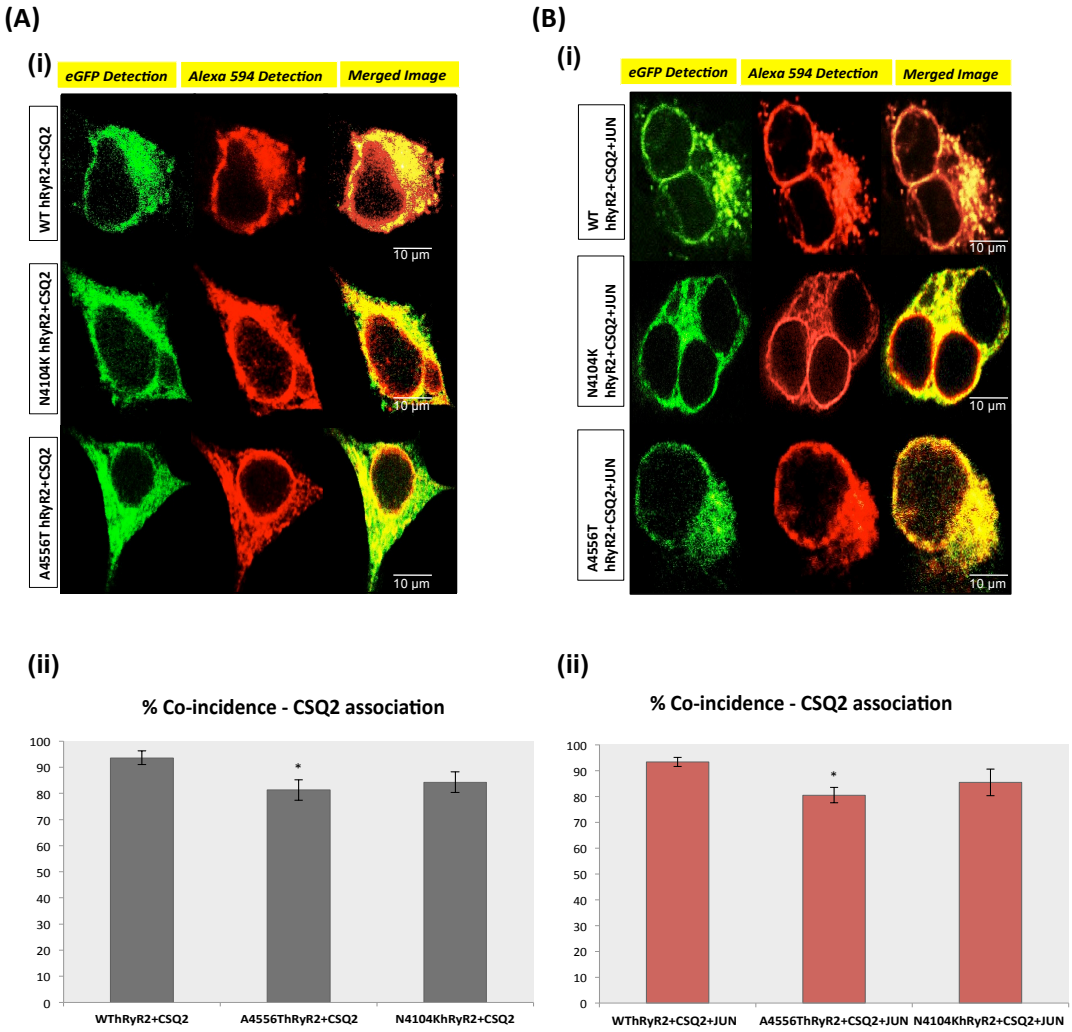

Figure 5.5: Evidence of reduced CSQ2 binding to the A4556T hRyR2 mutation by immunofluorescent co-localisation: *The top panels illustrate high-resolution images of transfected cells with detection of: eGFP-hRyR2 expression identified as green pixels (left images), CSQ2/JUN detection identified as red pixels (middle images) and a merge of the two (right images), which appear as yellow pixels and used to assess the degree of co-localisation. Immunofluorescent detection of CSQ2 in cells transfected with (A) hRyR2+CSQ2 only and (B) hRyR2+CSQ2+JUN are shown. The resultant pixel counting data (presented as the mean % co-incident pixels ± S.E.M) is represented in (A) and (B), (ii) as bar graphs, where 8-12 images in each instance were counted and any significant differences detected using a Student's t-test (GraphPad Prism), where * = p<0.05 (compared with WT hRyR2+CSQ2 (A) (ii) or CSQ2+JUN (B) (ii), respectively). Co-localisation of CSQ2 appeared significantly reduced when co-expressed with A4556T mutant channels.*

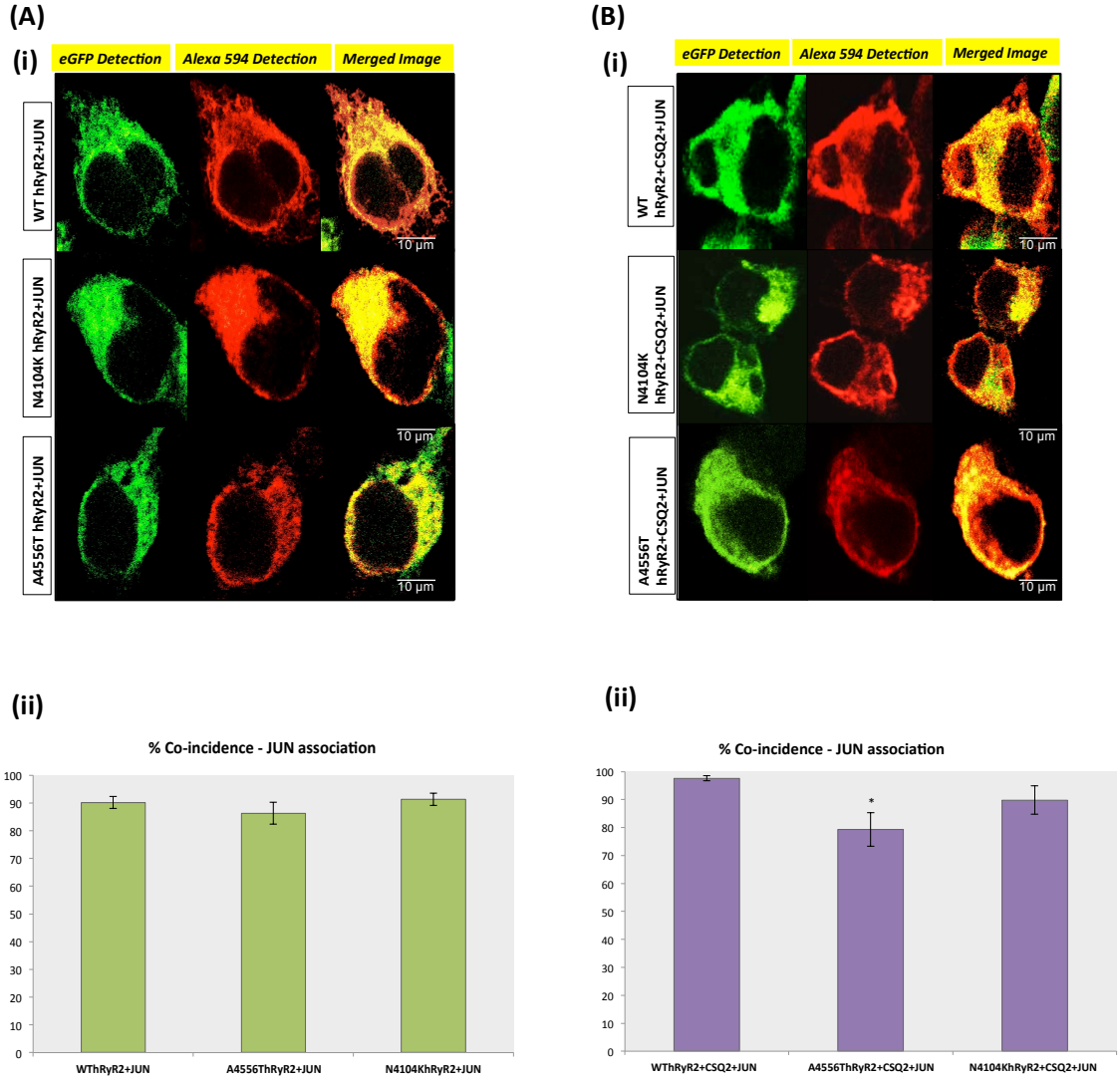

Figure 5.6: Evidence of reduced JUN binding to the A4556T hRyR2 mutation by immunofluorescent co-localisation: *Top panels illustrate high-resolution images of transfected cells with detection of: eGFP-hRyR2 expression identified as green pixels (left images), CSQ2/JUN detection identified as red pixels (middle images) and a merge of the two (right images), which appeared as yellow pixels and was used to assess the degree of co-localisation. Immunofluorescent detection of JUN in cells transfected with (A) hRyR2+JUN only and (B) hRyR2+CSQ2+JUN are demonstrated. The resultant pixel counting data (presented as the mean % co-incident pixels ± S.E.M) is represented in the bottom panels (A) and (B), (ii) as bar graphs, where 8-12 images in each instance were counted and any significant differences detected using a Student's t-test (* = p<0.05). Compared with WThRyR2, co-localisation of JUN appeared significantly reduced with the A4556T mutant, but only when co-expressed in the presence of CSQ2 (B), (ii).*

5.3.4. Assessment of protein-protein interactions between hRyR2 and the luminal accessory proteins using co-immunoprecipitation:

A series of Co-IP experiments were carried out to further examine the association of WT and mutant hRyR2 with CSQ2 and JUN (individually and in combination (CSQ2+JUN)). The aim of using this technique was not only to assess the ability of each luminal accessory protein to directly interact with hRyR2, but also to study the effect hRyR2 mutation may have on the ability of CSQ2 and/or JUN to bind with the Ca^{2+} release channel. In addition, although previously published by Zhang et al (1997) Co-IP was used to demonstrate a direct protein-protein interaction between recombinant CSQ2 and JUN in this investigation for completeness.

Proteins captured by μMACS™ columns (Figure 2.5), were eluted from anti-GFP microbeads (coupled to eGFP-hRyR2) and resolved by SDS-PAGE. Bound proteins were subsequently detected by Western blot analysis. Figure 5.7 illustrates two examples of Western blot detection, with protein bands corresponding to co-immunoprecipitated CSQ2 and JUN shown in A (i) and (ii), respectively. In order to normalise the signal from the eluate (solubilised material) for expression of the luminal protein of interest, unsolubilised mixed membranes (50μg) were loaded and resolved alongside the corresponding experimental samples (as shown in Figure 5.7, A (i) and (ii)). Densitometric analysis was used to assess the signals obtained from the immunoprecipitates, where an n=5 blots were analysed for each mixed membrane sample tested, i.e., WT/mutant hRyR2 co-expressing CSQ2 and/or JUN.

Interestingly, Co-IP investigations demonstrated that human cardiac muscle CSQ2 could directly interact with hRyR2 channels in the absence (Figure 5.7 (A), (i)) of other binding proteins, namely cardiac JUN in this project. To our knowledge, this is the first biochemical evidence to show a direct interaction of the Ca^{2+} binding protein with hRyR2. In the presence of JUN, CSQ2 was also found to be immunoprecipitated from hRyR2 channels. Likewise, a direct interaction of JUN with hRyR2 channels was seen in the presence (Figure 5.7 (A), (ii)) and absence of CSQ2 co-expression. Represented in Figure 5.7 (B), (i)-(iv) as a series of bar graphs, densitometric analysis of Western blot signals revealed that A4556T and N4104K hRyR2 channels appear to associate with CSQ2 and JUN to the same extent as WT, suggesting that these particular mutants do not alter the protein-protein interactions between the luminal accessory proteins and hRyR2.

Although the focus in this investigation was to examine the binding of the luminal proteins to hRyR2 channels, further Co-IP investigations were completed to establish if CSQ2 and JUN interact directly with each other (as proposed by Zhang et al., 1997). Still using the µMACS™ system, detergent-solubilised hRyR2+CSQ2+JUN mixed membranes (previously standardised for hRyR2 expression, as demonstrated in Figure 5.1) were instead incubated with µMACS™ Protein A microbeads labelled with α-CSQ2 antibody (section 2.4.3.6). As illustrated in Figure 5.8, to detect the presence of JUN in the immunoprecipitates, the collected eluates were resolved by SDS-PAGE and detection achieved by Western blot analysis. Since the primary aim of this investigation was to examine the interaction of CSQ2 and JUN with hRyR2 channels, densitometric analysis was not carried out the Western blot signals that examined the direct association between CSQ2 and JUN. However, JUN was successfully immunoprecipitated from solubilised hRyR2+CSQ2+JUN-expressing membranes by α-CSQ2 labelled microbeads (Figure 5.8), indicating a direct binding interaction between the luminal accessory proteins.

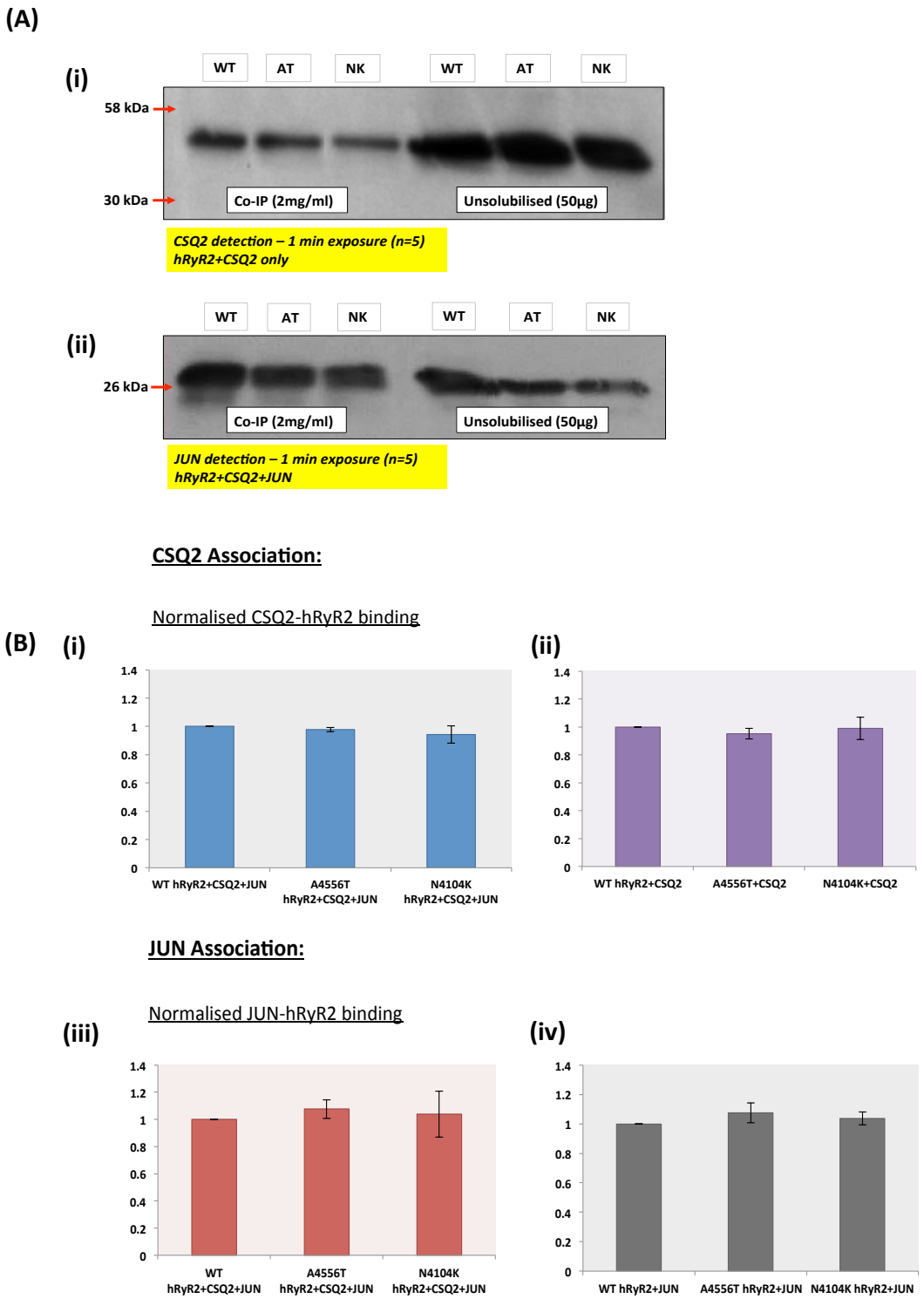

Figure 5.7: Co-immunoprecipitation demonstrates that mutation does not alter the interaction of CSQ2 or JUN with hRyR2: *Examples of Western blot signals obtained from the detection of CSQ2 or JUN expression in captured immunoprecipitates are shown in* ***(A) i*** *and* ***ii****, respectively. Detection of CSQ2 in solubilised mixed membranes expressing hRyR2+CSQ2 only demonstrate that the luminal protein can bind directly to hRyR2 channels in the absence of other interacting proteins (****(A),i****). Unsolubilised material was resolved and detected alongside the experimental samples, such that the signals obtained in the eluate could be normalised for CSQ2/JUN expression by densitometry. Mutant hRyR2 channels were found to associate with CSQ2 and JUN to the same extent as WThRyR2 channels, as represented here as a series of bar graphs* ***(B), i-iv****. An n=5 blots were analysed for each Co-IP study of CSQ2 or JUN immunoprecipitation when expressed alone or in combination (CSQ2+JUN) with hRyR2 and no statistically significant difference in WT/mutant RyR2 binding of luminal proteins was evident (assessed using one-way ANOVA and Tukey-Kramer post test (GraphPad Prism).*

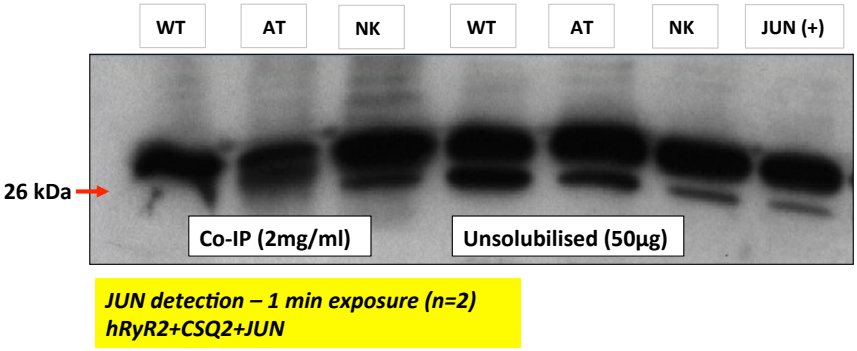

Figure 5.8: Direct protein-protein interactions between CSQ2 and JUN demonstrated by co-immunoprecipitation: *JUN was successfully detected in solubilised hRyR2+CSQ2+JUN immunoprecipitates captured by protein A microbeads coupled with a α-CSQ2 antibody. As in previous Co-IP investigations, corresponding unsolubilised material was resolved alongside the experimental samples. JUN (+) highlights JUN detection in an unsolubilised mixed membrane sample expressing JUN only, included as a positive control. The appearance of an additional band underneath the cardiac JUN signal in some lanes during Western blotting has been reported in previous studies and has been attributed to the presence of an internal methionine at amino acid residue 30 (Lim et al., 2000). Upon assessing all Western signals generated that corresponded to JUN expression, only a single band was evident in 54% of blots, whilst in the other 46% a second band was evident (but appeared substantially fainter).*

5.4 Discussion:

- Immunofluorescent staining was used to identify cells co-expressing CSQ2/JUN and WT/mutant hRyR2 where accessory proteins routinely achieved higher transfection efficiencies than those seen for hRyR2. Assessment of co-incident pixels found that WT and N4104K hRyR2 associate with the luminal proteins to a similar extent, whilst A4556T hRyR2 display a significantly reduced association with CSQ2 and JUN.

- Assessment of protein-protein interactions using co-immunoprecipitation and subsequent Western blotting demonstrated for the first time, the ability of CSQ2 to bind directly to hRyR2 channels, in the absence of JUN. Furthermore, direct binding of JUN alone and in the presence of CSQ2 to hRyR2 channels was established. Densitometric analysis of Western signals evidenced similar binding of CSQ2 and JUN to both WT and mutant hRyR2. The diminished association of CSQ2 and JUN with A4556T hRyR2 channels could not be replicated using this technique.

5.4.1. Immunofluorescence staining confirms successful co-expression of CSQ2 and JUN with hRyR2 in HEK293 cells:

Following imaging of immunofluorescently labelled CSQ2 and JUN (Figure 5.3), it was established that high transfection efficiencies of CSQ2 and JUN were achieved by co-expression with both WT and mutant hRyR2 channels, and that the efficiencies obtained were comparable (Figure 5.2). As illustrated in Figure 5.3 and discussed in section 5.3.1, the luminal proteins and eGFPhRyR2 were predominantly expressed within the same cells of a population. This was vital to reliably assess the functional response of WT and mutant hRyR2 to luminal protein co-expression and indicated the ability of the proteins to associate *in situ*.

Further to the immunofluorescence investigations described in Chapter 3 (section 3.3.5 and Figure 3.9) to confirm correct trafficking of all co-expressed proteins to the ER of HEK293 cells, it was also recognised that JUN might play an important role in CSQ2 retention. As demonstrated in Figure 5.4, as well as a reticular pattern of CSQ2 staining in proximal ER regions (also observed by Houle et al., 2006), much brighter fluorescence signals were observed in the peri-nuclear regions of cells when CSQ2 was co-expressed in the presence of JUN (i.e., cells transfected with hRyR2+CSQ2+JUN). Precisely how CSQ2, (being a small protein without a membrane spanning domain) is retained in the

junctional SR, has been the subject of a number of investigations. Milstein et al (2009) suggested that CSQ2 polymerisation is responsible for its retention in the jSR, since this is the first cellular compartment with ionic conditions favourable for CSQ2 polymerisation in cardiomyocytes; but did not discuss the potential involvement of the luminal accessory proteins (Milstein et al., 2009). It was however suggested by Knollmann et al (2010), that JUN (and TRD1) might help anchor a mesh of linear CSQ2 polymers to the mouth of the RyR2 Ca^{2+} release channels. The involvement of JUN in CSQ2 retention is supported by co-immunoprecipitation investigations in this project (Figures 5.7 and 5.8) and as demonstrated by Zhang et al (1997), where JUN is immunoprecipitated with both CSQ2 and RyR2 channels.

5.4.2. Examination of the protein-protein interactions between WT or mutant hRyR2 with CSQ2 and/or JUN using immunofluorescent co-localisation and co-immunoprecipitation:

The possibility that hRyR2 mutation may alter protein-protein interactions between CSQ2, JUN and the Ca^{2+} release channel were investigated in this chapter. Since the N4104K mutant resides on the cytosolic side of the hRyR2 channel, whilst A4556T is located on the luminal side, another aim was to establish if the location of the mutation could be a determinant of altered binding.

In addition to its use in the assessment of CSQ2 and JUN intracellular trafficking within HEK293 cells and establishing transfection efficiencies, immunofluorescence analysis was also used to measure the extent of co-localisation between the luminal accessory proteins and WT/mutant hRyR2 (Figures 5.5 and 5.6). As described in section 5.2.1, the direct overlay of eGFP- (hRyR2 detection) and Alexa® 594 (CSQ2 or JUN detection) images enabled the degree of co-localisation between the two signals to be calculated (George et al., 2003a). As represented as bar graphs in Figure 5.5 (A and B (ii)), co-incident pixel counting demonstrated that the co-localisation of CSQ2 with A4556T hRyR2 channels was significantly reduced, both when expressed alone and in the presence of JUN. This reduced binding could provide a possible explanation for the lack of CSQ2 inhibition evident in A4556T+CSQ2 only-expressing HEK293 cells in Ca^{2+} imaging investigations (Figure 4.17). However, inhibition of channel activity was apparent in HEK293 co-expressing A4556T+CSQ2+JUN (Figure 4.17). Furthermore, in cells transfected with hRyR2+JUN or +CSQ2+JUN, JUN co-localisation also appeared significantly decreased when co-expressed with the A4556T mutant. However, this was only evident when the protein was co-expressed in the presence of CSQ2 (Figure 5.6, B (ii)).

It is interesting that the A4556T mutation is located on the luminal side of the Ca^{2+} release channel and positioned very close to a proposed JUN binding site on the M5-M6 linker of RyR2 at residues 4520-4553 (Altschafl et al., 2011, Dulhunty et al., 2012). Given the observed decrease in co-localisation of both CSQ2 and JUN with the A4556T hRyR2 channel, it could be suggested that the mutant disrupts this JUN-RyR2 binding site, which could also be the site at which JUN anchors CSQ2 within close proximity to RyR2 channels. Although a decrease in JUN co-localisation with the A4556T mutant was also evident in Figure 5.6, B (i), (when expressed alone), the reduction was not calculated as significantly different from WT and N4104K hRyR2 channels. JUN has however been shown to associate at more than one site on RyR2 channels, for example luminal residues 78-210 also bind to a region that encompasses the pore loop at residues 4789-4846 (Altschafl et al., 2011).

Co-immunoprecipitation was used to assess the ability of CSQ2 and JUN to bind to each other and directly to hRyR2, in combination and individually. This technique was also used to further examine if the association of the luminal proteins with hRyR2 is altered by mutation. Co-IP investigations revealed that human cardiac muscle CSQ2 could directly interact with hRyR2 channels both in the absence (shown in Figure 5.7, A, (i)) and presence of cardiac JUN. This appears to be the first biochemical evidence to demonstrate a direct interaction of the Ca^{2+} binding protein with hRyR2 channels. Similarly, a direct interaction of JUN with hRyR2 channels was also observed in the presence (Figure 5.7 (A), (ii)) and absence of CSQ2 co-expression, consistent with previous research studies (section 5.1.3). Demonstrated previously by Zhang et al (1997), Co-IP was also used to observe a direct protein-protein interaction between recombinant CSQ2 and JUN in our experimental system, as illustrated in Figure 5.8.

In contrast to the immunofluorescent co-localisation findings discussed previously, densitometric analysis of Western blot signals obtained in Co-IP experiments demonstrated that A4556T- and N4104K hRyR2 channels associate with CSQ2 and JUN to the same extent as WT hRyR2, represented in Figure 5.7, B, (i)-(iv) as a series of bar graphs. This may suggest that mutants do not disrupt the protein-protein interactions between hRyR2, CSQ2 and JUN. However, the discrepancies between the results could also reflect limitations of the technique. The samples for example were standardised twice, once for hRyR2 expression (Figure 5.1) and then for CSQ2/JUN expression, following densitometric analysis of Western signals. Standardisation of hRyR2 was required to ensure equivalent protein binding to the anti-GFP microbeads, whilst the Western signals corresponding to the luminal proteins needed to be normalised to account for differences

in the expression levels of CSQ2/JUN amongst different mixed membrane preparations. It is thus possible that subtle changes could be missed. The results were however also prepared without luminal protein normalisation (data not shown) and still no statistical differences were calculated. The accuracy of densitometric analysis may have been improved by generating a standard curve from serial dilutions of each membrane preparation across an SDS-PAGE gel and subsequent Western blotting, or use of a loading control (such as actin, ~42 kDa) alongside experimental samples to correct for any errors in loading or transfer efficiencies (Taylor et al., 2013). Loading excessive amounts of the membrane preparation such that the Western signals were near saturation when analysed could have also hindered the detection of true changes in protein-protein interaction, as suggested by Mollica et al., 2009. Due to the somewhat variable nature of transient transfections (see Figure 3, Appendix), loading 50µg of each mixed membrane preparation was deemed the most sufficient amount for adequate signal detection.

Given the functional heterogeneity of CPVT-linked RyR2 mutations identified in previous investigations (Thomas et al., 2004, 2010) and between N4104K and A4556T hRyR2 in this project (see Chapter 4), the possibility that RyR2 mutants can disrupt protein-protein interactions of the channel complex can not be ruled out as a contributing factor in the pathogenesis of cardiac disease.

Chapter 6

General Discussion

6.1. Closing Discussion and Future Work:

The principal aim of this investigation was to establish if CPVT-linked mutant hRyR2 channels interact or respond differently to luminal accessory protein regulation by CSQ2, JUN and TRD1, proteins predicted to form a quaternary complex with RyR2 and to act as a luminal Ca^{2+} sensor for channel activity (Györke et al., 2004, Zhang et al., 2014). It is well documented that defective cytosolic and/or luminal Ca^{2+} sensing by RyR2 channels contributes to the aberrant Ca^{2+} release seen in CPVT (reviewed in Thomas et al., 2010). In addition, some CPVT-linked CSQ2 mutations result in a nonsense transcript effectively causing a knockout of the protein, which results in loss of SR Ca^{2+} buffering and Ca^{2+} binding capacity or association with RyR2 channels, which culminates in accelerated restitution of Ca^{2+} release (Terentyev et al., 2006, Rizzi et al., 2008). Evidently, defective luminal regulation of hRyR2 is implicated in arrhythmogenesis and this is the first study to examine how mutant hRyR2 channels respond to luminal accessory protein co-expression.

Two CPVT-linked hRyR2 mutations were examined: N4104K and A4556T, which reside on the cytosolic and luminal side of the channel, respectively. Since CSQ2, JUN and/or TRD1 are predicted to associate within the SR lumen, the location of the hRyR2 mutation could have been an important factor in detecting any differences in their interaction or response (i.e. luminal accessory protein association/effects may only be disrupted by mutations located on the luminal portion of the channel). Biochemical and functional assessment of luminal accessory protein interaction with WT hRyR2 were compared to that of the mutants. WT data were also used to inform on the respective roles of the accessory proteins in hRyR2 regulation.

To avoid species variability, often reported in the literature (described in Chapter 3, section 3.1.1, Qin et al., 2009, Wei et al., 2009b) the aim was to use only human isoforms of both RyR2 and the luminal accessory proteins, where a recombinant approach was employed. Expression constructs in (pcDNA3.1hygro$^{(+)}$) for human cardiac muscle CSQ2 and JUN were successfully generated, as outlined in Chapter 3, section 3.2.1 and 3.3.1-3.3.3. Specific amplification of cardiac TRD1 however proved problematic (Figure 3.2, section 3.4.1), which was largely due to the fact that at the time this work was carried out, the human cardiac muscle TRD1 sequence was unknown. Although a number of different primers were used in PCR amplification reactions, in an attempt to amplify TRD1 (section 3.3.1, Figure 3.1), without knowing the exact human sequence even undertaking a BLAST search for sequence homologies with the prospective amplicons isolated (cloned into TOPO® vector) proved difficult. In future work, the human cardiac muscle TRD1 sequence

published by Roux-Buisson et al (2012), could be consulted to re-design the PCR primers, in particular the reverse 3' primer, since the TRD1 sequence is reported to display its greatest divergence in the C-terminal region of the protein (Kobayashi and Jones, 1999, Roux-Buisson et al., 2012). Since TRD1 could not be successfully isolated, this project focussed exclusively on the response of WT/mutant hRyR2 channels to CSQ2 and JUN co-expression, both as a complex and expressed individually with the Ca^{2+} release channel. A mammalian HEK293 heterologous system was chosen to co-express WT and mutant hRyR2 with the luminal accessory proteins. Expression in HEK293 cells eliminated the need for purification and allowed the luminal proteins to associate with hRyR2 channels *in situ*.

The generation of HEK293 stable cells lines expressing CSQ2 and/or JUN is discussed in Chapter 3, sections 3.2.2. The original intent was to use these stable cells, and transfect them with eGFP-hRyR2, for use in all functional and protein-protein interaction investigations. However, the growth rate of the stable cell lines was much slower than anticipated, which consequently reduced the transfection efficiencies of transient eGFP-hRyR2 expression (using $CaPO_4$ precipitation). Since [^{3}H] ryanodine binding (Chapter 4) and co-immunoprecipitation assays (Chapter 5) require high levels of hRyR2 expression, the material for use in these experiments was generated by large-scale transient transfection of WT/mutant eGFP-hRyR2 with CSQ2 and/or JUN in an equimolar ratio. Using this optimised method, high transfection efficiencies of all co-expressed proteins were achieved, and as immunofluorescence studies proved that the transfection efficiency for JUN/CSQ2 was nearly twice that of hRyR2 (being expressed in ~% of the cells), it was judged that cells expressing hRyR2 would likely also be expressing the luminal accessory protein of choice as well, enabling complex formation. Accordingly, expression levels obtained for all proteins were sufficiently high as assessed by Western Blotting.

Stable cell lines were however essential for use in single-cell Ca^{2+} imaging, where it was necessary that each cell imaged, expressed the luminal accessory protein(s) of interest. Cells co-expressing WT or mutant hRyR2 could be identified by their caffeine response (Thomas et al., 2004). To obtain sufficient eGFP-hRyR2 transfection efficiencies in these cells, Effectene® reagent was used, the rationale for which included that fact that this method required less DNA and was therefore less cytotoxic than the $CaPO_4$ precipitation.

The functional assays used to assess the influence of CSQ2 and JUN on the intracellular Ca^{2+} regulation of WT and mutant hRyR2 are described in Chapter 4. The Ca^{2+} dependence of [^{3}H] ryanodine binding for WT and mutant hRyR2 channels in the absence and presence of CSQ2 and/or JUN was examined. When assessed alone (i.e., in the

absence of accessory proteins), notable differences in the Ca^{2+} activation profile of the hRyR2 mutants, compared to WT channels, were found. Although the half-maximal [Ca^{2+}] for activation of A4556T hRyR2 channels was not significantly different from that of the WT, the binding of [^{3}H] ryanodine was significantly higher at every Ca^{2+} concentration >1μM. This may have been due to a standardisation problem, due to vastly different expression levels, or it could reflect a genuine effect of the mutant on the association/dissociation of [^{3}H] ryanodine. If this was to be investigated further, the mutant could be explored at the single channel level with a reversible ryanoid (such as Ryanodol, used by Sigalas et al., 2009) so as to verify this assumption by the measurements of ryanoid association and dissociation rates (as in Tanna et al., 1998, Sigalas et al., 2009). The primary aim of the [^{3}H] ryanodine assay however, was to explore the sensitivity of Ca^{2+} activation, which for this mutant was no different to WT. In contrast, N4104K hRyR2 channels displayed a significantly sensitised Ca^{2+} activation profile, indicating that these mutations are functionally heterogeneous. Demonstration of this concept is an important contribution to the field, since as discussed in Chapter 1 (sections 1.8-1.8.3) the mechanism behind CPVT-linked hRyR2 dysfunction is often attributed in the literature to a single unifying factor, such as an altered interaction of FKBP12.6 with hRyR2 (section 1.8.1). It is however likely that the form of channel dysfunction is mutation-specific, possibly determined by its location in the polypeptide. The different modes of channel dysfunction found in this work between CPVT-linked mutants N4104K and A4556T are summarised as a schematic in Figure 6.1, and directly compared with WT hRyR2 (A-C).

To ascertain any functional effects conferred by luminal accessory protein co-expression, the aforementioned [^{3}H] ryanodine binding experiments were repeated in the presence of CSQ2 and/or JUN. However, no significant changes in the response of WT or mutant hRyR2 channels to Ca^{2+} activation were evident. Since differences were identified in single-cell Ca^{2+} imaging studies, it was concluded that the [^{3}H] ryanodine binding technique may not have been sensitive enough to detect subtle changes in the Ca^{2+} response imparted by CSQ2 and/or JUN (section 4.4.2). Alternatively, it is possible that the use of high salt conditions (used to optimise RyR2 P_o (Chopra et al., 2009, Euden et al., 2013)) could have disrupted protein-protein interactions between RyR2 channels and the luminal proteins, such that any functional effects were diminished. Indeed, it was demonstrated using co-immunoprecipitation studies that luminal protein association was diminished, albeit not significantly, under high salt conditions and this may have been enough to cause a functional effect. In future work, these experiments could be repeated using lower salt conditions, but it is unlikely using recombinant RyR2 that sufficient [^{3}H] ryanodine binding counts would be achieved.

Ca^{2+} imaging investigations proved more suitable in examining regulation of mutant hRyR2 by CSQ2 and/or JUN (Chapter 4). First, the properties of the SCR parameters (section 4.3.3) in HEK293 cells expressing WT and mutant hRyR2 channels alone were assessed. Figures 4.12 and 4.13 illustrate the similarity between the SCR properties of WT and A4556T channels, where no parameters were found to be statistically different. On the contrary, SCR events in cells expressing N4104K hRyR2 channels appeared completely different (Figures 4.12 and 4.13), where amplitude and duration were significantly reduced (compared to WT channels); whilst the SCR events appeared much faster (measured as an increase in SCR frequency). These differences needed to be considered when assessing any changes introduced by luminal protein co-expression. The alterations in the SCR parameters in stable HEK293 cells expressing CSQ2 and JUN alone or in combination with WT hRyR2 channels are described in detail in section 4.3.4, Figures 4.14 and 4.15. In the presence of the luminal proteins, properties such as the SCR event duration and inter-event duration were significantly enhanced, thereby reducing the frequency of events. Co-expression with CSQ2 in particular, both alone and in the presence of JUN, seemed to have a notable inhibitory effect on hRyR2 SCR activity (Figure 1.6 (A and B). This inhibition has been reported by others using different experimental systems (Jones et al., 1998, Beard et al., 2005, Györke et al., 2004). Despite the altered properties of SCR events evident in cells expressing N4104K channels alone, both A4556T and N4104K channels responded in a similar manner as WThRyR2 to CSQ2 and JUN co-expression (4.16-4.19). Surprisingly however, the inhibitory effects of CSQ2 co-expressed alone with hRyR2 channels (seen with WT and N4104K) were diminished in cells expressing A4556T channels (Figure 1.6 (C)). This is a novel finding of a previously uncharacterised, luminallly located hRyR2 mutation and will be of interest in further investigations.

In future work, the findings of the Ca^{2+} imaging studies could be verified by assessing WT or mutant hRyR2 channels in the presence of CSQ2 and/or JUN at the single channel level. Both cytosolic and luminal Ca^{2+} activation could be assessed using this technique, where conditions either side of the hRyR2 channel (reconstituted into a lipid bilayer) can be manipulated. This however would require extensive optimisation, starting with the decision of whether each protein should be purified and added back to the hRyR2 channel (as carried out by Györke et al., 2004) or the recording of heavy ER preparations (mixed membranes) should be optimised. If mixed membranes were to be used, different permeant ions (such as K^+, Cs^+, $Ba^{2+}$and Ca^{2+}) would need to be tested, in order to establish a sufficient signal to noise ratio where the activity of RyR2 channels could be clearly identified amongst other ion channels (such as Cl^- and K^+) that would also incorporate into the lipid membrane. In addition, a strategy to identify changes imparted by

the luminal proteins would need to be devised. Purification of the luminal proteins is another option, which again would require the development of a reliable purification strategy. Györke et al (2004) used two different expression systems to purify dog CSQ2, JUN and TRD1, suggesting that sufficient levels of expression may have been problematic. Recombinant dog calsequestrin was cloned into the bacterial expression vector pET5a (as used in Kobayashi et al, 2000), whilst JUN (Zhang et al, 1997) and TRD1 (Kobayashi and Jones, 1999) were both isolated and purified by infecting Sf21 insect cells with baculovirus encoding the recombinant proteins (Gyorke et al, 2004). Furthermore, in order to confidently determine the functional effects of the CSQ2 and/or JUN-hRyR2 interaction and establish if mutants respond differently, a reliable method to detect re-association/dissociation of the luminal proteins would need to be devised. Gaburjakova et al (2013) suggested that this issue is likely to be the reason why conflicting findings have been reported upon investigating the functional role of CSQ2 at the single channel level.

Chapter 5 describes the examination of WT and mutant hRyR2 interactions with the luminal accessory proteins. Demonstrated by immunofluorescent co-localisation and subsequent co-incident pixel counting (described in section 4.3.3), the interaction of CSQ2 with the previously uncharacterised A4556T channels was significantly reduced when expressed both alone and in the presence of JUN (Figure 5.5 and illustrated in Figure 1.6 (C)). Furthermore, a decrease in JUN binding with A4556T channels was also identified, but only when co-expressed in the presence of CSQ2 (Figure 5.6 and 6.1 (C)). No differences in the association of CSQ2 or JUN with N4104K channels (compared with WT hRyR2) were detected. This altered interaction of A4556T channels with CSQ2 could explain why in Ca^{2+} imaging investigations, the inhibitory effects of the luminal protein on channel activity was reduced in cells co-expressing CSQ2 only (Figure 4.17). If this were the case however, I would have also expected to see the same effect in HEK293 cells expressing A4556T, CSQ2 and JUN.

The ability of CSQ2 and JUN to bind both individually and in combination to WT/mutant hRyR2 channels was also explored using co-immunoprecipitation (section 5.3.4). In contrast to immunofluorescent co-localisation studies, both A4556T and N4104K hRyR2 channels were found to bind to CSQ2 and JUN to the same extent as WT channels (Figure 5.7). It is possible that since Western blot signals used for densitometric analysis were standardised twice, first for hRyR2 expression and then for luminal accessory protein expression (which differed between mixed membrane samples, section 5.4.2), subtle differences in the interaction between these proteins could have been missed. As illustrated in Figure 1.6 (A), Co-IP experiments biochemically demonstrated for the first

time the ability of human cardiac CSQ2 to bind directly to hRyR2 channels in the absence of any additional accessory proteins (i.e, JUN). Since the literature suggests that CSQ2 is only anchored within close proximity to hRyR2 via its association with JUN and/or TRD1 (as shown in Figure 1.2), this finding is a major contribution to the field.

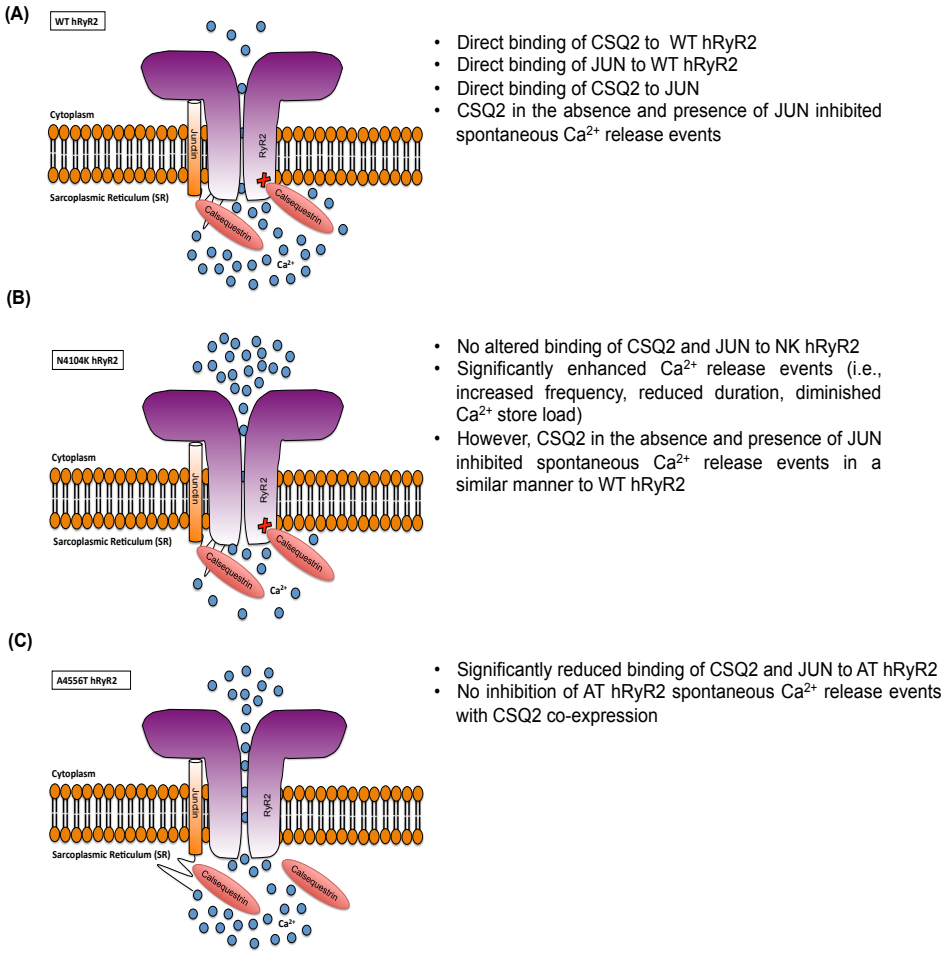

Figure 6.1: Schematic summarising the major findings of this work:
(A) *Illustrates the ability CSQ2 to bind directly to WT hRyR2 alone and via its association with JUN. CSQ2 co-expression appeared to have an inhibitory effect on hRyR2 channel activity (indicated with a red cross).* ***(B)*** *N4104K channels responded similarly to luminal protein co-expression, where an inhibitory effect on channel gating was observed in the presence of CSQ2 (expressed alone and with JUN). This mutant however displayed enhanced sensitivity to activating Ca^{2+} evident in both [^{3}H] ryanodine binding assays and Ca^{2+} imaging investigations; resulting in elevated SCR activity and a significantly reduced ER Ca^{2+} load, indicative of Ca^{2+} leak through the channel.* ***(C)*** *In Ca^{2+} imaging studies, no notable inhibitory effects of CSQ2 (when expressed alone) on A4556T hRyR2 activity were evident. Thus, this mutant did not respond in the same manner as WT and N4104K hRyR2 to CSQ2 co-expression. Demonstrated by co-immunofluorescent co-localisation and subsequent co-incident pixel counting, lack of an inhibitory effect may have been due to significantly reduced protein-protein associations between CSQ2 and A4556T hRyR2. Furthermore, JUN binding (when expressed in the presence of CSQ) was also significantly diminished in A4556T hRyR2 channels.*

In future work, it would be beneficial to investigate the interaction of mutant (and WT) hRyR2 with CSQ2 and/or JUN using a more sensitive technique, such as Surface Plasmon Resonance. Briefly, recombinant GST-fusion proteins corresponding to CSQ2 and JUN could be created and immobilised to the surface of a sensor chip (Blayney et al., 2010). To measure the affinity and binding kinetics between the proteins, WT or mutant hRyR2 could then be used as an analyte, and passed in solution over the chip surface, to which the luminal accessory proteins are bound (Hutsell et al., 2010, Blayney et al., 2010). Furthermore, the co-immunoprecipitation studies used in this investigation could be repeated, but instead using the stable HEK293 cells expressing CSQ2 and/or JUN. This would eliminate the need for further standardisation to account for luminal protein expression. However, since these investigations require high-levels of hRyR2, the protocol for transient transfection of hRyR2 in stable HEK293 cells would first need to be further optimised. In summary, these studies find that CPVT-linked hRyR2 mutant channels are functionally heterogeneous and that dysfunction of some mutants is unlikely to be caused by a lack of response to luminal accessory protein (e.g. N4104K). However, CSQ2 was found to bind directly to the WT channel, having a similar inhibitory effect as seen in the presence of JUN (its anchoring protein – Zhang et al., 1997). This study suggests that the A4556T mutation results in reduced CSQ2 binding to the channel resulting in altered regulation, however this was not found using all detection methods and requires verification by more sophisticated methods.

As discussed in Chapter 1, section 1.7, ß-blockers represent the first line in CPVT treatment. However, this treatment is often insufficient with many patients still suffering potentially fatal symptoms (Mackrill, 2010, Liu et al., 2011). The work carried out in this project provides evidence of the functional heterogeneity that exists between CPVT-linked mutations and demonstrates that therapeutic interventions may need to be tailored towards the specific pathogenic properties of a given RyR2 mutant, with consideration towards their location and severity.

N4104K RyR2 channels showed sensitised Ca^{2+} activation and aberrant Ca^{2+} release both in the absence and presence of luminal accessory proteins. Previous reports have suggested that gain-of-function mutations, such as N4104K, alter the ability of RyR2 channels to close during diastole, resulting in enhanced SCR release (described as Ca^{2+} leak, Jiang et al., 2004, 2005) and a decreased SR Ca^{2+} store (as demonstrated in Figure 4.13). Suppression of this enhanced SCR release (or SOICR) by decreasing RyR2 luminal Ca^{2+} sensitivity has been proposed as a promising antiarrhythmic treatment for patients harboring such mutations (Hunt et al., 2007, Zhou et al., 2011, Chen et al., 2014). However, the extent to which SOICR is eliminated needs to be controlled, since complete

inhibition also triggers arrhythmogenesis (Chen et al., 2014). A major challenge in drug development is to identify compounds with the ability to reduce diastolic Ca^{2+} leak without affecting RyR2 channel gating during systole (Mackrill, 2010, McCauley and Wehrens, 2011, Fischer et al., 2013). Hunt et al 2007 demonstrated that a 1,4-benzothiazepine derivative K201 (or JTV519) significantly reduced the occurrence of SOICR in HEK293 cells expressing WT hRyR2 (in Ca^{2+} imaging studies) and inhibited [^{3}H] ryanodine binding to both WT and N4104K RyR2 channels, diminishing the enhanced basal activity seen with CPVT-linked mutants (as demonstrated in this work, Figure 4.6). SOICR inhibition and subsequent stabilisation of the closed state (deduced from the fact that [^{3}H] ryanodine binding is reduced and the activation threshold increased with K201 treatment) occurred the absence of FKBP12.6, despite previous reports suggesting that the effectiveness of the drug stems from its ability to enhance FKBP12.6-RyR2 binding (Wehrens et al, 2004). Altered Ca^{2+} sensitivity however was only evident with the use of higher (μM) K201 concentrations, and thus seems unsuitable for use in patient clinical trials (Hunt et al., 2007). Another drug found to successfully suppress SOICR occurrence is carvedilol, which interestingly is one of the most effective ß-blockers used in preventing arrhythmia in HF patients (Zhou et al., 2011). Independent of its ability to inhibit ß-adrenergic stimulation, Zhou et al (2011) demonstrated that of the 14 known ß-blockers tested, only carvedilol displayed a direct effect on RyR2 gating, reducing RyR2 channel P_o at the single channel level. The concentrations of carvedilol required to effectively inhibit SOICR however, were much higher than those required as a ß-blocker, raising concern of adverse reactions when used in *vivo* (Zhou et al, 2011). To overcome this effect, the group demonstrated the use of carvedilol analogs (such as VK-II-86, tested in mice harbouring a CPVT-linked mutant and HEK293 cells), which retained their ability to suppress SOICR activity whilst having much lower actions as ß-blockers (Zhou et al, 2011). These analogs combined with an alternative ß-blocker (such as metoprolol) could improve protection against arrhythmia in CPVT patients with a mutation that displays a gain-of-function phenotype (Zhou et al., 2011). A4556T hRyR2 channels displayed similar SCR event properties to WT hRyR2 in the absence of accessory protein expression (Figure 4.13); however, the inhibitory effect of CSQ2 co-expression was diminished in cells expressing A4556T hRyR2. As discussed previously (section 5.4.2), this effect may have been caused by a disruption in the protein-protein associations between CSQ2 and A4556T hRyR2 (Figure 5.5). To date, only a few drugs have been proposed to enhance the interaction of RyR2 with its accessory proteins, such as the aforementioned K201, which has been proposed to stabilise the binding of FKBP12.6 (Wehrens et al, 2004, Mackrill, 2010), though this is in dispute (Hunt et al., 2007). The development of therapeutic agents to modify the binding interaction between RyR2 and CSQ2 may facilitate the treatment of CPVT mutants such as A4556T.

Appendix

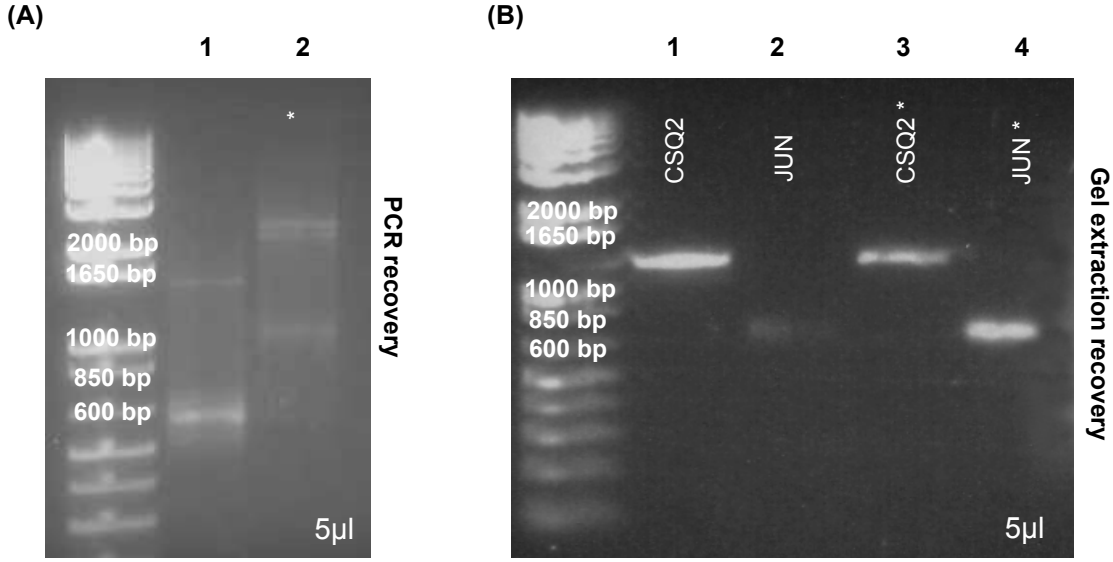

<u>Figure 1:</u> Visualisation of PCR/gel extraction products by agarose gel electrophoresis: *Original images that were cropped for presentation purposes in Chapter 3, Figure 3.2 are shown.* ***(A)*** *Demonstrates the PCR products generated in attempts to isolate TRD1. As indicated with an asterisk (lane 2), these products are shown in (Figure 3.2, B, (ii)) which were obtained following PCR amplification using a reverse primer designed to target the pACT2 vector (see section 3.3.1). Lane 1 corresponds to the same PCR recovered products shown in Figure 3.2 B, (iii), however the same recovery loaded on a different gel is shown in the chapter. (B) Illustrates the gel extraction recovery products of CSQ2 and JUN shown in Figure 3.2 (D) as highlighted with asterisks. Lanes 1 (CSQ2) and 2 (JUN) shown are the same as lanes 3 and 4, respectively. However, these were not shown in Figure 3.2, due to the loading error in lane 2.*

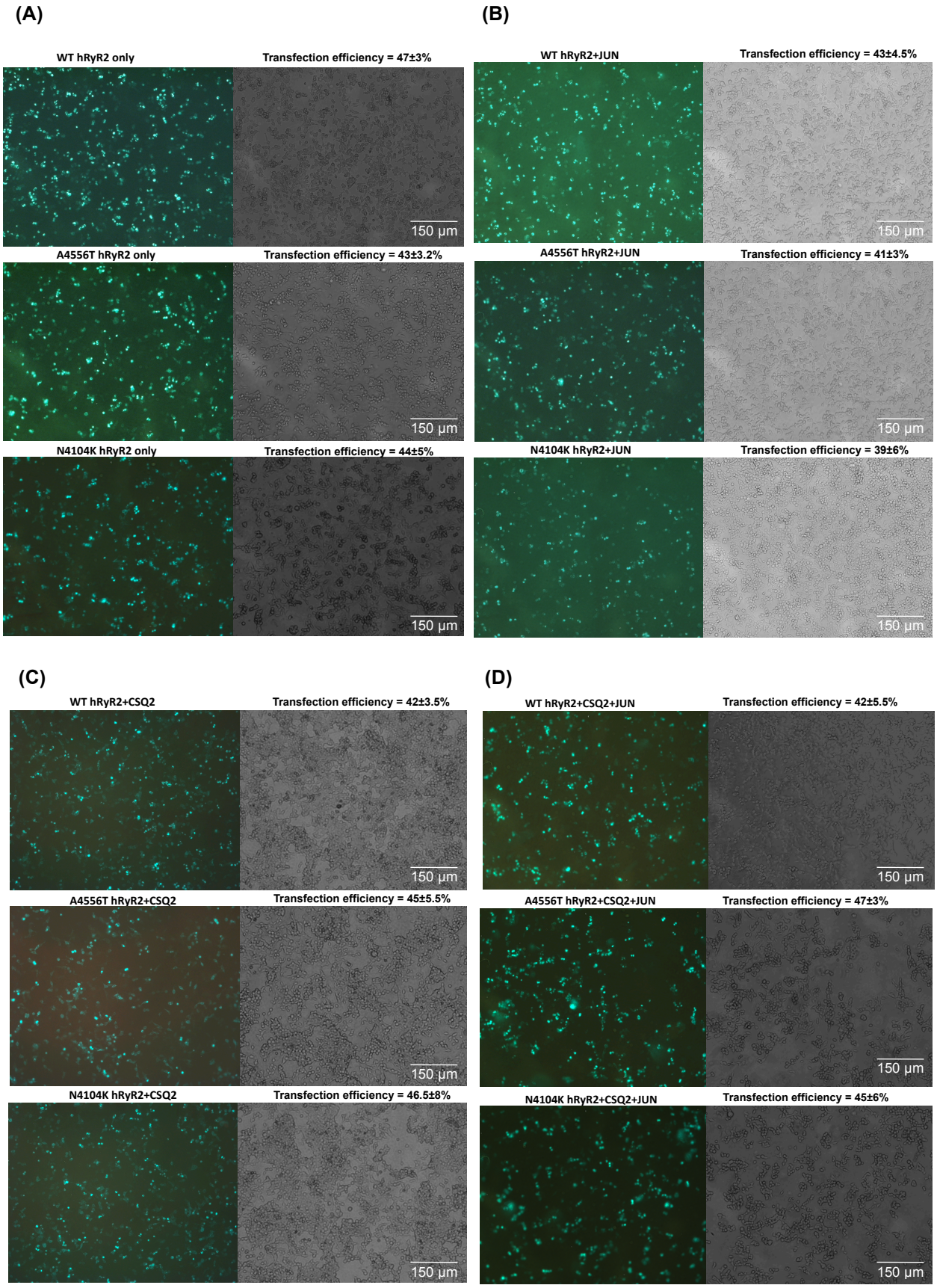

Figure 2: Comparable hRyR2 transfection efficiencies in HEK293 cell populations: *Illustrated are representative fluorescent images (and corresponding phase images) of HEK293 cell populations transfected with (A) hRyR2 only, (B) hRyR2+JUN, (C) hRyR2+CSQ2 and (D) hRyR2+CSQ2+JUN. Comparable transfection efficiencies were obtained in cells transfected with WT or mutant hRyR2, and the efficiencies were unaffected by co-expression with the accessory proteins.*

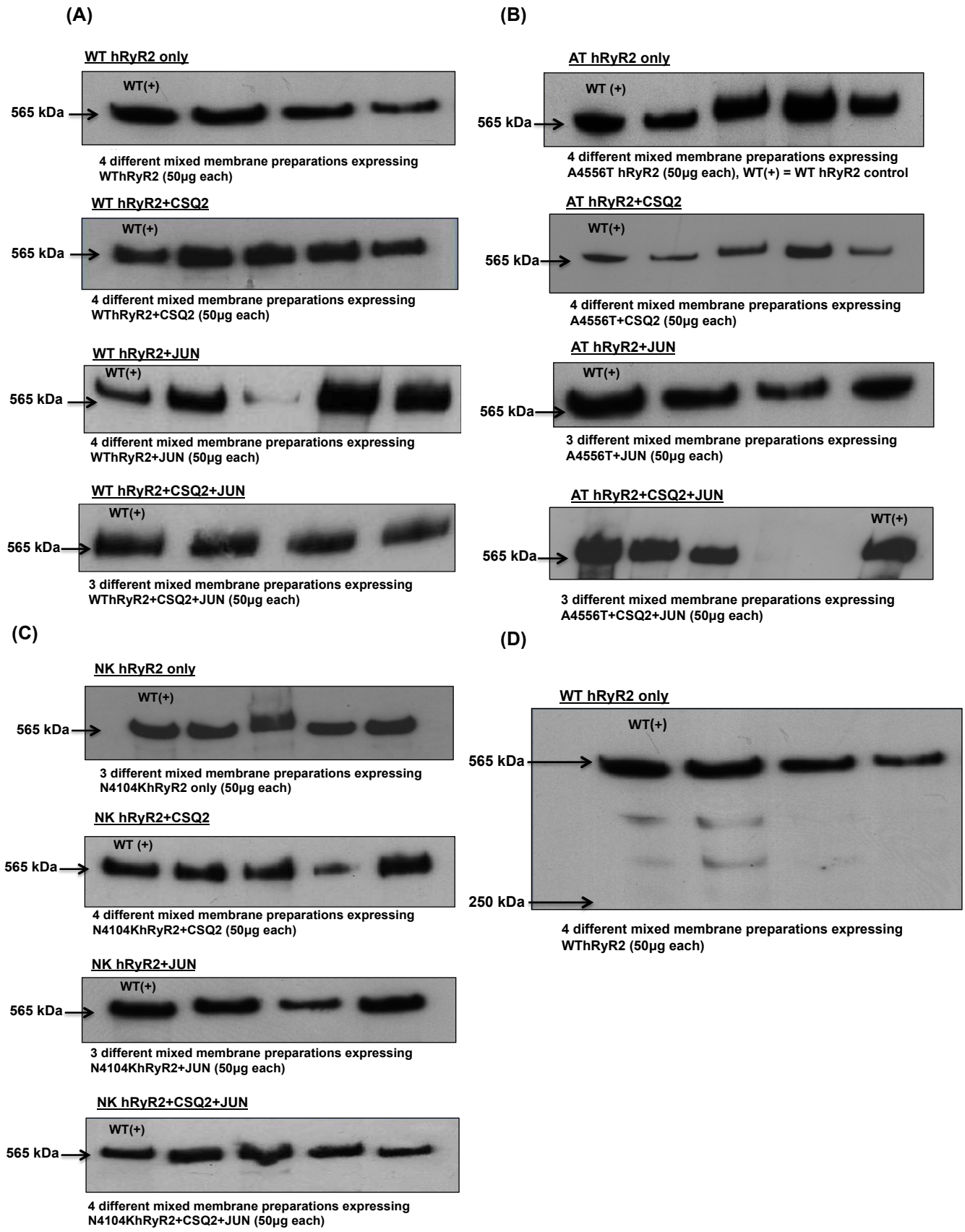

Figure 3: Additional Western blots of hRyR2 expression: *Illustrated are representative Western blot signals obtained following SDS-PAGE of mixed membrane samples expressing (A) WT hRyR2, (B) A4556T (AT) hRyR2 and (C) N4104K (NK) hRyR2 alone and in the presence of CSQ2 and/or JUN. WT (+) refers to a positive WT hRyR2 only control loaded alongside test samples. (D) hRyR2 signals (WT shown) were detected at 565 kDa (fainter signals below this band are breakdown products of the protein), above the highest reference band of the pre-stained Kaleidoscope™ marker (Bio-Rad) at 250 kDa.*

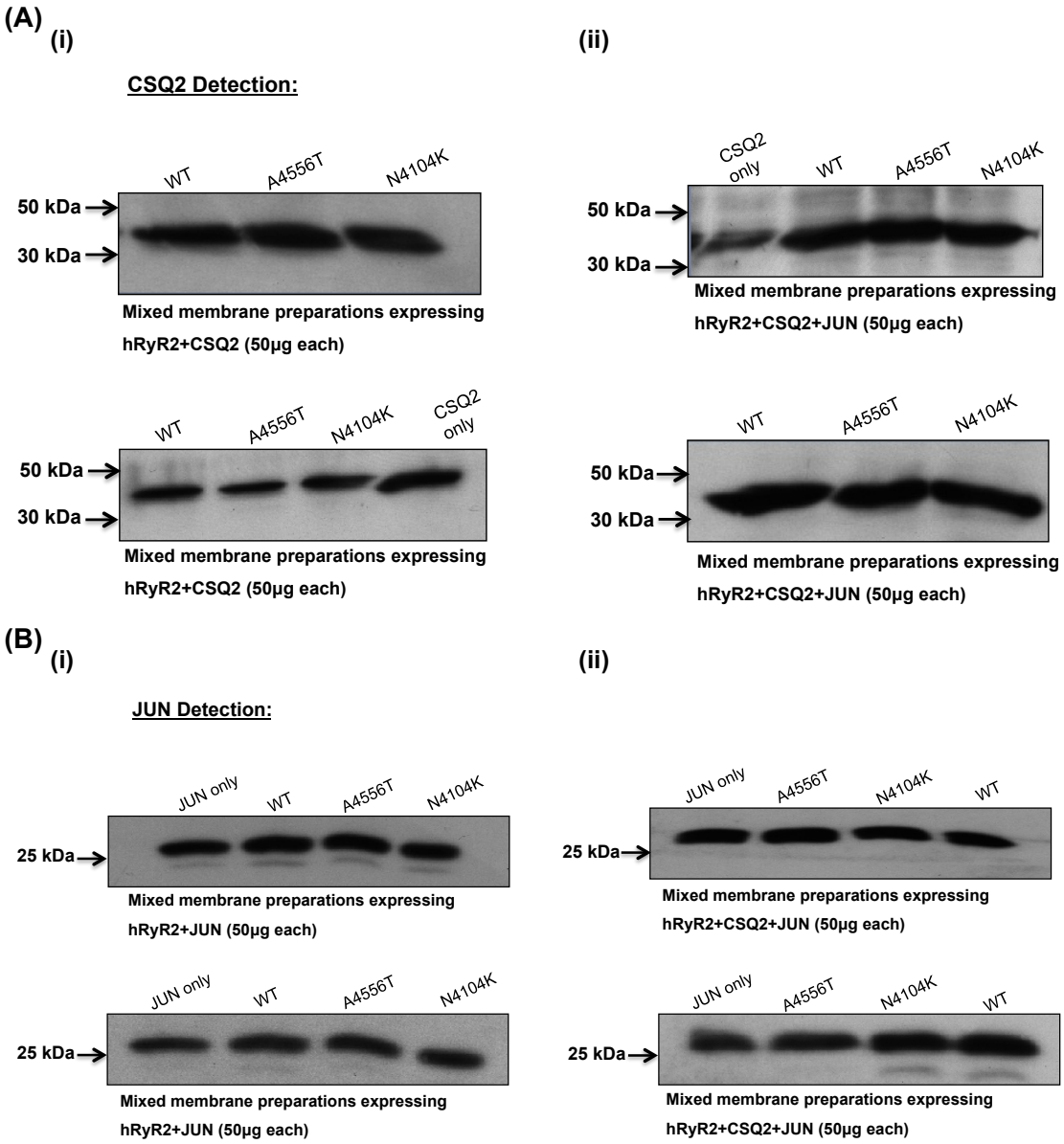

Figure 4: Additional Western blots of CSQ2 and JUN expression: *Illustrated are representative western blot signals obtained following SDS-PAGE of mixed membrane samples expressing* ***(A)*** *hRyR2+CSQ2 (i) and hRyR2+CSQ2+JUN (ii) – CSQ2 detection shown and* ***(B)*** *hRyR2+JUN (i) and hRyR2+CSQ2+JUN (ii) – JUN detection shown. CSQ2 and JUN only refers to mixed membrane samples generated from HEK293 cells transfected with CSQ2 and JUN only, respectively.*

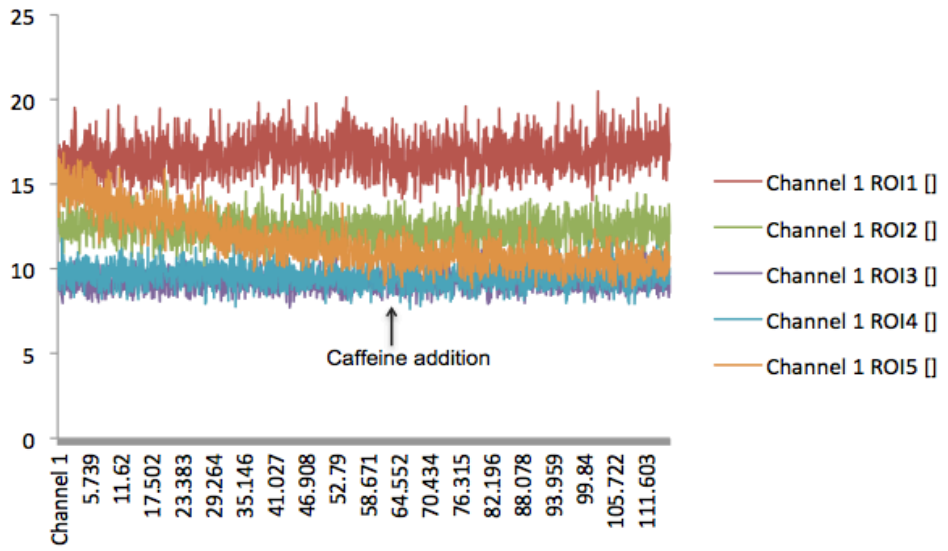

Figure 5: Untransfected HEK293 loaded with Fluo-3 did not display spontaneous Ca^{2+} release events or respond to caffeine addition: *As discussed in Chapter 4, section 4.2.2, cells successfully transfected with hRyR2 could be identified by their caffeine response and in Ca^{2+} imaging investigations these cells displayed SCR activity. In control experiments, untransfected HEK293 cells were loaded with Fluo-3 and imaged by confocal microscopy. As shown, untransfected HEK293 (5 cells selected here, also called regions of interest (ROI)) did not display SCR events or respond to 10mM caffeine application.*

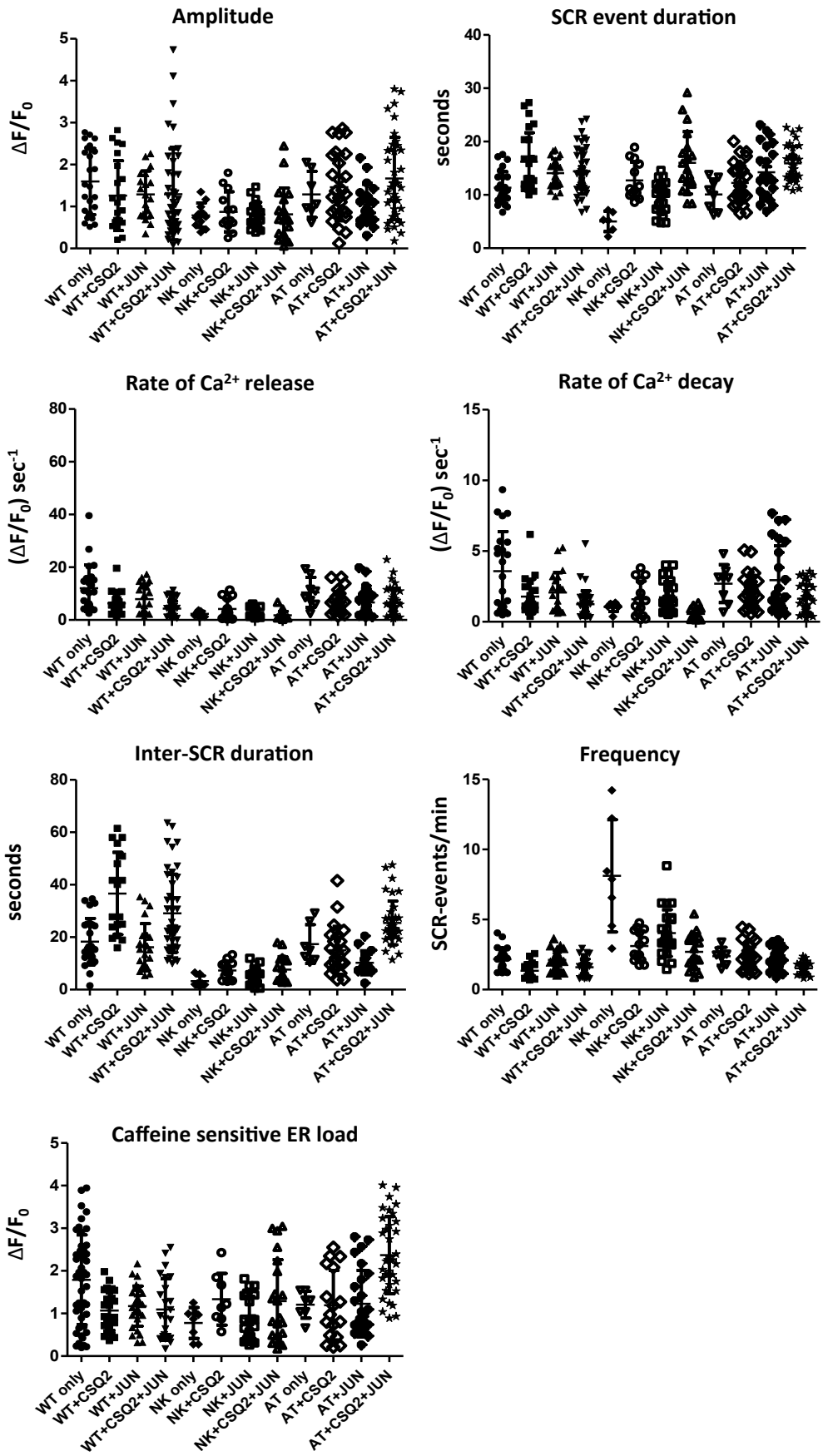

Figure 6: Column scatter plots of all Ca^{2+} imaging data: *Described in Chapter 4, sections 4.3.3-4.3.6, all properties of the SCR events evident in cells expressing WT or mutant hRyR2 in the presence/absence of luminal accessory proteins CSQ2 and JUN were assessed. Shown here are column scatter plots of all the collected data, constructed using GraphPad Prism. Outliers were detected and removed using the GraphPad Prism Grubbs' test (graphpad.com).*

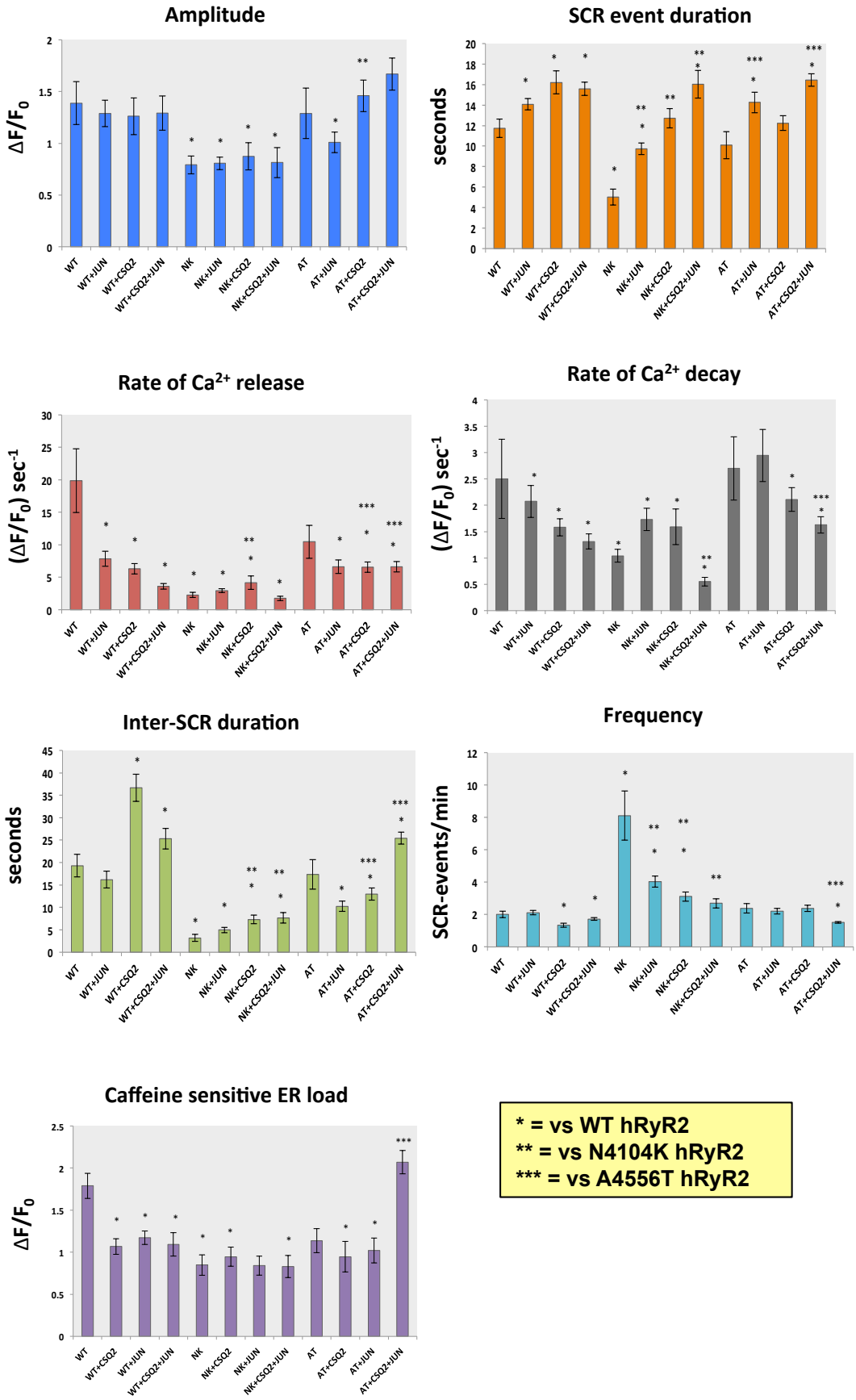

Figure 7: Bar graphs of all Ca^{2+} imaging data: *All experimental data generated from assessment of the SCR event parameters in cells expressing WT or mutant hRyR2 in the presence/absence of luminal accessory proteins CSQ2 and JUN (Chapter 4, sections 4.3.3-4.3.6) are summarised here. Calculated using one-way ANOVA and a Tukey-Kramer post-test (GraphPad Prism), parameters that were statistically different from WT/A4556T/N4104K only are indicated.*

References

Ahmed, H. and PhD, H.A. 2004. *Principles and Reactions of Protein Extraction, Purification, and Characterization*. CRC Press.

Altschafl, B.A., Arvanitis, D.A., Fuentes, O., Yuan, Q., Kranias, E.G. and Valdivia, H.H. 2011. Dual role of junctin in the regulation of ryanodine receptors and calcium release in cardiac ventricular myocytes. *Journal of Physiology* 589(Pt 24), pp. 6063–6080.

Arvanitis, D.A., Vafiadaki, E., Sanoudou, D. and Kranias, E.G. 2011. Histidine-rich calcium binding protein: the new regulator of sarcoplasmic reticulum calcium cycling. *Journal of Molecular and Cellular Cardiology* 50(1), pp. 43–49.

Balog, E.M., Fruen, B.R., Shomer, N.H. and Louis, C.F. 2001. Divergent Effects of the Malignant Hyperthermia-Susceptible Arg615→Cys Mutation on the $Ca^{2+}$and Mg^{2+}Dependence of the RyR1. *Biophysical journal* 81(4), pp. 2050–2058.

Balshaw, D.M., Xu, L., Yamaguchi, N., Pasek, D.A. and Meissner, G. 2001. Calmodulin binding and inhibition of cardiac muscle calcium release channel (ryanodine receptor). *The Journal of biological chemistry* 276(23), pp. 20144–20153.

Bassani, J.W., Bassani, R.A. and Bers, D.M. 1994. Relaxation in rabbit and rat cardiac cells: species-dependent differences in cellular mechanisms. *Journal of Physiology* pp. 279-293.

Beard, N.A., Casarotto, M.G., Wei, L. and Varsányi, M. 2005. Regulation of Ryanodine Receptors by Calsequestrin: Effect of High Luminal Ca^{2+} and Phosphorylation. *Biophysical journal* 88(5), pp. 3444-3454.

Beard, N.A., Laver, D.R. and Dulhunty, A.F. 2004. Calsequestrin and the calcium release channel of skeletal and cardiac muscle. *Progress in Biophysics and Molecular Biology* 85(1), pp. 33–69.

Beard, N.A., Sakowska, M.M., Dulhunty, A.F. and Laver, D.R. 2002. Calsequestrin is an inhibitor of skeletal muscle ryanodine receptor calcium release channels. *Biophysical Journal* 82(1 Pt 1), pp. 310–320.

Beard, N.A., Wei, L. and Dulhunty, A.F. 2009. Control of muscle ryanodine receptor calcium release channels by proteins in the sarcoplasmic reticulum lumen. *Clinical and Experimental Pharmacology and Physiology* 36(3), pp. 340–345.

Beavers, D.L., Wang, W., Ather, S., Voigt, N., Garbino, A., Dixit, S.S., Landstrom, A.P., et al. 2013. Mutation E169K in junctophilin-2 causes atrial fibrillation due to impaired RyR2 stabilization. *Journal of the American College of Cardiology* 62(21), pp. 2010–2019.

Berridge, M.J., Bootman, M.D. and Roderick, H.L. 2003. Calcium signalling: dynamics, homeostasis and remodelling. *Nature Reviews Molecular Cell Biology* 4, pp. 517-529.

Bers, D.M. 2001. *Excitation-Contraction Coupling and Cardiac Contractile Force*. Springer Science & Business Media.

Bers, D.M. 2008. Calcium cycling and signaling in cardiac myocytes. *Annu Rev Physiol* 70, pp. 23–49.

Bers, D.M. 2002. Cardiac excitation–contraction coupling. *Nature* 415(6868), pp. 198–205.

Bers, D.M. 2004. Macromolecular complexes regulating cardiac ryanodine receptor function. *Journal of molecular and cellular cardiology* 37(2), pp. 417–429.

Bers, D.M. and Guo, T. 2005. Calcium signaling in cardiac ventricular myocytes. *Annals of the New York Academy of Sciences* 1047, pp. 86-98.

Blayney, L.M., Jones, J.-L., Griffiths, J. and Lai, F.A. 2010. A mechanism of ryanodine receptor modulation by FKBP12/12.6, protein kinase A, and K201. *Cardiovascular Research* 85(1), pp. 68–78.

Bridge, J.H., Smolley, J.R. and Spitzer, K.W. 1990. The relationship between charge movements associated with ICa and INa-Ca in cardiac myocytes. *Science* 248(4953), pp. 376–378.

Capes, E.M., Loaiza, R. and Valdivia, H.H. 2011. Ryanodine receptors. *Skeletal Muscle* 1(1), p.18.

Carter, S., Colyer, J. and Sitsapesan, R. 2006. Maximum phosphorylation of the cardiac ryanodine receptor at serine-2809 by protein kinase a produces unique modifications to channel gating and conductance not observed at lower levels of phosphorylation. *Circulation research*. 98, pp. 1506-1513.

Carter, S., Pitt, S.J., Colyer, J. and Sitsapesan, R. 2011. Ca^{2}+-dependent phosphorylation of RyR2 can uncouple channel gating from direct cytosolic Ca^{2}+ regulation. *The Journal of membrane biology* 240(1), pp. 21–33.

Cerrone, M., Colombi, B., Santoro, M., di Barletta, M.R., Scelsi, M., Villani, L., Napolitano, C., et al. 2005. Bidirectional ventricular tachycardia and fibrillation elicited in a knock-in mouse model carrier of a mutation in the cardiac ryanodine receptor. *Circulation research* 96(10), pp. e77–82.

Chelu, M.G., Danila, C.I., Gilman, C.P. and Hamilton, S.L. 2004. Regulation of ryanodine receptors by FK506 binding proteins. *Trends in Cardiovascular Medicine* 14(6), pp. 227–234.

Chen, C. and Okayama, H. 1987. High-efficiency transformation of mammalian cells by plasmid DNA. *Molecular and cellular biology* 7(8), pp. 2745–2752.

Chen, H., Valle, G., Furlan, S., Nani, A., Gyorke, S., Fill, M. and Volpe, P. 2013. Mechanism of calsequestrin regulation of single cardiac ryanodine receptor in normal and pathological conditions. *The Journal of General Physiology* 142(2), pp. 127–136.

Chen, W., Wang, R., Chen, B., Zhong, X., Kong, H. and Bai, Y. 2014. The ryanodine receptor store-sensing gate controls Ca^{2+} waves and Ca^{2+}-triggered arrhythmias. *Nature medicine*, 20(2). pp. 184–192.

Cheng, H. and Lederer, W.J. 2008. Calcium sparks. *Physiological reviews*, 88(4). pp. 1491–1545.

Cheng, H., Lederer, W.J. and Cannell, M.B. 1993. Calcium sparks: elementary events underlying excitation-contraction coupling in heart muscle. *Science* 262(5134), pp. 740–744.

Ching, L.L., Williams, A.J. and Sitsapesan, R. 2000. Evidence for $Ca(^{2+})$ activation and inactivation sites on the luminal side of the cardiac ryanodine receptor complex. *Circulation research* 87(3), pp. 201–206.

Chopra, N., Yang, T., Asghari, P., Moore, E.D., Huke, S., Akin, B., Cattolica, R.A., et al. 2009. Ablation of Triadin Causes Loss of Cardiac Ca^{2+} Release Units, Impaired Excitation-Contraction Coupling, and Cardiac Arrhythmias. *Proceedings of the National Academy of Sciences of the United States of America* 106(18), pp. 7636–7641.

Copello, J.A., Barg, S., Onoue, H. and Fleischer, S. 1997. Heterogeneity of Ca^{2+} gating of skeletal muscle and cardiac ryanodine receptors. *Biophysical journal* 73(1), pp. 141–156.

Cozens, B. and Reithmeier, R.A. 1984. Size and shape of rabbit skeletal muscle calsequestrin. *The Journal of biological chemistry* 259(10), pp. 6248–6252.

d'Amati, G., Bagattin, A., Bauce, B., Rampazzo, A., Autore, C., Basso, C., King, K., et al. 2005. Juvenile sudden death in a family with polymorphic ventricular arrhythmias caused by a novel RyR2 gene mutation: evidence of specific morphological substrates. *Human Pathology* 36(7), pp. 761–767.

Deivanayagam, C. and Carson, M. 2000. Structure of FKBP12.6 in complex with rapamycin. *Section D: Biological Crystallography* D56, pp. 266-271.

del Pino, P., Pelaz, B., Zhang, Q. and Maffre, P. 2014. Protein corona formation around nanoparticles–from the past to the future. *Materials Horizons* (1), pp. 301–313.

di Barletta, M.R., Viatchenko-Karpinski, S., Nori, A., Memmi, M., Terentyev, D., Turcato, F., Valle, G., et al. 2006. Clinical phenotype and functional characterization of CASQ2 mutations associated with catecholaminergic polymorphic ventricular tachycardia. *Circulation* 114(10), pp. 1012–1019.

Di Pasquale, E., Lodola, F., Miragoli, M. and Denegri, M. 2013. CaMKII inhibition rectifies arrhythmic phenotype in a patient-specific model of catecholaminergic polymorphic ventricular tachycardia. *Cell death & Differentiation* Vol 4, p. e843.

Dirksen, W.P., Lacombe, V.A., Chi, M., Kalyanasundaram, A., Viatchenko-Karpinski, S., Terentyev, D., Zhou, Z., et al. 2007. A mutation in calsequestrin, CASQ2D307H, impairs Sarcoplasmic Reticulum Ca^{2+} handling and causes complex ventricular arrhythmias in mice. *Cardiovascular Research* 75(1), pp. 69–78.

Du, G.G., Imredy, J.P. and MacLennan, D.H. 1998. Characterization of recombinant rabbit cardiac and skeletal muscle Ca^{2+} release channels (ryanodine receptors) with a novel [3H]ryanodine binding assay. *Journal of Biological Chemistry* 273(50), pp. 33259–33266.

Du, G.G., Sandhu, B. and Khanna, V.K. 2002. Topology of the Ca^{2+} release channel of skeletal muscle sarcoplasmic reticulum (RyR1). *Proc Natl Acad Sci U.S.A* 99(26), pp. 16725-30.

Dulhunty, A., Wei, L. and Beard, N. 2009. Junctin - the quiet achiever. *The Journal of Physiology* 587(13), pp. 3135–3137.

Dulhunty, A.F., Wium, E., Li, L., Hanna, A.D., Mirza, S., Talukder, S., Ghazali, N.A., et al. 2012. Proteins within the intracellular calcium store determine cardiac RyR channel activity and cardiac output. *Clinical and Experimental Pharmacology and Physiology* 39(5), pp. 477–484.

Efremov, R.G., Leitner, A., Aebersold, R. and Raunser, S. 2015. Architecture and conformational switch mechanism of the ryanodine receptor. *Nature*. (517), pp. 39–

43.

Eldar, M., Pras, E. and Lahat, H. 2003. A missense mutation in the CASQ2 gene is associated with autosomal-recessive catecholamine-induced polymorphic ventricular tachycardia. *Trends in Cardiovascular Medicine* 13(4), pp. 148–151.

Euden, J., Mason, S.A., Viero, C., Thomas, N.L. and Williams, A.J. 2013. Investigations of the contribution of a putative glycine hinge to ryanodine receptor channel gating. *Journal of Biological Chemistry* 288(23), pp. 16671–16679.

Fabiato, A. and Fabiato, F. 1975. Contractions induced by a calcium-triggered release of calcium from the sarcoplasmic reticulum of single skinned cardiac cells. *Journal of Physiology* 249(3), pp. 469–495.

Fan, G.-C., Yuan, Q. and Kranias, E.G. 2008. Regulatory roles of junctin in sarcoplasmic reticulum calcium cycling and myocardial function. *Trends in cardiovascular medicine* 18(1), pp. 1–5.

Fan, G.-C., Yuan, Q., Zhao, W., Chu, G. and Kranias, E.G. 2007. Junctin is a prominent regulator of contractility in cardiomyocytes. *Biochemical and biophysical research communications* 352(3), pp. 617–622.

Farrell, E.F., Antaramian, A., Rueda, A., Gómez, A.M. and Valdivia, H.H. 2003. Sorcin inhibits calcium release and modulates excitation-contraction coupling in the heart. *The Journal of biological chemistry* 278(36), pp. 34660–34666.

Fearnley, C.J. and Roderick, H.L. 2011. Calcium signaling in cardiac myocytes. *Cold Spring Harbor Perspect Biol* 3, p. a004242.

Feng, Y., Valley, M.T., Lazar, J., Yang, A.L., Bronson, R.T., Firestein, S., Coetzee, W.A., et al. 2009. SRp38 regulates alternative splicing and is required for Ca(2+) handling in the embryonic heart. *Developmental cell* 16(4), pp. 528–538.

Fischer, T.H., Neef, S. and Maier, L.S. 2013. The Ca-calmodulin dependent kinase II: a promising target for future antiarrhythmic therapies? *Journal of Molecular and Cellular Cardiology* 58, pp. 182–187.

Fisher, J.D., Krikler, D. and Hallidie-Smith, K.A. 1999. Familial polymorphic ventricular arrhythmias: a quarter century of successful medical treatment based on serial exercise-pharmacologic testing. *Journal of the American College of Cardiology* 34(7), pp. 2015–2022.

Franzini-Armstrong, C. 2005. The Assembly of Calcium Release Units in Cardiac Muscle. *Annals of the New York Academy of Sciences* 1047(1), pp. 76–85.

Franzini-Armstrong, C., Kenney, L.J. and Varriano-Marston, E. 1987. The structure of calsequestrin in triads of vertebrate skeletal muscle: a deep-etch study. *The Journal of cell biology* 105(1), pp. 49–56.

Franzini-Armstrong, C., Protasi, F. and Ramesh, V. 1999. Shape, Size, and Distribution of Ca^{2+} Release Units and Couplons in Skeletal and Cardiac Muscles. *Biophysical journal* 77(3), pp. 1528–39.

Fruen, B.R., Bardy, J.M. and Byrem, T.M. 2000. Differential Ca^{2+} sensitivity of skeletal and cardiac muscle ryanodine receptors in the presence of calmodulin. *American Journal of physiology* 279(3), pp. c724–33.

Gaburjáková, M., Bal, N.C., Gaburjáková, J. and Periasamy, M. 2013. Functional interaction between calsequestrin and ryanodine receptor in the heart. *Cellular and molecular life sciences : CMLS* 70(16), pp. 2935–2945.

Galfré, E., Pitt, S.J., Venturi, E., Sitsapesan, M., Zaccai, N.R., Tsaneva-Atanasova, K., O'Neill, S., et al. 2012. FKBP12 activates the cardiac ryanodine receptor Ca^{2+}-release channel and is antagonised by FKBP12.6. *PloS one* 7(2), pp. e31956–e31956.

George, C.H., Higgs, G.V., Mackrill, J.J. and Lai, F.A. 2003a. Dysregulated ryanodine receptors mediate cellular toxicity: restoration of normal phenotype by FKBP12.6. *Journal of Biological Chemistry* 278(31), pp. 28856–28864.

George, C.H., Higgs, G.V. and Lai, F.A. 2003b. Ryanodine receptor mutations associated with stress-induced ventricular tachycardia mediate increased calcium release in stimulated cardiomyocytes. *Circulation Research* 93(6), pp. 531–540.

George, C.H., Jundi, H., Thomas, N.L., Scoote, M., Walters, N., Williams, A.J. and Lai, F.A. 2004. Ryanodine receptor regulation by intramolecular interaction between cytoplasmic and transmembrane domains. *Molecular Biology of the Cell* 15(6), pp. 2627–2638.

George, C.H., Jundi, H., Walters, N., Thomas, N.L., West, R.R. and Lai, F.A. 2006. Arrhythmogenic mutation-linked defects in ryanodine receptor autoregulation reveal a novel mechanism of Ca^{2+} release channel dysfunction. *Circulation research* 98(1), pp. 88–97.

George, C.H., Kendall, J.M., Campbell, A.K. and Evans, W.H. 1998. Connexin-aequorin chimerae report cytoplasmic calcium environments along trafficking pathways leading to gap junction biogenesis in living COS-7 cells. *Journal of Biological Chemistry* 273(45), pp. 29822–29829.

Gergs, U., Berndt, T., Buskase, J., Jones, L.R., Kirchhefer, U., Müller, F.U., Schlüter, K.-D., et al. 2007. On the role of junctin in cardiac Ca^{2+} handling, contractility, and heart failure. *American Journal of Physiology - Heart and Circulatory Physiology* 293(1), pp. H728–H734.

Giannini, G., Conti, A., Mammarella, S., Scrobogna, M. and Sorrentino, V. 1995. The ryanodine receptor/calcium channel genes are widely and differentially expressed in murine brain and peripheral tissues. *The Journal of Cell Biology* 128(5), pp. 893–904.

Goonasekera, S.A., Beard, N.A., Groom, L., Kimura, T., Lyfenko, A.D., Rosenfeld, A., Marty, I., et al. 2007. Triadin binding to the C-terminal luminal loop of the ryanodine receptor is important for skeletal muscle excitation contraction coupling. *The Journal of General Physiology* 130(4), pp. 365–378.

Gorman, C.M., Howard, B.H. and Reeves, R. 1983. Expression of recombinant plasmids in mammalian cells is enhanced by sodium butyrate. *Nucleic acids research* 11(21), pp. 7631–7648.

Graham, F.L., Smiley, J., Russell, W.C. and Nairn, R. 1977. Characteristics of a human cell line transformed by DNA from human adenovirus type 5. *The Journal of general virology* 36(1), pp. 59–74.

Gregory, K.N., Ginsburg, K.S., Bodi, I., Hahn, H., Marreez, Y.M.A., Song, Q., Padmanabhan, P.A., et al. 2006. Histidine-rich Ca binding protein: a regulator of sarcoplasmic reticulum calcium sequestration and cardiac function. *Journal of*

Molecular and Cellular Cardiology 40(5), pp. 653–665.

Guo, A., Cala, S.E. and Song, L.-S. 2012. Calsequestrin accumulation in rough endoplasmic reticulum promotes perinuclear Ca^{2+} release. *Journal of Biological Chemistry* 287(20), pp. 16670–16680.

Guo, T., Cornea, R.L., Huke, S., Camors, E., Yang, Y., Picht, E., Fruen, B.R., et al. 2010. Kinetics of FKBP12.6 binding to ryanodine receptors in permeabilized cardiac myocytes and effects on Ca sparks. *Circulation research* 106(11), pp. 1743–1752.

Guo, W. and Campbell, K.P. 1995. Association of triadin with the ryanodine receptor and calsequestrin in the lumen of the sarcoplasmic reticulum. *The Journal of biological chemistry* 270(16), pp. 9027–9030.

Guo, W., Jorgensen, A.O., Jones, L.R. and Campbell, K.P. 1996. Biochemical characterization and molecular cloning of cardiac triadin. *The Journal of biological chemistry* 271(1), pp. 458–465.

Györke, S. and Carnes, C. 2008. Dysregulated sarcoplasmic reticulum calcium release: Potential pharmacological target in cardiac disease. *Pharmacology & Therapeutics* 119(3), pp. 340–354.

Györke, I. and Györke, S. 1998. Regulation of the cardiac ryanodine receptor channel by luminal Ca^{2+} involves luminal Ca^{2+} sensing sites. *Biophysical journal* 75(6), pp. 2801–2810.

Györke, I., Hester, N., Jones, L.R. and Györke, S. 2004. The role of calsequestrin, triadin, and junctin in conferring cardiac ryanodine receptor responsiveness to luminal calcium. *Biophysical Journal* 86(4), pp. 2121–2128.

Györke, S. 2009. Molecular basis of catecholaminergic polymorphic ventricular tachycardia. *Heart Rhythm* 6(1), pp. 123–129.

Györke, S. and Terentyev, D. 2007. Modulation of ryanodine receptor by luminal calcium and accessory proteins in health and cardiac disease. *Cardiovascular Research* 77(2), pp. 245–255.

Hain, J., Nath, S., Mayrleitner, M., Fleischer, S. and Schindler, H. 1994. Phosphorylation modulates the function of the calcium release channel of sarcoplasmic reticulum from skeletal muscle. *Biophysical Journal* 67(5), pp. 1823–1833.

Hamilton, S.L. and Serysheva, I.I. 2009. Ryanodine receptor structure: progress and challenges. *The Journal of biological chemistry* 284(7), pp. 4047–4051.

Hamilton, S.L., Serysheva, I. and Strasburg, G.M. 2000. Calmodulin and Excitation-Contraction Coupling. *Physiology* 15(6), pp. 281–284.

He, Z., Dunker, A.K., Wesson, C.R. and Trumble, W.R. 1993. $Ca(^{2+})$-induced folding and aggregation of skeletal muscle sarcoplasmic reticulum calsequestrin. The involvement of the trifluoperazine-binding site. *The Journal of biological chemistry* 268(33), pp. 24635–24641.

Herzog, A., Szegedi, C., Jona, I., Herberg, F.W. and Varsanyi, M. 2000. Surface plasmon resonance studies prove the interaction of skeletal muscle sarcoplasmic reticular $Ca(^{2+})$ release channel/ryanodine receptor with calsequestrin. *FEBS letters* 472(1), pp. 73–77.

Holmberg, S.R. and Williams, A.J. 1990. The cardiac sarcoplasmic reticulum calcium-release channel: modulation of ryanodine binding and single-channel activity. *Biochimica et biophysica acta* 1022(2), pp. 187–193.

Hong, C.-S., Cho, M.-C., Kwak, Y.-G., Song, C.H., Lee, Y.-H., Lim, J.S., Kwon, Y.K., et al. 2002. Cardiac remodeling and atrial fibrillation in transgenic mice overexpressing junctin. *FASEB journal : official publication of the Federation of American Societies for Experimental Biology* 16(10), pp. 1310–1312.

Hong, C.S., Kwak, Y.G., Ji, J.H., Chae, S.W. and Kim, D.H. 2001. Molecular cloning and characterization of mouse cardiac junctate isoforms. *Biochemical and biophysical research communications* 289(4), pp. 882–887.

Hong, C.-S., Kwon, S.-J. and Do Han Kim 2007. Multiple functions of junctin and junctate, two distinct isoforms of aspartyl beta-hydroxylase. *Biochemical and Biophysical Research Communications* 362(1), pp. 1–4.

Hong, C.-S., Kwon, S.-J., Cho, M.-C., Kwak, Y.-G., Ha, K.-C., Hong, B., Li, H., et al. 2008. Overexpression of junctate induces cardiac hypertrophy and arrhythmia via altered calcium handling. *Journal of Molecular and Cellular Cardiology* 44(4), pp. 672–682.

Hopkins, R.F., Wall, V.E. and Esposito, D. 2012. Optimizing transient recombinant protein expression in mammalian cells. *Methods in molecular biology (Clifton, N.J.)* 801, pp. 251–268.

Houle, T.D., Ram, M.L. and Cala, S.E. 2004. Calsequestrin mutant D307H exhibits depressed binding to its protein targets and a depressed response to calcium. *Cardiovascular Research* 64(2), pp. 227–233.

Houle, T.D., Ram, M.L., McMurray, W.J. and Cala, S.E. 2006. Different endoplasmic reticulum trafficking and processing pathways for calsequestrin (CSQ) and epitope-tagged CSQ. *Experimental Cell Research* 312(20), pp. 4150-4161.

Huke, S. and Bers, D.M. 2008. Ryanodine receptor phosphorylation at Serine 2030, 2808 and 2814 in rat cardiomyocytes. *Biochemical and biophysical research communications* 376(1), pp. 80–85.

Hulme, J.T., Scheuer, T. and Catterall, W.A. 2004. Regulation of cardiac ion channels by signaling complexes: role of modified leucine zipper motifs. *Journal of molecular and cellular cardiology* 37(3), pp. 625–631.

Hutsell, S.Q., Kimple, R.J. and Siderovski, D.P. 2010. High-affinity immobilization of proteins using biotin-and GST-based coupling strategies. *Surface Plasmon Resonance, Methods Mol Biol.* 627, pp. 75-90.

Hwang, H.S., Nitu, F.R., Yang, Y., Walweel, K., Pereira, L., Johnson, C.N., Faggioni, M., et al. 2014. Divergent regulation of ryanodine receptor 2 calcium release channels by arrhythmogenic human calmodulin missense mutants. *Circulation research* 114(7), pp. 1114–1124.

Ikemoto, N. and Yamamoto, T. 2002. Regulation of calcium release by interdomain interaction within ryanodine receptors. *Frontiers in Bioscience* 7, pp. d671–83.

Jabbari, J., Jabbari, R., Nielsen, M.W., Holst, A.G., Nielsen, J.B., Haunsø, S., Tfelt-Hansen, J., et al. 2013. New exome data question the pathogenicity of genetic variants previously associated with catecholaminergic polymorphic ventricular

tachycardia. *Circulation. Cardiovascular genetics* 6(5), pp. 481–489.

Huang, X., Fruen, B., Farrington, D.T., Wagenknecht, T. and Liu, Z. 2012. Calmodulin-binding locations on the skeletal and cardiac ryanodine receptors. *Journal of Biological Chemistry* 287(36), pp. 30328–30335.

Huang, X., Liu, Y., Wang, R., Zhong, X., Liu, Y., Koop, A., Chen, S.R.W., et al. 2013. Two potential calmodulin-binding sequences in the ryanodine receptor contribute to a mobile, intra-subunit calmodulin-binding domain. *Journal of cell science* 126(Pt 19), pp. 4527–4535.

Hunt, D.J., Jones, P.P., Wang, R., Chen, W., Bolstad, J., Chen, K., Shimoni, Y., et al. 2007. K201 (JTV519) suppresses spontaneous Ca2+ release and [3H]ryanodine binding to RyR2 irrespective of FKBP12.6 association. *Biochemical Journal* 404(3), pp. 431–438.

Jiang, D., Chen, W., Wang, R., Zhang, L. and Chen, S.R.W. 2007. Loss of luminal Ca^{2+} activation in the cardiac ryanodine receptor is associated with ventricular fibrillation and sudden death. *Proceedings of the National Academy of Sciences of the United States of America* 104(46), pp. 18309–18314.

Jiang, D., Wang, R., Xiao, B., Kong, H., Hunt, D.J., Choi, P., Zhang, L., et al. 2005. Enhanced store overload-induced Ca^{2+} release and channel sensitivity to luminal Ca^{2+} activation are common defects of RyR2 mutations linked to ventricular tachycardia and sudden death. *Circulation research* 97(11), pp. 1173–1181.

Jiang, D., Xiao, B., Yang, D., Wang, R., Choi, P., Zhang, L., Cheng, H., et al. 2004. RyR2 mutations linked to ventricular tachycardia and sudden death reduce the threshold for store-overload-induced Ca^{2+} release (SOICR). *PNAS* 101(35), pp. 13062–13067.

Jiang, D., Xiao, B., Zhang, L. and Chen, S.R.W. 2002. Enhanced basal activity of a cardiac Ca^{2+} release channel (ryanodine receptor) mutant associated with ventricular tachycardia and sudden death. *Circulation research* 91(3), pp. 218–225.

Jones, L.R.L., Suzuki, Y.J.Y., Wang, W.W., Kobayashi, Y.M.Y., Ramesh, V.V., Franzini-Armstrong, C.C., Cleemann, L.L., et al. 1998. Regulation of Ca^{2+} signaling in transgenic mouse cardiac myocytes overexpressing calsequestrin. *Journal of Clinical Investigation* 101(7), pp. 1385–1393.

Jones, L.R., Zhang, L., Sanborn, K., Jorgensen, A.O. and Kelley, J. 1995. Purification, primary structure, and immunological characterization of the 26-kDa calsequestrin binding protein (junctin) from cardiac junctional sarcoplasmic reticulum. *The Journal of biological chemistry* 270(51), pp. 30787–30796.

Jordan, M. and Wurm, F. 2004. Transfection of adherent and suspended cells by calcium phosphate. *Methods (San Diego, Calif.)* 33(2), pp. 136–143.

Kang, C.B., Hong, Y., Dhe-Paganon, S. and Yoon, H.S. 2008. FKBP family proteins: immunophilins with versatile biological functions. *NeuroSignals* 16(4), pp. 318–325.

Katz, G., Arad, M. and Eldar, M. 2009. Catecholaminergic polymorphic ventricular tachycardia from bedside to bench and beyond. *Current problems in cardiology* 34(1), pp. 9–43.

Kawamura, M., Ohno, S., Naiki, N., Nagaoka, I., Dochi, K., Wang, Q., Hasegawa, K., et al. 2013. Genetic background of catecholaminergic polymorphic ventricular

tachycardia in Japan. *Circulation journal : official journal of the Japanese Circulation Society* 77(7), pp. 1705–1713.

Kawasaki, T. and Kasai, M. 1994. Regulation of calcium channel in sarcoplasmic reticulum by calsequestrin. *Biochemical and Biophysical Research Communications* 199(3), pp. 1120–1127.

Kermode, H., Williams, A.J. and Sitsapesan, R. 1998. The Interactions of ATP, ADP, and Inorganic Phosphate with the Sheep Cardiac Ryanodine Receptor. *Biophysical journal* 74(3), pp. 1296–1304.

Kiarash, A. 2004. Defective glycosylation of calsequestrin in heart failure. *Cardiovascular Research* 63(2), pp. 264–272.

Kim, E., Youn, B., Kemper, L., Campbell, C., Milting, H., Varsányi, M. and Kang, C. 2007. Characterization of Human Cardiac Calsequestrin and its Deleterious Mutants. *Journal of Molecular Biology* 373(4), pp. 1047–1057.

Kirchhefer, U. 2004. Age-dependent biochemical and contractile properties in atrium of transgenic mice overexpressing junctin. *AJP: Heart and Circulatory Physiology* 287(5), pp. H2216–H2225.

Kirchhefer, U., Hanske, G., Jones, L.R., Justus, I., Kaestner, L., Lipp, P., Schmitz, W., et al. 2006. Overexpression of junctin causes adaptive changes in cardiac myocyte $Ca(^{2+})$ signaling. *Cell calcium* 39(2), pp. 131–142.

Kirchhof, P., Klimas, J., Fabritz, L., Zwiener, M., Jones, L.R., Schäfers, M., Hermann, S., et al. 2007. Stress and high heart rate provoke ventricular tachycardia in mice expressing triadin. *Journal of molecular and cellular cardiology* 42(5), pp. 962–971.

Knollmann, B.C. 2009. New roles of calsequestrin and triadin in cardiac muscle. *The Journal of Physiology* 587(Pt 13), pp. 3081–3087.

Knollmann, B.C. 2010. A 'rough' journey to the sarcoplasmic reticulum—implications of altered calsequestrin trafficking for cardiac arrhythmia. *Journal of molecular and cellular cardiology* 49(4), pp. 554–555.

Knollmann, B.C., Chopra, N. and Hlaing, T. 2006. Casq2 deletion causes sarcoplasmic reticulum volume increase, premature Ca^{2+} release, and catecholaminergic polymorphic ventricular tachycardia. *J Clin Invest* pp. 2510-2520

Kobayashi, Y.M. and Jones, L.R. 1999. Identification of triadin 1 as the predominant triadin isoform expressed in mammalian myocardium. *The Journal of biological chemistry* 274(40), pp. 28660–28668.

Kobayashi, Y.M., Alseikhan, B.A. and Jones, L.R. 2000. Localization and characterization of the calsequestrin-binding domain of triadin 1. Evidence for a charged beta-strand in mediating the protein-protein interaction. *The Journal of biological chemistry* 275(23), pp. 17639–17646.

Kong, H., Jones, P.P., Koop, A., Zhang, L., Duff, H.J. and Chen, S.R.W. 2008. Caffeine induces Ca^{2+} release by reducing the threshold for luminal Ca^{2+} activation of the ryanodine receptor. *Biochemical Journal* 414(3), p. 441-52.

Kujala, K., Paavola, J., Lahti, A., Larsson, K., Pekkanen-Mattila, M., Viitasalo, M., Lahtinen, A.M., et al. 2012. Cell model of catecholaminergic polymorphic ventricular tachycardia reveals early and delayed afterdepolarizations. *PloS one* 7(9), p. e44660.

Kuwajima, G., Futatsugi, A., Niinobe, M. and Nakanishi, S. 1992. Two types of ryanodine receptors in mouse brain: skeletal muscle type exclusively in Purkinje cells and cardiac muscle type in various neurons. *Neuron* 9(6), pp. 1133-42.

Lahat, H., Pras, E., Olender, T., Avidan, N., Ben-Asher, E., Man, O., Levy-Nissenbaum, E., et al. 2001. A missense mutation in a highly conserved region of CASQ2 is associated with autosomal recessive catecholamine-induced polymorphic ventricular tachycardia in Bedouin families from Israel. *American journal of human genetics* 69(6), pp. 1378–1384.

Lai, F.A. and Meissner, G. 1989. The muscle ryanodine receptor and its intrinsic Ca^{2+} channel activity. *Journal of bioenergetics and biomembranes*, pp. 227-246.

Lai, F.A., Erickson, H.P., Rousseau, E., Liu, Q.Y. and Meissner, G. 1988. Purification and reconstitution of the calcium release channel from skeletal muscle. *Nature* 331(6154), pp. 315–319.

Laitinen, P.J., Swan, H. and Kontula, K. 2003. Molecular genetics of exercise-induced polymorphic ventricular tachycardia: identification of three novel cardiac ryanodine receptor mutations and two common calsequestrin 2 amino-acid polymorphisms. *European Journal of Human Genetics* 11(11), pp. 888–891.

Lakatta, E.G. 2004. Beyond Bowditch: the convergence of cardiac chronotropy and inotropy. *Cell calcium* 35(6), pp. 14–14.

Lanner, J.T., Georgiou, D.K., Joshi, A.D. and Hamilton, S.L. 2010. Ryanodine Receptors: Structure, Expression, Molecular Details, and Function in Calcium Release. *Cold Spring Harbor Perspectives in Biology* 2(11), pp. a003996–a003996.

Laver, D.R. 2007. Ca^{2+} stores regulate ryanodine receptor Ca^{2+} release channels via luminal and cytosolic Ca^{2+} sites. *Clinical and experimental pharmacology & physiology* 34(9), pp. 889–896.

Laver, D.R. 2010. Regulation of RyR channel gating by Ca^{2+}, Mg^{2+} and ATP. *Structure and Function of Calcium Release Channels, San Diego: Elsevier Academic Press Inc* pp. 69-89.

Laver, D.R. and Honen, B.N. 2008. Luminal Mg^{2+}, a key factor controlling RYR2-mediated Ca^{2+} release: cytoplasmic and luminal regulation modeled in a tetrameric channel. *Journal of General Physiology* 132(4), pp. 429–446.

Lee, H.G., Kang, H., Kim, D.H. and Park, W.J. 2001. Interaction of HRC (histidine-rich $Ca(^{2+})$-binding protein) and triadin in the lumen of sarcoplasmic reticulum. *The Journal of biological chemistry* 276(43), pp. 39533–39538.

Lee, K.W., Maeng, J.-S., Choi, J.Y., Lee, Y.R., Hwang, C.Y., Park, S.S., Park, H.K., et al. 2012. Role of Junctin protein interactions in cellular dynamics of calsequestrin polymer upon calcium perturbation. *Journal of Biological Chemistry* 287(3), pp. 1679–1687.

Leenhardt, A., Lucet, V., Denjoy, I., Grau, F., Ngoc, D.D. and Coumel, P. 1995. Catecholaminergic polymorphic ventricular tachycardia in children. A 7-year follow-up of 21 patients. *Circulation* 91(5), pp. 1512–1519.

Li, J., Imtiaz, M.S., Beard, N.A., Dulhunty, A.F., Thorne, R., vanHelden, D.F. and Laver, D.R. 2013. ß-Adrenergic stimulation increases RyR2 activity via intracellular Ca^{2+} and Mg^{2+} regulation. *PLoS ONE* 8(3), pp. e58334–e58334.

Li, L., Desantiago, J. and Chu, G. 2000. Phosphorylation of phospholamban and troponin I in β-adrenergic-induced acceleration of cardiac relaxation. *American Journal of Physiology, Heart and Circulation Physiology* 278(3), pp. H769-79.

Li, P. and Chen, S.R. 2001. Molecular basis of Ca(2)+ activation of the mouse cardiac Ca(2)+ release channel (ryanodine receptor). *The Journal of General Physiology* 118(1), pp. 33–44.

Lim, K.Y., Hong, C.-S. and Do Han Kim 2000. cDNA cloning and characterization of human cardiac junctin. *Gene* 255(1), pp. 35–42.

Liu, N., Denegri, M., Ruan, Y., Avelino-Cruz, J.E., Perissi, A., Negri, S., Napolitano, C., et al. 2011. Short communication: flecainide exerts an antiarrhythmic effect in a mouse model of catecholaminergic polymorphic ventricular tachycardia by increasing the threshold for triggered activity. *Circulation Research* 109(3), pp. 291–295.

Liu, Y., Kimlicka, L., Hiess, F., Tian, X., Wang, R., Zhang, L., Jones, P.P., Van Petegem, F. and Chen, S.R.W. 2013. The CPVT-associated RyR2 mutation G230C enhances store overload-induced Ca^{2+} release and destabilizes the N-terminal domains. *The Biochemical journal* 454(1), pp. 123–131.

Liu, N., Ruan, Y., Denegri, M., Bachetti, T., Li, Y., Colombi, B., Napolitano, C., et al. 2011. Calmodulin kinase II inhibition prevents arrhythmias in RyR2(R4496C+/-) mice with catecholaminergic polymorphic ventricular tachycardia. *Journal of molecular and cellular cardiology* 50(1), pp. 214–222.

Liu, Z., Zhang, J., Sharma, M.R. and Li, P. 2001. Three-dimensional reconstruction of the recombinant type 3 ryanodine receptor and localization of its amino terminus *PNAS USA* 98(11), pp. 6104-9.

Loaiza, R., Benkusky, N.A., Powers, P.P., Hacker, T., Noujaim, S., Ackerman, M.J., Jalife, J., et al. 2013. Heterogeneity of ryanodine receptor dysfunction in a mouse model of catecholaminergic polymorphic ventricular tachycardia. *Circulation research* 112(2), pp. 298–308.

Lokuta, A.J., Meyers, M.B., Sander, P.R., Fishman, G.I. and Valdivia, H.H. 1997. Modulation of cardiac ryanodine receptors by sorcin. *The Journal of biological chemistry* 272(40), pp. 25333–25338.

MacDougall, L.K., Jones, L.R. and Cohen, P. 1991. Identification of the major protein phosphatases in mammalian cardiac muscle which dephosphorylate phospholamban. *European Journal of Biochemistry* 196(3), pp. 725–734.

Mackrill, J.J. 1999. Protein-protein interactions in intracellular Ca^{2+}-release channel function. *The Biochemical journal* 337 (Pt 3), pp. 345–361.

Mackrill, J.J. 2010. Ryanodine receptor calcium channels and their partners as drug targets. *Biochemical pharmacology* 79(11), pp. 1535–1543.

MacLennan, D.H. and Chen, S. 2009. Store overload-induced Ca^{2+} release as a triggering mechanism for CPVT and MH episodes caused by mutations in RYR and CASQ genes. *The Journal of Physiology* 587(Pt 13), pp. 3113-3115.

MacLennan, D.H. and Wong, P.T. 1971. Isolation of a calcium-sequestering protein from sarcoplasmic reticulum. *Proceedings of the National Academy of Sciences of the United States of America* 68(6), pp. 1231–1235.

Marks, A.R. 1996. Cellular functions of immunophilins. *Physiological reviews* 76(3), pp. 631–49.

Marty, I., Fauré, J., Fourest-Lieuvin, A., Vassilopoulos, S., Oddoux, S. and Brocard, J. 2009. Triadin: what possible function 20 years later? *The Journal of Physiology* 587(Pt 13), pp. 3117–3121.

Marx, S.O. and Marks, A.R. 2013. Dysfunctional ryanodine receptors in the heart: new insights into complex cardiovascular diseases. *Journal of molecular and cellular cardiology* 58, pp. 225–231.

Marx, S.O., Gaburjakova, J. and Gaburjakova, M. 2001. Coupled gating between cardiac calcium release channels (ryanodine receptors). *Circulation* 88(11), pp. 1151-8.

Marx, S.O., Ondrias, K. and Marks, A.R. 1998. Coupled gating between individual skeletal muscle Ca^{2+} release channels (ryanodine receptors). *Science* 281(5378), pp. 818–821.

Marx, S.O., Reiken, S., Hisamatsu, Y., Jayaraman, T., Burkhoff, D., Rosemblit, N. and Marks, A.R. 2000. PKA phosphorylation dissociates FKBP12.6 from the calcium release channel (ryanodine receptor): defective regulation in failing hearts. *Cell* 101(4), pp. 365–376.

Mason, S.A., Viero, C., Euden, J., Bannister, M., West, D., Chen, S.R.W. and Williams, A.J. 2012. The contribution of hydrophobic residues in the pore-forming region of the ryanodine receptor channel to block by large tetraalkylammonium cations and Shaker B inactivation peptides. *Journal of General Physiology* 140(3), pp. 325–339.

Massignan, T., Stewart, R.S., Biasini, E. and Solomon, I.H. 2010. A novel, drug-based, cellular assay for the activity of neurotoxic mutants of the prion protein. *Journal of Biological Chemistry* 285(10), pp. 7752–65.

McCauley, M.D. and Wehrens, X.H.T. 2011. Targeting ryanodine receptors for anti-arrhythmic therapy. *Acta pharmacologica Sinica* 32(6), pp. 749–757.

McFarland, T.P., Milstein, M.L. and Cala, S.E. 2010. Rough endoplasmic reticulum to junctional sarcoplasmic reticulum trafficking of calsequestrin in adult cardiomyocytes. *Journal of Molecular and Cellular Cardiology* 49(4), pp. 556–564.

Medeiros-Domingo, A. and Bhuiyan, Z.A. 2009. The RyR2-encoded ryanodine receptor/calcium release channel in Patients Diagnosed Previously With Either Catecholaminergic Polymorphic Ventricular Tachycardia or Genotype Negative, Exercise-Induced Long QT syndrome: a comprehensive open reading frame mutational analysis. *J Am Coll Cardiol*, 54(22), pp. 2065-74.

Meissner, G. 1988. Ionic permeability of isolated muscle sarcoplasmic reticulum and liver endoplasmic reticulum vesicles. *Methods in enzymology* 157, pp. 417–437.

Meissner, G. 2004. Molecular regulation of cardiac ryanodine receptor ion channel. *Cell Calcium* 35(6), pp. 621–628.

Meli, A.C., Refaat, M.M., Dura, M., Reiken, S., Wronska, A., Wojciak, J., Carroll, J., et al. 2011. A novel ryanodine receptor mutation linked to sudden death increases sensitivity to cytosolic calcium. *Circulation research* 109(3), pp. 281–290.

Meyers, M.B.M., Puri, T.S.T., Chien, A.J.A., Gao, T.T., Hsu, P.H.P., Hosey, M.M.M. and Fishman, G.I.G. 1998. Sorcin associates with the pore-forming subunit of voltage-dependent L-type Ca^{2+} channels. *The Journal of biological chemistry* 273(30), pp. 18930–18935.

Miller, S.L.W., Currie, S., Loughrey, C.M., Kettlewell, S., Seidler, T., Reynolds, D.F., Hasenfuss, G., et al. 2005. Effects of calsequestrin over-expression on excitation-contraction coupling in isolated rabbit cardiomyocytes. *Cardiovascular Research* 67(4), pp. 667–677.

Milstein, M.L., Houle, T.D. and Cala, S.E. 2009. Calsequestrin isoforms localize to different ER subcompartments: evidence for polymer and heteropolymer-dependent localization. *Experimental Cell Research* 315(3), pp. 523–534.

Mitchell, R.D., Simmerman, H.K. and Jones, L.R. 1988. Ca^{2+} binding effects on protein conformation and protein interactions of canine cardiac calsequestrin. *The Journal of biological chemistry* 263(3), pp. 1376–1381.

Mollica, J.P., Oakhill, J.S., Lamb, G.D. and Murphy, R.M. 2009. Are genuine changes in protein expression being overlooked? Reassessing Western blotting. *Analytical Biochemistry* 386(2), pp. 270–275.

Mukherjee, S., Thomas, N.L. and Williams, A.J. 2012. A mechanistic description of gating of the human cardiac ryanodine receptor in a regulated minimal environment. *Journal of General Physiology* 140(2), pp. 139–158.

Mukherjee, S., Thomas, N.L. and Williams, A.J. 2014. Insights into the Gating Mechanism of the Ryanodine-Modified Human Cardiac Ca^{2+}-Release Channel (Ryanodine Receptor 2). *Molecular pharmacology* 86(3), pp. 318–329.

Murphy, R.M., Mollica, J.P. and Beard, N.A. 2011. Quantification of calsequestrin 2 (CSQ2) in sheep cardiac muscle and Ca^{2+}-binding protein changes in CSQ2 knockout mice. *American Journal of Physiology Heart Circ Physiol,* 300(2), pp. H595-H604.

Murray, B.E. and Ohlendieck, K. 1998. Complex formation between calsequestrin and the ryanodine receptor in fast- and slow-twitch rabbit skeletal muscle. *FEBS letters* 429(3), pp. 317–322.

Nakai, J., Imagawa, T., Hakamata, Y. and Shigekawa, M. 1990. Primary structure and functional expression from cDN A of the cardiac ryanodine receptor/calcium release channel. *FEBS letters* 271(1-2), pp. 169–177.

Nishi, M., Mizushima, A., Nakagawara, K.I. and Takeshima, H. 2000. Characterization of human junctophilin subtype genes. *Biochemical and Biophysical Research Communications* 273(3), pp. 920–927.

Novak, A., Lorber, A., Itskovitz-Eldor, J. and Binah, O. 2012. Modeling Catecholaminergic Polymorphic Ventricular Tachycardia using Induced Pluripotent Stem Cell-derived Cardiomyocytes. *Rambam Maimonides medical journal* 3(3), p. e0015.

Novák, P. and Soukup, T. 2011. Calsequestrin distribution, structure and function, its role in normal and pathological situations and the effect of thyroid hormones. *Physiological research / Academia Scientiarum Bohemoslovaca* 60(3), pp. 439–452.

Nyegaard, M., Overgaard, M.T., Søndergaard, M.T., Vranas, M., Behr, E.R., Hildebrandt, L.L., Lund, J., et al. 2012. Mutations in calmodulin cause ventricular

tachycardia and sudden cardiac death. *American journal of human genetics* 91(4), pp. 703–712.

O'Brian, J.J., Ram, M.L., Kiarash, A. and Cala, S.E. 2002. Mass spectrometry of cardiac calsequestrin characterizes microheterogeneity unique to heart and indicative of complex intracellular transit. *Journal of Biological Chemistry* 277(40), pp. 37154–37160.

Oda, T., Yano, M., Yamamoto, T., Tokuhisa, T., Okuda, S., Doi, M., Ohkusa, T., et al. 2005. Defective regulation of interdomain interactions within the ryanodine receptor plays a key role in the pathogenesis of heart failure. *Circulation* 111(25), pp. 3400–3410.

Ondrias, K., Marx, S.O. and Gaburjakova, M. 1998. FKBP12 Modulates Gating of the Ryanodine Receptor/Calcium Release Channel. *Annals of the New York Academy of Sciences* 853, pp. 149–56.

Otsu, K., Fujii, J., Periasamy, M., Difilippantonio, M., Uppender, M., Ward, D.C. and MacLennan, D.H. 1993. Chromosome Mapping of Five Human Cardiac and Skeletal Muscle Sarcoplasmic Reticulum Protein Genes. *Genomics* 17(2), pp. 507–509.

Papadakis, M., Raju, H., Behr, E.R., De Noronha, S.V., Spath, N., Kouloubinis, A., Sheppard, M.N., et al. 2013. Sudden cardiac death with autopsy findings of uncertain significance: potential for erroneous interpretation. *Circulation. Arrhythmia and electrophysiology* 6(3), pp. 588–596.

Patton, C., Thompson, S. and Epel, D. 2004. Some precautions in using chelators to buffer metals in biological solutions. *Cell calcium* 35(5), pp. 427–431.

Park, H.J., Wu, S., Dunker, A.K. and Kang, C.H. 2003. Polymerization of Calsequestrin Implications for Ca^{2+} Regulation. *Journal of Biological Chemistry* Vol 278, pp. 16176-16182.

Pessah, I.N., Stambuk, R.A. and Casida, J.E. 1987. Ca^{2+}-activated ryanodine binding: mechanisms of sensitivity and intensity modulation by Mg^{2+}, caffeine, and adenine nucleotides. *Molecular pharmacology*, 31(3), pp. 232–238.

Ponting, C., Schultz, J. and Bork, P. 1997. SPRY domains in ryanodine receptors (Ca(2+)-release channels). *Trends in Biochemical Sciences* 22(6), pp. 193–194.

Postma, A.V., Denjoy, I., Kamblock, J., Alders, M., Lupoglazoff, J.-M., Vaksmann, G., Dubosq-Bidot, L., et al. 2005. Catecholaminergic polymorphic ventricular tachycardia: RYR2 mutations, bradycardia, and follow up of the patients. *Journal of medical genetics* 42(11), pp. 863–870.

Priori, S.G. and Chen, S.R.W. 2011. Inherited dysfunction of sarcoplasmic reticulum Ca^{2+} handling and arrhythmogenesis. *Circulation research* 108(7), pp. 871–883.

Priori, S.G., Napolitano, C., Memmi, M., Colombi, B., Drago, F., Gasparini, M., DeSimone, L., et al. 2002. Clinical and molecular characterization of patients with catecholaminergic polymorphic ventricular tachycardia. *Circulation* 106(1), pp. 69–74.

Priori, S.G., Napolitano, C., Tiso, N., Memmi, M., Vignati, G., Bloise, R., Sorrentino, V., et al. 2001. Mutations in the cardiac ryanodine receptor gene (hRyR2) underlie catecholaminergic polymorphic ventricular tachycardia. *Circulation* 103(2), pp. 196–200.

Prins, D. and Michalak, M. 2011. Organellar calcium buffers. *Cold Spring Harbor Perspectives in Biology* 3(3), p. a004069.

Pritchard, T.J. and Kranias, E.G. 2009. Junctin and the histidine-rich Ca^{2+} binding protein: potential roles in heart failure and arrhythmogenesis. *Journal of Physiology* 587(Pt 13), pp. 3125–3133.

Prosser, B.L., Hernández-Ochoa, E.O. and Schneider, M.F. 2011. S100A1 and calmodulin regulation of ryanodine receptor in striated muscle. *Cell Calcium* 50(4), pp. 323–331.

Qin, J., Valle, G., Nani, A., Nori, A., Rizzi, N., Priori, S.G., Volpe, P., et al. 2008. Luminal Ca^{2+} regulation of single cardiac ryanodine receptors: insights provided by calsequestrin and its mutants. *The Journal of General Physiology* 131(4), pp. 325–334.

Qin, J., Valle, G., Nani, A., Chen, H., Ramos-Franco, J., Nori, A., Volpe, P., et al. 2009. Ryanodine receptor luminal Ca^{2+} regulation: swapping calsequestrin and channel isoforms. *Biophysical journal* 97(7), pp. 1961–1970.

Radwański, P.B., Belevych, A.E., Brunello, L., Carnes, C.A. and Györke, S. 2013. Store-dependent deactivation: cooling the chain-reaction of myocardial calcium signaling. *Journal of molecular and cellular cardiology* 58, pp. 77–83.

Ranatunga, K.M., Moreno-King, T.M., Tanna, B., Wang, R., Chen, S.R.W., Ruest, L., Welch, W., et al. 2005. The Gln4863Ala mutation within a putative, pore-lining trans-membrane helix of the cardiac ryanodine receptor channel alters both the kinetics of ryanoid interaction and the subsequent fractional conductance. *Molecular pharmacology* 68(3), pp. 840–846.

Reiken, S., Lacampagne, A., Zhou, H., Kherani, A., Lehnart, S.E., Ward, C., Huang, F., et al. 2003. PKA phosphorylation activates the calcium release channel (ryanodine receptor) in skeletal muscle: defective regulation in heart failure. *The Journal of Cell Biology* 160(6), pp. 919–928.

Rizzi, N., Liu, N., Napolitano, C., Nori, A. and Turcato, F. 2008. Unexpected structural and functional consequences of the R33Q homozygous mutation in cardiac calsequestrin a complex arrhythmogenic cascade in a knock in mouse model. *Circulation* 103(3), pp. 298–306.

Rossi, D. and Sorrentino, V. 2002. Molecular genetics of ryanodine receptors Ca^{2+}-release channels. *Cell calcium* 32(5-6), pp. 307–319.

Rossi, D., Bencini, C., Maritati, M., Benini, F., Lorenzini, S., Pierantozzi, E., Scarcella, A.M., et al. 2014. Distinct regions of triadin are required for targeting and retention at the junctional domain of the sarcoplasmic reticulum. *The Biochemical journal* 458(2), pp. 407–417.

Roux-Buisson, N., Cacheux, M., Fourest-Lieuvin, A., Fauconnier, J., Brocard, J., Denjoy, I., Durand, P., et al. 2012. Absence of triadin, a protein of the calcium release complex, is responsible for cardiac arrhythmia with sudden death in human. *Human Molecular Genetics* 21(12), pp. 2759–2767.

Sambrook, J., Fritsch, E.F. and Maniatis, T. 1989. Molecular cloning.

Samsó, M., Wagenknecht, T. and Allen, P.D. 2005. Internal structure and visualization of transmembrane domains of the RyR1 calcium release channel by cryo-EM. *Nature*

Structural & Molecular Biology 12(6), pp. 539–544.

Sato, Y., Ferguson, D.G., Sako, H., Dorn, G.W., Kadambi, V.J., Yatani, A., Hoit, B.D., et al. 1998. Cardiac-specific overexpression of mouse cardiac calsequestrin is associated with depressed cardiovascular function and hypertrophy in transgenic mice. *The Journal of biological chemistry* 273(43), pp. 28470–28477.

Scheinman, M.M. and Lam, J. 2006. Exercise-induced ventricular arrhythmias in patients with no structural cardiac disease. *Annual review of medicine* 57, pp. 473–484.

Scott, B.T., Simmerman, H.K., Collins, J.H., Nadal-Ginard, B. and Jones, L.R. 1988. Complete amino acid sequence of canine cardiac calsequestrin deduced by cDNA cloning. *Journal of Biological Chemistry* 263(18), pp. 8958–8964.

Scoote, M. and Williams, A.J. 2004. Myocardial calcium signalling and arrhythmia pathogenesis. *Biochemical and Biophysical Research Communications* 322(4), pp. 1286–1309.

Scoote, M. and Williams, A.J. 2002. The cardiac ryanodine receptor (calcium release channel): emerging role in heart failure and arrhythmia pathogenesis. *Cardiovascular Research* 56(3), pp. 359–372.

Scriven, D.R.L., Asghari, P. and Moore, E.D.W. 2013. Microarchitecture of the dyad. *Cardiovascular Research* 98(2), pp. 169–176.

Shan, J., Kushnir, A. and Betzenhauser, M.J. 2010. Phosphorylation of the ryanodine receptor mediates the cardiac fight or flight response in mice. *The Journal of Clinical Investigation* 120(12), pp. 4388–4398.

Shannon, T.R., Wang, F. and Bers, D.M. 2005. Regulation of cardiac sarcoplasmic reticulum Ca release by luminal [Ca^{2+}] and altered gating assessed with a mathematical model. *Biophysical journal* 89(6), pp. 4096–110.

Sharma, M.R.M., Penczek, P.P., Grassucci, R.R., Xin, H.B.H., Fleischer, S.S. and Wagenknecht, T.T. 1998. Cryoelectron microscopy and image analysis of the cardiac ryanodine receptor. *Journal of Biological Chemistry* 273(29), pp. 18429–18434.

Shin, D.W., Ma, J. and Kim, D.H. 2000. The asp-rich region at the carboxyl-terminus of calsequestrin binds to $Ca(^{2+})$ and interacts with triadin. *FEBS letters* 486(2), pp. 178–182.

Sigalas, C., Bent, S., Kitmitto, A., O'Neill, S. and Sitsapesan, R. 2009. $Ca(^{2+})$-calmodulin can activate and inactivate cardiac ryanodine receptors. *British Journal of Pharmacology* 156(5), pp. 794–806.

Singh, V.P., Rubinstein, J., Arvanitis, D.A., Ren, X., Gao, X., Haghighi, K., Gilbert, M., et al. 2013. Abnormal calcium cycling and cardiac arrhythmias associated with the human Ser96Ala genetic variant of histidine-rich calcium-binding protein. *Journal of the American Heart Association* 2(5), p. e000460.

Sitsapesan, R. and Williams, A.J. 1998. *The Structure and Function of Ryanodine Receptors*. Imperial College Press, pp. 269-290.

Sitsapesan, R.R. and Williams, A.J. 1994. Regulation of the gating of the sheep cardiac sarcoplasmic reticulum $Ca(^{2+})$-release channel by luminal Ca^{2+}. *Journal of Membrane Biology* 137(3), pp. 215–226.

Slupsky, J.R., Ohnishi, M., Carpenter, M.R. and Reithmeier, R.A. 1987. Characterization of cardiac calsequestrin. *Biochemistry (Washington)* 26(20), pp. 6539–6544.

Song, L., Alcalai, R., Arad, M., Wolf, C.M., Toka, O., Conner, D.A., Berul, C.I., et al. 2007. Calsequestrin 2 (CASQ2) mutations increase expression of calreticulin and ryanodine receptors, causing catecholaminergic polymorphic ventricular tachycardia. *Journal of Clinical Investigation* 117(7), pp. 1814–1823.

Sönnichsen, B.B., Füllekrug, J.J., Van, P.P.N., Diekmann, W.W., Robinson, D.G.D. and Mieskes, G.G. 1994. Retention and retrieval: both mechanisms cooperate to maintain calreticulin in the endoplasmic reticulum. *Journal of Cell Science* 107 (Pt 10), pp. 2705–2717.

Stevens, S.C.W., Terentyev, D., Kalyanasundaram, A., Periasamy, M. and Györke, S. 2009. Intra-sarcoplasmic reticulum Ca^{2+} oscillations are driven by dynamic regulation of ryanodine receptor function by luminal Ca^{2+} in cardiomyocytes. *Journal of Physiology* 587(Pt 20), pp. 4863–4872.

Sumitomo, N., Harada, K., Nagashima, M., Yasuda, T., Nakamura, Y., Aragaki, Y., Saito, A., et al. 2003. Catecholaminergic polymorphic ventricular tachycardia: electrocardiographic characteristics and optimal therapeutic strategies to prevent sudden death. *Heart (British Cardiac Society)* 89(1), pp. 66–70.

Swan, H., Laitinen, P. and Kontula, K. 2005. Calcium Channel Antagonism Reduces Exercise‐Induced Ventricular Arrhythmias in Catecholaminergic Polymorphic Ventricular Tachycardia Patients with RyR2 Mutations. *Journal of Cardiovasc Electrophysiol* 16(2), pp. 162-6.

Szegedi, C.S., Sarkozi, S., Herzog, A., Jona, I. and Varsányi, M. 1999. Calsequestrin: more than 'only'a luminal Ca^{2+} buffer inside the sarcoplasmic reticulum. *The Biochemical journal* 337(Pt 1), pp. 19-22.

Swan, H., Piippo, K., Viitasalo, M., Heikkilä, P., Paavonen, T., Kainulainen, K., Kere, J., et al. 1999. Arrhythmic disorder mapped to chromosome 1q42-q43 causes malignant polymorphic ventricular tachycardia in structurally normal hearts. *Journal of the American College of Cardiology* 34(7), pp. 2035–2042.

Takeshima, H., Komazaki, S., Nishi, M., Iino, M. and Kangawa, K. 2000. Junctophilins: a novel family of junctional membrane complex proteins. *Molecular cell* 6(1), pp. 11–22.

Taylor, S.C., Berkelman, T., Yadav, G. and Hammond, M. 2013. A defined methodology for reliable quantification of Western blot data. *Molecular Biotechnology* 55(3), pp. 217–226.

Tanna, B., Welch, W., Ruest, L., Sutko, J.L. and Williams, A.J. 1998. Interactions of a reversible ryanoid (21-amino-9alpha-hydroxy-ryanodine) with single sheep cardiac ryanodine receptor channels. *Journal of General Physiology* 112(1), pp. 55–69.

Tateishi, H., Yano, M. and Mochizuki, M. 2008. Defective domain-domain interactions within the ryanodine receptor as a critical cause of diastolic Ca^{2+} leak in failing hearts. *Cardiovascular Research* 81(3), pp. 536-45.

Tencerová, B., Zahradníková, A., Gaburjáková, J. and Gaburjáková, M. 2012. Luminal Ca^{2+} controls activation of the cardiac ryanodine receptor by ATP. *Journal of General Physiology* 140(2), pp. 93–108.

Terentyev, D. 2005. Triadin Overexpression Stimulates Excitation-Contraction Coupling and Increases Predisposition to Cellular Arrhythmia in Cardiac Myocytes. *Circulation Research* 96(6), pp. 651–658.

Terentyev, D., Nori, A., Santoro, M., Viatchenko-Karpinski, S., Kubalova, Z., Gyorke, I., Terentyeva, R., Vedamoorthyrao, S., Blom, N.A., Valle, G., Napolitano, C., Williams, S.C., Volpe, P., Priori, S.G., and Gyorke, S. 2006. Abnormal interactions of calsequestrin with the ryanodine receptor calcium release channel complex linked to exercise-induced sudden cardiac death. *Circulation research* 98(9), pp. 1151–1158.

Terentyev, D., Viatchenko-Karpinski, S., Gyorke, I., Terentyeva, R. and Gyorke, S. 2003a. Protein phosphatases decrease sarcoplasmic reticulum calcium content by stimulating calcium release in cardiac myocytes. *The Journal of Physiology* 552(Pt 1), pp. 109–118.

Terentyev, D., Viatchenko-Karpinski, S., Gyorke, I., Volpe, P., Williams, S.C. and Gyorke, S. 2003b. Calsequestrin determines the functional size and stability of cardiac intracellular calcium stores: Mechanism for hereditary arrhythmia. *Proceedings of the National Academy of Sciences of the United States of America* 100(20), pp. 11759–11764.

Tester, D.J., Dura, M., Carturan, E., Reiken, S., Wronska, A., Marks, A.R. and Ackerman, M.J. 2007. A mechanism for sudden infant death syndrome (SIDS): stress-induced leak via ryanodine receptors. *Heart Rhythm* 4(6), pp. 733–739.

Thevenon, D., Smida-Rezgui, S., Chevessier, F., Groh, S., Henry-Berger, J., Romero, N.B., Villaz, M., et al. 2003. Human skeletal muscle triadin: gene organization and cloning of the major isoform, Trisk 51. *Biochemical and biophysical research communications* 303(2), pp. 669–675.

Thomas, N.L., George, C.H. and Lai, F.A. 2004. Functional heterogeneity of ryanodine receptor mutations associated with sudden cardiac death. *Cardiovascular Research* 64(1), pp. 52–60.

Thomas, N.L. and Williams, A.J. 2012. Pharmacology of ryanodine receptors and Ca^{2+}-induced Ca^{2+} release. *Wiley Interdisciplinary Reviews: Membrane Transport and Signaling* 1(4), pp. 383–397.

Thomas, N.L., George, C.H. and Lai, F.A. 2006. Role of ryanodine receptor mutations in cardiac pathology: more questions than answers? *Biochemical Society transactions* 34(Pt 5), pp. 913–918.

Thomas, N.L., George, C.H., Williams, A.J. and Lai, F.A. 2007. Ryanodine receptor mutations in arrhythmias: advances in understanding the mechanisms of channel dysfunction. *Biochemical Society transactions* 35(Pt 5), pp. 946–951.

Thomas, N.L., Lai, F.A. and George, C.H. 2005. Differential Ca^{2+} sensitivity of RyR2 mutations reveals distinct mechanisms of channel dysfunction in sudden cardiac death. *Biochemical and biophysical research communications* 331(1), pp. 231–238.

Thomas, N.L., Maxwell, C., Mukherjee, S. and Williams, A.J. 2010. Ryanodine receptor mutations in arrhythmia: The continuing mystery of channel dysfunction. *FEBS letters* 584(10), pp. 2153–2160.

Tijskens, P. 2003. Junctin and calsequestrin overexpression in cardiac muscle: the role of junctin and the synthetic and delivery pathways for the two proteins. *Journal of Molecular and Cellular Cardiology* 35(8), pp. 961–974.

Timerman, A.P., Ogunbumni, E., Freund, E., Wiederrecht, G., Marks, A.R. and Fleischer, S. 1993. The calcium release channel of sarcoplasmic reticulum is modulated by FK-506-binding protein. Dissociation and reconstitution of FKBP-12 to the calcium release channel of skeletal muscle sarcoplasmic reticulum. *Journal of Biological Chemistry* 268(31), pp. 22992–22999.

Tiso, N., Stephan, D.A., Nava, A., Bagattin, A., Devaney, J.M., Stanchi, F., Larderet, G., et al. 2001. Identification of mutations in the cardiac ryanodine receptor gene in families affected with arrhythmogenic right ventricular cardiomyopathy type 2 (ARVD2). *Human Molecular Genetics* 10(3), pp. 189–194.

Treves, S., Feriotto, G., Moccagatta, L., Gambari, R. and Zorzato, F. 2000. Molecular cloning, expression, functional characterization, chromosomal localization, and gene structure of junctate, a novel integral calcium binding protein of sarco(endo)plasmic reticulum membrane. *The Journal of biological chemistry* 275(50), pp. 39555–39568.

Tripathy, A. and Meissner, G. 1996. Sarcoplasmic reticulum lumenal Ca^{2+} has access to cytosolic activation and inactivation sites of skeletal muscle Ca^{2+} release channel. *Biophysical journal* 70(6), pp. 2600-2615.

Tripathy, A., Xu, L., Mann, G. and Meissner, G. 1995. Calmodulin activation and inhibition of skeletal muscle Ca^{2+} release channel (ryanodine receptor). *Biophysical Journal* 69(1), pp. 106–119.

Tunwell, R., Wickenden, C., Bertrand, B. and Shevchenko, V. 1996. The human cardiac muscle ryanodine receptor-calcium release channel: identification, primary structure and topological analysis. *The Biochemical journal* 318 (Pt 2), pp. 477-87.

Uehara, A., Yasukochi, M., Mejía-Alvarez, R., Fill, M. and Imanaga, I. 2002. Gating kinetics and ligand sensitivity modified by phosphorylation of cardiac ryanodine receptors. *Pflügers Archiv : European journal of physiology* 444(1-2), pp. 202–212.

Valle, G., Boncompagni, S., Sacchetto, R., Protasi, F. and Volpe, P. 2014. Post-natal heart adaptation in a knock-in mouse model of calsequestrin 2-linked recessive catecholaminergic polymorphic ventricular tachycardia. *Experimental Cell Research* 321(2), pp. 178–189.

Van Petegem, F. 2012. Ryanodine Receptors: Structure and Function. *Journal of Biological Chemistry* 287(38), pp. 31624–31632.

Venetucci, L.A. and Eisner, D.A. 2008. Calsequestrin mutations and sudden death: a case of too little sarcoplasmic reticulum calcium buffering? *Circulation research* 103(3), pp. 223–225.

Venetucci, L.A., Trafford, A.W., O'Neill, S.C. and Eisner, D.A. 2008. The sarcoplasmic reticulum and arrhythmogenic calcium release. *Cardiovascular Research* 77(2), pp. 285–292.

Viatchenko-Karpinski, S., Terentyev, D. and Györke, I. 2004. Abnormal calcium signaling and sudden cardiac death associated with mutation of calsequestrin. *Circulation* 94(4), pp. 471-7.

Wang, W., Landstrom, A.P., Wang, Q., Munro, M.L., Beavers, D., Ackerman, M.J., Soeller, C., et al. 2014. Reduced junctional Na+/Ca2+-exchanger activity contributes to sarcoplasmic reticulum Ca2+ leak in junctophilin-2-deficient mice. *American Journal of Physiology - Heart and Circulatory Physiology*, 307(9), pp. H1317–H1326.

Wang, S., Trumble, W.R., Liao, H., Wesson, C.R., Dunker, A.K. and Kang, C.H. 1998. Crystal structure of calsequestrin from rabbit skeletal muscle sarcoplasmic reticulum. *Nature structural biology* 5(6), pp. 476–483.

Wang, R., Zhang, L., Bolstad, J., Diao, N., Brown, C., Ruest, L., Welch, W., et al. 2003. Residue Gln4863 within a predicted transmembrane sequence of the Ca^{2+} release channel (ryanodine receptor) is critical for ryanodine interaction. *Journal of Biological Chemistry* 278(51), pp. 51557–51565.

Wehrens, X.H.T. 2007. Leaky ryanodine receptors cause delayed afterdepolarizations and ventricular arrhythmias. *European heart journal* 28(9), pp. 1054–1056.

Wehrens, X.H., Lehnart, S.E., Huang, F., Vest, J.A., Reiken, S.R., Mohler, P.J., Sun, J., et al. 2003. FKBP12.6 Deficiency and Defective Calcium Release Channel (Ryanodine Receptor) Function Linked to Exercise-Induced Sudden Cardiac Death. *Cell* 113(7), pp. 829–840.

Wehrens, X.H.T., Lehnart, S.E. and Marks, A.R. 2005. Intracellular calcium release and cardiac disease. *Annu Rev Physiol* 67, pp. 69–98.

Wehrens, X.H.T., Lehnart, S.E., Reiken, S.R., Deng, S.-X., Vest, J.A., Cervantes, D., Coromilas, J., et al. 2004. Protection from cardiac arrhythmia through ryanodine receptor-stabilizing protein calstabin2. *Science (New York, N.Y.)* 304(5668), pp. 292–296.

Wehrens, X.H.T., Lehnart, S.E., Reiken, S., Vest, J.A., Wronska, A. and Marks, A.R. 2006. Ryanodine Receptor/Calcium Release Channel PKA Phosphorylation: A Critical Mediator of Heart Failure Progression. *Proceedings of the National Academy of Sciences of the United States of America* 103(3), pp. 511–518.

Wei, L., Gallant, E.M., Dulhunty, A.F. and Beard, N.A. 2009a. Junctin and triadin each activate skeletal ryanodine receptors but junctin alone mediates functional interactions with calsequestrin. *The international journal of biochemistry & cell biology* 41(11), pp. 2214–2224.

Wei, L., Hanna, A.D., Beard, N.A. and Dulhunty, A.F. 2009b. Unique isoform-specific properties of calsequestrin in the heart and skeletal muscle. *Cell Calcium* 45(5), pp. 474–484.

Wetzel, G.T., Ding, S. and Chen, F. 2000. Molecular cloning of junctin from human and developing rabbit heart. *Molecular genetics and metabolism* 69(3), pp. 252–258.

Wium, E., Dulhunty, A.F. and Beard, N.A. 2012. A skeletal muscle ryanodine receptor interaction domain in triadin. *PloS one* 7(8), p. e43817.

Wu, H.-D., Xu, M., Li, R.-C., Guo, L., Lai, Y.-S., Xu, S.-M., Li, S.-F., et al. 2012. Ultrastructural remodelling of $Ca(^{2+})$ signalling apparatus in failing heart cells. *Cardiovascular Research* 95(4), pp. 430–438.

Xiao, B., Zhong, G., Obayashi, M., Yang, D. and Chen, K. 2006. Ser-2030, but not Ser-2808, is the major phosphorylation site in cardiac ryanodine receptors responding to protein kinase A activation upon beta-adrenergic stimulation in normal and failing hearts. *The Biochemical journal* 396(1), pp. 7-16.

Xiao, J., Tian, X., Jones, P.P., Bolstad, J. and Kong, H. 2007. Removal of FKBP12. 6 does not alter the conductance and activation of the cardiac ryanodine receptor or the susceptibility to stress-induced ventricular arrhythmias. *The Journal of Biological*

Chemistry 282(48), pp. 34828–38.

Xu, L. and Meissner, G. 1998. Regulation of cardiac muscle Ca^{2+} release channel by sarcoplasmic reticulum lumenal Ca^{2+}. *Biophysical journal* 75(5), pp. 2302–2312.

Xu, L. and Meissner, G. 2004. Mechanism of Calmodulin Inhibition of Cardiac Sarcoplasmic Reticulum Ca^{2+} Release Channel (Ryanodine Receptor). *Biophysical Journal* 86(2), pp. 797–804.

Xu, X., Yano, M., Uchinoumi, H., Hino, A. and Suetomi, T. 2010. Defective calmodulin binding to the cardiac ryanodine receptor plays a key role in CPVT-associated channel dysfunction. *Biochemical and Biophysical Research Communications* 394(3), pp. 660-666.

Yamamoto, T. and Ikemoto, N. 2002. Spectroscopic monitoring of local conformational changes during the intramolecular domain-domain interaction of the ryanodine receptor. *Biochemistry (Washington)* 41(5), pp. 1492–1501.

Yan, Z., Bai, X-C., Yan, C., Wu, J., Li, Z., Xie, T., Peng, W., et al. 2015. Structure of the rabbit ryanodine receptor RyR1 at near-atomic resolution. *Nature* 517(7532), pp. 50–55.

Yang, Z., Ikemoto, N., Lamb, G.D. and Steele, D.S. 2006. The RyR2 central domain peptide DPc10 lowers the threshold for spontaneous Ca^{2+} release in permeabilized cardiomyocytes. *Cardiovascular Research* 70(3), pp. 475–485.

Yano, M., Yamamoto, T., Kobayashi, S. and Matsuzaki, M. 2009. Role of ryanodine receptor as a Ca^{2+} regulatory center in normal and failing hearts. *Journal of Cardiology* 53, pp. 1-7.

Yuan, Q., Fan, G.-C., Dong, M., Altschafl, B., Diwan, A., Ren, X., Hahn, H.H., et al. 2007. Sarcoplasmic reticulum calcium overloading in junctin deficiency enhances cardiac contractility but increases ventricular automaticity. *Circulation* 115(3), pp. 300–309.

Yuchi, Z., Lau, K. and Van Petegem, F. 2012. Disease mutations in the ryanodine receptor central region: crystal structures of a phosphorylation hot spot domain. *Structure (London, England : 1993)* 20(7), pp. 1201–1211.

Zahradníková, A. and Zahradník, I. 2012. Construction of calcium release sites in cardiac myocytes. *Frontiers in physiology* Vol 3, p. a322.

Zahradníková, A., Dura, M. and Györke, I. 2003. Regulation of dynamic behavior of cardiac ryanodine receptor by Mg^{2+} under simulated physiological conditions. *American Journal of Physiology Cell Physiology* 285(5), pp. C1059–70.

Zamparelli, C., Ilari, A., Verzili, D., Giangiacomo, L., Colotti, G., Pascarella, S. and Chiancone, E. 2000. Structure-function relationships in sorcin, a member of the penta EF-hand family. Interaction of sorcin fragments with the ryanodine receptor and an Escherichia coli model system. *Biochemistry (Washington)* 39(4), pp. 658–666.

Zhang, J., Chen, B., Guo, A., Zhou, Q., Tan, Z., Wu, G., Song, L.-S., et al. 2013. A Luminal Calcium Sensing Mutation of the Cardiac Ryanodine Receptor Diminishes Calcium Waves and Stress -Induced Ventricular Tachycardias in Calsequestrin Null Mice. *Biophysical journal* 104, p. 441.

Zhang, J., Chen, B., Zhong, X., Mi, T., Guo, A., Zhou, Q., Tan, Z., et al. 2014. The

cardiac ryanodine receptor luminal Ca^{2+} sensor governs Ca^{2+} waves, ventricular tachyarrhythmias and cardiac hypertrophy in calsequestrin-null mice. *The Biochemical journal* 461(1), pp. 99–106.

Zhang, L., Franzini-Armstrong, C., Ramesh, V. and Jones, L.R. 2001. Structural alterations in cardiac calcium release units resulting from overexpression of junctin. *Journal of molecular and cellular cardiology* 33(2), pp. 233–247.

Zhang, L., Kelley, J., Schmeisser, G., Kobayashi, Y.M. and Jones, L.R. 1997. Complex formation between junctin, triadin, calsequestrin, and the ryanodine receptor. Proteins of the cardiac junctional sarcoplasmic reticulum membrane. *The Journal of biological chemistry* 272(37), pp. 23389–23397.

Zhou, Q., Xiao, J., Jiang, D., Wang, R., Vembaiyan, K., Wang, A., Smith, C.D., et al. 2011. Carvedilol and its new analogs suppress arrhythmogenic store overload–induced Ca2+ release. *Nature Medicine* 17(8), pp. 1003–1009.

Zhu, L., Zhong, X., Chen, S. and Banavali, N. 2013. Modeling a ryanodine receptor N-terminal domain connecting the central vestibule and the corner clamp region. *Journal of Biological Chemistry* 288(2), pp. 903-914.

Zissimopoulos, S., Seifan, S., Maxwell, C., Williams, A.J. and Lai, F.A. 2012. Disparities in the association of the ryanodine receptor and the FK506-binding proteins in mammalian heart. *Journal of cell science* 125(Pt 7), pp. 1759–1769.

Zorzato, F., Fujii, J., Otsu, K., Phillips, M., Green, N.M., Lai, F.A., Meissner, G., et al. 1990. Molecular cloning of cDNA encoding human and rabbit forms of the Ca^{2+} release channel (ryanodine receptor) of skeletal muscle sarcoplasmic reticulum. *Journal of Biological Chemistry* 265(4), pp. 2244–2256.